

WL-TR-97-4057

**RESEARCH IN ADVANCED MATERIALS PROCESSING  
AND PROCESS MODELING**

Samuel P. Owusu-Ofori (Principal Investigator)  
Devdas M. Pai & Robert L. Sadler (Co-Investigators)  
North Carolina A&T State University  
1601 E. Market Street  
Greensboro, NC 27411



May 1997

Final Report For Period July 29, 1993 through April 30, 1997

Approved for public release; distribution unlimited

**MATERIALS DIRECTORATE  
WRIGHT LABORATORY  
AIR FORCE MATERIEL COMMAND  
WRIGHT-PATTERSON AIR FORCE BASE, OHIO 45433-7734**

19980512 002

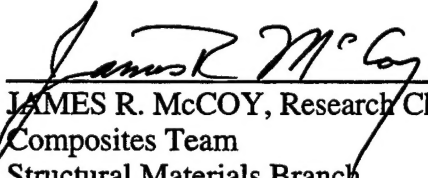
DTIC QUALITY INSPECTED 3

## NOTICE


USING GOVERNMENT DRAWINGS, SPECIFICATIONS, OR OTHER DATA INCLUDED IN THIS DOCUMENT FOR ANY PURPOSE OTHER THAN GOVERNMENT PROCUREMENT DOES NOT IN ANY WAY OBLIGATE THE US GOVERNMENT. THE FACT THAT THE GOVERNMENT FORMULATED OR SUPPLIED THE DRAWINGS, SPECIFICATIONS, OR OTHER DATA DOES NOT LICENSE THE HOLDER OR ANY OTHER PERSON OR CORPORATION; OR CONVEY ANY RIGHTS OR PERMISSION TO MANUFACTURE, USE, OR SELL ANY PATENTED INVENTION THAT MAY RELATE TO THEM.

THIS REPORT IS RELEASABLE TO THE NATIONAL TECHNICAL INFORMATION SERVICE (NTIS). AT NTIS, IT WILL BE AVAILABLE TO THE GENERAL PUBLIC, INCLUDING FOREIGN NATIONS.

THIS TECHNICAL REPORT HAS BEEN REVIEWED AND IS APPROVED FOR PUBLICATION.

  
JAMES R. McCOY, Research Chemist  
Composites Team  
Structural Materials Branch

  
L. SCOTT THEIBERT, Chief  
Structural Materials Branch  
Nonmetallic Materials Division

  
ROGER D. GRISWOLD, Assistant Chief  
Nonmetallic Materials Division  
Materials and Manufacturing Directorate

Do not return copies of this report unless contractual obligations or notice on a specific document requires its return.

REPORT DOCUMENTATION PAGE			Form Approved OMB No. 0704-0188	
Public reporting burden for this collection of information is estimated to average 1 hour per response, including the time for reviewing instructions, searching existing data sources, gathering and maintaining the data needed, and completing and reviewing the collection of information. Send comments regarding this burden estimate or any other aspect of this collection of information, including suggestions for reducing this burden, to Washington Headquarters Services, Directorate for Information Operations and Reports, 1215 Jefferson Davis Highway, Suite 1204, Arlington, VA 22202-4302, and to the Office of Management and Budget, Paperwork Reduction Project (0704-0188), Washington, DC 20503.				
1. AGENCY USE ONLY (Leave blank)		2. REPORT DATE May 1997		3. REPORT TYPE AND DATES COVERED Final Report for 29 July 1993 - 30 April 1997
4. TITLE AND SUBTITLE Research in Advanced Materials Processing and Process Modeling			5. FUNDING NUMBERS C: F33615-93-C-5337 PE: 62102F PR: 2419 TA: 30 WU: 04	
6. AUTHOR(S) Samuel P. Owusu-Ofori, Devdas M. Pai, and Robert L. Sadler				
7. PERFORMING ORGANIZATION NAME(S) AND ADDRESS(ES) North Carolina A & T State University 1601 E. Market Street Greensboro NC 27411			8. PERFORMING ORGANIZATION REPORT NUMBER	
9. SPONSORING / MONITORING AGENCY NAME(S) AND ADDRESS(ES) POC: J. McCoy, AFRL/MLBC, 937-255-9063 Materials Directorate Wright Laboratory Air Force Materiel Command Wright-Patterson AFB OH 45433-7734			10. SPONSORING / MONITORING AGENCY REPORT NUMBER  WL-TR-97-4057	
11. SUPPLEMENTARY NOTES				
12a. DISTRIBUTION / AVAILABILITY STATEMENT  Approved for public release; distribution unlimited.			12b. DISTRIBUTION CODE	
13. ABSTRACT (Maximum 200 words)  In resin transfer molding (RTM), the liquid matrix is pumped into the mold to infiltrate a preform assembled in the mold and under compressive stresses. The matrix tends to flow around the preform periphery, along the path(s) of least resistance and arrive at the vents before the entire preform is impregnated, causing the part to be defective. This phenomenon is known as "race tracking." A preform-mold misfit could waste an entire part since recovery from a non-fill is not possible. The primary goal of this research was to develop and demonstrate a practical quantitative method for evaluating the preform-mold fit with the mold closed before the matrix is injected. The preform-mold fit is determined by probing the ready-to-inject mold assembly with nitrogen and collecting the exhaust gas through a series of flow meters located along the periphery of the mold. Experiments have been developed to test the instrumentation and the methodology for the prediction of the characteristics of the resin flow front with satisfactory results.				
14. SUBJECT TERMS resin transfer molding, race-tracking, composite processing, process control, process monitoring,			15. NUMBER OF PAGES 207	
			16. PRICE CODE	
17. SECURITY CLASSIFICATION OF REPORT UNCLASSIFIED	18. SECURITY CLASSIFICATION OF THIS PAGE UNCLASSIFIED	19. SECURITY CLASSIFICATION OF ABSTRACT UNCLASSIFIED	20. LIMITATION OF ABSTRACT SAR	

## CONTENTS

LIST OF FIGURES	vi
LIST OF TABLES	viii
FOREWORD	x
SUMMARY	xi
 CHAPTER 1 INTRODUCTION	 1
1.1 Need for Composite Materials	1
1.2 Composite Materials Fabrication	2
1.2.1 Autoclave Molding	2
1.2.2 Compression Molding	3
1.2.3 Pultrusion	4
1.2.4 Filament Winding	6
1.2.5 Elastic Reservoir Molding	7
1.2.6 Tube Rolling	7
1.2.7 Resin Transfer Molding	9
1.3 Defects	9
1.4 Autoclave Molding versus RTM	10
1.5 Research in Resin Transfer Molding	11
1.5.1 Flow Pattern	13
1.5.2 Fiber-Resin System	13
1.5.3 Material Properties	14
1.5.4 Vacuum Assistance	15
1.5.5 Process Parameters	16
1.5.6 Race Tracking	17
1.5.7 Process Monitoring and Control	19
1.6 Objective and Scope	19
 CHAPTER 2 EXPERIMENTAL SETUP AND PROCEDURE	 21
2.1 Process Variables	21
2.1.1 Viscosity of Resin	21
2.1.2 Resin Back Pressure	23
2.1.3 Flow Rate / Pump Speed	23
2.1.4 Air Content in the Resin/Catalyst Mixture	29
2.1.5 Resin/Catalyst Mix Ratio	33
2.1.6 Evacuation of the Mold	34
2.1.7 Uniformity of Preform and Placement of Preform in Mold	36
2.1.8 Temperatures	36
2.2 Mold Design and Construction	36
2.3 Description of Sensors	38
2.3.1 Mass Flow Meters	38
2.3.2 Pressure Transducer	39
2.4 Description of Data Acquisition System	40



2.4.1	Data Acquisition System Hardware	40
2.4.2	Description of LabView Software	40
2.5	Instrument Specifications	41
2.6	Description of Experimental Setup	43
2.6.1	Experimental Setup for N <sub>2</sub> Gas Introduction	43
2.6.2	Experimental Setup for RTM/Resin Impregnation	46
2.7	Summary of Levels of Variables	49
2.8	Data Collection Scheme for N <sub>2</sub> Gas Flow Rates	50
2.9	Data Collection of Back Pressure during RTM	53
2.10	Development of Database	53
2.11	Materials Properties	55
2.11.1	Specific Gravity, Fiber Volume and Void Content	55
2.11.2	Compression Test	56
2.11.3	Transverse Short-Beam Shear Testing	59
2.12	Non-Destructive Evaluation	59
CHAPTER 3	RESULTS AND OBSERVATIONS	63
3.1	Nitrogen Flow Data	63
3.1.1	Raw Nitrogen Flow Rates	63
3.1.2	Normalized Flow Rates	63
3.1.3	Gas Flow Parameter	63
3.2	Resin Flow Data	65
3.2.1	Flow Front Height Ratios	66
3.2.2	Back Pressure	72
3.3	Material Properties	72
3.3.1	Compression Test	72
3.3.2	Short-Beam Shear Test	76
3.3.3	Specific Gravity, Fiber Volume Fraction and Void Content	76
3.3.4	Ultrasonic Test Results	78
CHAPTER 4	ANALYSIS AND DISCUSSION OF RESULTS	82
4.1	Prediction of Skewness of Resin Flow Front	82
4.1.1	Prediction Based On Relative Percent Cumulative Flow	82
4.1.2	Prediction Based on Gas Flow Ratio	88
4.1.3	Prediction Based on Gas Flow Parameter	90
4.1.4	Summary of Resin Flow Prediction Methods	94
4.2	Prediction of Race Tracking	95
4.2.1	Characterization of Flow Front by Height Ratios	95
4.2.2	Characterization of Flow Front by Flow Front Angle	96

4.2.3	Parameterization of Flow Front	99
4.2.4	Correlation of Flow Front and Gas Flow Parameter	99
4.2.5	Limits of Gas Flow Parameter	103
4.3	Verification of Method	105
4.3.1	Verification using Flat Panels	105
4.3.2	Verification using 3-D Demonstration Part	110
4.4	Material Properties	110
4.4.1	Physical Properties	112
4.4.2	Mechanical Properties	112
4.4.3	Relationship among Material Properties	117
CHAPTER 5	CONCLUSIONS AND RECOMMENDATIONS	121
CHAPTER 6	REFERENCES	124
APPENDIX A:	NITROGEN FLOW RATE DATA	126
APPENDIX B:	NORMALIZED GAS FLOW DATA	130
APPENDIX C:	GAS FLOW PARAMETERS	134
APPENDIX D:	GAS FLOW DATA WITH DIGITIZED FLOW FRONTS	138
APPENDIX E:	C-SCAN IMAGES FOR PANELS S2P1-S2P10	159
APPENDIX F:	RACE-TRACKING / FINAL FILL PREDICTION CHARTS	170
APPENDIX G:	FLOW FRONT ANGLES	178
APPENDIX H:	LABVIEW OUTPUT -VERIFICATION TESTS	187
APPENDIX I:	RESULTS - MATERIAL PROPERTIES	199

## LIST OF FIGURES

	Page
Figure 1-1 Schematic of Bagging in Autoclave Molding	3
Figure 1-2 Schematic of Compression Molding	4
Figure 1-3 Schematic of Pultrusion	5
Figure 1-4 Schematic of Filament Winding	6
Figure 1-5 Schematic of Elastic Reservoir Molding	8
Figure 1-6 Schematic of Tube Rolling	9
Figure 1-7 Schematic of Resin Transfer Molding	10
Figure 1-8 Flow Front Illustrating Race Tracking	12
Figure 2-1 Experimental Scheme	22
Figure 2-2 Plot of Viscosity versus Time	25
Figure 2-3 Plot of Viscosity versus Temperature	26
Figure 2-4 Pump Head, Flow Rate and Tube Calibration	27
Figure 2-5 Tube Expansion, Flow Rate and Back Pressure	30
Figure 2-6 Pump Cumulative Flow versus Time	35
Figure 2-7 Engineering Drawing of the Mold	37
Figure 2-8 Port Configuration	44
Figure 2-9 Schematic for Nitrogen Data Acquisition	47
Figure 2-10 Schematic for Flow Front Data Acquisition	48
Figure 2-11 Port Configuration for Nitrogen Injection	51
Figure 2-12 LabView User Interface for Nitrogen Injection	52
Figure 2-13 LabView User Interface for Resin Injection	54
Figure 2-14 Panel Showing Sample Regions for Tests	57
Figure 2-15 Modified IITRI Compression Test Fixture and Test Specimen	58
Figure 2-16 Test Fixture and Sample for Short Beam Shear Test	60
Figure 2-17 Schematics of Pulse-Echo and Through-Transmission Methods	61
Figure 2-18 Schematics of Pulse-Echo Display Systems	62
Figure 3-1 Traced and Corresponding Digitized Flow Front - Sample 1	67
Figure 3-2 Traced and Corresponding Digitized Flow Front - Sample 2	68
Figure 3-3 Traced and Corresponding Digitized Flow Front - Sample 3	69
Figure 3-4 Schematic of A Flow Front	70
Figure 3-5 Plots of Flow Front Height Ratios - Sample 1	70
Figure 3-6 Plots of Flow Front Height Ratios - Sample 2	71
Figure 3-7 Plots of Flow Front Height Ratios - Sample 3	71
Figure 3-8 Plot of Inlet Pressure versus Time - Sample 1	72
Figure 3-9 Plot of Inlet Pressure versus Time - Sample 2	73

Figure 3-10	Plot of Inlet Pressure versus Time - Sample 3	73
Figure 3-11	Typical Compressive Stress-Strain Diagram	75
Figure 3-12	Typical Shear Stress-Strain Diagram	77
Figure 3-13	Typical Flow Front and Corresponding C-Scan Image (S2P1)	81
Figure 4-1	Air Flow Data and Resin Flow Front - S1P1	83
Figure 4-2	Air Flow Data and Resin Flow Front - S1P2	84
Figure 4-3	Air Flow Data and Resin Flow Front - S1P3	85
Figure 4-4	Air Flow Data and Resin Flow Front - S1P4	86
Figure 4-5	Air Flow Data and Resin Flow Front - S1P5	87
Figure 4-6	Resin Flow Front Parameters	96
Figure 4-7	Height Ratio for A Good Flow Front - S2P2	97
Figure 4-8	Height Ratio for A Poor Flow Front - S1P3	97
Figure 4-9	Flow Front Angle for A Good Flow Front - S2P2	98
Figure 4-10	Flow Front Angle for A Poor Flow Front - S1P3	98
Figure 4-11	Definition of Flow Front Angle Area	100
Figure 4-12	Scatter Plots of Gas Flow Parameters versus Flow Front Angle Area	101
Figure 4-13	Normal Distribution Showing Limits of Gas Flow Parameter	104
Figure 4-14	Flow Chart of Methodology for Prediction of Resin Flow	106
Figure 4-15	Flow Front for S3P1	107
Figure 4-16	Flow Front for S3P2	107
Figure 4-17	Flow Front for S3P3	108
Figure 4-18	Flow Front for S3P4	108
Figure 4-19	Flow Front for S3P5	109
Figure 4-20	Flow Front for S3P6	109
Figure 4-21	3-D Demonstration Part	111
Figure 4-22	Flow Front for S4P1	113
Figure 4-23	Flow Front for S4P2	113
Figure 4-24	Flow Front for S4P3	114
Figure 4-25	Flow Front for S4P4	114
Figure 4-26	Flow Front for S4P5	115
Figure 4-27	Specific Gravity versus Number of Plies	116
Figure 4-28	Fiber Volume Fraction versus Number of Plies	116
Figure 4-29	Void Content versus Resin Flow Rate	117

## LIST OF TABLES

		Page
Table 2-1	Viscosity Test for Mix Ratio 100:17	24
Table 2-2	Viscosity Test for Mix Ratio 100:22	25
Table 2-3	Pump Head Test	26
Table 2-4	Tube Calibration	29
Table 2-5	Pump Test against Pressure	31
Table 2-6	Pump Calibration	32
Table 2-7	Tube Calibration for Test with Corn Syrup	33
Table 2-8	Pump Test against Pressure with Corn Syrup	33
Table 2-9	Mold Filling with Corn Syrup	34
Table 2-10	Mix Ratio Test by Making Panels	36
Table 3-1	Raw N <sub>2</sub> Flow Rates (q <sub>i</sub> ) - standard liters per minute	64
Table 3-2	Normalized N <sub>2</sub> Flow Rates	65
Table 3-3	Gas Flow Parameters (P <sub>L</sub> , P <sub>R</sub> )	66
Table 3-4	Compressive Strength - Sample Test Results (S2P1)	74
Table 3-5	Average Compressive Strengths of Panels	74
Table 3-6	Shear Strength - Sample Test Results (S2P1)	76
Table 3-7	Average Shear Strengths of Panels	78
Table 3-8	Fiber Volume Fraction - Sample Test Results (S2P1)	79
Table 3-9	Average Fiber Volume Fraction of Panels	79
Table 3-10	Percent Void Content - Sample Test Results (S2P1)	80
Table 3-11	Average Void Content of Panels	80
Table 4-1	Prediction Table Using Relative Percent Flow; All-Ports-Open	89
Table 4-2	Success Rate in Prediction Using Relative Percent Gas Flow Rates	90
Table 4-3	Success Rate in Prediction of Skewness Using Gas Flow Ratio; Ports (3+4+7) and (1+2+5)	91
Table 4-4	Success Rate in Prediction of Skewness Using Gas Flow Ratio; Ports (3+7) and (2+5)	91
Table 4-5	Success Rate in Prediction of Skewness Using Gas Flow Ratio; Ports (3) and (2)	91
Table 4-6	Success Rate in Prediction of Skewness Using Gas Flow Ratio; Ports (3+4) and (1+2)	91
Table 4-7	Success Rate in Prediction of Skewness Using Gas Flow Ratio; Ports (5) and (7)	91
Table 4-8	Significance Test for Difference of Gas Flow Parameters; Ports (3+4+7) And (1+2+5)	92
Table 4-9	Significance Test for Difference of Gas Flow Parameters; Ports (3+7) And (2+5)	92
Table 4-10	Significance Test for Difference of Gas Flow Parameters; Ports (3+4) And (1+2)	92

Table 4-11	Significance Test for Difference of Gas Flow Parameters; Ports (7) and (5)	93
Table 4-12	Significance Test for Difference of Gas Flow Parameters; Ports (3) and (2)	93
Table 4-13	Success Rate in Prediction of Skewness Using Gas Flow Parameters; Ports (3+4+7) and (1+2+5)	93
Table 4-14	Success Rate in Prediction of Skewness Using Gas Flow Parameters; Ports (3+7) and (2+5)	94
Table 4-15	Success Rate in Prediction of Skewness Using Gas Flow Parameters; Ports (3) and (2)	94
Table 4-16	Success Rate in Prediction of Skewness Using Gas Flow Parameters; Ports (3+4) and (1+2)	94
Table 4-17	Success Rate in Prediction of Skewness Using Gas Flow Parameters; Ports (5) and (7)	94
Table 4-18	Correlation of Gas Flow Parameters versus Flow Front Angle Area	102
Table 4-19	Limits of Gas Flow Parameters	103
Table 4-20	Normalized Data and Gas Flow Parameters ( $P_L$ , $P_R$ ); 2-D Verification Part	105
Table 4-21	Normalized Data and Gas Flow Parameters ( $P_L$ , $P_R$ ); 3-D Demonstration Part	112
Table 4-22	Correlation Coefficients between Material Properties and Fill Time	119
Table 4-23	Correlation Coefficients between Material Properties and Race-Tracking Index	120

## **FOREWORD**

This final technical report covers the work performed under Air Force Contract F33615-93-C-5337, "Advanced Materials Processing and Product Modeling," from July 30, 1993 through April 30, 1997. This contract was sponsored by the Wright Laboratory, Materials Directorate, Air Force Materiel Command, Wright-Patterson Air Force Base, Ohio. It was administered by WL/MLBC with Lt. Terry Christiansen and Dr. James R. McCoy as the technical monitors. Dr. Samuel P. Owusu-Ofori, served as the principal investigator with Dr. Devdas Pai and Professor Robert Sadler as the co-investigators. Four graduate students, Dharmesh Shah, Prafulkumar Vyas, Marcus Green, and Deryl Alexander used parts of this work to develop their thesis topics. Several other graduate students were also involved with various aspects of the project. The experiments were conducted at the laboratories of the Center for Composite Materials Research (CCMR), North Carolina A&T State University with the assistance of the staff, especially Professor Leon Skeen.

## SUMMARY

In Resin Transfer Molding (RTM), the liquid matrix is pumped into the mold to infiltrate a preform assembled in the mold and under compressive stresses. The matrix tends to flow around the preform periphery, along the path(s) of least resistance and arrive at the vents before the entire preform is impregnated causing the part to be defective. This phenomenon is known as "race tracking." A preform-mold misfit could waste an entire part since recovery from a non-fill is not possible.

The primary goal of this research is to develop and demonstrate a practical quantitative method for evaluating the preform-mold fit with the mold closed before the matrix is injected. The preform-mold fit is determined by probing the ready-to-inject mold assembly with nitrogen and collecting the exhaust gas through a series of flow meters located along the periphery of the mold. The resin flow front is monitored as the process progresses. The gas flow rates are used to develop a parameter, the gas flow parameter and the resin flow rates near the sides of the mold have been used to develop a parameter, the resin flow front angle index, to represent the actual resin flow. It has been demonstrated that the gas flow parameter and the resin flow index have a significant correlation between them. Thus, by correlating the flow characteristics of the nitrogen introduced into the mold with the resin flow characteristics the predictions of the skewness of the flow front and the degree of race tracking can be made with a high degree of accuracy. An automatic advisory system has been developed to collect the nitrogen data, analyze it and inform the operator of the possible direction of the skewness of resin flow front and the severity of the race tracking phenomenon.

Experiments have been developed to test the instrumentation and the methodology for the prediction of the characteristics of the resin flow front with satisfactory results. This report describes the development of the experimental procedures, the methodology for the prediction of the mold-preform fit as indicated by the degree of skewness of the resin flow front, the setup and testing of the automatic advisory system.



## CHAPTER 1

### INTRODUCTION

As the century comes to a close and we approach a new millennium, it is the expectation, the directive and the destiny of man to make significant advances in all areas of technology. Prognosticators have long since determined that the 21<sup>st</sup> century will be defined by efficient and fast machines utilized on a daily basis. Throughout history, new technologies have not only been defined by new inventions but also by the application of a new material to an old technology to create a better one. This is very evident in the field of materials engineering. As the progression of man continued and tools evolved from sticks to stones to metal alloys, the ingenuity of the applied technology also progressed along.

#### 1.1 Need for Composite Materials

The basic need for composite materials follows the natural process of evolution as a result of technology. The desire and the eventual requirement that processes and equipment perform at faster and more efficient rates provide the incentive for the implementation of composite materials into the fabric of everyday objects. Composite materials are being widely used in industry and are rapidly replacing the conventional construction materials. The reason for their popularity is that they offer a combination of strength and modulus that is comparable to or better than many traditional metallic materials. Because of their low specific gravity, the strength-to-weight and the modulus-to-weight ratios are markedly superior to those of metallic materials. Also, the fatigue strength-to-weight ratios as well as the fatigue damage tolerance of most of the composite materials are excellent. Thus, the inherent advantages of composite materials make them attractive. Specifically, the high strength-weight-ratio and stiffness-weight-ratio make composites the ideal application in instances where weight and structural integrity are of primary concern.

Applications of composites range from aerospace to automotive; from sporting goods to marine engineering. The aircraft industry uses composite materials for the primary reason that with the reduced weight, higher speeds and increased payloads are possible. They are also used to manufacture rotor blades for many military and commercial helicopters. The space industry uses composite materials for weight reduction. Due to their near zero coefficient of thermal expansion, they are used for support structures for mirrors and lenses on space stations, which are exposed to surface temperatures ranging from 100 °C to -100 °C. The automotive industry uses composite materials for body components such as hood or door panels, radiator supports, door frames and bumper reinforcement beams. The sporting goods industry uses composite materials for tennis rackets, racquetball rackets, fishing rods, bicycle frames, skis, sailboats and kayaks, surf boards, javelins and helmets. The marine applications of composites are boat hulls, decks, bulkheads, frames, masts and spars.

## **1.2 Composite Materials Fabrication**

As is the case with most new technologies, the application of composite materials is cost prohibitive in both material and manufacturing aspects. The primary concern involves the manufacturing processes required to fabricate these materials.

Fiber-reinforced composite materials are mainly composed of fibers and the resin mixture. The latter is known as the matrix. In general, there are two principal steps in manufacturing laminated fiber-reinforced composite materials. The first step is the lay-up process, which is basically the arrangement of the unidirectional or woven fibers in a matrix, called lamina; followed by the stacking of these laminae into laminates. In this broad definition of the fabrication process, the application of the matrix is considered a sub-category of the lay-up process. The fibers and matrices are available separately or in combination; commonly known as pre-impregnated fibers or prepregs. Prepregs are fibers which have been saturated with a resinous material prior to use in the fabrication process and are utilized as the fiber component in the final fabrication process (Jones, 1975). The second step is the curing process. The curing process is the drying or polymerization of the resinous matrix material to form a permanent bond between fibers and between laminae (Jones, 1975). This may be conducted at room temperature or be accelerated by the application of heat. There are three primary methods for the lay-up process: (1) winding and laying, (2) molding and (3) continuous lamination.

Many factors including part size, cost, scheduling and time constraints determine the selection of the appropriate process and curing. The most prominent processes under the three classes are (Mallick, 1988) listed below and described briefly.

1. Autoclave Molding
2. Compression Molding
3. Pultrusion
4. Filament Winding
5. Elastic Reservoir Molding
6. Tube Rolling
7. Resin Transfer Molding

### **1.2.1 Autoclave Molding**

The parts made by this process are of high quality, from the strength as well as dimensional point of view. However, autoclave molding is an expensive fabrication process. This process is predominantly used in the aerospace industry, where high production rates are not an important consideration. An aluminum tool plate, nylon film, bleeder mat, porous Teflon sheet, prepreg (fiber plus resin), porous Teflon sheet, bleeder mat, nylon film, aluminum caul plate, nylon film, breather mat and nylon film, are "bagged up". "Bagging up" means it is laid up in the sequence listed above. An example of a vacuum bag assembly is shown in Figure 1-1.

Prepreg contains fibers in a partially cured epoxy resin. Typically, the resin is 42% of the total weight of the prepreg. Plies are trimmed from the prepreg roll into the desired shape, size and orientation. The layers of prepreg are laid at different angles per the specified design. The whole stack is put in a vacuum chamber. Application of heat cures the resin and vacuum squeezes out the excess resin.

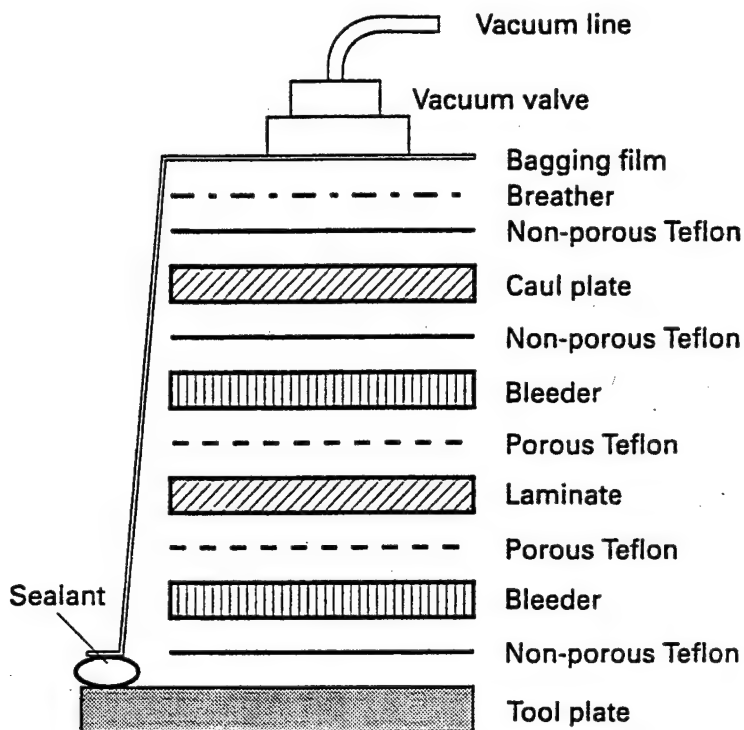


Figure 1-1 Schematic of bagging in autoclave molding

The main drawback of this process is its high cost and the limitation of the size of part since the process requires a closed chamber. Close control has to be maintained over fiber orientation, stacking sequence and the number of plies. Care must be taken to maintain the filament gap between two sheets in the same layer as well as avoid filament crossovers. Broken filaments, foreign matter and debris should not be permitted.

### 1.2.2 Compression Molding

Compression molding uses matched molds to transform sheet-molding compounds (SMCs) into finished products. Its principal advantage is its ability to quickly produce complex parts. Also, parts with non-uniform thickness; and features such as ribs, bosses, flanges, holes and shoulders can be incorporated during manufacture. This eliminates secondary operations such as drilling. The entire process can be automated and used for high volume production.

The process involves placement of precut and weighed amounts SMCs, usually a stack of several rectangular plies called a charge, onto the bottom of a preheated mold cavity as shown in Figure 1-2. The ply dimensions are selected to cover about 60 to 70 % of the mold surface area. The mold is closed quickly after the charge placement, and the top half of the mold is lowered at a constant rate until the pressure on the charge increases to a preset level. With increasing pressure the sheet molding compounds in the mold start to flow and fill the cavity. The molding pressure and temperature depend on the specific material being used and geometry of the final product.

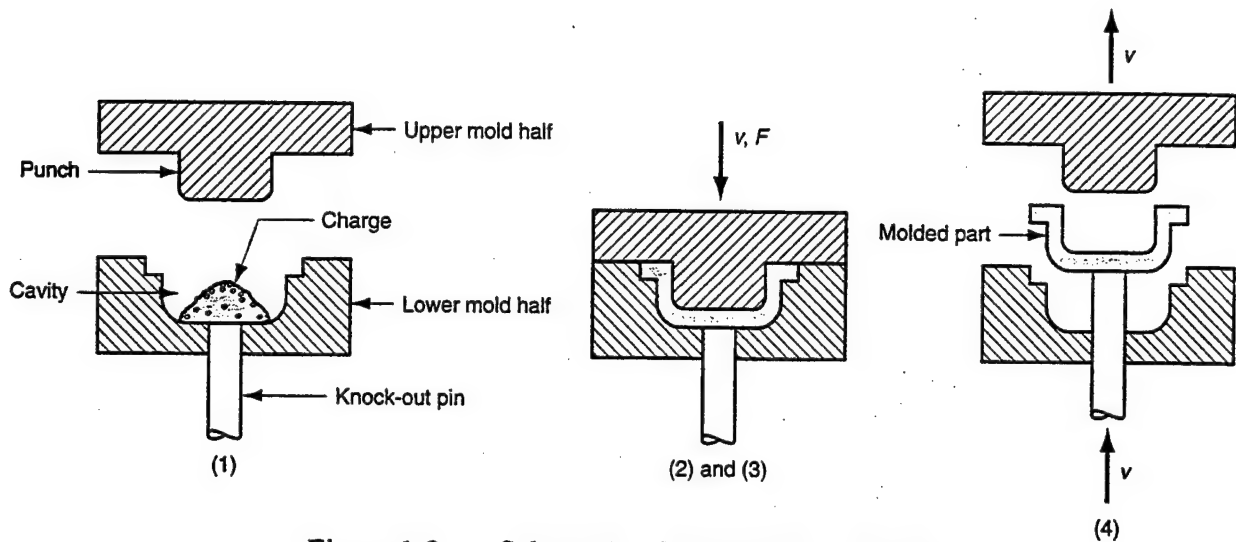


Figure 1-2 Schematic of Compression Molding

Molding defects include voids, blisters, fiber buckling, sink marks and knit lines. Voids are caused by the entrapment of air or other gases in the molded part. Blisters are inter-laminar cracks formed at the end of molding, due to excessive gas pressure in the interior region of the molded part. The delaminated area near the surface may bulge into a dome-shaped blister due to entrapped gas pressure. In molding processes involving long resin flow paths, it is extremely difficult to control the fiber orientation. Abrupt changes in thickness, any obstruction in the flow path or presence of high shear zones can deviate the fiber orientation. As a result, the molded part may become anisotropic with its strength and modulus higher in the direction of flow orientation than in the transverse direction. During compression molding of a charge having continuous fibers, flow is possible only in the transverse direction of the fibers. If excessive transverse flow is allowed, the continuous fibers on the surface may buckle near the end of the flow path. Knit lines are linear domains of poor fiber orientation and are formed by the joining of two divided flow fronts. The strength of the part in the direction normal to the knit line is reduced. Sink marks are small surface depressions normally observed above ribs in compression molded parts. Warpage is another defect found in thin molded parts.

### 1.2.3 Pultrusion

Pultrusion is a continuous molding process for producing long straight structural members with a constant cross-sectional area. Some of the common pultruded products are rods, hollow tubes, flat sheets, various types of beams, angles, channels, etc. The total fiber content in a pultruded member may be as high as 70% by weight for glass.

Figure 1-3 shows the schematic of a typical pultrusion line. Continuous strands of fiber and mats are pulled from one end into a bath which contains liquid resin, mixed with additives such as curing agent, colorant, ultraviolet stabilizer and fire retardants. To improve the surface finish of the product, thermoplastic surfacing veils are sometimes added. The fiber resin stream is pulled through a series of preformers and then through a

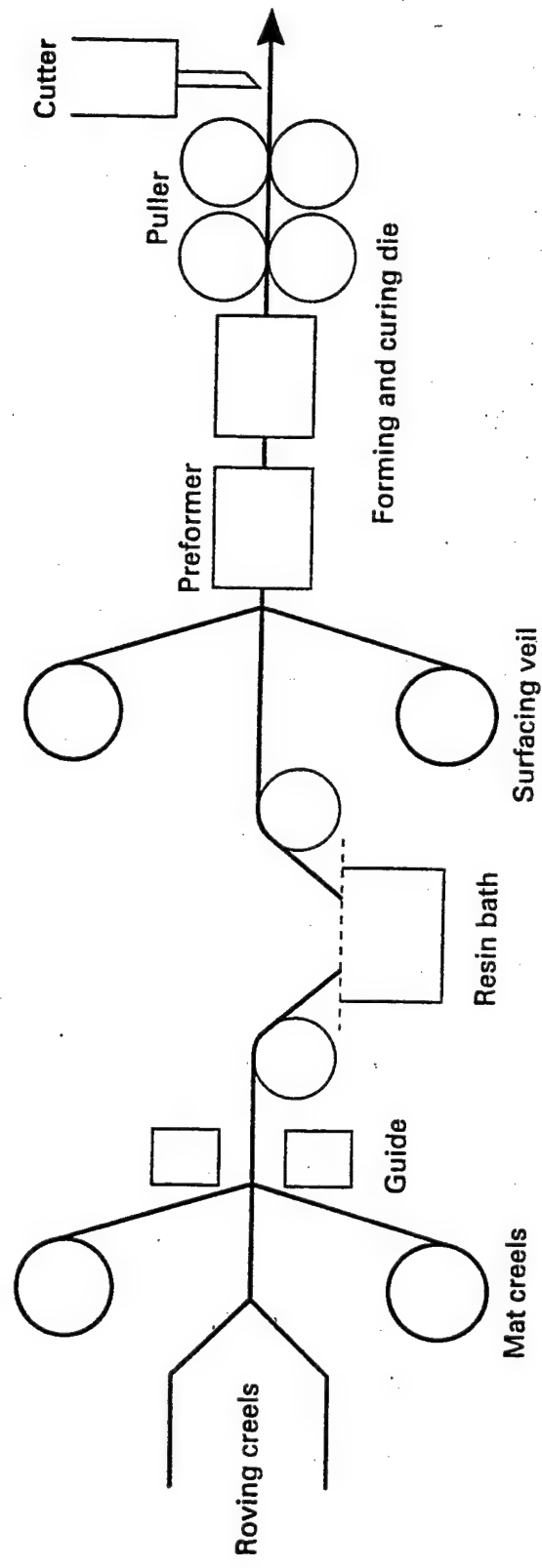


Figure 1-3 Schematic of Pultrusion

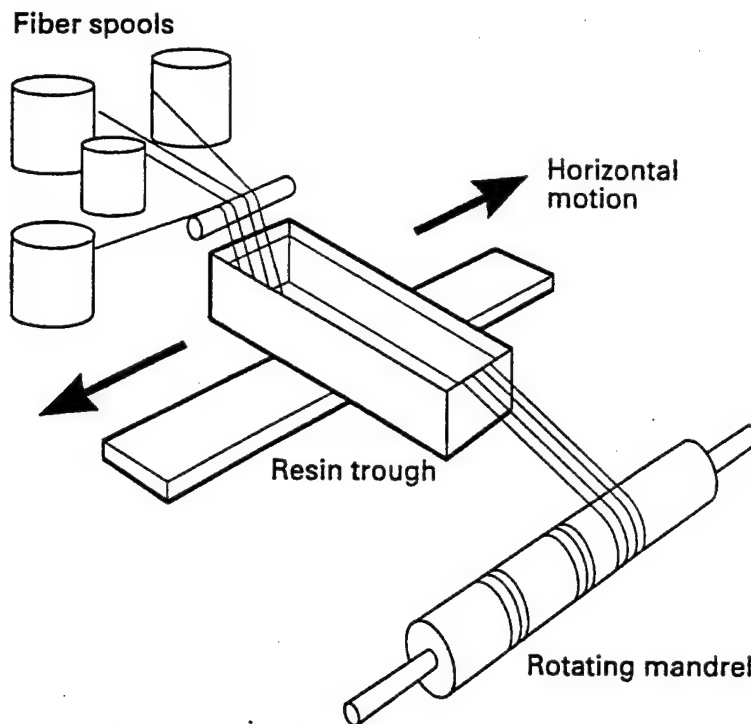


Figure 1-4 Schematic of Filament Winding

preheated die. The preformers distribute the fiber bundles evenly, squeeze out the excess resin and bring the material to its final configuration. The final shaping, compaction and curing takes place in the die, which has a gradually tapering section along its length. The entrance section of the die is usually water cooled to prevent premature curing of the resin. The rest of the die is heated either by oil or electric heaters. A number of pulling blocks pulls the cured member out of the die. After cooling with air or water, it is cut into required lengths by a diamond-impregnated saw at the end of the line.

However, this process is limited to products with constant cross-sectional areas. The process is very temperature-sensitive - even small changes in temperature affect the resin curing, and, thus, the surface finish. Any deviation from the designed pulling force results in defective parts.

#### 1.2.4 Filament Winding

Filament winding is generally used for fabrication of axisymmetric parts. Among the applications of filament winding are automotive drive shafts, helicopter blades, oxygen tanks, pipelines, spherical pressure vessels, conical rocket motor cases, and large underground gasoline storage tanks. The filament winding process is also used to manufacture prepreg sheets or continuous fiber-reinforced sheet molding compounds.

In this process, a band of resin-impregnated rovings or monofilaments are wrapped around a rotating mandrel (Figure 1-4) and cured to produce axisymmetric hollow parts. A large number of fiber rovings are pulled from a series of creels into a liquid resin bath containing liquid resin, catalyst, and other ingredients such as pigments and UV adsorbents. Fiber tension is controlled by the fiber guide or scissor bars located between each creel and the resin bath. Just before the fibers enter the resin bath, they are

usually gathered into a band by passing them through a textile board or a stainless steel comb. The resin-impregnated rovings are then pulled through a wiping device to remove the excess resin and control the resin coating thickness around each roving. Once the rovings have been thoroughly impregnated and wiped, they are gathered in a flat band, using a straight bar, a ring or a comb, and positioned on the mandrel. The band is usually located on the carriage, which traverses back and forth parallel to the mandrel like the tool on a lathe. The traversing speed of the carriage and the winding speed of the mandrel are controlled to create the desired winding angle patterns. After winding a number of layers to generate the desired thickness, the filament wound part is cured with the mandrel in place. The mandrel is extracted from the part.

Some of the common defects found in products manufactured by filament winding are voids, delaminations, and fiber wrinkles. Voids may be caused due to poor fiber wet-out, entrapped air in the resin or excessive resin squeezed out of the interior layers due to high fiber tension. Excessive time lapse between two consecutive layers causes delaminations. This defect is prominent in resin with a limited pot life. Wrinkles are formed due to improper winding tension and misaligned rovings.

### **1.2.5 Elastic Reservoir Molding**

In elastic reservoir molding (Figure 1-5), a sandwich of liquid resin-impregnated open celled foam and face layers of dry continuous strand mat, woven roving, or cloth is placed in a heated mold and pressed with a molding pressure of 75 to 150 psi. The foam at the center of the sandwich is usually a flexible polyurethane that acts as an elastic reservoir for the catalyzed liquid resin. As the foam is compressed, the resin flows out vertically and wets the face layers. Upon curing, a sandwich of low-density core and fiber-reinforced skins is formed. The advantages of elastic reservoir molding are low tooling cost, better control of properties, and a better stiffness to weight ratio. The process is generally restricted to the manufacture of thin panels of simple geometry, like bus roof panels, radar reflecting surfaces, automotive body panels, and luggage carriers.

### **1.2.6 Tube Rolling**

Circular tubes for space trusses or bicycle frames are often fabricated from prepreg by a rolling technique. In this process, precut lengths of prepreg are rolled onto a removable mandrel by a number of techniques (Figure 1-6). The uncured tube is wrapped with a heat shrinkable film or sleeve and cured at elevated temperatures in an air-circulating oven. As the outer wrap shrinks the air entrapped between the layers is squeezed out at the ends. For a better surface finish the curing operation can be performed in a close fitting steel tube or a split steel mold. The outer steel also prevents the mandrel from sagging at high temperature used for curing. After curing, the mandrel and the steel tube are removed and a hollow tube is formed. The advantages of tube rolling over filament winding are low tooling cost, simple operation, better resin content control and distribution, and faster production rate. The process is however limited to simple lay-ups containing 0° and 90° layers.

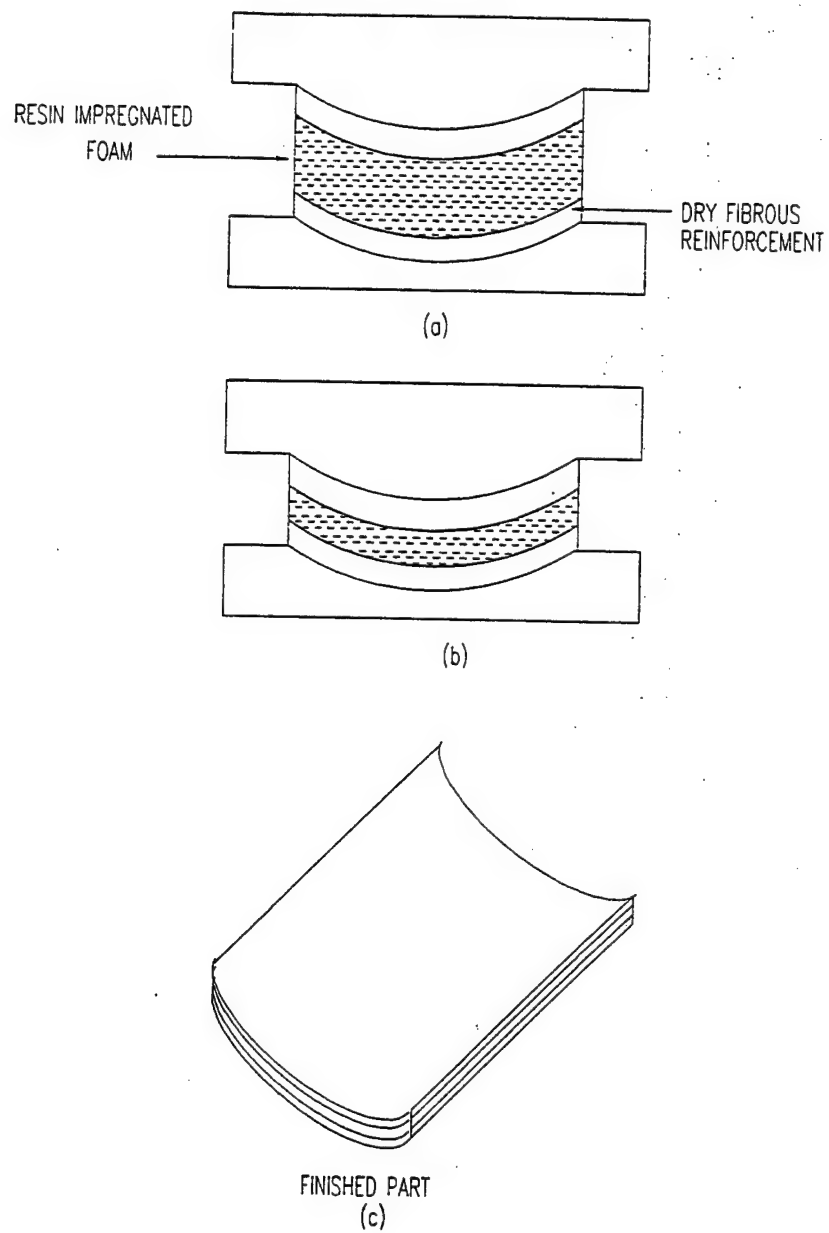


Figure 1-5 Schematic of Elastic Reservoir Molding



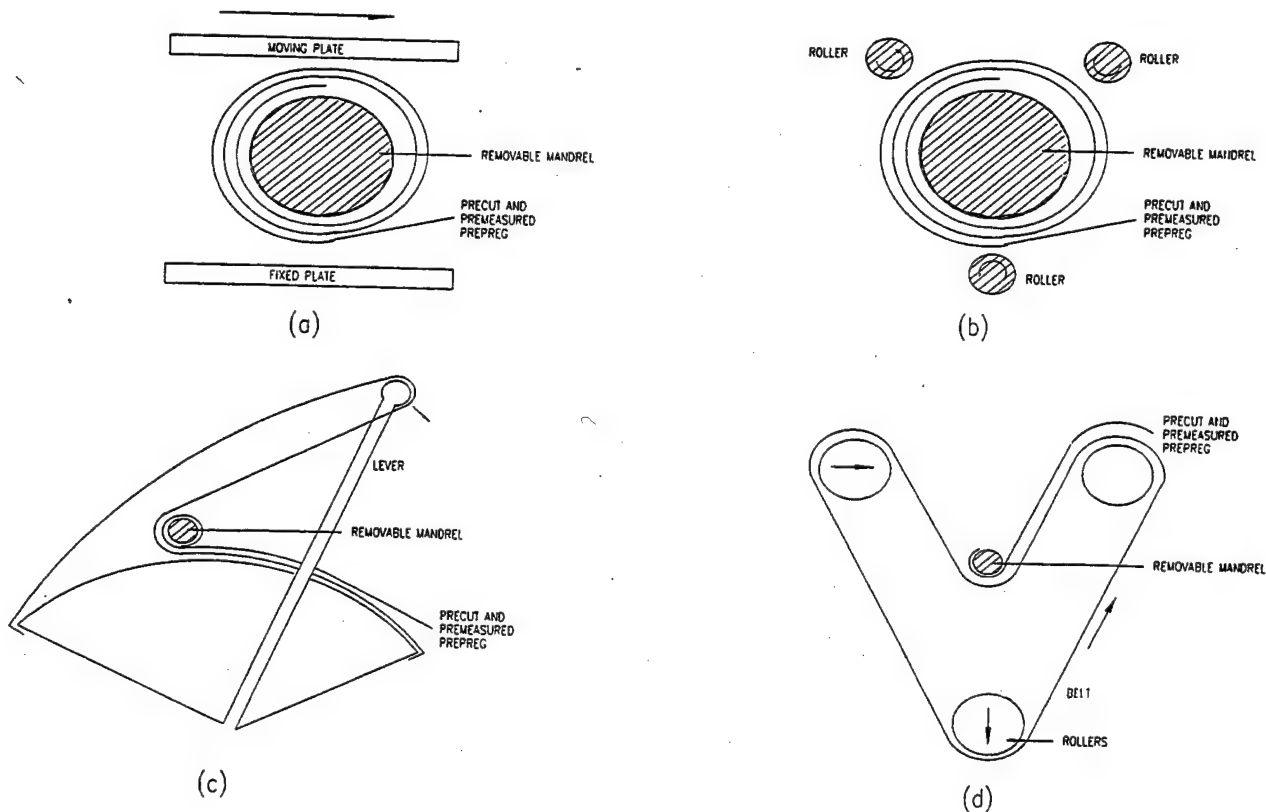


Figure 1-6 Schematic of Tube Rolling

### 1.2.7 Resin Transfer Molding

In RTM, several layers of dry continuous strand mat, woven roving, or cloth are placed in the bottom half of a two-part mold (Figure 1-7). The mold is closed and the catalyzed liquid resin is pumped in via a sprue. The resin injection pressure is usually in the range of 10 to 100 psi. As the resin enters the mold, it impregnates the fibers. Depending on the type of the resin-catalyst mixture, the curing is either performed at room temperature or at an elevated temperature in an air-circulated oven. After the cured part is pulled out of the mold, it is often necessary to trim the part at the outer edges to make it conform to the exact dimensions. Compared to other fabrication processes, RTM has a very low tooling cost and simple mold clamping requirements. A second advantage is its ability to encapsulate parts such as metal ribs, stiffeners and inserts within the molded laminate. The process has been successfully used to mold parts such as cabinet walls, chair and bench seats, hoppers, water tanks, bath tubs, and boat hulls.

### 1.3 Defects

As with most manufacturing processes, one must be cognizant of defects. Advanced composites are not immune to such imperfections. The defects can have a direct relation to the mechanical properties of the finished product. Typical defects include:

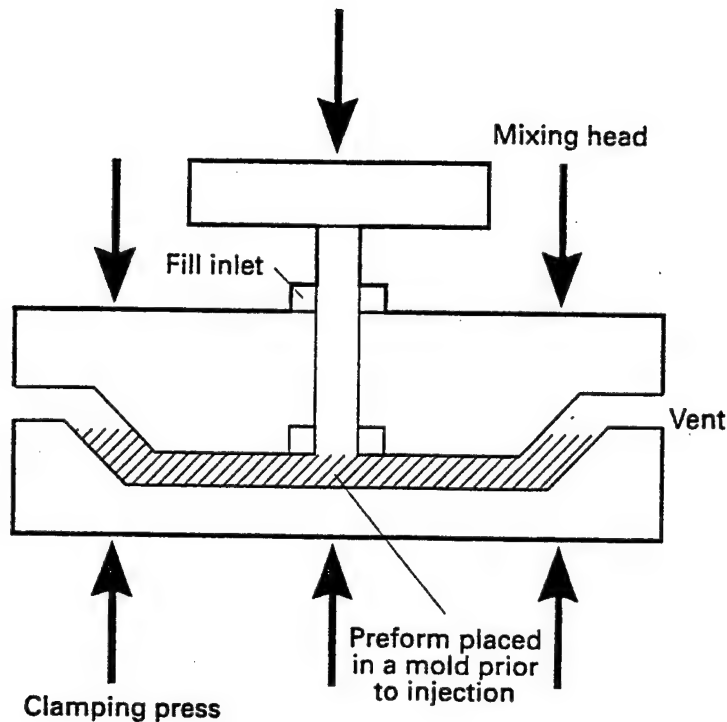


Figure 1-7 Schematic of Resin Transfer Molding

1. Incomplete curing of resin
2. Excess resin between layers
3. Incorrect orientation of laminae principal material directions
4. Damaged fibers
5. Inclusion of foreign matter
6. Inter-laminar voids due to air entrapment or delamination
7. Excess matrix voids and porosity
8. Variations in thickness
9. Wrinkles due to improper layer alignment

An understanding of the mechanisms for the formation of these defects and the ability to predict and eliminate them are of great interest to the industry. Development of the RTM process to compete with the autoclave method is of particular interest.

#### 1.4 Autoclave Molding versus RTM

At the present moment, the autoclave process is the predominant method of manufacturing composites in the aerospace industry (Mallick, 1988). This is due to the high levels of precision and reliability in the manufacture of parts through this methodology. However, this process allows only pre-impregnated materials or

"prepregs" to be used and requires strict control of both the temperature and pressure. The basic premise of the autoclave process is actually a derivative of a more general method known as vacuum forming. The autoclave utilizes pressures in excess of atmospheric to produce high-density parts (Matthews and Rawlings, 1994). Heat is also used in conjunction with the pressure to assist in the cure phase of the laminate, in addition to aiding the flow of excess resin from the laminate. The primary drawback of the autoclave process is that large amounts of energy and labor are necessary from the initial to the final stages. Not only does this include the efforts necessary to hand lay-up the laminae, but also includes the cost and efforts required inspecting the part at each successive step (Brosius and Wadsworth, 1991).

RTM provides a less labor-intensive process, coupled with a reduction in material cost and utilities. The RTM process has its genesis in the automotive industry, where cost and productivity are of the utmost concern. A renewed interest in RTM has occurred largely due to advances in the material and the process. As it pertains to the materials, recent advances have produced a new series of matrix materials with mechanical properties equivalent to those used in prepreg materials. In addition, advances in the material fabrication and weaving processes have allowed the production of complex preforms that possess mechanical properties superior to those fabricated by the lay-up of a uniaxial prepreg.

RTM is a closed mold system. The premise of this procedure is to pump a low viscosity resin into the mold. The resin, being injected at a relatively low pressure would eventually infiltrate the preform and subsequently form a composite after completion of the curing procedures. Utilizing pressures of low magnitude allows for the use of inexpensive molds. Production of larger and more complex shapes can be produced cheaply as a result of the reduced tooling costs. However, the infiltration phase is typically slow, unpredictable and extensive, thus increasing the overall production time, due in part to the relatively low pressures (Matthews and Rawlings, 1994).

The RTM process has been refined to a degree such that the resulting void content compares well with that of its autoclave-produced counterpart. This is not to say that extensive research in RTM is unnecessary. On the contrary, the most intense scrutiny focuses on the skewness of the resin flow, which may lead to "race tracking," which typically occurs during the introduction of the resin (Figure 1-8). The tendency of the resin to follow the path of least resistance leads the resin to flow more readily around the edges of the preform, as opposed to flowing in a uniform manner throughout the entire preform. Once the resin prematurely reaches the exit ports of the mold, the air trapped in the mold has the potential to create voids or micro-voids in the material. The entrapment of air due to race tracking produces a part with micro-void content, which could adversely affect the mechanical properties of the panel.

## **1.5 Research in RTM**

The beneficial characteristics associated with resin transfer have encouraged efforts to refine and cultivate the technology. As a result, a plethora of research is being pursued in order to more readily understand and harness the variables associated with RTM. Some of the relevant analyses and observations determined by previous research

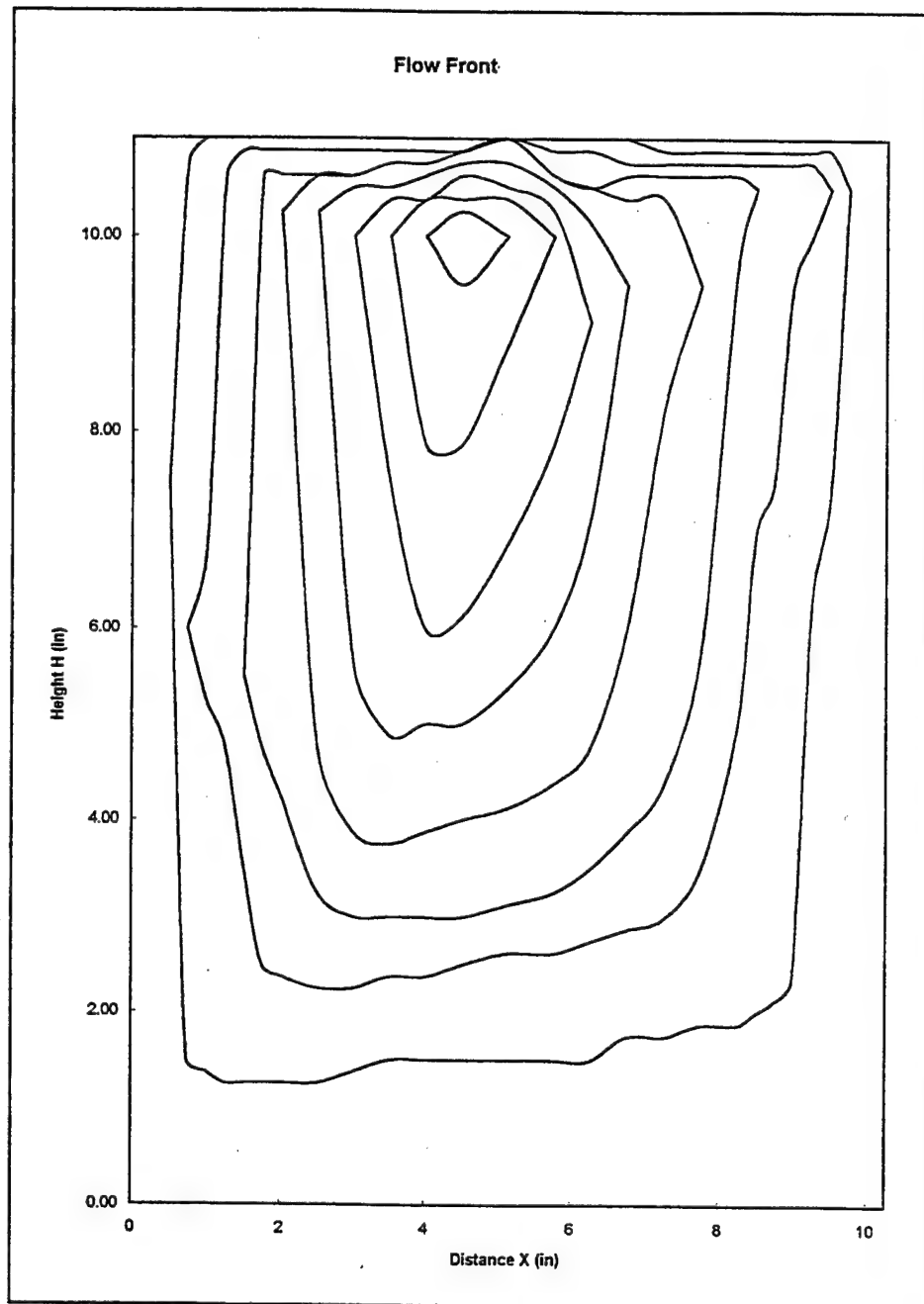


Figure 1-8 Flow Front Illustrating Race Tracking

are presented in this section. The most pertinent research are those which focus on the process variables of RTM, the development and control of void content, and the analysis/prevention of race tracking and voids.

### **1.5.1 Flow Pattern**

A lot of research has been done on the prediction of the flow pattern in the RTM process. Most of it is done using Darcy's Law for flow. Computer programs are written to simulate the flow pattern under different boundary conditions.

Coulter et al., (1988), modeled the resin flow during the RTM process. Assuming that no macroscopic fiber motion occurs during resin injection, the resin flow inside the mold can be modeled as a flow through a porous media. The flow is modeled in 2-D as an isothermal fluid moving through a porous medium using Darcy's Law. A numerical code is developed to simulate resin impregnation. The code is validated through a comparison with results previously presented in the literature (Martin and Son, 1986) and then used for complex boundary conditions. The code generates the fronts for the streamlines, X and Y direction velocity and pressure distribution. However, no supporting experimental data has been generated.

A simplified resin flow calculation of the RTM process is given by Cai (1992), which gives closed form solutions of some simple mold sections with various inlet boundary conditions. Darcy's Law for flow is used for the solutions. Some basic concepts for mold design and vent arrangements are revealed. These are, (a) inlets and outlets should be arranged such that shorter flow paths are possible; (b) the resin flow should be arranged from larger sides to smaller sides, or from outside to the inside, which guarantees rapid reduction of unoccupied volume. A set of formulas and charts are derived for various one dimensional flow cases, which can be used to estimate the fill time, wet length and operating equipment requirements. Estimates for the filling time of complicated sections are made using the same principle. The complicated sections are broken down to simple sections and the filling time for each of them is calculated. The sections are then assembled and a total filling time is estimated. The results compare favorably with the results obtained using other computer simulation models. However, no supporting experimental data has been generated.

### **1.5.2 Fiber-Resin System**

Stark et al., (1990), have studied the different fiber-resin combinations used in the RTM process. A comparative study of mechanical properties of different epoxy and bismaleimide resins is done. Parts are made with different resins and bismaleimides using RTM process. The fabric selected is 8-harness satin weave Celion G30-500 3k. Mechanical properties of the fabricated parts are compared. Epoxy and bismaleimides are found to be excellent resin choices for the RTM process due to their ease of processing. The physical properties of parts made using the above group of resins and the RTM process are comparable to those obtained with low pressure autoclave molding.

In the selection of the catalyst, the primary factor considered was the viscosity of the matrix. Ideally, the viscosity of the matrix should approach 250 cP (Heyward and Harris, 1990). In experiments preceding this project, Senibi (Senibi et al., 1993) found

that Dow Chemical's Tactix 123<sup>®</sup> resin and Pacific Anchor's Ancamine 1770<sup>®</sup> catalyst possess sufficient viscosity for their experiments.

Once again, Senibi (Senibi et al., 1993) provided guidance in the selection of the fiber material. In similar experiments, woven 8-harness satin weave graphite cloth was utilized. The ease of cutting, the uniformity, and the level of reliability in controlling the fiber volume (by stacking a distinct number of layers) were the variables considered when the selection of the type of fiber and number of layers for the RTM experiments were determined. The number of layers, six in this instance, was chosen to yield a fiber volume of approximately 40 percent (Senibi et al., 1993).

### **1.5.3 Material Properties**

Ideally, the final results of composite research are to provide low cost, high strength alternative materials for some of today's manufacturing applications. A primary concern is the ability to consistently fabricate quality parts. The material properties can be affected by a myriad of variables inherent to the resin/mold system, including microvoids and the cure cycle process.

#### **Micro-Void Content**

From the very beginning of RTM research, the level of void content has been a primary concern. In fact, extensive time and effort have been invested to determine and reduce the number of voids formed in composite panels. Careful preparation of the composite components and dedicated attention to the minimization of all sources of air and leaks may reduce the number of inadvertent voids in an RTM-produced composite (Stabler, 1991). Ramifications of high void content include diminished physical properties and poor finish (Patel et al., 1995). The most common and highly probable causes of void formation in composite panels are entrapment of air in the system, partial evaporation of mold release agent(s), and the volatility of chemicals during curing. Process variables that contribute to the level of void content include injection pressure, mold temperature, pressure during curing, resin characteristics and properties, and reinforcement properties. To date, there appears to be no effective way of having a part with zero void content. Autoclave and vacuum-bag type methods seem to control some of the variables conducive to void formation, but poor wetting and void content are still evident.

From the research performed by Patel, Rohatgi and Lee, there appears to be some vehicle(s) through which microvoids are formed. In the analysis of micro scale flow behavior, it was observed that differences in permeability of the fiber tows and the gaps in between tows caused fingering, a flow pattern with a definite lead-lag characteristic. The magnitude of the fingering phenomena is largely dependent on the relative magnitudes of the capillary and the hydrodynamic pressures (Patel et al.). One conclusion of their research of particular interest is that void formation is largely dependent on two specific phenomena of microflow: fingering at the flow front and transverse flow. Inhomogenities in the fiber mat usually trap the voids and prevent the flow from carrying away the voids. It was also determined that the use of mold-releasing

agents tended to facilitate the presence of voids, due to the lowering of the solid surface energy by these agents.

### **Mechanical Properties**

All variables, from the most predominant to those relatively obscure, determine the success or failure of the mechanical behavior of the composite panel. The improvement of the mechanical properties of composites, more specifically, tensile and compressive strengths, flexural and shear moduli, are the primary reasons for the desire to use composites as the eventual replacement of the metals now in use.

In recent experiments, it was found that laminates with moderately high (40 - 48 %) fiber volume fraction reinforced with non-woven fabrics, and plain weave laminates made in the RTM process, have mechanical properties which fall within close proximity to theoretical values found using classical lamination theory (Wang and Li, 1994). Further research has also been done on computer algorithms which serve to model the strengths of a composite material, given the basic fiber and matrix properties. Zhu and Zong have refined a previous statistical tensile strength model to provide an accurate tensile strength for a composite with unidirectionally arranged fibers. In addition, the researchers' model surmised that a higher composite strength would result from having lesser strength dispersion, smaller ineffective length and higher matrix shear moduli (Zhu and Zong, 1992).

Hayward et al., (1990), have studied the effect of vacuum assistance, injection pressure, mold temperature and resin viscosity, in the properties of resin transfer molded flat plates. The plates are made of glass fiber/reinforced polyester resin. Some of the plates are also made of carbon fiber/epoxy. It is found that the application of vacuum greatly increases the wettability of the fibers within the mold. This reduces the porosity levels, improves the mechanical properties and gives a better appearance. A number of plates have been manufactured using injection pressures varying from 50 to 400 kPa. There is relatively little variation in the shear strength values for different pressures. The flexural strength, however, shows a slight decrease with increase in injection pressure. The effect of mold temperature was studied by varying it from 20 °C to 40 °C. Following the molding process, the plates were post-cured for 24 hours at 45 °C. No significant difference in the shear strength or flexural strength was found. Composites have been successfully manufactured using resin viscosities ranging from ~100 cP to ~3500 cP. Lower viscosity resins are found to produce good panels, whereas the higher viscosity resins do not sufficiently penetrate the reinforcement and wet out the fibers.

#### **1.5.4 Vacuum Assistance**

The process known as regular RTM (RRTM) is one in which a liquid catalyzed thermosetting resin matrix is injected into a closed mold containing a fiber preform (Senibi et al., 1993). Although, the RRTM process has been in existence for approximately 50 years, the major drawbacks of high micro-void content and low fiber volume content still remain. These two drawbacks are the primary limitations of quality in composites manufactured by RRTM.

The basic premise of vacuum-assisted RTM (VARTM) is identical to the principles found in RRTM, with the exception of utilizing a vacuum to assist the process.



The mold is evacuated prior to matrix introduction and the vacuum is maintained until the mold is completely filled. In previous experiments, Heyward and Harris (Heyward and Harris, 1990) found that vacuum assistance improved the wetting of the fibers and a corresponding improvement in the mechanical properties, most notably the flexural strength and short beam shear strength. Further independent research also determined that VARTM reduced the percentage of micro-voids, compared to similar runs using RRTM and Controlled Leak Vacuum RTM (CLVRTM). Senibi et al., (1993), have done some preliminary research on the VARTM process using graphite fiber and Tactix 123 resin with Millamine 5260 catalyst. They have compared the void contents of composite plates for different flow rates and number of plies. Use of vacuum results in a lower void content. Also, with the use of vacuum, higher fill rates can be achieved without affecting the void content. However, the sealing of the mold plays a very important role in determining the number of voids. An improperly sealed mold dramatically increases the void content of the plate.

### **1.5.5 Process Parameters**

In the initial analysis of RTM, it has been found that there are myriads of variables that contribute to the outcome of the final product. The factors that possess a direct relationship to composites fabricated with the RTM process include the fiber type, orientation, surface treatment, ply sequence, volume fraction, resin composition, mold geometry, injection pressure, the application of vacuum assistance and ambient conditions (Young and Tseng, 1994). Initial investigations also yielded more variables to consider, such as mold temperature, air content of the matrix, injection rate, and placement of preform in the mold (Shah, 1995). By the use of experiments and investigation of previous research, the effects of variables were examined to determine the most significant ones. Heyward and Harris, (1990), found that VARTM greatly improved the wettability of the fibers within the mold and noted that vacuum assistance does not have the same effect as an increase of resin injection pressure.

During a resin fill, there are two types of flow that occur, one being the flow which distributes the resin throughout the mold cavity, the second being the penetration of the resin in the fiber bundle (Young and Tseng, 1994). The two phenomena, macro flow and micro flow, are governed by Darcy's law and capillary action, respectively. The primary objective of the study performed by Young and Tseng was to gage the effects of manufacturing variables upon the RTM process. More specifically, the influence of resin injection pressure, preheated mold temperatures and vacuum assistance upon the final quality of the part were of primary concern. The effects of these variables were determined by comparison of the flexural strength of the resulting panels. The three point bending test and tensile tests were used in order to determine the values for the flexural strength, the tensile strength, and the accompanying moduli for both. The ultimate goal was to determine the ramifications the different fabrication variables had upon the wetting degree and the final quality of the final parts. During the course of the study, panels were manufactured at different combinations of injection pressures, preheated temperatures of the mold, and vacuum assistance. As a result of the study, the researchers concluded that the most significant factor in final part quality and mechanical properties was the injection pressure, based upon the level of void content present.



Overall, low injection pressures tended to yield better results, due to more favorable wetting. However, when low injection pressure is used, coupled with a preheated mold temperature, local voids are more prone to form, due to the increased resin viscosity and low pressure gradient distribution in the mold cavity. In addition, it was discovered that different fiber types influenced the wetting mechanism, due to bundle size and weaving configurations and that vacuum assistance had a positive effect upon the mechanical properties of the final product (Heyward and Harris, 1990).

Further research into the pressure distribution in the mold during RTM by Gong (Gong, 1993) revealed a viable model for the prediction of the effect(s) of the preform's compressibility and relaxation upon the pressure distribution for one-dimensional RTM. In performing this research, Gong ascertains that the accurate prediction of process characteristics is complicated by the influence of complications in the impregnation environment. These complications include the deformation of braided preforms while under the hydraulic pressure. Subsequently, the permeability of the preform is also compromised in various regions of the preform. In fact, there seems to be evidence to the fact that at high flow rates, the preform compressibility affects the pressure drop in such a way that a non-linear pressure growth with time results at the inlet. In addition, the predicted value for the pressure found by using Darcy's law is overestimated mostly due to the absence of proper consideration for the effect of the compressibility and the relaxation of the matrix upon the pressure in the mold. For this analysis, Gong assumed that the preform permeability was non-homogeneous in one direction only, the flow profile would be flat, and that the resin impregnation was isothermal and Newtonian in behavior. Gong concludes that the modeling of the preform compressibility is largely dependent on the moving resin from impacting on the preform and stretching the fiber bundles and the relaxation is a result of the recoiling of the fibers after having been stretched by the resin front. Thus, the compressibility region is located at the front region of the characteristic length, which is determined by the preform compressibility and relaxation time. Gong also states that the compressibility is influenced by the injection velocity, which results in a non-linear relationship between the pressure gradient and the flow rate.

#### **1.5.6 Race Tracking**

In recent research, heavy emphasis has been placed on some of the more dynamic aspects of composite manufacture to determine the root causes of part imperfections stemming from fabrication. Some of the pertinent areas of interest are the causes and effects of race tracking and the real-time observation of the resin impregnation process.

In 1994, Fong and Lee (1994) performed a permeability study, with the primary goal of discovering and defining the effects of the preform on the flow patterns. During the course of the experiments, it was discovered that the permeability might be a function of two entities, the porosity and the orientation of the preform. The permeability tends to change during the introduction of the matrix to the preform at which point the preform fibers begin to stretch. This subsequent rearrangement of the preform fibers affects the permeability in the following manner: A flow parallel to the stretch direction results in an increase in permeability while a perpendicular flow causes a reduction. The porosity of the preform also appears to have a direct relation to the permeability. These factors in

turn affect the resin flow pattern. After further investigation, it was determined that there must be some additional phenomena, which caused the large differential between the actual flow pattern and the simulated pattern. The third, and perhaps most critical factor is the change in porosity and permeability as a result of bending-induced thickness changes known as the bending effect. Once this was integrated and accounted for in the flow front simulation, the simulation and the experiments agreed reasonably well. As a result, it was concluded that all three phenomena contributed to the irregular flow front patterns, but that the bending effect had the most profound impact and played a significant role in causing the observed race tracking.

Other significant causes of race tracking can be attributed to the precision between the dimensions of the mold and those of the preform width and the state of the fiber structure at the edge of the preform (Han et al., 1993). Even in utilizing edge compression of the preform, the race tracking effects were mitigated, but not totally eliminated. Race tracking led to reduced inlet pressures and altered matrix flow patterns, leading to the formation of dry spots.

As evidenced by the varying degrees of influence that the variables have upon the final part, there is a need to control and monitor the most crucial variables. A design for manufacture methodology, which compensates for manufacturing uncertainties, has been proposed (Chao et al., 1992). The rationale upon which the research was based is to reduce the variations in the manufacturing parameters that lead to inconsistent mechanical properties and macrostructure of a fibrous laminated composite materials part. Due to the intrinsic differences in the fabrication processes between metals and composites, and the subsequent increase in design variables, the desire for this technology looms large. Initially, the assumption is made that a problem of this type and its associated variables are random in nature (Chao et al., 1992). Thus, having defined composite fabrication as a stochastic optimal design problem, the desire now is to determine a solution that converts the stochastic optimal design problem to an equivalent deterministic design problem. This is accomplished through the implementation of a chance-constrained programming technique. The primary variables of concern were the ply thickness, the fiber orientation and the fiber volume fraction. These variables were significant in the final analysis because of the direct relation between them and the dynamic response of the manufactured part. The results obtained suggested that the application of random variables and conversion to equivalent deterministic values constitute a reasonable course of action for a design for manufacture methodology in the design of fibrous laminated composite structures.

In previous studies of the cure cycle for fibrous laminated composites, the emphasis focused upon specific materials and systems. Thus, any foundation upon which to determine the optimum cure cycle was non-existent unless using previously researched material. In order to eliminate the heuristic approach to cure cycle selection, Pitchumani and Yao (Pitchumani and Yao, 1992) present a generalized analysis of the cure cycle. This was done by idealizing the expressions for the cure kinetics and simplifying said expressions by using dimensionless representatives of the process and product parameters. It was their contention that by using a non-dimensional analysis, a reduction of process and product parameters occurs, in addition to the elimination of process-specific or material-specific research related to the optimum cure. The optimum cure

cycle was defined as the magnitude and duration of a cure temperature that yielded a homogeneously cured product in the minimum possible cycle time. The application of this procedure was not limited by the choice of process or material, thus, allowing widespread implementation in all fabrication processes.

### 1.5.7 Process Monitoring and Control

One crucial area of research is a method to monitor the RTM process as it is being conducted, *in situ* process monitoring. The various procedures in which the resin flow may be monitored may be categorized in two ways: Embedded or Non-embedded. Some of the more involved methods of embedded flow sensors include pressure transducers, dielectric sensors, and frequency-dependent electromagnetic sensors. Kikuchi et al., (1994), expanded upon a technology first proposed by Walsh: the use of an electrically conductive grid positioned in the mold cavity to gage the flow progression by changes in the electrical conductivity and/or the resin rheology during flow. This technology, known as *SMART* (Sensors Mounted As Roving Threads) weave, involves the placement of conductive wires within a non-conductive medium, the preform. The utilization of the technique was found to be successful, within limited bounds. The visually recorded and electrically-sensed flow profiles were compared and deemed identical, and the time responses were the same within fractions of a second. The *SMART* weave was found to be accurate at slow flow rates, but unsuitable for fast injection molding processes. In addition, the basic premise of the procedure calls for the introduction of a foreign object (electrical wires) to the process and its components, thus, introducing new variables to an already complicated system. Care would have to be taken to ensure none of the other conductive material(s) in the process or process equipment affected the sensors capabilities, in addition to limiting the selection of matrices to those which have low resistivity.

Addison (Addison et al., 1992) proposed the use of laser-based ultrasound (LBU) to complete this task. The advent of in-process monitoring would allow for accurate observation of the resin in progress, and provide preliminary information about areas most likely to have voids. Most importantly, a procedure such as this would remove the ambiguity in the determination of complete fiber wetting, as is the case when using visual inspection. In previous attempts to monitor the process, piezoelectric transducers were used to relay the pertinent data. However, the major failing of these transducers was the reliability at elevated temperatures, thus, providing the impetus for the application of laser-based ultrasound. In the experiments using LBU to monitor the progression of the resin, it was found that the level of completely wetted fibers could significantly lag the level of the flow front during an RTM process. Ultimately, it was concluded that laser-based ultrasound is a technology that could be further refined to provide in-process monitoring. Laser-based ultrasound also permits the testing of mold design and configurations and provides guidance to determine if the entry and exit ports allow for complete wetting of the fibers and sufficient resin penetration.

### 1.6 Objective and Scope

Unlike the autoclave process, RTM does not require the application of high pressure and thereby has a very low tooling cost. Additionally, not all of the new textile

constructions are available yet in prepreg form. Thus, they are not readily suitable for the autoclave molding process.

The void content in the RTM process is normally not as low as that obtained from the autoclave process, owing to the formation of micro-voids during mold filling. As the resin is injected in the mold, it takes the path of least resistance. If this high permeability path should be along the periphery of the preform, the resin tends to flow along the periphery leading to a phenomenon called "race tracking." Usually race tracking is caused by a loose fit between the preform and mold periphery, which allows the resin to arrive at the exit vents before the entire mold is filled. The mold may eventually fill, but the micro-void content may be high, especially in "islands" that were the last to fill.

The primary objective of this project is to develop and demonstrate a technique for evaluating the preform-mold fit and the potential for race tracking with the mold closed and ready for resin injection for VARTM. The approach is to probe the mold-preform assembly with a non-reactive fluid before the resin is injected. The probing action is then used to predict the resin flow pattern and any potential for race tracking. This may allow for the re-adjustment of the mold-preform fit until a satisfactory flow pattern is predicted before making the irreversible decision to pump in resin. The results of the effort will be beneficial in reducing the amount of rejects due to non-fill and voids, thus, yielding savings in time, money, labor, material and utilities.

The material system to be investigated is graphite-epoxy. Flat panels be will used to develop the technique and a 3-dimensional demonstration part used to test the extent of application of the technique.

## CHAPTER 2

### EXPERIMENTAL SETUP AND PROCEDURE

The objectives of the experiments are to obtain the necessary reliable data to enable the prediction of the nature of the resin flow front. The experimental plan involves (1) pre-process, (2) in-process and (3) post-process measurements. Figure 2-1 shows a schematic of the experimental plan. The pre-process experiments are designed for two purposes. The first one is to determine the appropriate combination of resin flow rate and viscosity in order to avoid premature gelation. It is also necessary to determine the flow rates and pressures for the nitrogen injection. Measurements involve the inlet pressure for the nitrogen and the flow rates at each exit port of the mold. These data are organized and stored before the resin injection. The in-process measurements are the resin flow rate, the back pressure and the flow front pattern at regular time intervals. The post-process measurements involve the mechanical and physical properties of the part after the curing operation. This is to ensure that the material properties are acceptable and to validate the conclusions drawn from the results of the experiment. The relationship between the resin front flow pattern and the properties is also of interest.

#### 2.1 Process Variables

From the literature and previous experiments, the variables that may influence the RTM process characteristics and subsequently the product quality are:

1. Resin viscosity
2. Back pressure
3. Flow rate / pump speed
4. Air content in the resin + catalyst mixture
5. Resin + catalyst mix ratio
6. Mold evacuation
7. Uniformity of preform dimensions
8. Placement of preforms in mold
9. Mold temperature
10. Cure cycle (temperature and time)

Some of the variables have been screened initially. The interest is to obtain the operating ranges for these variables. Each variable is described in some detail below.

##### 2.1.1 Viscosity of Resin

Resin viscosity and pot life are two of the important variables that affect the quality of the final product. Lower viscosities are preferable so that the resin will penetrate and wet the fibers. In general, viscosities ranging from 100 cP to 300 cP are desirable. The ideal viscosity range for a specific application depends on the fiber volume, fiber type, wet-out area and the mold design.

An experiment was conducted to monitor the viscosity of the catalyzed resin over a period twice as long as the mold fill time. If the viscosity of the resin were to change appreciably during the mold fill process, it would need to be carefully monitored during the process. The resin (Tactix 123) and catalyst (Ancamine 1770) were mixed in ratios

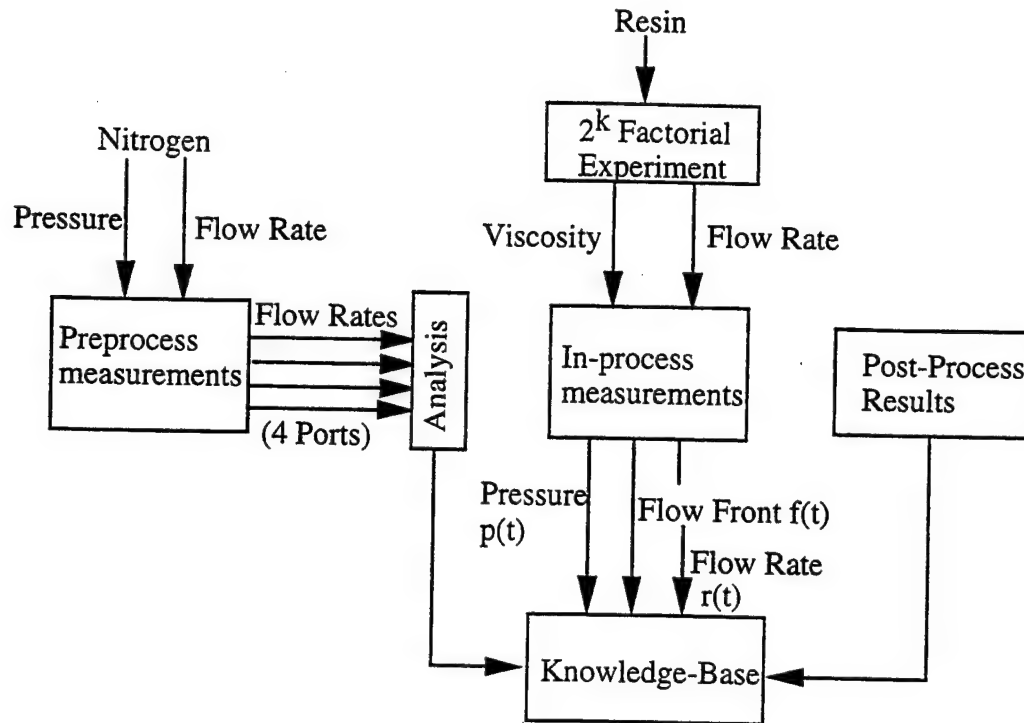


Figure 2-1 Experimental Scheme

varying from 100:17 to 100:22. These mix ratios were selected after panels were made with mix ratios ranging from 100:12 to 100:22. These experiments and their results are described later in this chapter. The viscometer used for the experiment is made by Labline Instruments Inc. (Model # 4537). The viscosity was measured every 3 minutes over a 1-hour period as follows:

1. Level the instrument.
2. Mix Tactix and Ancamine in a clean glass beaker, of diameter 70 mm. or more in the ratio 100:17 or 100:22 by weight.
3. Stir the mixture thoroughly.
4. Evacuate the resin filled beaker in the vacuum chamber for 5 min.
5. Place 500 ml. of the evacuated sample in another clean beaker.
6. Insert the recommended viscometer spindle (spindle # 2 in this case) and guard into the sample. Avoid the entrapment of air under the spindle plate. Insert the spindle so that half the notch is immersed in the resin.
7. Set spindle speed to 30 RPM.
8. Start the viscometer. Allow the spindle to rotate for 30 seconds. Note the reading.
9. Using a thermometer, note the temperature of the mixture.
10. Repeat step #8 and #9 every 3 minutes, for a total of 1 hour.

Each experiment is repeated three times for each mix ratio. The time of one hour was selected because, it is almost as twice as the longest mold fill time for the initial test panels made. The first reading in each case was taken at 8 minutes, as it takes about that



time to weigh, mix and evacuate the resin-catalyst mixture. The experimental data are given in Tables 2-1 and 2-2 and the respective plots are shown in Figures 2-2 and 2-3. The viscosity does not change significantly for about 1 hour. Thus, the pot life of the resin will allow us to run the experiment for a fill time not exceeding 1 hour.

### **2.1.2 Resin Back Pressure**

Back pressure is one of the variables to be monitored when the resin is being pumped in the mold. Experiments were conducted using corn syrup with viscosities of 150 cP and 350 cP to simulate the resin flow. The tube expansion was noted every minute while the syrup was being pumped in. The corresponding pressure was found from the tube expansion versus pressure calibration experiments. A pressure sensor was selected based on the tube expansion data when pumping liquid. Back pressure is to be monitored when the mold is probed with air as well as when the resin is pumped in. The sensor is placed near the inlet port of the mold to monitor the inlet pressure as the process progresses. The pressure sensor selected is of a diaphragm type and has a 0-100 psig range (Omega Model PX-613). The sensors as well as the diaphragm are made of stainless steel. The pressure sensor is supplied pre-calibrated and has a 0-5 V dc output. A conversion factor is to be applied to convert the voltage to pressure. The pressure sensor calibration was checked by connecting it to the nitrogen bottle and subjecting it to different pressures. The output voltage was converted to pressure and compared to the pressure reading on the nitrogen bottle pressure gage. The sensor is inverted and about 70 % of the tube connecting the vertical leg of the 'T' and the pressure sensor is filled with dark 'KARO' corn syrup. Corn syrup is used as a buffer between the resin and the sensitive steel diaphragm of the sensor. The resin is a thermoset type and once it sets on a surface, it is almost impossible to remove it from the surface, except by scraping it off. The buffer fluid (corn syrup), thus, protects the diaphragm. The density of the syrup is higher than that of the resin, and, thus, the resin floats on the syrup. The diaphragm needs to be cleaned thoroughly after each experiment. The syrup is very easily rinsed off with hot water.

### **2.1.3 Flow Rate / Pump Speed**

The pump procured for the experiment can be controlled either manually or from a computer terminal. The pump has a digital display. Either the flow rate or the pump RPM can be set for a particular tube size. The pump can display the cumulative volume of liquid pumped and the current flow rate or RPM. Speed or flow rate can be changed at any time during the process.

Since the back pressure in the mold increases as the process continues, it is necessary to study the behavior of the pump against a back pressure. The pump has to be checked on three aspects. First, whether it pumps a consistent volume of the fluid regardless of the input pressure. Second, whether the pump calibration for the particular tube size is accurate. Third, what back pressure it can pump the fluid against before it starts slipping.

Table 2-1: Viscosity Test for Mix Ratio 100:17

Time (Min.)	TEST 1		TEST 2*		TEST 3*	
	Viscosity (cP)	Temp (°F)	Viscosity (cP)	Temp (°F)	Viscosity (cP)	Temp (°F)
8	183	91				
11	171	102	174	100	147	106
14	179	100	166	101	144	118
17	180	102				
20	187	100	164	98	140	110
23	188	100				
26	196	100	167	99	146	114
29	199	106	168	108	146	117
32	210	106				
35	212	106	170	108	146	120
38	221	111				
41	230	111	170	112	143	117
44	243	113	160	114	142	118
47	238	116				
50	246	117	165	122	129	118
53	240	123				
56	250	125	160	122		
59	230	136	169	138		
62	234	138				
65	211	140				
68	211	142				

\* Sampling interval was 5 minutes. Readings have been staggered to reflect to the nearest minute.

### Flow Rate

The pump was initially checked for consistent delivery flow rate at various input pressures. The tubing size (24) and tube materials (neoprene) were entered. The pump was then set at a flow rate of 21.3 ml/min. and run for 1 minute. The height of the water supply reservoir was changed from 0 in. (level with the pump) to 7 in., 11 in., and -12 in. The pump delivered at a constant flow rate regardless of the supply pressure (Table 2-3 and Figure 2-4a). However, while the flow rate was constant, it was not the value set on the pump. The pump was calibrated after its behavior against back pressure was studied.

### Tube Expansion

The tube expansion versus pressure behavior was obtained. A neoprene tube was filled with air at various known pressures and the corresponding tube expansions were noted. The experimental procedure is as below:

1. Cut four pieces (105 cm long) of Fisherbrand™ size 24, black neoprene tubing.



Table 2.2: Viscosity Test for Mix Ratio 100:22

Time (Min.)	TEST 1		TEST 2		TEST 3	
	Viscosity (cP)	Temp. (°F)*	Viscosity (cP)	Temp. (°F)	Viscosity (cP)	Temp. (°F)
8	152		159	96	173	92
11	136		162	96	168	90
14	139		157	92	166	92
17	143		165	92	170	98
20	155		158	92	170	96
23	160		166	96	174	96
26	170		166	101	175	96
29	173		172	100	179	94
32	179		166	100	180	98
35	190		172	100	181	98
38	202		170	102	179	98
41	200		177	104	181	100
44	203		170	104	180	102
47	211		179	106	178	102
50	215		169	110	178	104
53	228		179	110	179	106
56	210		166	114	174	106
59	223		173	116	174	110
62	224		154	122	178	114
65	223		162	124	181	116
68	210		113	132	175	118

\* Temperature readings were not noted for Test 1.

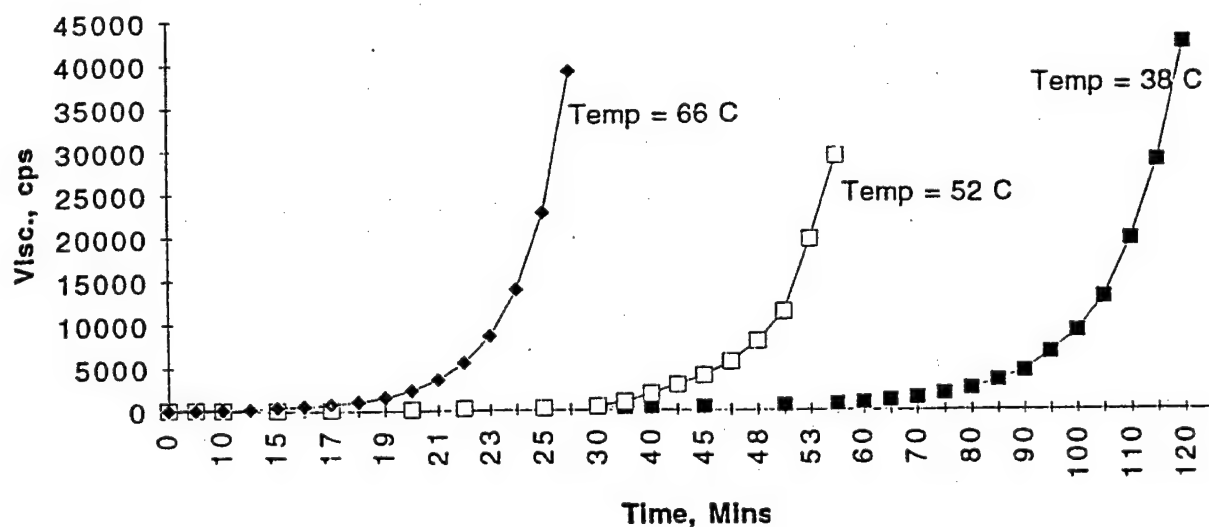


Figure 2.2 Plot of Viscosity versus Time

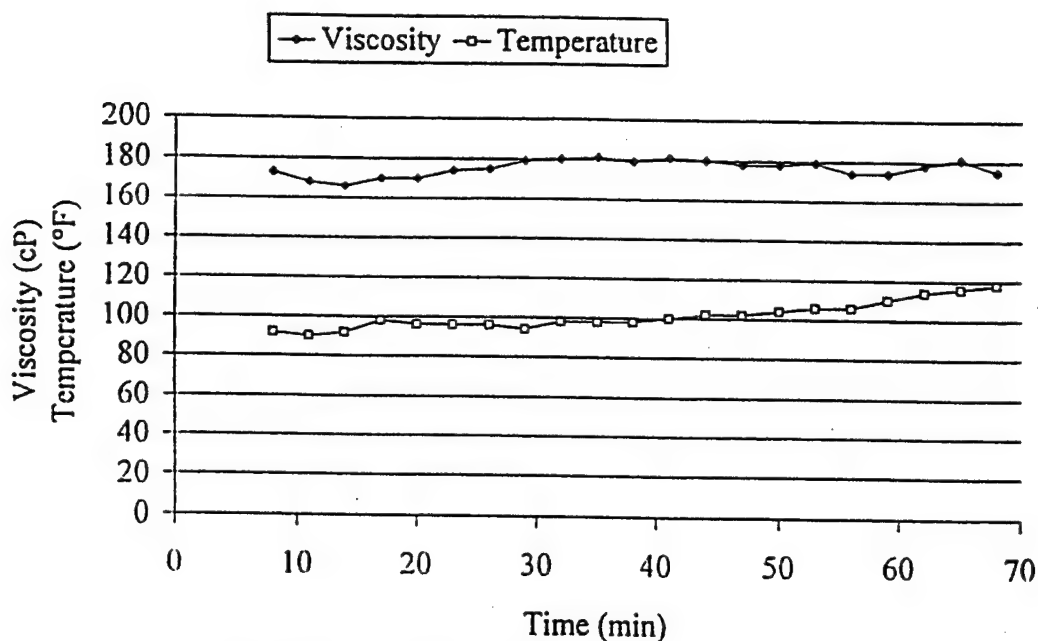


Figure 2.3 Plot of Viscosity versus Temperature

Table 2.3: Pump Head Test

EXPERIMENT #	Height of Output Reservoir (in.)	True Flow Rate (Water)	
		(set rate 21.3 ml/min.)	(set rate 43.2 ml/min.)
1	11	87.29	166.46
2	11	89.16	165.36
3	11	88.28	164.48
4	7	89.29	164.49
5	7	88.96	165.83
6	7		166.07
7	0	90.70	166.34
8	0	89.72	165.80
9	0		164.69
10	-12	89.67	164.03
11	-12	89.96	166.69
12	-12		165.58

2. Secure open end of tubing to pressure valve of nitrogen bottle.
3. Situate the dial gage such that the stem touches the tubing very lightly.
4. Zero the dial gage.
5. Clamp shut the open end of the tube.
6. Open the pressure valve on the bottle. Use the secondary release valve to control the amount of nitrogen released to the tubing.
7. Note the air pressure.

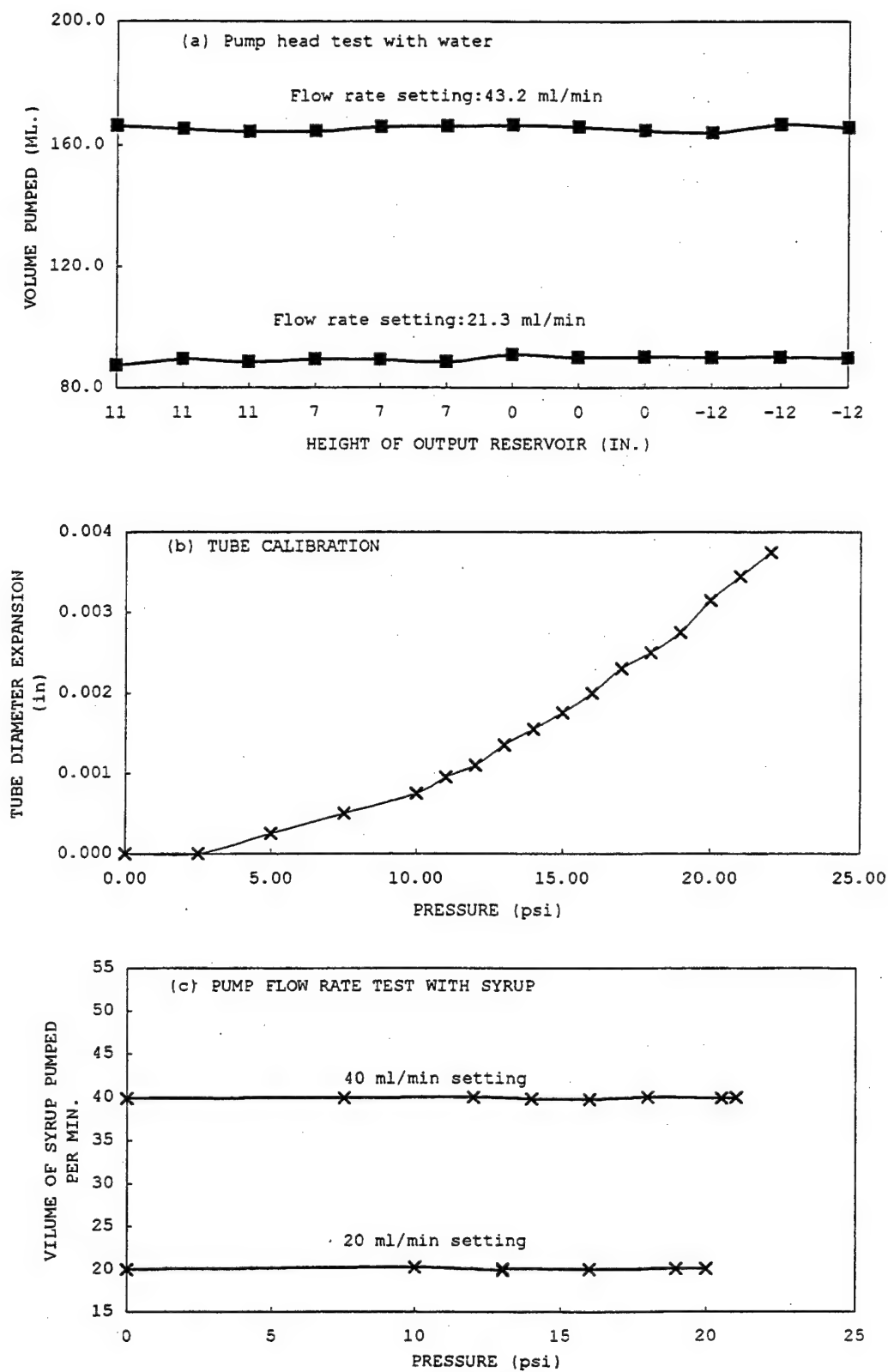


Figure 2-4 Pump Head, Flow Rate and Tube Calibration

8. Allow for the dial gage to settle and note the steady state reading of the tube expansion (after approx. 30 sec).
9. Increase air pressure in increments of 0.25 or 0.5 psi and repeat steps 7 and 8 until the desired maximum pressure is reached.
10. Close primary valve of the nitrogen bottle.
11. Release the clamp from one end of the tube and allow the nitrogen to escape. (see Table 2.4 for results and Figure 2.5 -a for the plot).

### **Back Pressure**

After the tubes have been calibrated, the same tubes were used to check the behavior of the pump against different back pressures.

The procedure is as below (see Table 2.5 for results and Figure 2.5-b for plot).

1. Connect one end of the tube to the inlet reservoir via the pump while pinching the other end of the hose to create different back pressures.
2. Set the pump at a particular flow rate and pump water.
3. Note the dial gage reading - it measures the tube expansion due to the back pressure.
4. Run the pump for 1 minute and collect the water in a pre-calibrated beaker.
5. Note the amount of water pumped.
6. From the calibration chart of Figure 2.5-a read off the back pressure corresponding to the tube expansion.
7. Change the back pressure using the clamp and repeat steps 2 - 6 at least five times for a particular flow rate for each tube.

### **Pump Calibration**

The next step is to calibrate the pump to display the same amount of fluid as it pumps. The pump calibration procedure is given below:

1. Select the right tubing size (size 24).
2. Select the right tubing material (neoprene).
3. Set the pump to a particular flow rate.
4. Select a fluid, preferably water.
5. Start the pump and collect the water in a glass beaker.
6. Pump water for 1 minute.
7. Weigh the water in the beaker.
8. If not, then press the flow calibration switch and enter the actual volume of the water pumped (the amount of water in the beaker). Repeat steps 5 through 8 till the pump setting and the amount of water pumped is the same.
9. If the volume of the water pumped matches the pump setting, then the pump is already calibrated (see Table 2.6 for results).

A different set of tubes was used to check the behavior of the pump when pumping liquids of higher viscosities. For this experiment, corn syrup of viscosity 150 cP was used. The tube was calibrated as described above. The pump was set to flow rates of 20 ml/min. and 40 ml/min. The experimental procedure is the same as used for water, except syrup is used here. The back pressure is also created in the same manner. Tables 2.7 and 2.8 give the results (see Figure 2.4-b and c for plots).

Table 2.4: Tube Calibration

Pressure (psi)	TUBE DIAMETER EXPANSION (in)			
	Tube #1*	Tube #2	Tube #3	Tube #4
2.50	0.00000	0.00000	0.00000	0.00030
3.75	0.00000	0.00000	0.00000	0.00055
5.00	0.00000	0.00000	0.00000	0.00080
6.25	0.00050	0.00040	0.00100	0.00105
7.50	0.00045	0.00060	0.00135	0.00140
8.75	0.00080	0.00080	0.00175	0.00180
10.00	0.00135	0.00135	0.00210	0.00225
11.00	0.00190	0.00175	0.00250	0.00265
12.00	0.00235	0.00230	0.00285	0.00315
13.00	0.00285	0.00290	0.00320	0.00355
14.00	0.00355	0.00340	0.00360	0.00400
15.00	0.00420	0.00395	0.00415	0.00445
16.00		0.00450	0.00460	0.00490
17.00		0.00520	0.00565	0.00540
18.00		0.00610	0.00630	0.00600
19.00		0.00665	0.00670	0.00645
20.00		0.00745	0.00730	0.00715
21.00		0.00810	0.00785	0.00770
22.00		0.00870	0.00840	0.00825
23.00		0.00930	0.00890	0.00880
24.00		0.00995	0.00950	0.00955
25.00		0.01080	0.01010	0.01010

Tube #1 was subjected to a maximum pressure of 15 psi.

Two molds were filled with corn syrup of viscosities 150 cP and 350 cP to observe the performance of the pump under simulated "realistic" conditions. When starting, the pump cumulative volume reading was set to zero. The syrup reservoir was also calibrated to read the volume of syrup pumped. The pump was set at 40 ml/. The tube reading was taken as zero, when the syrup first entered the mold. Both pump and tube were read at 1-minute intervals and ½ minute intervals for the 150 cP syrup and the 350 cP syrup, respectively. Results are presented in Table 2.9 and Figure 2.6.

#### 2.1.4 Air Content in the Resin / Catalyst Mixture

When the resin and catalyst mixture is mixed initially by stirring, air gets entrapped in the mixture. Entrapped air in the resin + catalyst mixture is one of the undesirable factors that affect the quality of the finished product. The greater the number of voids in the mixture, the higher the likelihood for micro-void content in the finished product. To minimize this, the mixture is evacuated in the vacuum chamber for 5 minutes at 1 Torr before it is pumped in the mold. When the mixture is being evacuated it seems to boil, which is actually the entrapped air being sucked out.

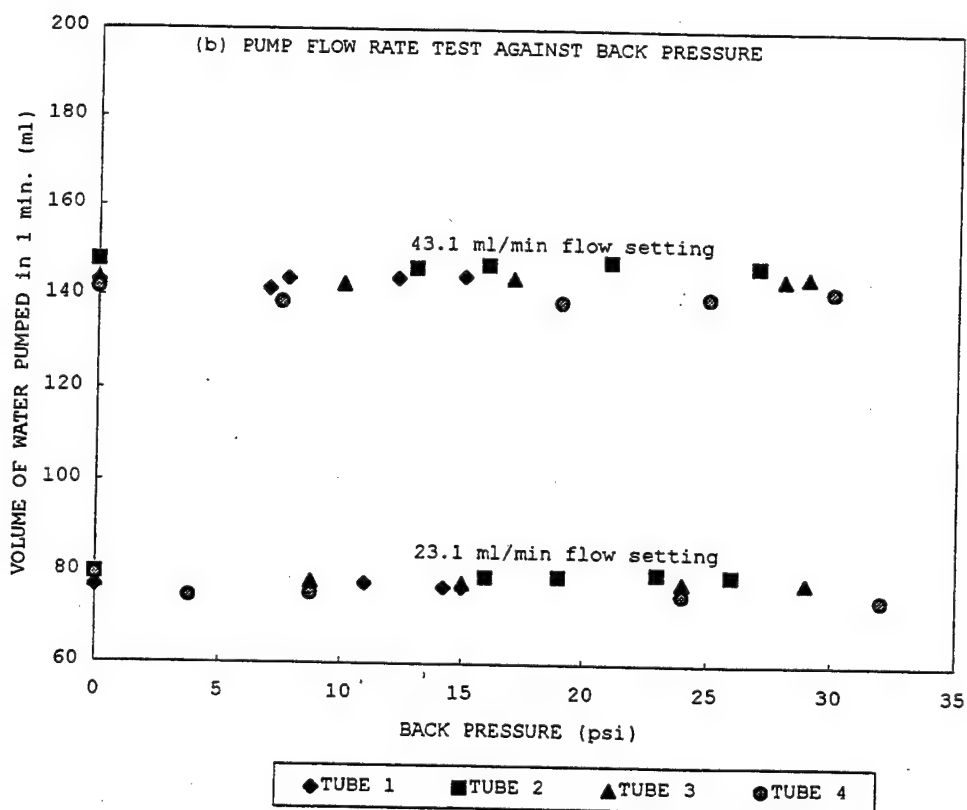
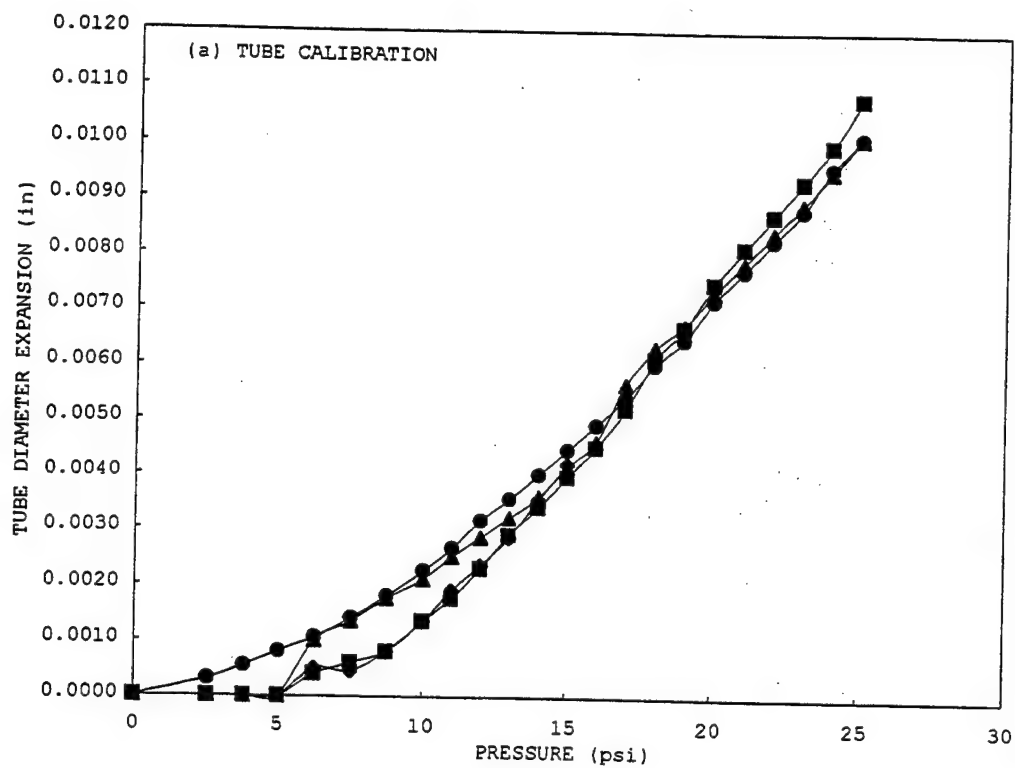


Figure 2-5 Tube Expansion, Flow Rate and Back Pressure

Table 2.5: Pump Test against Pressure

Experiment #	Pump Setting (ml/min.)	TUBE #1		
		Dial Gage Reading(in)	Weight of Water Pumped (g)	Back Pressure (psi)
1	23.1	0.00000	76.90	0.00
2	23.1	0.00000	76.74	0.00
3	23.1	0.00370	76.83	14.25
4	23.1	0.00190	77.60	11.00
5	23.1	0.00400	76.83	15.00
6	43.1	0.00000	143.00	0.00
7	43.1	0.00000	143.61	0.00
8	43.1	0.00050	173.69	7.75
9	43.1	0.00030	141.44	7.00
10	43.1	0.00245	143.84	12.25
11	43.1	0.00400	144.26	15.00
Experiment #	Pump Setting (ml/min.)	TUBE #2		
		Dial Gage Reading(in)	Weight of Water Pumped (g)	Back Pressure (psi)
1	23.1	0.00000	79.78	0.00
2	23.1	0.00000	79.90	0.00
3	23.1	0.00435	79.00	16.00
4	23.1	0.01100	79.62	26.00
5	23.1	0.09400	79.86	23.00
6	23.1	0.00690	79.15	19.00
7	43.4	0.00000	147.57	0.00
8	43.1	0.00000	146.86	0.00
9	43.1	0.00265	146.12	13.00
10	43.1	0.01285	146.86	27.00
11	43.1	0.00820	147.58	21.00
12	43.1	0.00470	146.75	16.00
Experiment #	Pump Setting (ml/min.)	TUBE #3		
		Dial Gage Reading(in)	Weight of Water Pumped (g)	Back Pressure (psi)
1	23.1	0.00000	77.96	0.00
2	23.1	0.00000	76.70	0.00
3	23.1	0.00180	78.06	8.75
4	23.1	0.00940	78.10	24.00
5	23.1	0.00390	77.80	15.00
6	23.1	0.01435	78.20	29.00
7	43.4	0.00000	135.64	0.00
8	43.1	0.00000	143.46	0.00
9	43.1	0.00000	144.14	0.00
10	43.1	0.00215	142.65	10.00
11	43.1	0.01325	144.08	28.00
12	43.1	0.00545	144.01	17.00

Table 2.5 (Continued)

		TUBE #4		
1	23.1	0.00000	79.56	0.00
2	23.1	0.00000	74.85	0.00
3	23.1	0.00000	75.84	0.00
4	23.1	0.00060	74.67	3.75
5	23.1	0.00190	75.35	8.75
6	23.1	0.00975	75.24	24.00
7	23.1	0.01880	74.37	32.00
8	43.1	0.00000	141.68	0.00
9	43.1	0.00000	139.82	0.00
10	43.1	0.00000	140.36	0.00
11	43.1	0.00130	138.72	7.50
12	43.1	0.01060	139.91	25.00
13	43.1	0.00660	138.77	19.00
14	43.1	0.01595	141.52	30.00

Table 2.6: Pump Calibration

BEFORE CALIBRATION		
Pump Setting	Weight of Water Pumped (g)	
23.10	83.50	
23.10	81.26	
23.10	83.79	
43.10	152.79	
43.10	152.35	
43.10	157.04	
AFTER CALIBRATION		
Pump Setting	Weight of Water Pumped (g)	
153.00	157.00	
100.00	102.00	
50.00	51.00	
AFTER CALIBRATION		
Pump Setting	Weight of Syrup Pumped (g)	Volume of Syrup Pumped (ml)
50.00	63.40	49.60
75.00	98.96	77.40
100.00	127.91	100.00
125.00	163.17	127.67
150.00	193.83	151.60
WITH APPLICATION OF BACK PRESSURE		
50.00	67.21	52.58
75.00	99.09	77.53
100.00	131.39	102.80
125.00	164.37	128.60
150.00	197.09	154.20



Table 2.7: Tube Calibration for Test with Corn Syrup

Pressure (psi)	Tube Diameter Expansion (in)
0.0	0.00000
2.5	0.00000
5.0	0.00025
7.5	0.00050
10.0	0.00075
11.0	0.00095
12.0	0.00110
13.0	0.00135
14.0	0.00155
15.0	0.00175
16.0	0.00200
17.0	0.00230
18.0	0.00250
19.0	0.00275
20.0	0.00315
21.0	0.00345
22.0	0.00375

Table 2.8: Pump Test against Pressure with Corn Syrup

CORN SYRUP VISCOSITY 150 cP			
PUMP SETTING 20 ml/min.			
Tube Diameter Expansion (in)	Equivalent Air Pressure (psi)	Flow Rate	
		gms/min.	ml/min.
0.00000	0.0	25.48	19.94
0.00070	10.0	25.82	20.21
0.00125	13.0	25.37	19.85
0.00140	13.0	25.61	20.04
0.00195	16.0	25.51	19.96
0.00270	19.0	25.59	20.02
0.00305	20.0	25.59	20.02
PUMP SETTING 40 ml/min.			
0.00000	0.0	50.89	39.82
0.00060	7.5	51.03	39.93
0.00100	12.0	51.12	40.00
0.00155	14.0	50.85	39.79
0.00200	16.0	50.72	39.69
0.00250	18.0	51.04	39.94
0.00335	20.5	50.91	39.84
0.00350	21.0	50.99	39.90

### 2.1.5 Resin/Catalyst Mix Ratio

The manufacturer-recommended resin:catalyst mix ratio is 100 : 17 by weight. We studied other ratios at resin flow rates of 20 ml/min. and 40 ml/min. Panels made with the mix ratios of 100:12, 100:15 and 100:16 failed; the bonding between the fiber and the resin was bad and the layers of fabric could be easily peeled off.

Table 2.9: Mold Filling with Corn Syrup

PUMP SETTING 40 ml/min.			
MOLD FILLING WITH 150 cP CORN SYRUP			
TIME	CUMULATIVE FLOW (ml/min.)		
	PUMP	TUBE	
0.0	36.87		0.00
1.0	77.68		38.95
2.0	116.40		78.60
3.0	155.30		118.20
3.5	183.50		137.70
MOLD FILLING WITH 350 cP CORN SYRUP			
0.0	250.4		0.00
0.5	270.8		19.00
1.0	290.9		37.45
1.5	310.7		51.55
2.0	329.3		65.65
2.5	349.4		74.85
3.0	370.2		86.65
3.5	389.8		98.86
4.0	409.8		110.63
4.5	429.5		124.93

The first plate was made with a mix ratio of 100:12 and a flow rate of 20 ml/min. The plate failed. The next two panels were made with a mix ratio of 100:22 and flow rates of 20 ml/min. and 40 ml/min. Both the panels were good. Since the ratio of 100:22 gave good results, this was set as the upper limit. The next step was to establish the minimum mix ratio at which good panels could be made at a flow rate of both 20 ml/min. and 40 ml/min. The next step was to establish a lower limit. Panels were made with a mix ratio of 100:15, 100:16, and 100:17 with the flow rate set at 20 ml/min. and 40 ml/min. The mix ratios of 100:15 and 100:16 gave unsatisfactory results. The mix ratios of 100:17 and 100:22 gave good results. A mix ratio of 100:17 was selected for all further experiments. Table 2-10 gives a summary of the results.

### 2.1.6 Evacuation of the Mold

Vacuum assisted RTM process is used throughout the project. Previous studies have shown that evacuating the mold before and during the process improved the quality of the finished product by reducing the micro-void content. A previous study has also shown that when the vacuum is used during the process, the first half of the mold is filled primarily due to the assistance of the vacuum while the other half of the mold is filled due to the positive pressure of the pump. In our process, the mold is evacuated with a vacuum pump for about half an hour before the resin is pumped in. The vacuum is held between 28 to 30 in. of mercury till the mold is completely filled.

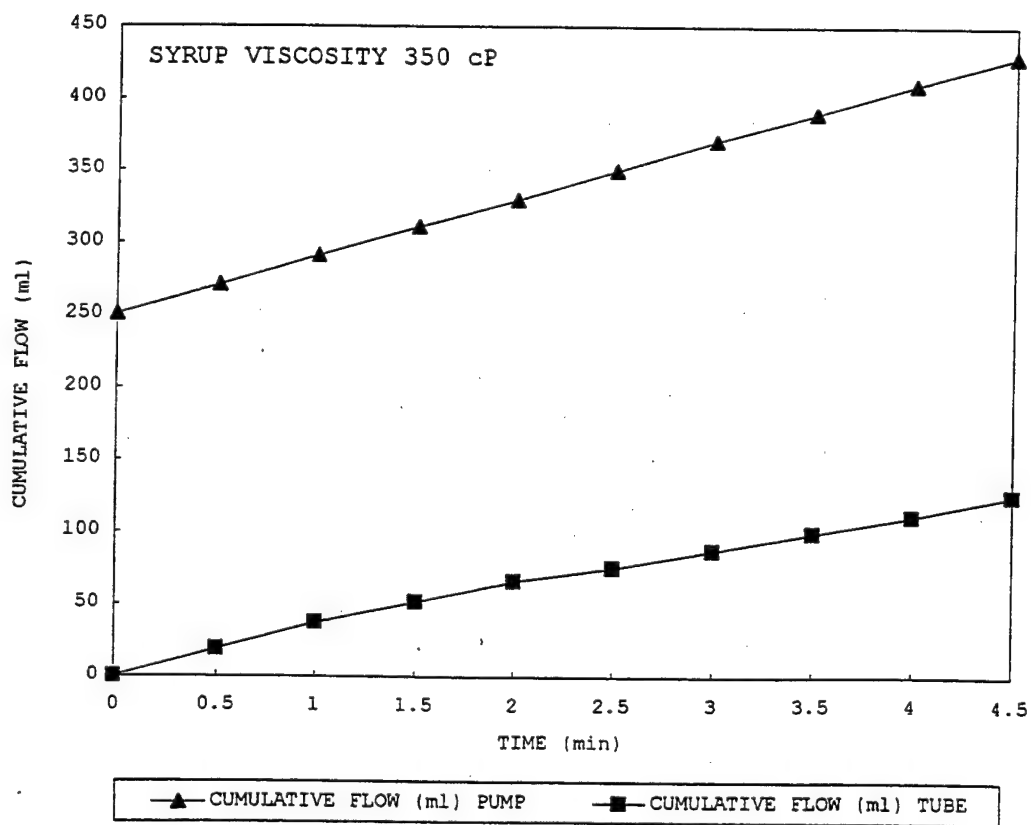
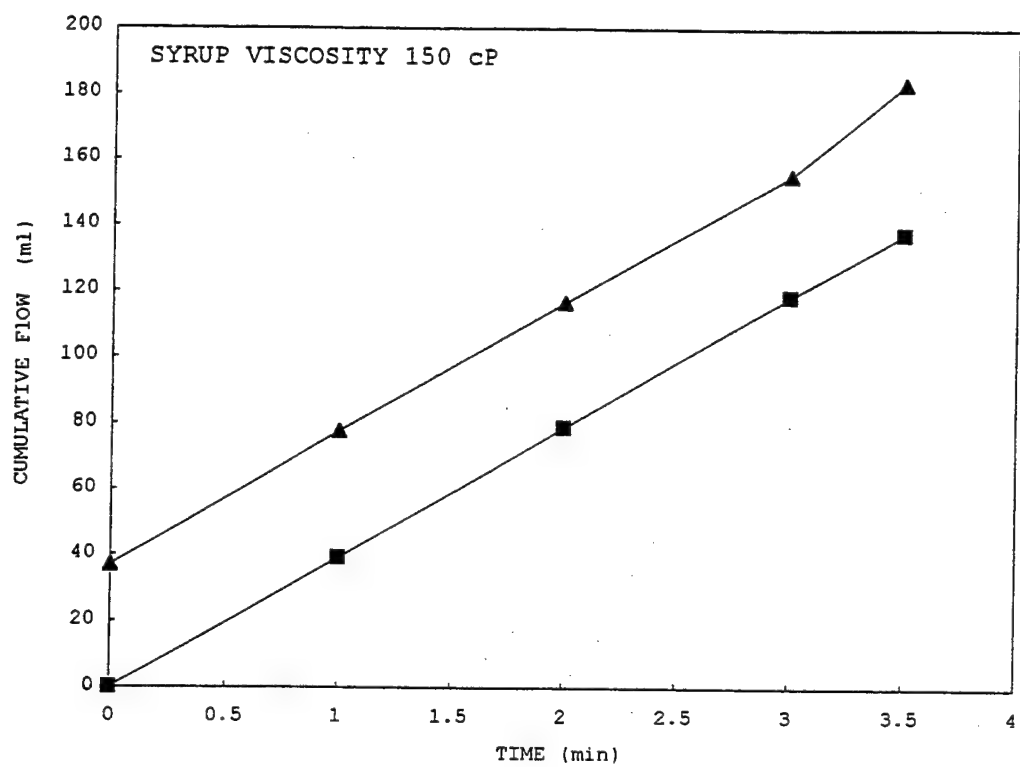


Figure 2-6: Pump Cumulative Flow versus Time

Table 2.10: Mix Ratio Test by Making Panels

Experiment #	Mix Ratio	Flow Rate (g/min.)	Panel Inspection Result
1	100:22	20	Good
2	100:12	20	Unsatisfactory
3	100:22	40	Good
4	100:15	20	Good
5	100:15	40	Unsatisfactory
6	100:15	40	Unsatisfactory
7	100:16	40	Good
8	100:16	20	Unsatisfactory
9	100:17	20	Good
10	100:17	40	Good

### 2.1.7 Uniformity of Preform and Placement of Preform in Mold

One of the parameters in prediction of the flow front and the race tracking, is the mold-preform fit. The preform selected for the process is made of 8-harness satin weave graphite fabric. A template is made to the dimensions of the mold cavity. The template is then placed on the fabric and the fabric is cut using a razor. Care has to be taken to avoid fiber fallout from the edges. A poor preform fit could result in severe race tracking.

### 2.1.8 Temperatures

All mold-filling experiments were performed at room temperature. The cure process recommended by the resin manufacturer is 1 hour at 177 °F in the mold (first cure), followed by 2 hours at 350 °F for 2 hours after the plate is taken out of the mold (second cure). We have followed this recommendation closely.

## 2.2 Mold Design and Construction

The mold assembly for the RTM experiments consists of two distinct components; an acrylic cover plate and a carbon steel base plate, both rectangular in shape. The mold was specifically designed to produce rectangular-shaped, multi-layered composite panels. On the top surface of the metal base plate, a groove circumvents the interior edges of the mold. The purpose of the groove is to accommodate a 1/8" silicon rubber "O"-ring. The O-ring is the sole means of maintaining the integrity of the seal once the mold is closed. Previous experiments relied upon the application of a silicon sealant and a caulking type of sealant around the edges of the mold to ensure seal integrity. This procedure proved unreliable and time consuming, thus, precipitating the use of the O-ring (Shah, 1995). Features and physical dimensions of the mold base and its acrylic cover plate are given in Figure 2.7. Evident in the diagram are the three vent holes in the top edge, the single hole in the bottom edge, and the two holes on each side edge of the baseplate. All these are threaded to permit the insertion of a plastic 1/8 in. male connector adapter that facilitates the connection of tubing necessary to sense the N<sub>2</sub> gas flow and the injection of resin. Lastly, there are three threaded holes on the bottom face of the base plate, which facilitates composite plate removal.

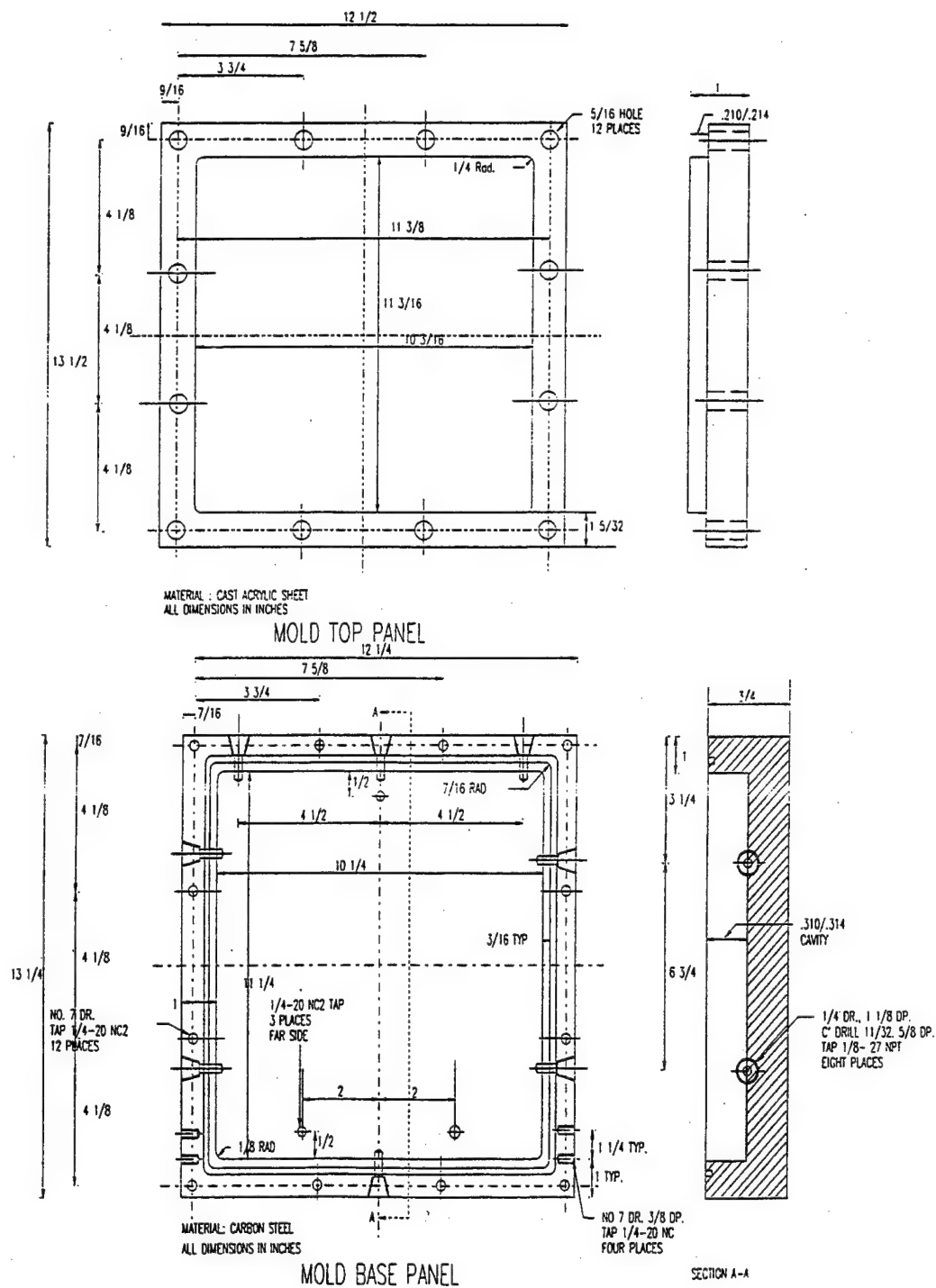


Figure 2-7 Engineering Drawing of the Mold

At measured intervals around the periphery of the acrylic plate, there are holes, which allow for the insertion of screws. The spacing of these holes was designed to correspond to the threaded screw holes located around the periphery of the metal base plate. In this fashion, the two plates are matched together and subsequently sealed. The interior surface of the acrylic sheet compresses the layers of preform to the steel lower bottom of the mold to hold it in place during the RTM process.

The selections of the acrylic for the faceplate and carbon steel for the baseplate were because of the inherent properties of both materials. The transparent nature of the acrylic allows for observation of the RTM process, as well as providing a high enough resistance to expansion caused by the heat of the oven during curing. The durability of the carbon steel is its principal advantage. The repetition necessary for RTM experimentation dictated the use of a material that could withstand the cyclic temperature changes when curing, as well as resist corrosion or contamination by the resin mixture. The dimensions of the top acrylic part are monitored closely and replaced when necessary.

## **2.3 Description of Sensors**

During the introduction of the  $N_2$  gas and the impregnation of the preform by the resin mixture, the fluid flow rates were continuously monitored. In order to achieve this, various sensing devices coupled with the data acquisition system and LabView<sup>TM</sup> software were integrated into the experimental setup. The nature of the resin mixture posed imminent danger to contact type sensing devices; therefore, the decision was made to sense phenomena that could be directly related to resin flow patterns without having to have the instrumentation come in direct contact with the resin mixture. The chosen parameters were the flow rates of a non-reactive gas (Nitrogen) and the back pressures experienced in the mold during the introduction of the  $N_2$  gas and during the complete resin fill. The success of sensing the selected parameters hinged upon two types of devices, mass flow meters and pressure transducers. The acquisition of these devices permitted the observation of changes in flow rate and pressure during the introduction of the  $N_2$  gas and the impregnation of the preform by the resin.

### **2.3.1 Mass Flowmeters**

The primary purpose of the research is to relate the flow rates and subsequent flow patterns of a non-reactive gas and the flow patterns exhibited by the resin during a mold fill. The measurement of the flow rates of the non-reactive gas is done using Omega FMA-5000 Series Electronic Mass Flowmeters. A 0-5 V dc output signal that is linearly proportional to the flow rate provided the translation from analog to digital conversion. The flowmeters can be calibrated for 13 different ranges, depending on the desired range. From previous tests, Shah (1995) determined the range of the flow rate to be no greater than 5 standard liters per minute (slm). A 9-pin "D" sub-connector for the output signal, input power, and remote display drive permitted the connection between the mass flowmeters and the data acquisition board.

The basic theory of the mass flowmeter operation is largely dependent on the difference in temperature. Gas enters the flow body and is directed into one of two paths.

The majority of the flow travels through the laminar flow bypass, thus creating a pressure drop that compels a portion of the flow to enter the sensor tube. The sensor tube is located directly above the bypass flow path. Two resistance detector coils surround the sensor tube, conducting a constant amount of heat into the gas stream. During operation, the gas flow tends to carry away some of the heat from the first coil to the second coil via convection. The subsequent temperature difference is the means through which the flow rate is measured by using the following formula:

$$\dot{m} = \frac{HN}{C_p \Delta T}$$

where

$\dot{m}$	=	Mass flow rate of gas (g/min.)
H	=	Constant amount of heat applied to sensor tube
N	=	Correction factor for molecular structure of gas
$C_p$	=	Coefficient of specific heat of gas (cal/g)
$\Delta T$	=	Temperature difference between downstream and upstream coils

The volume flow rate is the product of the mass flow rate and the density of the gas ( $N_2$ ).

### 2.3.2 Pressure Transducer

For the measurement of the pressure for both the  $N_2$  gas infiltration and the resin impregnation, the sensor of choice was an Omega® Thin Film Pressure Transducer. The selection of this type of pressure transducer facilitated its integration into the system, as well as providing a level of flexibility absent from other types. From previous experiments, the decision was made to utilize two pressure sensors, the first having a pressure sensing range of 0-15 psi for nitrogen injection and the second a range of 0-100 psi for resin injection. The sensors were equipped with a special connector, which permitted the pressure sensors wiring to connect with the data acquisition board, and subsequently the data acquisition system.

The basic theory of operation for the sensors is the conversion of one type of energy to another. Under normal operation, the pressure sensor is connected in series with the tubing or piping of interest. The pressure felt by the sensor is converted to an electrical voltage. This resultant voltage represents the fluid pressure experienced in the tubing. The conversion formula for voltage to pressure is a function of the operating pressure range of the sensor.

$$P = ((V_{out} - 1) * 3.75) \text{ For sensor with 0 - 15 psi range}$$

$$P = ((V_{out} - 1) * 25.0) \text{ For sensor with 0 - 100 psi range}$$

where

P	=	Pressure
$V_{out}$	=	Voltage output

For the pressure sensor, any voltage readings below the value of 1 V are considered as noise and are irrelevant in the calculation of the pressure. conversion formulas are based on the output voltage range (1 - 5 V dc) and the sensor pressure range.

## 2.4 Description of Data Acquisition System

The central component of the experimentation was the data acquisition system. The data acquisition was executed by a collection of hardware and software compiled specifically to collect the pertinent data before and during the RTM experiments. All data collected immediately prior to the RTM fill refers to the flow of  $N_2$  gas through the mold and the subsequent flow rates experienced at the exit ports. The primary sources of the sensing capabilities were mass flowmeters and pressure sensors.

### 2.4.1 Data Acquisition System Hardware

The primary components of the data acquisition system's hardware are the data acquisition board, the associated wiring, a power supply, and a Macintosh IIfx computer. The data acquisition board itself is comprised of various receptacles for wiring and resistors. The data acquisition board was configured in such a way that seven flow meters and one pressure sensor may be utilized simultaneously. The wiring is directly connected from the output serial ports of the Omega flow meters to the data acquisition board. Additional wiring is used to connect the data acquisition board directly to the serial ports of the computer system.

### 2.4.2 Description of LabView Software

The foundation of the experimental research is the software that enables the acquisition of the data, LabView for Macintosh. LabView is specifically geared towards data acquisition and instrumentation control. Unlike previous programs, LabView uses a graphical programming language to create programs in block diagram form. In this way, control panel(s) were created to facilitate the collection of data during the introduction of the  $N_2$  and the Tactix 123/Ancamine 1770 mixture. The programs in LabView are called *virtual instruments* or VIs. The VIs in LabView are the constitutive components of the entire software. These VIs may be used as the top-level programs or applied as subprograms contained within another program or outside of the main program.

The basis for the virtual instruments is a graphical programming language entitled G. The VI programs are created using pre-defined symbols and icons for all functions, such as mathematical operations, Boolean operations, and all connections for the sequence of operations. The VIs themselves are composed of the front panel, the block diagram and the icon/connector. The front panel is the graphical representation of the virtual instrument. Typically, the front panel is the first and only interaction a layperson will have with LabView. In this interface, all virtual controls, such as knobs, levers, buttons, etc., are put into place to facilitate any adjustments needed during the data acquisition. The block diagram represents the VI main program. In essence, the block diagram is analogous to the source code of text-based programs. This segment is where symbols are used to perform the various operations and decisions necessary to complete the required tasks. The third component of the virtual instrument is the icon/connector. This device allows for the VI to be used in other applications or block diagrams. The icon graphically represents the VI or subVI in the block diagram of other VIs. The function of the icon is to hide the connector and its terminals, unless chosen for viewing. The connector terminals determine where the input and output *wires* of the icon must be placed in order to function. The terminals are graphical representations of the parameters



of a subroutine or a function. These terminals correspond to the controls and indicators provided on the front panel of the VI. These controls and indicators provide the means through which numerical data flow can be manipulated and observed during the course of the process.

## **2.5 Instrument Specifications**

At this juncture, the specifications of instruments, hardware and software are determined. The following specifications are provided to enable the reader to generate a similar experimental setup.

### **1. Viscometer specifications:**

Manufacturer: Labline Instruments Inc.  
Model: 4537  
Electric supply: 120 V, 60 Hz  
Accuracy:  $\pm 0.1\%$  of full scale in use  
Repeatability:  $\pm 0.2\%$  of full scale in use  
Ambient temperature:  $+10\text{ }^{\circ}\text{C}$  to  $+40\text{ }^{\circ}\text{C}$   
Resolution: 0.01 to 100 cP depending on range and model  
Humidity: 5% to 95% RH non-condensing  
Range: 10 to 1,000,000 cP  
Number of ranges: 32  
Spindle rpm: 0.3, 0.6, 1.5, 3, 6, 12, 30, 60

### **2. Pressure sensor specifications**

Manufacturer: Omega Engineering, Inc.  
Model: PX 613-100G5V  
Range: 0 - 100 psig  
Excitation: 10 - 30 V dc unregulated  
Output: 1-5 V dc (3-wire)  
Supply current:  $<3.0\text{ mA}$   
Output impedance: 100 ohms  
Accuracy:  $\pm 0.4\%$  BFS (Best Fit Straight Line)  
Hysteresis:  $\pm 0.2\%$  full scale  
Repeatability:  $\pm 0.05\%$  full scale  
Stability:  $\pm 1\%$ /year  
Durability: 100 million cycles  
Operating temperature:  $-55$  to  $195\text{ }^{\circ}\text{F}$   
Compensated temperature:  $-20$  to  $180\text{ }^{\circ}\text{F}$   
Thermal zero effect:  $\pm 0.04\%$  full scale/ $^{\circ}\text{F}$   
Thermal span effect:  $\pm 0.04\%$  full scale/ $^{\circ}\text{F}$   
Proof pressure: 200%  
Burst pressure: 800%  
Gages: Thin film polysilicon  
Diaphragm: 17 - 4PH stainless steel  
Case: 300 series stainless steel  
Pressure connection:  $\frac{1}{4}$  in. NPT

Electrical connection: Connector type, Mating connector, PTO6F-8-4S

Weight: 4.5 oz without cable

Response time: 1 ms

Construction: sealed

3. Pump specifications:

Manufacturer: Masterflex

Model: MR-07550-90, 60 rpm

Pump heads: Masterflex Easyload MR-07158-12

Pump mounting: Two pumps

Flow rate capacity: 0.06 to 228 ml/min.

Cumulative volume capacity: 0.01 l to 99999 l

Automatic speed control: 1 to 60 rpm

Speed regulation: 0.02 rpm measured over 1 minute

Start/stop control: As a stand-alone controller, the dynamic brake will stop the output shaft within 0.05 revolution after the stop button is pressed. In the remote computer linked mode a combination of dynamic braking and a closed loop servo will stop the output shaft with an accuracy much better than 1/100<sup>th</sup> revolution

Power line connector: Standard US 3-wire, 115 V operation, grounded

Operating range: 0 to 40 °C

Relative humidity: 20 % to 90% non-condensing

Cabinet dimensions: 10 in.w. x 6-3/4 in. h. x 8 in. d.

Weight: 15 lb

Front panel construction: reverse screen control key designations, matte finish polyester, with integrated clear display window.

4. Air flow meter specifications:

Manufacturer: Omega Engineering, Inc.

Model: FMA-5609

Accuracy: 2% full scale including linearity over 15-25 °C and 5-60 psia; 4% full scale over 0-50 °C and 1-150 psia

Temperature coefficient: 0.15% of full scale/°C

Pressure coefficient: 0.02% of full scale/psi

Maximum gas pressure: 150 psig

Gas and ambient temperature: 32-122 °F

Leak integrity (std cm<sup>3</sup>/s He): 1 x 10<sup>-4</sup>

5. Fabric specifications:

8-harness satin weave graphite fabric with no finish. It is woven from 3 K tow supplied to the fabric vendor (BGF industries Inc.) by Toho (Fiber / tow manufacturer) and has Toho's standard on it. The weight is 10 oz per sq. yard and is woven with 23.5 warp ends per inch and 23.0 fill ends per inch.

6. Clear tubing specs.

Fisherbrand™ Catalog # 14-169-7e, Material: Tygon

Tube ID: ¼ in. Tube OD: ½ in.

Wall thickness: 1/8 in.

Durometer hardness: SHORE A, 65

Maximum operating temperature: 165 °F

- Highly flexible, non aging, non oxidizing
7. Neoprene tubing specs
    - Masterflex Catalog # 6404-24
    - Tube ID: ¼ in.
    - Tube size: 24
    - Hose barb size: ¼ in.
    - Flow range (6 to 600 rpm): 17 to 170 ml/min.
    - Maximum pressure, continuous: 25 psig
    - Maximum pressure, intermittent: 40 psig
    - Maximum vacuum: 30 in of Hg
    - Suction lift: 29 ft of water
    - Operating temperature: 60 to 275 °F
  8. 'O' Ring specification
    - McMaster-Carr Catalog # 96505K23
    - Material: Silicone
    - Diameter: 1/8i
    - Operating temperature: 65 to 400 °F, 500 °F intermittent
    - Durometer hardness: Shore A, 70
  9. Vacuum pump specification
    - Make: Sargent-Welch Scientific Co.
    - Model: 1405
    - Free air displacement: 60 lpm
    - Guaranteed partial pressure blankoff: 0.1 mtorr
    - Pump speed: 525 rpm
    - Number of stages: 2

## **2.6 Description of Experimental Setup**

The procedure involves two distinct steps in the testing process. One is to measure the N<sub>2</sub> gas flow rates and inlet pressures during probing; the second is to record the flow front at time intervals during resin impregnation. The back pressure is also monitored to ensure that the capacity of the pump was not exceeded. The conversion of the experimental setup from gas introduction to the resin impregnation requires only the addition or removal of pertinent sensors and equipment. The experimental setup for the RTM process is a slight modification of the general RTM arrangement. The two distinct facets of the experiment require two VIs in LabView to accommodate the different types of data being collected. In our setup, seen in Figure 2-8, there were seven flowmeters available to monitor the N<sub>2</sub> gas flow from every port along the mold.

### **2.6.1 Experimental Setup for N<sub>2</sub> Gas Introduction**

1. Using a putty knife or any type of scraping device, remove all resin debris from the interior surfaces and entrance/exit ports of the acrylic plate and the steel plate. During this operation, it may be necessary to use a drill to clean out the entrance and exit ports of the steel mold.

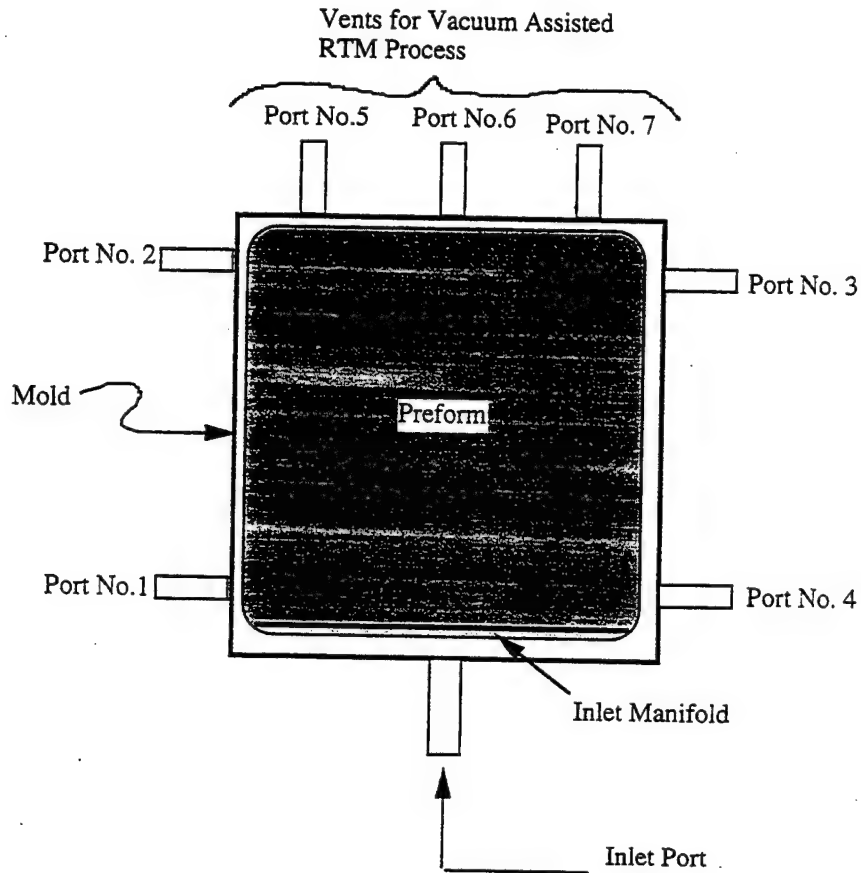


Figure 2-8 Port Configuration

2. Using Trewax brand wax or any automotive wax, coat both the acrylic plate and the steel plate. After 5 minutes, buff and polish the wax with a clean cloth. Repeat this step three times, leaving a light coat after the third iteration.
3. Cut a 43 5/8" length of the cylindrical silicon rubber (1/8 in. diameter) to be used as the "O"-ring to seal the mold. The ends of the "O"-ring should be joined together using LocTite Quickset industrial adhesive. Setting time is usually 5 minutes.
4. Cut eleven 1-inch strips of Teflon tape. Wrap one piece of tape around the threaded portion of eight threaded male pipe adapters, being sure to wrap the tape in a clockwise direction.
5. Place one wrapped threaded male pipe adapter in each of the threaded orifices around the periphery of the steel plate (three openings on top surface, two on each side, one on bottom surface). Using a standard socket wrench, tighten the pipe adapters until firmly placed in the mold.
6. Repeat Step 4 using three wrapped short hexagonal bolts and the remaining pieces of tape. These are inserted in the screw holes located on the bottom face of the mold. The screws should be placed in the holes from the back side of the steel plate so that the heads of the screws face away from the front face of the steel plate.

7. Cut six rectangular shapes of the graphite 8-harness satin weave fabric. Each shape should be cut to the exact size of the interior of the mold cavity. This was done by using a template made of soft metal or cardboard.
8. With the mold cavity lying horizontally on a flat surface, place the six layers of fabric in the mold. The placement of the fabric should be in such a way that the bottom three layers are facing upwards, and the top three layers should face downwards.
9. Place the "O"-ring in the groove in the inner cavity of the steel mold plate.
10. Place the acrylic cover on top of the mold cavity, being sure to align the openings provided for the insertion of screws.
11. Position the four bolt bars in the order T-Top, B-Bottom, L-Left, and R-Right.
12. Tighten the bolts in the sequence given by the numbers stamped on the face of the bolt bars. Use a torque wrench to tighten each bolt to a maximum torque of 36 in-lb.
13. Attach both of the triangle-shaped stands to each side of the mold. Place the mold assembly on the stands such that the entire assembly is vertical.
14. Cut seven 1-inch strips of Teflon tape. Using the male reducer fittings, wrap the threaded 1/8" diameter side of the male reducer fittings. After wrapping the tape, insert the reducer fittings in the "Flow In" receptacles of each of the seven Omega FMA-5000 Series Electronic Mass Flowmeters.
15. Insert one Omega FMA-5000 Series Electronic Mass Flowmeters Power Pack into the power jack of each flowmeter.
16. Insert a nine-pin connector into the nine-pin output jack for each flowmeter.
17. Connect the open ends of each of the seven nine-pin connector wiring and the pressure sensor connector wiring to the data acquisition board and connect the "hot" wire of the pressure sensor to a separate power source.
18. Connect the data acquisition board to the appropriate ports of the Macintosh IIc.
19. Cut seven 36-inch lengths of amber Fisher Scientific Latex laboratory flexible tubing (1/4 in. x 3/32 in.). One tube should be connected to each of the threaded ends of the seven flow meters.
20. Cut two pieces of black Masterflex Norprene size 24 tubing, of lengths 41 5/6 in. and 37 3/8 in., respectively.
21. Connect one end of the short tubing to one of the horizontal barbed ends of a Cole-Parmer male pipe tee. Connect one end of the longer tubing to the opposite barbed end. Secure the open ends of the longer tubing and the shorter tubing to the N<sub>2</sub> gas bottle and the male pipe fitting located at the bottom of the mold, respectively. Secure all connections with high pressure hose clamps.
22. Secure one end of a Cross brass connector to the threaded end of the Omega Thin Film Pressure Transducer. Insert a taped male pipe adapter in the other end of the brass connector.
23. Cut a 20" length of Fisherbrand Flexible Clear Plastic Tubing. Secure the one end to the male pipe adapter connected to the pressure sensor. Fill 18 inches of the tubing with Karo Dark corn syrup. Secure the other end of this length to the open barbed end of the male pipe tee. Secure all tubing/adaptor connections with high pressure hose clamps.

24. Attach the open ends of the seven amber latex tubes to the male pipe adapter at its corresponding port. (i.e., The tubing connected to flow meter No. 1 should match with port 1 of the mold, and so forth.)
25. Collect the  $N_2$  gas flow rate per section 2.8.

This procedure represents the general methodology for the preparation of the collection of  $N_2$  gas flow data. Figure 2-9 shows a schematic of the mold during the  $N_2$  data collection. Until replacement is necessary, the "O"-ring, the pressure sensor and the brass connector may be reused.

### **2.6.2 Experimental Setup for RTM/Resin Impregnation**

This simply requires that the hoses and tubes connected to the mold for nitrogen injection be removed; the side ports be plugged; and the top vents be connected to a vacuum pump. The inlet port is connected to the resin tank via the peristaltic pump. The setup is seen in Figure 2-10. The detailed procedure is as follows:

1. Remove all amber latex tubes connections from the mold.
2. Remove and save the male pipe adapters from ports 1-4.
3. Wrap the threaded ends of four 1/8" NPT diameter black pipe plugs with Teflon tape.
4. Insert the four wrapped plugs in the threaded holes formerly occupied by the male pipe adapters.
5. Cut four lengths of clear plastic tubing, the first three being at least 8 inches, the fourth piece at least 25 inches.
6. Connect the three shorter pieces to the left, right and lower barbed ends of a Cross 4-way pipe adapter. The fourth and longest piece should connect to the upper barbed end, which should point in a direction away from the mold assembly. Secure all connections with high-pressure hose clamps.
7. The open ends of the three short pieces should be connected to the three male pipe adapters labeled ports 5 - 7. The end of the longest tube should connect to a flask used as an overflow resin reservoir. Secure all connections with high-pressure hose clamps.
8. Using a test tube holder of appropriate size, suspend a resin reservoir at a level at least 6 inches above that of the top of the mold assembly. The placement of the reservoir should be at least 2 feet away from the mold in order to accommodate the placement of the peristaltic pump.
9. Disconnect the black peristaltic pump tubing from the nozzle of the  $N_2$  gas bottle and connect this end to the tip of the resin reservoir.
10. Place the peristaltic pump such that it is situated midway between the resin reservoir and the mold assembly.
11. Feed the black tubing through the head of the peristaltic pump.
12. Use two adjustable Hoffman tubing clamps to seal off the tubing leading from the pressure sensor to the mold assembly entrance port. Place the first clamp just above the level of the Karo™ Dark corn syrup in the Fisherbrand Flexible Clear Plastic tubing. The second is placed just below the entrance port of the mold assembly.
13. Secure vacuum tubing to barbed fitting on the flask with a hose clamp.

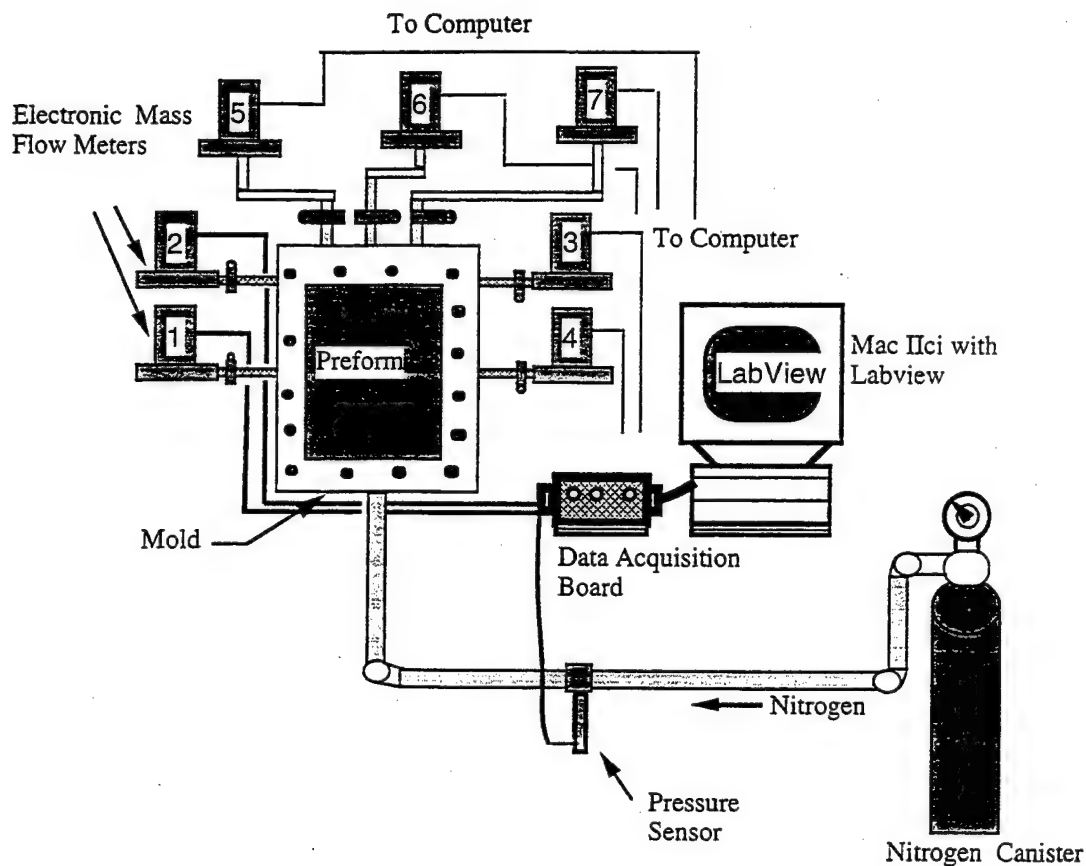


Figure 2-9 Schematic for Nitrogen Data Acquisition

14. Turn on vacuum pump. After the gage reads at least 28 in. Hg, allow the vacuum to run for 30 minutes.
15. At the 25-minute mark of running the vacuum, mix Tactix 123 and Ancamine 1770 in a clean beaker. The weight mix ratio should be 100 parts resin to 17 parts catalyst (100:17 mix ratio by weight).
16. Stir the mixture thoroughly with a tongue depressor.
17. Place the beaker with the resin mixture in an evacuation chamber. Close the chamber and evacuate for approximately 5 minutes. If the resin mixture begins to bubble and spill out of the beaker, relieve the vacuum temporarily (through a release valve) until the resin level settles in the beaker and resume the evacuation procedure.

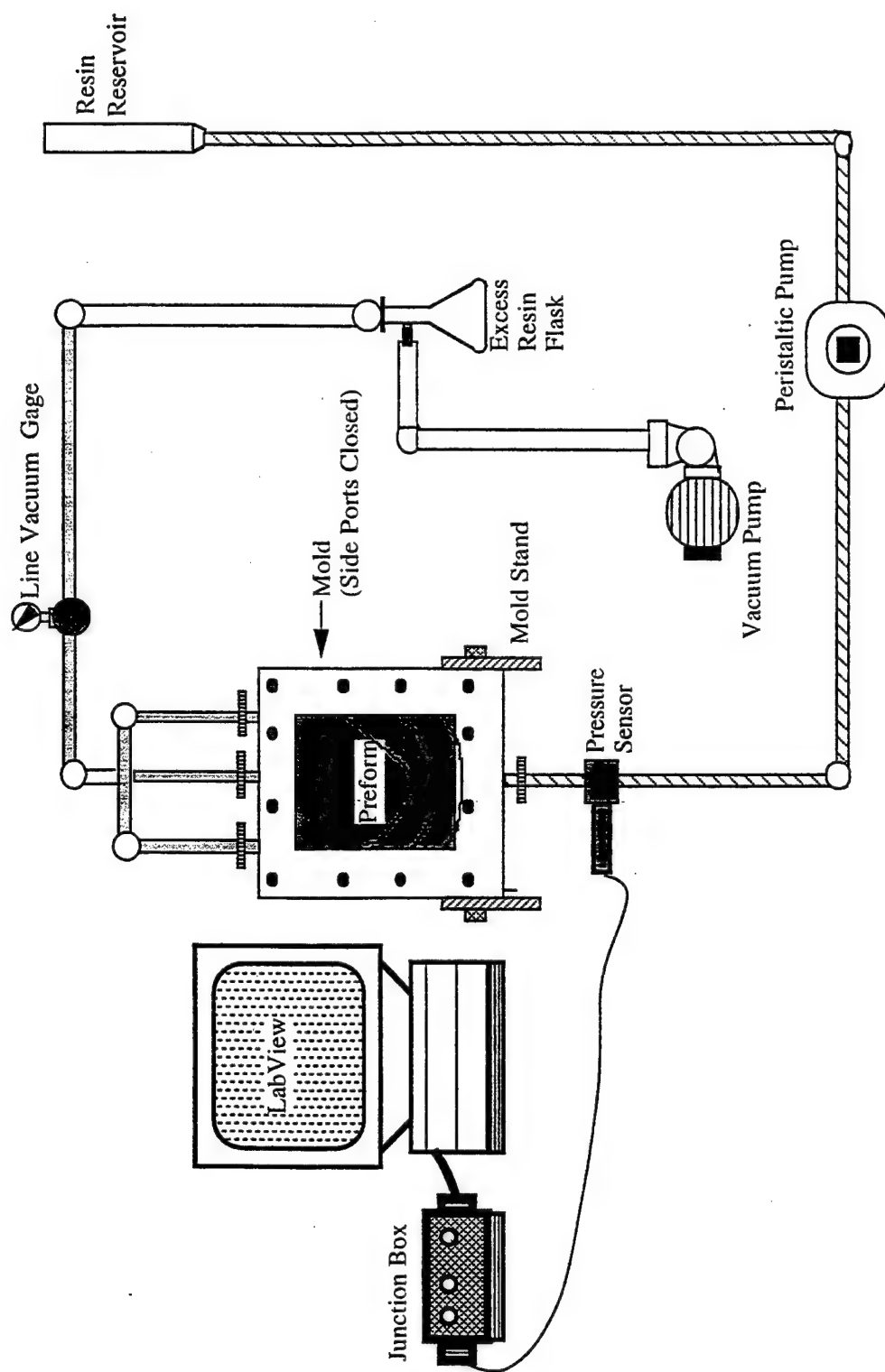


Figure 2-10 Schematic for Flow Front Data Acquisition



18. After the evacuation of the resin, remove the beaker from the chamber and pour the resin mixture into the resin reservoir.
19. Cut a rectangular sheet of plastic that is the approximate size of the acrylic mold cover of the mold assembly. Use Scotch adhesive tape to affix the plastic sheet to the front of the acrylic mold cover.
20. Turn on the peristaltic pump, setting the flow rate at 30 milliliters per minute (30 ml/min.). At this point, the vacuum should still be running, and will remain on for the duration of the experiment.
21. Allow the resin mixture to flow until it has reached the level of the corn syrup in the clear plastic tubing. At this point, release both adjustable clamps, with the clamp located on the transparent tubing being released first.
22. At the first sign of the entrance of resin in the mold, initialize the Resin Pressure Read VI in LabView.
23. Collect the data as explained in Section 2.9.
24. After the mold has been filled, turn off the peristaltic pump and close off the tubing for both the entrance and exit ports using two adjustable clamps. Cut the excess tubing just after the position of the clamps, such that the adjustable clamps prevent any resin from spilling out of the mold assembly.
25. Place the entire mold assembly in a preheated oven set at a temperature of 177 °F for exactly 1 hour.
26. Dispose of the excess resin mixture in a designated disposal can for resin.
27. Discard any remaining tubing and wipe away excess or spilled resin mixture.
28. After the first cure cycle, disassemble the mold assembly.
29. Remove all male pipe adapters, short and long hexagonal bolts and tubing.
30. Using three long bolts, insert the bolts in the three bolt holes located on the backside of the mold assembly. Tighten the bolts until the plate is ejected from the steel mold cavity.
31. Clean all reusable equipment that came in contact with the resin mixture (vacuum flask, hose clamps, etc.) with a solvent.
32. Place the plate in an oven preheated to a temperature of 350 °F. The plate is to be cured for 2 hours.

Unlike the procedure for the introduction of  $N_2$  gas, all steps of this procedure must remain intact to ensure the integrity of the testing configuration. None of these steps may be omitted; however, the four male pipe adapters removed at the conclusion of the  $N_2$  gas experiment may be reused. After the completion of the resin injection, the cleaning procedures outlined at the end of this procedure and the beginning of the  $N_2$  gas procedure have to be done to repeat the experiment.

## 2.7 Summary of Levels of Variables

For this experiment, the variables include the resin matrix viscosity, the resin matrix mix ratio, the peristaltic pump flow rate and the dimensions of the preform. The pot life and approximate viscosity of the resin mixture were found using a Lab-Line Instruments Inc. viscometer, and following the guidelines of the *Standard Test Method for Viscosity of Epoxy Resins and Related Components* (ASTM D2393-86). There was

the need to establish the proper setting for the peristaltic pump used to introduce the resin into the mold.

In summary, the following levels of the variables were throughout the project.

- |                                |   |
|--------------------------------|---|
| 1. Mix ratio                   | 100:17  |
| 2. Pump flow rate              | 30 ml / min.  |
| 3. Resin evacuation time       | 5 min. at 1 Torr  |
| 4. Mold temperature            | Room temperature  |
| 5. Curing time and temperature | 1 hour at 177 °F in mold followed by<br>2 hours at 350 °F out of the mold |
| 5. Nitrogen inlet pressure     | Enough to have a maximum flow rate of ~ 4 slm                             |
| 6. Vacuum                      | 28 to 30 in. Hg from ½ hour before to end of process                      |

The variables to be monitored are:

1. Air flow readings during the air probing stage.
2. Pressure during the air probing stage.
3. Back pressure when resin is being pumped in.

## **2.8 Data Collection Scheme for N<sub>2</sub> Gas Flow Rates**

The collection of the N<sub>2</sub> gas data requires precise steps to be followed to ensure the data were collected and saved appropriately. The general process for data collection is the initial procedure to be reviewed. While collecting N<sub>2</sub> gas data, there were four different configurations that hopefully, simulated various conditions of the mold. These four conditions involved the closure of specific ports to force flow through the remaining open ports. This was done in an effort to determine which port(s) combinations yielded the best correlation between N<sub>2</sub> gas data and the resin flow front(s). The four configurations (Figure 2-11) are:

1. No ports closed
2. Top ports closed
3. Lower ports closed
4. Side ports closed

Typically, 100 - 105 readings at a scan rate of one reading per second were collected and the average used as the value of the flow rate. In those instances where the configuration required no data from a particular port or ports, short lengths of hose clamped at one end replaced the hose connection to the flow meter at the mold to create the effect of closure. Unless otherwise noted, all remaining ports were to be unimpeded or "Open". In the case of the pressure sensor, no additional steps are needed after making the necessary connections for the power/output signal. The LabView user interface for the nitrogen injection is shown in Figure 2-12.

### **Data Collection**

1. Open the flow valve of the N<sub>2</sub> gas bottle.
2. Adjust the valve of the N<sub>2</sub> gas bottle such that the flow meter with the highest flow rate reading does not exceed 5 standard liters per minute (slm).

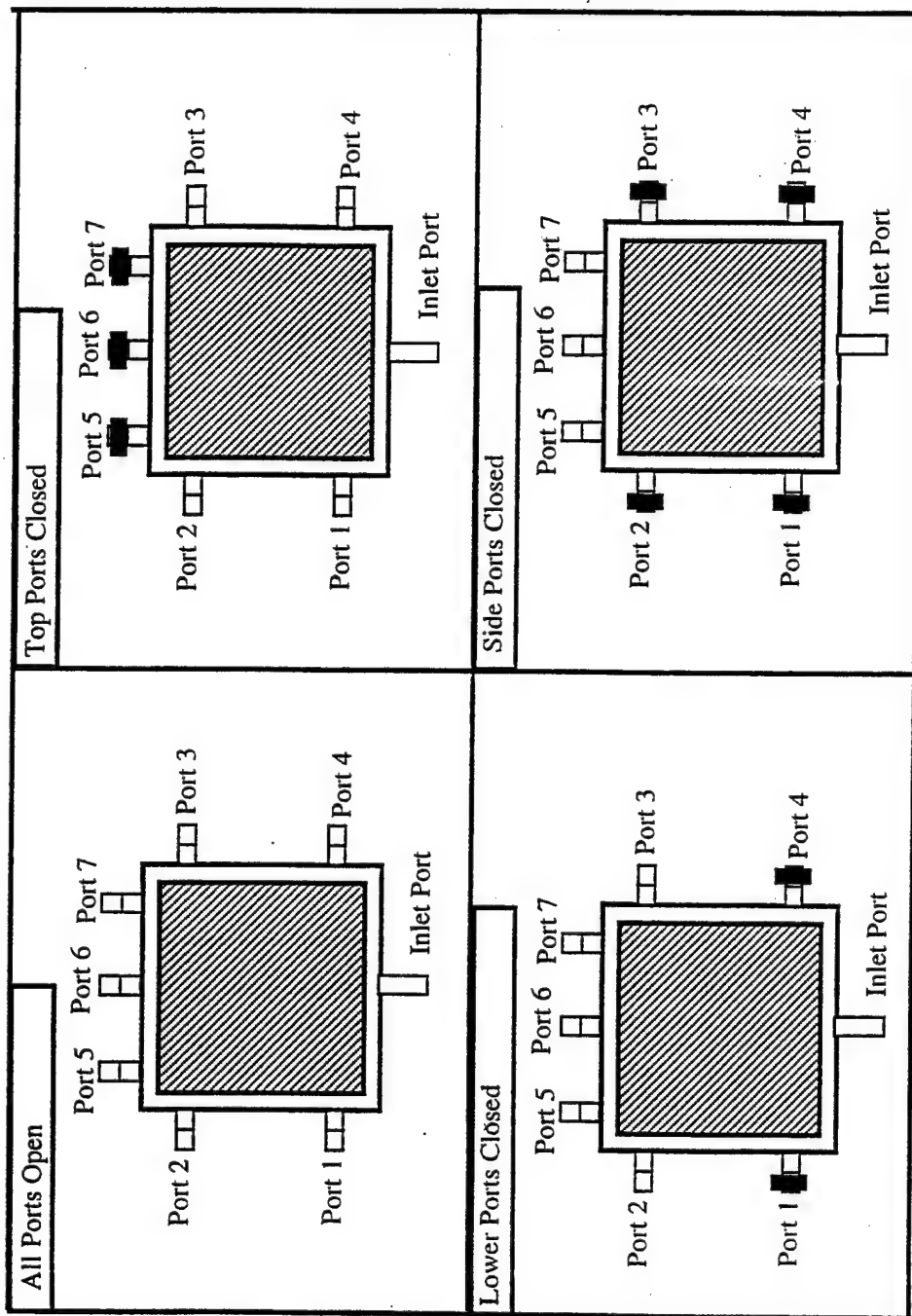


Figure 2-11 Port Configuration for Nitrogen Injection

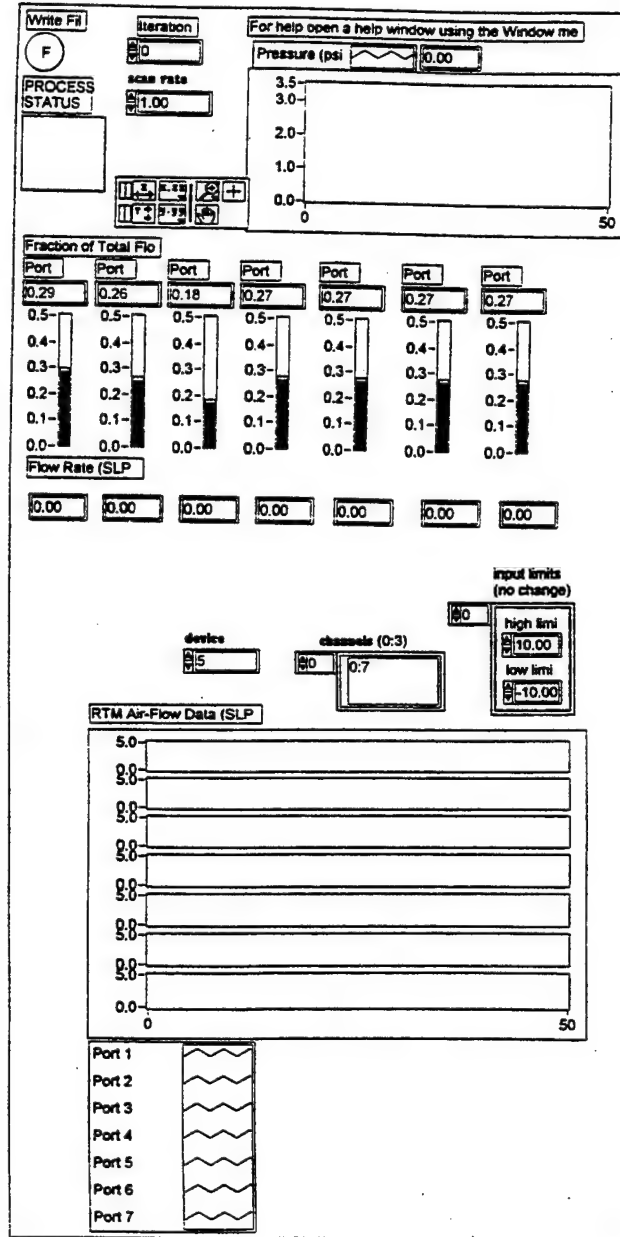


Figure 2-12 LabView User Interface for Nitrogen Injection

3. Initialize the Flow Rate VI in LabView once the flowmeter readings stabilize.
4. Clear the data from previous trials by clicking on the "Clear" key represented by the "hand" icon on the display.
5. Click the "Write File" icon of the front panel to the "On" position.
6. Click the "+" icon to initiate the data collection.
7. After taking approximately 100 readings from all seven ports, click the "Stop" button to cease data acquisition.
8. Save the data to a file.

The data yielded by the Pressure Read VI give the flow rates of the respective ports, ranging in values of 0 to 5 slm, providing that the  $N_2$  gas pressure was appropriately set, and the values for the back pressure during the  $N_2$  gas introduction. The pressure data were given in terms of voltages, therefore the application of the conversion equations referred to in Section 2.3 were necessary.

## 2.9 Data Collection of Back Pressure during Resin Impregnation

The LabView user interface at this stage is shown in Figure 2-13.

1. Click the "hand" icon on the face panel to clear data from previous trials.
2. Set the "Channel Read" icon to Channel #4. If this is not done, the data *will not* be recorded!
3. Click the "Write File" icon of the front panel to the "ON" position.
4. Set the desired scan rate for the data acquisition (2 scans/second).
5. Click the "+" icon to initiate the data collection.
6. Starting from the first sight of resin in the mold, manually trace the flow front or use a Macintosh digital camera to take a digital image of the flow front at a predetermined time interval, typically 1 minute.
7. Repeat Step 5 until the RTM fill has reached its conclusion, and all three top ports (5, 6, and 7) have resin flowing through to the vacuum flask.
8. Click the "STOP" button to cease data acquisition.
9. Save the data to a file.

The data yielded by the Resin Pressure Read VI will have two important variables, the time and the back pressure. Once again, the application of the conversion factors introduced in Section 2.3 are necessary to transform the output voltages from the pressure sensor into equivalent pressures. The time at each reading was derived from the set scan rate, 2 scans per second, thus delivering 120 data points per minute.

## 2.10 Development of Database

The driving force behind every experiment performed was to develop a viable database that could be utilized to predict the resin flow pattern. The development of such a resource would allow for the analysis and comparison of the  $N_2$  gas data to flow patterns exhibited during an actual RTM fill. This end may be achieved through data conversion and analysis. By establishing a foundation of data, we were able to use this for comparisons and prediction in the RTM trials to follow.

The database constituted the sole means by which the prediction of the flow patterns and race tracking were derived. The development of the database was not only

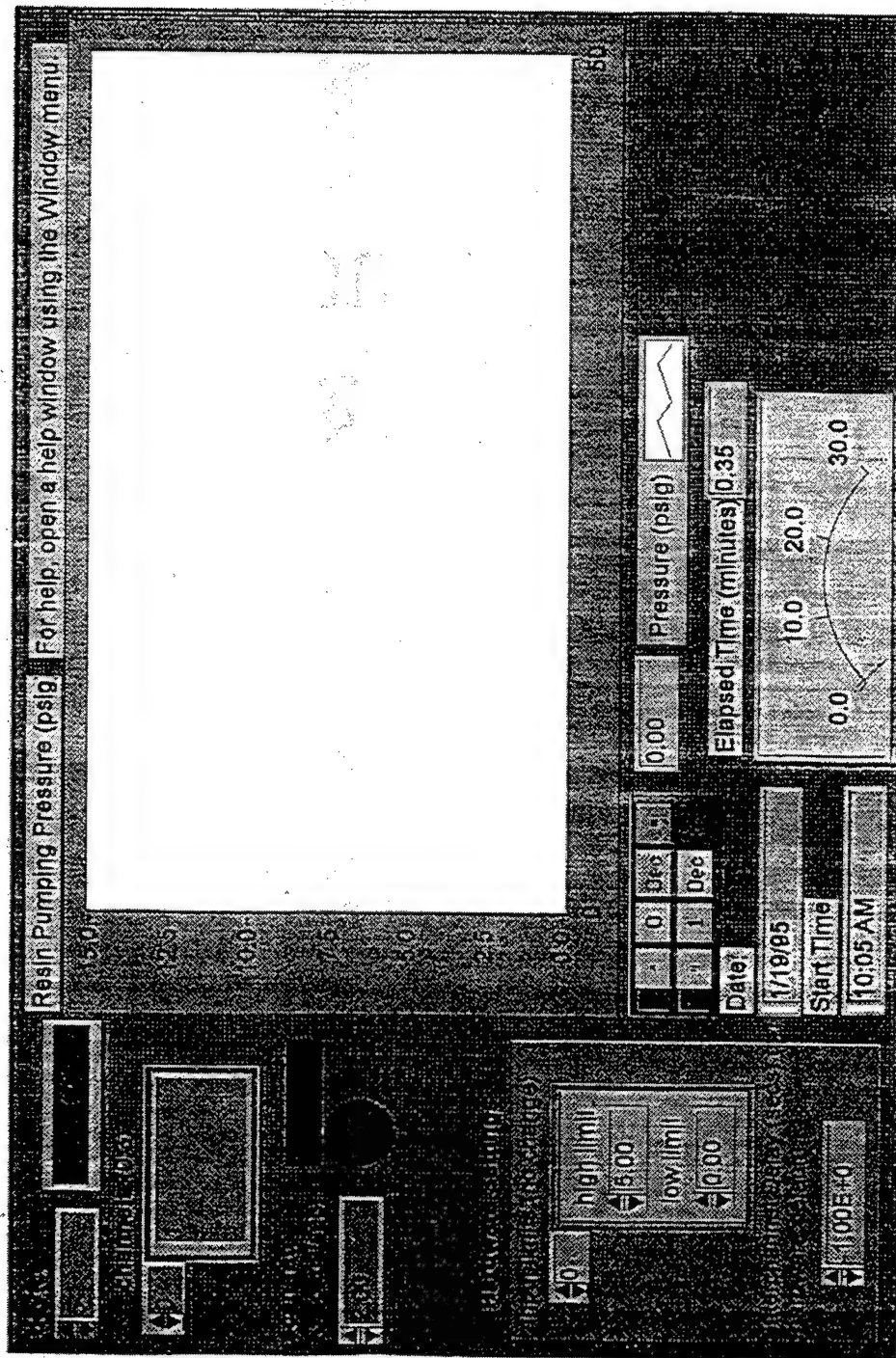


Figure 2-13 Labview User Interface for Resin Injection

predicated on the need to predict the flow pattern but also to determine what, if any, effects significantly influence the system. In order to simulate these effects, certain manipulations were done during the  $N_2$  gas infiltration. As the control, the first set of 10 panels was fabricated with no changes in the system. The second set of 10 panels was used to determine the effect of removing the cover after each procedure. Thus, for each panel of the second set,  $N_2$  gas tests using all four configurations were performed when the preform was initially placed into the mold, similar to the first set, and then the tests were reiterated after removing and replacing the cover plate. Theoretically, the removal of the acrylic cover allowed the preform in the mold to relax and reposition itself microscopically, thus, altering the flow pattern of the  $N_2$  gas and the resin mixture. A third set of panels was used to verify any results and theories regarding the pattern of flow.

All data collected during these trials were used in an effort to establish a pattern that could discern certain characteristics. First, a pattern indicating skewed resin flow was the ultimate goal. The primary purpose of the research is to relate a non-reactive fluid flow in the mold to the flow of the resin. Based on the data accumulated from the first two sets, it was evident that some pattern or correlation between the gas flow and resin flow could be established, either through statistical analysis or a discernible or derived pattern exhibited in the system. From this, it was hoped that a clear range of flow rate values or distinct flow phenomena would emerge and define a pattern of behavior in the mold which could subsequently be related to the resin flow.

Some of the underlying goals were to establish the effect of allowing the preform to relax and reform and the effectiveness of shifting the fabric, and how these slight modifications altered the flow of the  $N_2$  gas and the resin mixture flow pattern. These observations may eventually allow for pre-process modification to mitigate for race tracking.

## **2.11 Material Properties**

It is necessary to ensure that the panels produced have satisfactory physical and mechanical properties. This serves as a validating process for the data collected during the experiments. Selected physical and mechanical properties were measured. The physical properties are the specific gravity, fiber volume, and void content. The mechanical properties studied are the compression strength and the inter-laminar shear strength. The methods used to determine the material properties are discussed.

### **2.11.1 Specific Gravity, Fiber Volume and Void Content**

The fiber content of the reinforced resin composites was determined by the acid digestion method. In this test, the resin matrix is digested in a concentrated nitric acid solution. The void content can also be calculated using this method and the concept of constant volume. The density was first determined using *Test for Specific Gravity and Density of Plastics by Displacement* (ASTM D792-66). Once the density of each specimen was determined, the fiber content was evaluated from weight to volume ratio.

The test specimen consisted of 1.00 in. by 0.750 in. squares cut from a flat laminate having a  $0^\circ$  unidirectional fiber orientation, and a thickness of 0.100 in. Each specimen had a weight ranging from 2.250 g to 2.500 g in order to provide enough fibers



for the test and guard against a large error due to the loss of fibers during the test. All edges of the specimen were sanded until they were smooth to prevent air bubbles from being trapped inside of the specimen, thus, allowing for an accurate calculation of density. The specimens were also cleaned with acetone to rid them of any impurities that would interfere with the data.

The panel was divided into sections and samples taken from each region. Figure 2-14 shows a typical panel with the locations from which the acid digestion samples were cut. Each specimen was weighed and the density calculated per ASTM D792-66. The fiber volume and void content was determined as follows: The specimens were placed in separate flasks containing 30 ml. of 70% nitric acid to digest the epoxy resin. They were fit with reflux condensers and placed in a water bath at 75 °C. When the digestion was complete, the remaining fibers were filtered in crucibles and washed several times with distilled water and once with acetone. The crucibles containing the fibers were placed in an oven at 100 °C for 1 hour to remove the moisture. The crucibles were then weighed to determine the weight of the fibers by subtracting the empty crucible weight prior to the test from the crucible containing the fibers after the test. The fiber volume and void content are then calculated given the densities of the composite, the fiber, and the resin. The results are presented in the next Chapter.

### **2.11.2 Compression Test**

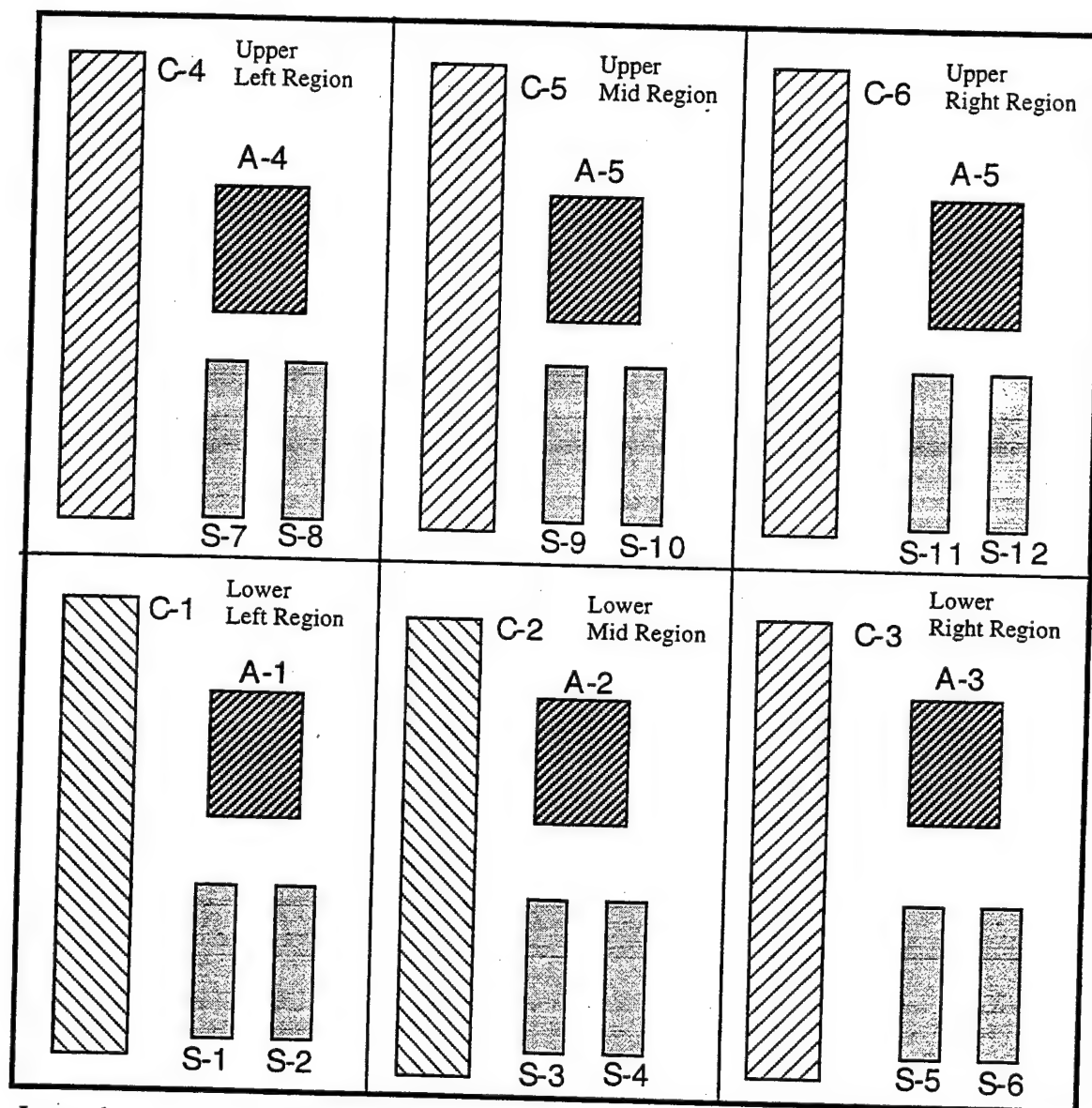
Axial compression is usually done by end loading or shear loading. Due to the sensitivity of the failure modes, shear loading through bonded tabs is usually used for composite materials. The compressive load is applied by shear as it acts along the wedge grips. The tests were conducted according to ASTM D3410-87 test standards. The Modified IITRI Test Specimen and Test Fixture was used in this study (Figure 2-15).

The modified IITRI test specimen with tapered cross-ply glass / epoxy tabs was used for this study. These 0° unidirectional-fiber specimens have a nominal width of 0.750 in., a thickness of 0.142 in., and an unsupported gauge length of 1.00 in. Specimens were taken from six regions of each composite panel. Figure 2.14 shows how a typical panel was divided into regions. The six regions are:

1. Lower Left
2. Lower Middle
3. Lower Right
4. Upper left
5. Upper Middle
6. Upper Right

The six specimens were strain-gauged in the axial direction on one side, and the transverse on the other face. The specimens were tested in compression using the IITRI test fixture in a uniaxial testing machine. A displacement-controlled load was applied at a constant strain rate of 0.02 in./min. The stroke displacement load, and strains were recorded at 2-second intervals with an automatic data acquisition system. Each specimen was tested to failure. The Young's modulus, Poisson ratio and the ultimate compressive strength were determined for each test. The results are provided in the next chapter.

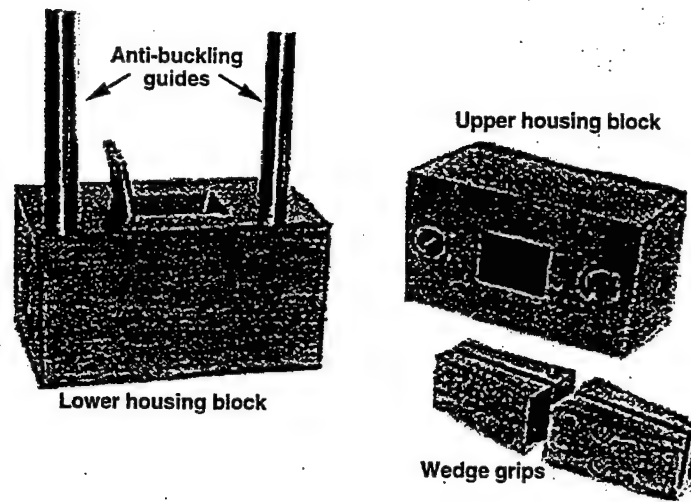




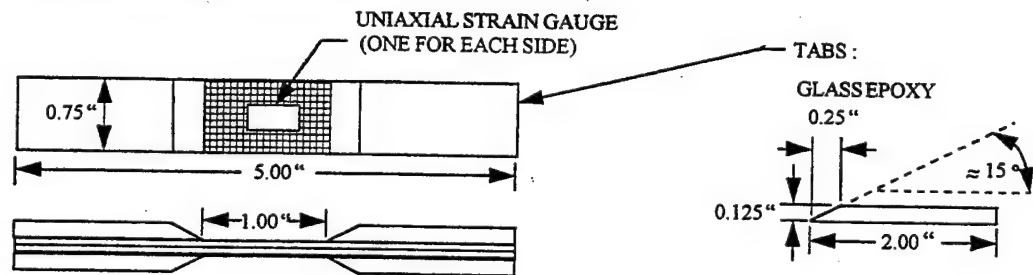
Legend:

- C - Compression Test Specimen
- S - Short Beam Shear Test Specimen
- A - Acid Digestion Test Specimen

Figure 2-14 Panel showing Test Sample Regions for Tests



# **COMPRESSION SPECIMEN\*\***



**\*\*ASTM D3410**

**Figure 2-15 Modified IITRI Compression Test Fixture and Test Specimen**

### 2.11.3 Transverse Short-Beam Shear Testing

The shear strength is usually determined by the interply strength of parallel fiber reinforced plastics. The data collected cannot be used as design criteria, but used for comparative testing of composites if all failures are in horizontal shear. Horizontal shear occurs when cracks appear in the resin matrix of the composite causing delamination. These shear tests were performed according to ASTM D2344-84. Figure 2-16 shows the test specimen and fixture. The test fixture consists of two 0.125 in diameter dowel pins that are fixed on the lower half of the test fixture. These pins can slide horizontally to accommodate the span required for the test. The top half of the fixture is fitted with a 0.250-in. diameter dowel pin. The two halves are aligned by two longer dowel pins that stick up from the lower half and slide into ball bearing sleeves fixed in the top half of the test fixture.

The specimens are short beams cut from a flat laminate having 0° unidirectional fiber orientation. They have a thickness of approximately 0.100 in. Figure 2-14 also shows the regions where the test specimens were cut from. Since the composite panels were constructed of a plain weave textile graphite fabric, some modifications were made to the test specimen and setup. The specimens were limited by the span length to thickness and specimen length to thickness ratios based upon the type of filaments used as reinforcement, the Young's modulus, and mode of failure. Since delamination must occur horizontally between the plies of the reinforcement material, through trial and error, the span was changed to 0.60 in. and the length of the specimen was changed to 0.8 in. 10 specimens were tested; of approximate dimensions 0.250 in. x 0.800 in. x 0.100 in.

The test specimen is placed and centered across the two smaller dowel pins. The top half slides down so that the top dowel pin touches approximately the center point of the test specimen. The specimen is then loaded at a rate of 0.050 in./min. until failure occurs. The breaking load and the inter-laminar shear strength are determined.

### 2.12 Non-Destructive Evaluation

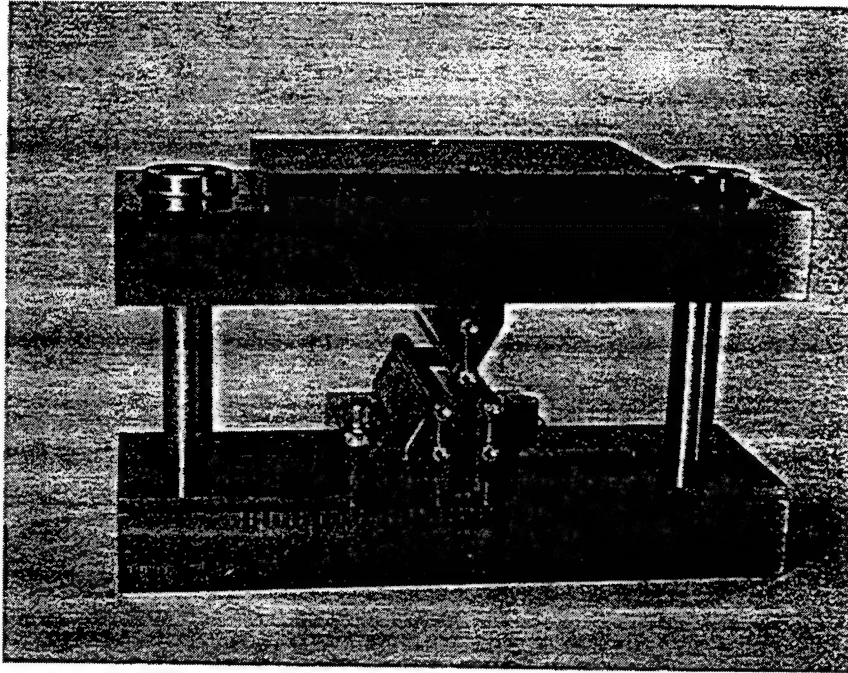
All the above tests involve the destruction of the material and require tremendous amounts of time. A faster approach was explored by means of non-destructive evaluation. The idea was that if we were able to obtain data from a non-destructive test and if that data could be related to the material properties, then it would be easier to determine the respective properties without going through all the destructive steps.

Ultrasonic testing was selected as the method of choice to non-destructively evaluate the part and to indirectly obtain the pertinent properties. A disturbance at the end of a solid travels through the solid in a finite time as a result of vibrations of the molecules, atoms or particles present. Ultrasonics refers to these vibration waves above the audible range. Discontinuities or defects cause scattering and reflection of the waves, and the detection of the reflected or transmitted waves permits the defect to be located. Our idea is to explore the possibility of using the ultrasonic technique to detect microvoid content in the panels.

## SHORT BEAM SHEAR TEST FIXTURE (ASTM D 2344)

MODEL NO. CU-SB (LOW CARBON STEEL)

MODEL NO. WTF-SB (17-4PH STAINLESS)



Assembled Fixture with Specimen in Place

An assembled short beam shear test fixture is shown in the above photograph, with a typical test specimen mounted in it. This fixture is commonly used to test composite materials in interlaminar (through-the-thickness) shear, in general accordance with ASTM Standard D 2344

Figure 2-16 Test Fixture and Sample for Short Beam Shear Test

Several factors affect the results of the ultrasonic test. Figure 2-17 shows schematics of the Pulse-Echo (PE) and the Through-Transmission (TT) methods through a solid with a defect. The PE method uses a Transmitter/Receiver (T/R) transducer while the transmission method uses two separate transducers to receive the signals. The transmission method is used when small defects are present which do not give adequate reflection signals. Furthermore, the TT method is quite common and often used for thin sheets since the PE test creates a dead zone effect for thin sections. Thus, the TT method is used to obtain the signal data for the non-destructive evaluations.

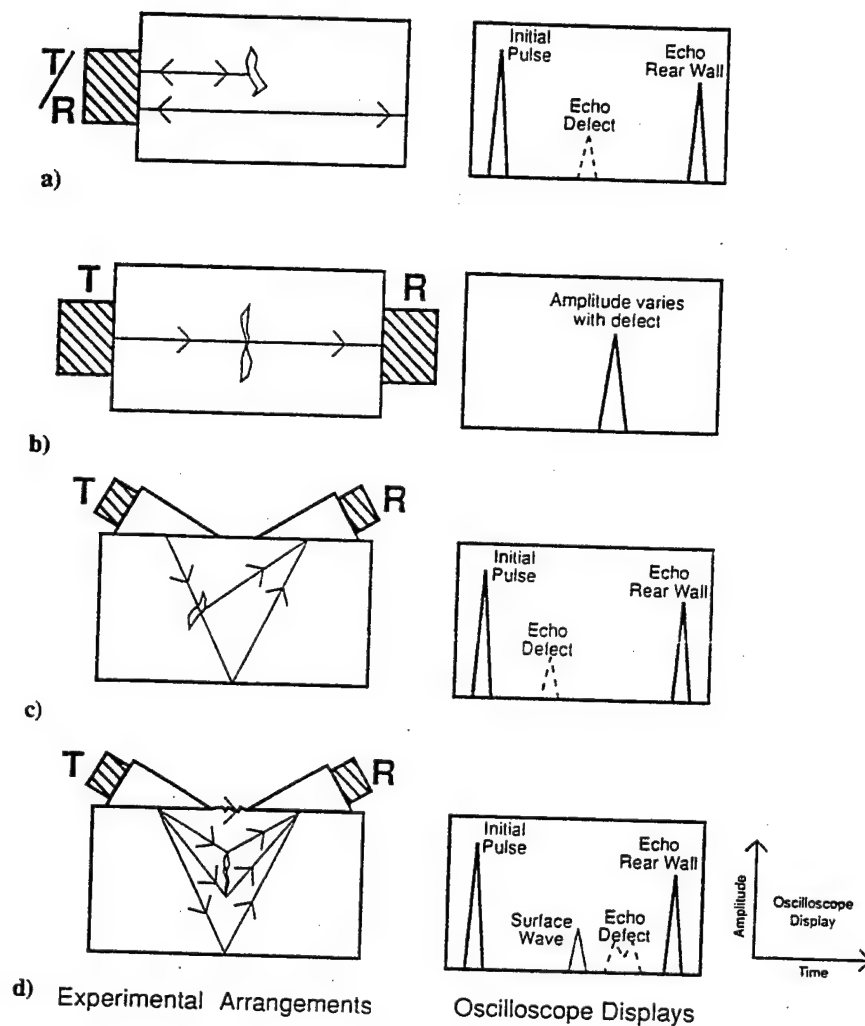
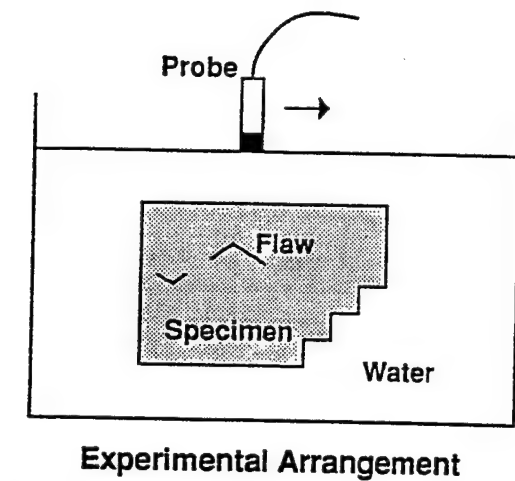
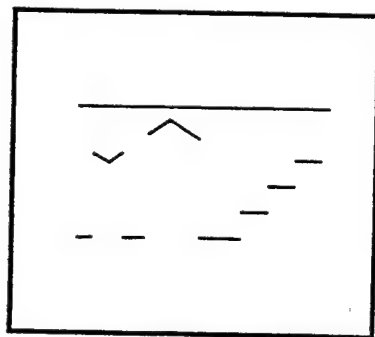


Figure 2-17 Schematics of Pulse-Echo and Through-Transmission Methods

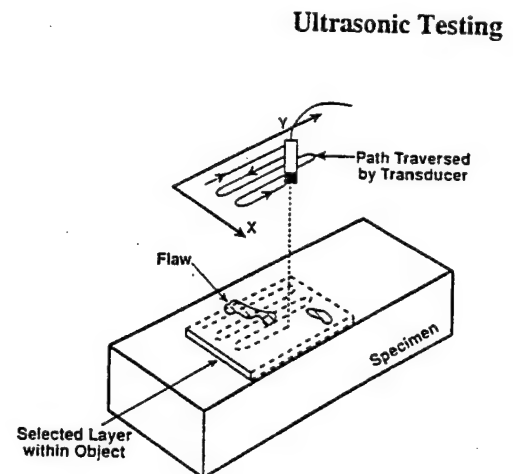
Since this is exploratory research, the frequency of transmission which provides the most reliable results will be sought. Frequencies ranging from 1 to 10 MHz were explored. A coupling medium is usually used to provide a suitable sound path between the transducer and the test surface to increase the transmission of the ultrasound pulse energy. We have used both water and air as couplants in for comparison. The part may be completely immersed in water or provided as squirt between the transducer and the surface. The transducers are made of piezoelectric single crystals of  $\alpha$ -quartz.



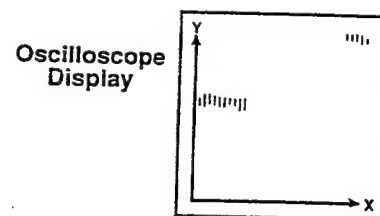
(a)



(b)



(a)



(b)

Figure 2-18 Schematics of Pulse-Echo Display Systems

The ultrasonic echoes can be displayed in several modes, providing one-, two- or three-dimensional data. In the A-Scan method the pulse circuit and the data acquisition system (oscilloscope) time-base are usually synchronized by a pulse from a timer-trigger circuit. A schematic is presented in Figure 2-18a. The horizontal sweep depends on time; the vertical amplitude depends on the signal from the probe. The emitted pulse and the later reflections are used to determine the distance from the flaw and the size. The B-Scan method (Figure 2-18b) is a series of plots of the A-Scan signal, obtained by moving the probe along an axis to provide a 2-dimensional view of the flaws present. The C-Scan method also involves a series of A-Scan results obtained in a plane, thus, providing 3-dimensional data. In the C-Scan (Figure 2-18c) the pulse echoes are restricted to those returning during a fixed time interval. The echo pattern will be from discontinuities at a specific level of the object.

## CHAPTER 3

### RESULTS AND OBSERVATIONS

The experimental procedures, the mold preparation method, the data acquisition procedure and the setup have been discussed in the previous chapter. The airflow through each port and the inlet pressure when the mold is probed with the gas are monitored. The resin flow front and the back pressure during the resin injection are also monitored. This chapter presents sample data and calculated results. Complete data are provided in the Appendices.

#### 3.1 Nitrogen Flow Data

The first step in the investigation was to relate all observations to the resin flow phenomena. The overall purpose was to somehow relate the flow of the gas to the flow pattern of the resin. The prediction method relies on the gas flow rates through each port. Sample data and the derivatives are presented below.

##### 3.1.1 Raw Nitrogen Flow Rates

Table 3.1 shows samples of the raw readings ( $q_i$ ) obtained from the flow meters. Zero is recorded for any ports closed during a particular run. The procedure is discussed in Section 2.8. The table also shows the pressure at which the gas enters the mold. Since precise valve control is not easy, the same pressure level was not possible for each experiment, and slight variations are seen. Appendix A contains the complete data set for the raw nitrogen flow rates.

##### 3.1.2 Normalized Flow Rates

In order to facilitate comparisons among tests and compensate for slightly different inlet pressures, all flow data were normalized with the average flow rate through all 7 ports for the particular trial. The resulting value was used as a dividend with the divisor being the data value received from the respective flow port. Thus, data are transformed as follows:

$$Q_i = q_i / q_{avg}$$

where  $Q_i$  = Normalized flow rate through the  $i^{\text{th}}$  port  
 $q_i$  = Flow rate through the  $i^{\text{th}}$  port (slm)  
 $q_{avg}$  = Average flow rate through all ports (slm)

Gas flow rates (raw data in Table 3-1) are automatically normalized as the reading is completed, as seen in Table 3-2. The data are assembled in Appendix B. The ensuing analyses make use of the normalized flows ( $Q_i$ ).

##### 3.1.3 Gas Flow Parameter

The initial step was to analyze the flow pattern displayed by the resin and compare that to the flow pattern of the  $N_2$  gas prior to the resin injection. The next task was to assemble the normalized flow data into a logical grouping that would facilitate the discovery of any patterns or trends.

Table 3-1: Raw N<sub>2</sub> Flow Rates (q<sub>i</sub>) - standard liters per minute

Plate ID: S1P1	Port #1	Port #2	Port #3	Port #4	Port #5	Port #6	Port #7	Pressure (psig)
No ports closed	2.101	1.028	3.925	3.745	2.795	3.500	2.681	4.620

Plate ID: S1P2	Port #1	Port #2	Port #3	Port #4	Port #5	Port #6	Port #7	Pressure (psig)
No ports closed	2.791	1.000	3.584	3.180	2.450	4.392	2.858	2.940

Plate ID: S1P6	Port #1	Port #2	Port #3	Port #4	Port #5	Port #6	Port #7	Pressure (psig)
No ports closed	1.793	1.316	1.252	2.616	2.082	3.829	2.473	2.710
Top ports closed	1.985	1.978	2.503	2.729	0.000	0.000	0.000	2.640
Lower ports closed	0.000	1.280	1.379	0.000	1.968	4.076	2.800	2.620
Side ports closed	0.000	0.000	0.000	0.000	2.565	5.215	3.689	2.710

Plate ID: S2P1	Port #1	Port #2	Port #3	Port #4	Port #5	Port #6	Port #7	Pressure (psig)
No ports closed	0.737	0.726	1.122	2.526	1.537	1.507	1.076	1.860
Top ports closed	1.339	2.608	2.688	3.597	0.000	0.000	0.000	2.040
Lower ports closed	0.000	1.207	1.689	0.000	3.364	2.513	2.198	2.050
Side ports closed	0.000	0.000	0.000	0.000	4.518	2.742	2.937	2.130

Plate ID: S2P2	Port #1	Port #2	Port #3	Port #4	Port #5	Port #6	Port #7	Pressure (psig)
No ports closed	2.158	1.125	1.563	3.114	1.354	1.961	1.912	3.590
Top ports closed	2.143	2.411	2.756	2.963	0.000	0.000	0.000	3.390
Lower ports closed	0.000	1.720	2.062	0.000	2.114	2.934	2.716	3.920
Side ports closed	0.000	0.000	0.000	0.000	3.362	3.779	3.889	4.060

Readings from selected ports and combinations were used to check how they corresponded to the flow patterns of the resin. The chosen combinations, given in Table 3-3, were primarily based on the port location. The left side of the mold was represented quantitatively by the average of the normalized flows through combinations of the left side ports (1, 2 and 5). Similarly, the right side was represented by the average of the normalized flows through combinations of right side ports (3, 4, and 7). We define the gas flow parameter  $P_L$  and  $P_R$  as follows:

$$\begin{aligned}
 P_L &= \text{Avg. } (Q_1, Q_2, Q_5) \text{ if no ports are closed} \\
 &= \text{Avg. } (Q_1, Q_2) \text{ if top ports are closed} \\
 &= \text{Avg. } (Q_2, Q_5) \text{ if lower ports are closed} \\
 &= (Q_5) \text{ if side ports are closed} \\
 P_R &= \text{Avg. } (Q_3, Q_4, Q_7) \text{ if no ports are closed} \\
 &= \text{Avg. } (Q_3, Q_4) \text{ if top ports are closed}
 \end{aligned}$$



Table 3-2: Normalized  $N_2$  Flow Rates ( $Q_i$ )

Plate ID: S1P1	Avg. flow	Port #1	Port #2	Port #3	Port #4	Port #5	Port #6	Port #7
No ports closed	2.825	0.744	0.364	1.389	1.326	0.989	1.239	0.949

Plate ID: S1P2	Avg. flow	Port #1	Port #2	Port #3	Port #4	Port #5	Port #6	Port #7
No ports closed	2.894	0.964	0.346	1.238	1.099	0.847	1.518	0.988

Plate ID: S1P6	Avg. flow	Port #1	Port #2	Port #3	Port #4	Port #5	Port #6	Port #7
No ports closed	2.195	0.817	0.600	0.571	1.192	0.949	1.745	1.127
Top ports closed	1.314	1.511	1.506	1.905	2.077	0.000	0.000	0.000
Lower ports closed	1.643	0.000	0.779	0.839	0.000	1.198	2.480	1.704
Side ports closed	1.639	0.000	0.000	0.000	0.000	1.566	3.183	2.252

Plate ID: S2P1	Avg. flow	Port #1	Port #2	Port #3	Port #4	Port #5	Port #6	Port #7
No ports closed	1.319	0.559	0.551	0.851	1.916	1.165	1.143	0.816
Top ports closed	1.462	0.916	1.784	1.839	2.461	0.000	0.000	0.000
Lower ports closed	1.516	0.000	0.796	1.114	0.000	2.219	1.420	1.450
Side ports closed	1.457	0.000	0.000	0.000	0.000	3.101	1.883	2.016

Plate ID: S2P2	Avg. flow	Port #1	Port #2	Port #3	Port #4	Port #5	Port #6	Port #7
No ports closed	1.884	1.146	0.597	0.829	1.653	0.719	1.041	1.015
Top ports closed	1.468	1.460	1.643	1.878	2.019	0.000	0.000	0.000
Lower ports closed	1.650	0.000	1.043	1.250	0.000	1.282	1.779	1.647
Side ports closed	1.576	0.000	0.000	0.000	0.000	2.134	2.398	2.468

= Avg. ( $Q_3$ ,  $Q_7$ ) if lower ports are closed

= ( $Q_7$ ) if side ports are closed

Thus, if any port is closed, its corresponding flow rate becomes zero and the remaining ports are used to evaluate  $P_L$  and  $P_R$ . In all instances, port 6 was considered a separate entity. The importance of port 6 has not been ignored, but its relevance in prediction of the resin flow pattern has not been determined at this stage. The complete data for the test panels are provided in Appendix C.

### 3.2 Resin Flow Data

Next, the resin flow front was recorded, to determine any correlation with the gas flow data. In each case, the resin flow front was traced manually at  $\frac{1}{2}$  to 1-minute intervals on transparent cellophane sheeting placed on the acrylic top during the actual resin impregnation. The hand-traced flow fronts were then digitized with a scanner. This image was vectorized and converted to a series of X, Y coordinate points along each flow line.

Table 3-3: Gas Flow Parameter ( $P_L$ ,  $P_R$ )

	$P_L$	$P_R$	$P_L$	$P_R$	$P_L$	$P_R$	
<i>Plate ID: SIP1</i>	<i>Ports</i> 1+2+5	<i>Ports</i> 3+4+7	<i>Ports</i> 2+5	<i>Ports</i> 3+7	<i>Ports</i> 1+2	<i>Ports</i> 3+4	<i>Port #6</i>
No ports closed	0.699	1.221	0.677	1.169	0.554	1.358	1.239

<i>Plate ID: SIP2</i>	<i>Ports</i> 1+2+5	<i>Ports</i> 3+4+7	<i>Ports</i> 2+5	<i>Ports</i> 3+7	<i>Ports</i> 1+2	<i>Ports</i> 3+4	<i>Port #6</i>
No ports closed	0.719	1.108	0.596	1.113	0.655	1.169	1.518

<i>Plate ID: SIP6</i>	<i>Ports</i> 1+2+5	<i>Ports</i> 3+4+7	<i>Ports</i> 2+5	<i>Ports</i> 3+7	<i>Ports</i> 1+2	<i>Ports</i> 3+4	<i>Port #6</i>
No ports closed	0.789	0.963	0.774	0.849	0.708	0.881	1.745
Top ports closed	1.006	1.328	0.753	0.953	1.509	1.991	0.000
Lower ports closed	0.659	0.848	0.988	1.272	0.389	0.420	2.480
Side ports closed	0.522	0.751	0.783	1.126	0.000	0.000	3.183

<i>Plate ID: S2P1</i>	<i>Ports</i> 1+2+5	<i>Ports</i> 3+4+7	<i>Ports</i> 2+5	<i>Ports</i> 3+7	<i>Ports</i> 1+2	<i>Ports</i> 3+4	<i>Port #6</i>
No ports closed	0.758	1.194	0.858	0.833	0.555	1.383	1.143
Top ports closed	0.900	1.433	0.892	0.919	1.350	2.150	0.000
Lower ports closed	1.005	0.855	1.508	1.282	0.398	0.557	1.420
Side ports closed	1.034	0.672	1.551	1.008	0.000	0.000	1.883

<i>Plate ID: S2P2</i>	<i>Ports</i> 1+2+5	<i>Ports</i> 3+4+7	<i>Ports</i> 2+5	<i>Ports</i> 3+7	<i>Ports</i> 1+2	<i>Ports</i> 3+4	<i>Port #6</i>
No ports closed	0.820	1.116	0.658	0.922	0.871	1.241	1.041
Top ports closed	1.034	1.299	0.821	0.939	1.552	1.948	0.000
Lower ports closed	0.775	0.996	1.162	1.448	0.521	0.625	1.779
Ports 1 - 4 closed	0.711	0.823	1.067	1.234	0.000	0.000	2.398

The numerical coordinates of the flow fronts were transcribed into a spreadsheet, which recreated each flow front in graphical form. Examples are seen in Figures 3-1 to 3-3, and the complete data are provided in Appendix D.

### 3.2.1 Flow Front Height Ratios

Race tracking occurs when the flow fronts at the sides of the mold run significantly ahead of the central front. Thus, data that reflect the relative positions of the flow front with respect to time could be helpful in characterizing the front. Figure 3-4 shows the schematic of a flow front. The relative change of the flow front location may be determined by the following three ratios:

1. Change in height to central height ( $\Delta H(t) / H_m(t)$ )
2. Height to central height ( $H(t) / H_m(t)$ )
3. Change in height to change in central height ( $\Delta H(t) / \Delta H_m(t)$ )

Sample plots of these ratios for each side of the flow front are seen in Figures 3-5 to 3-7. The data generated for each run are stored for analysis.

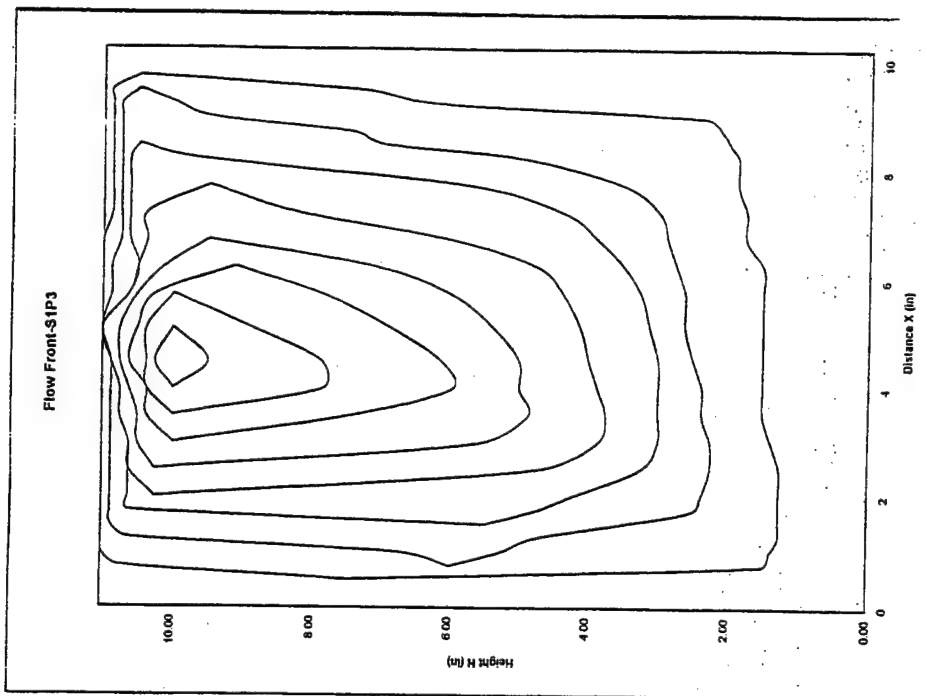
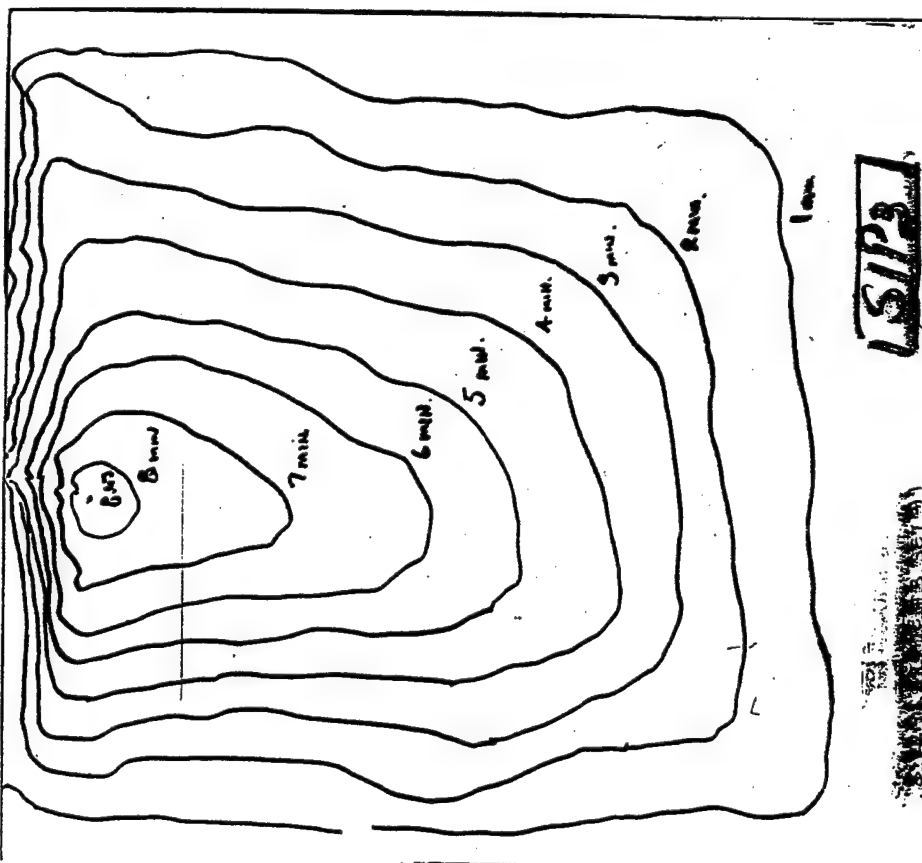


Figure 3-1 Traced and Corresponding Digitized Flow Front - Sample 1

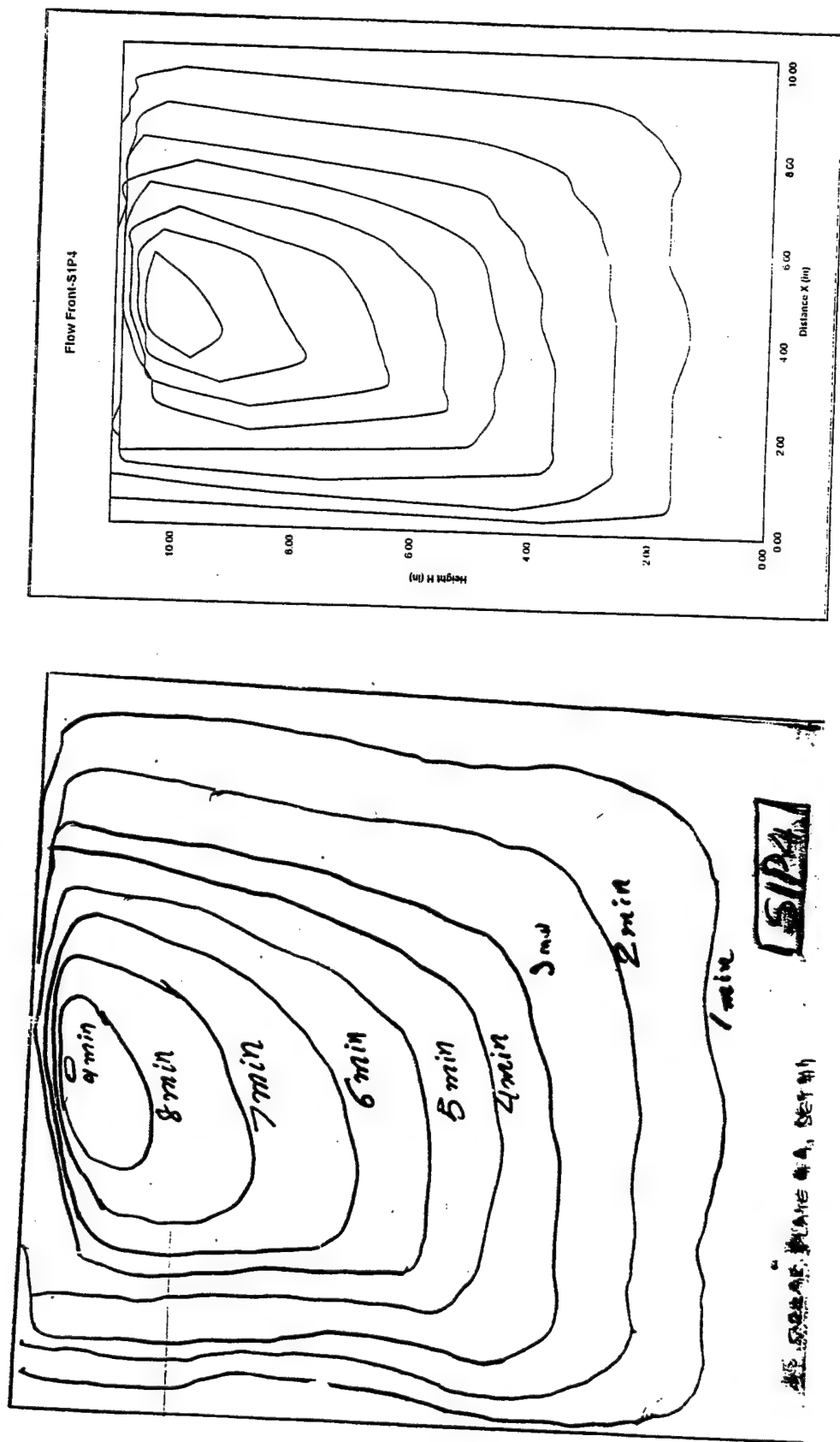


Figure 3-2 Traced and Corresponding Digitized Flow Front - Sample 2

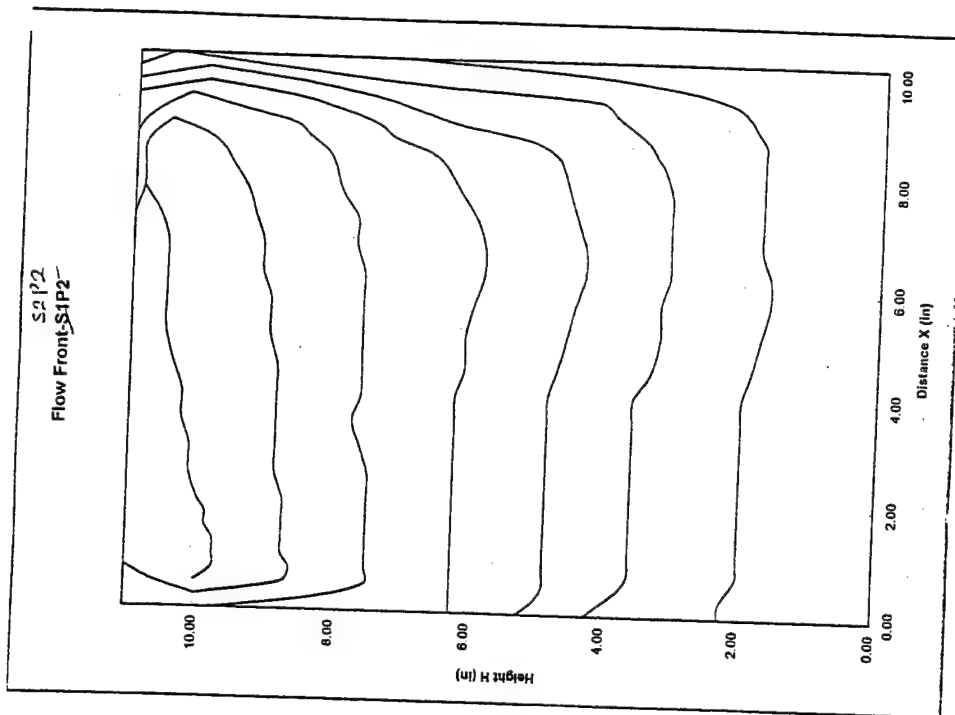
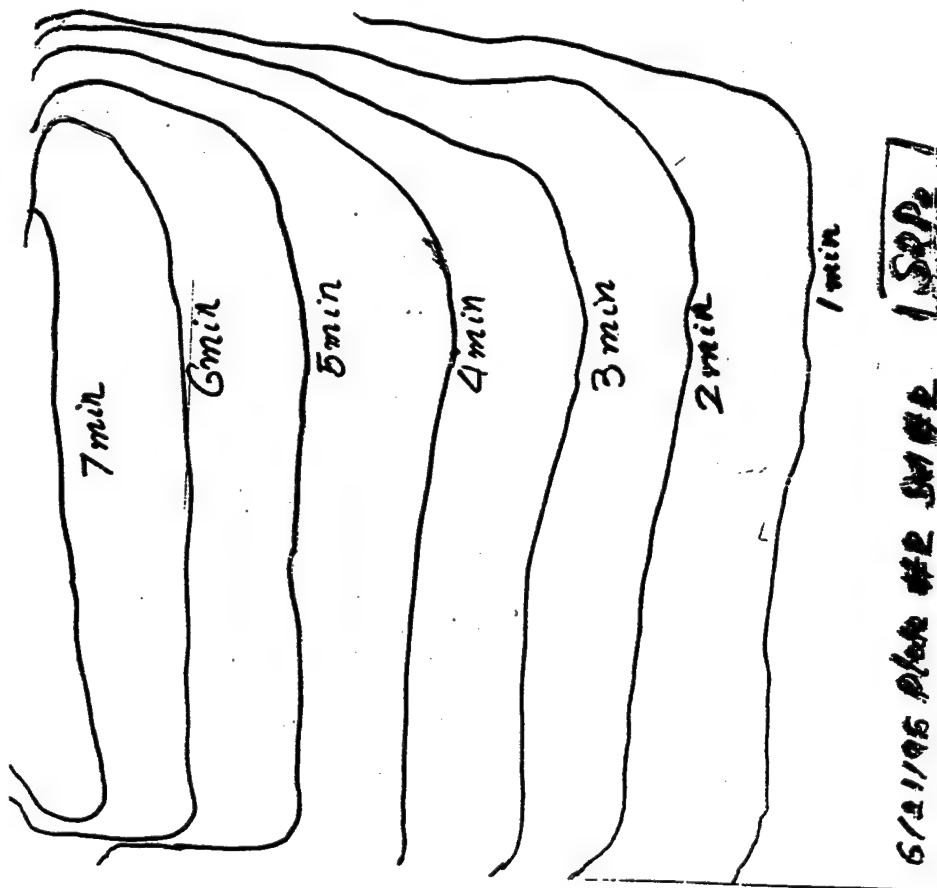


Figure 3-3 Traced and Corresponding Digitized Flow Front - Sample 3

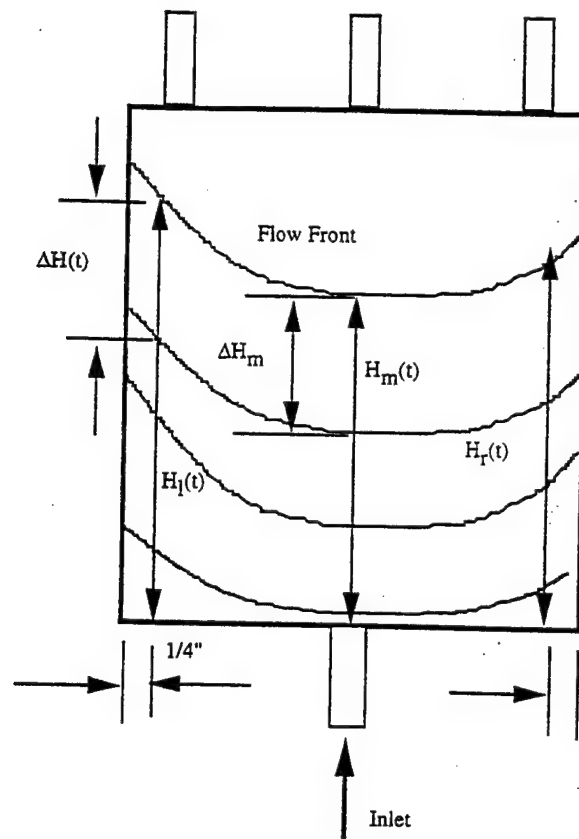


Figure 3-4 Schematic of a Flow Front

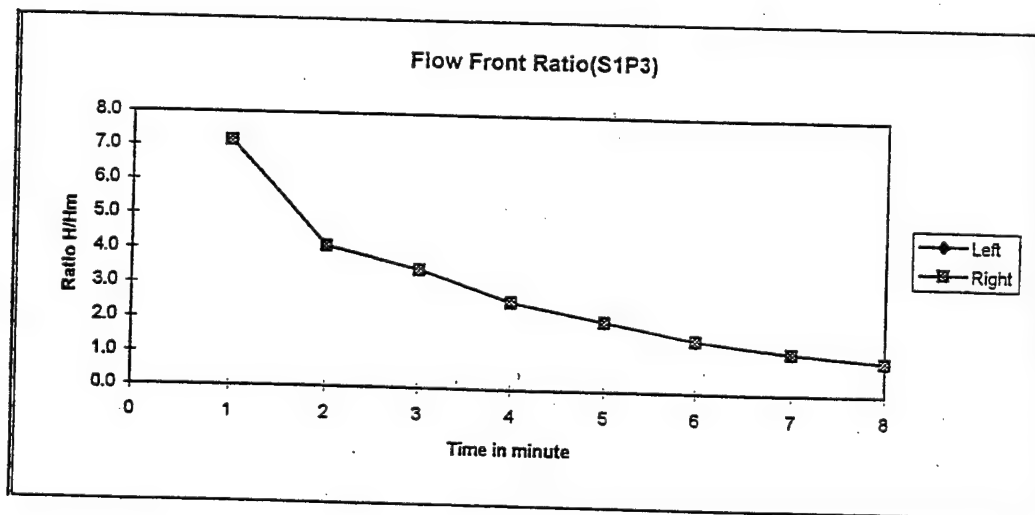


Figure 3-5 Plots of Flow Front Height Ratios - Sample 1

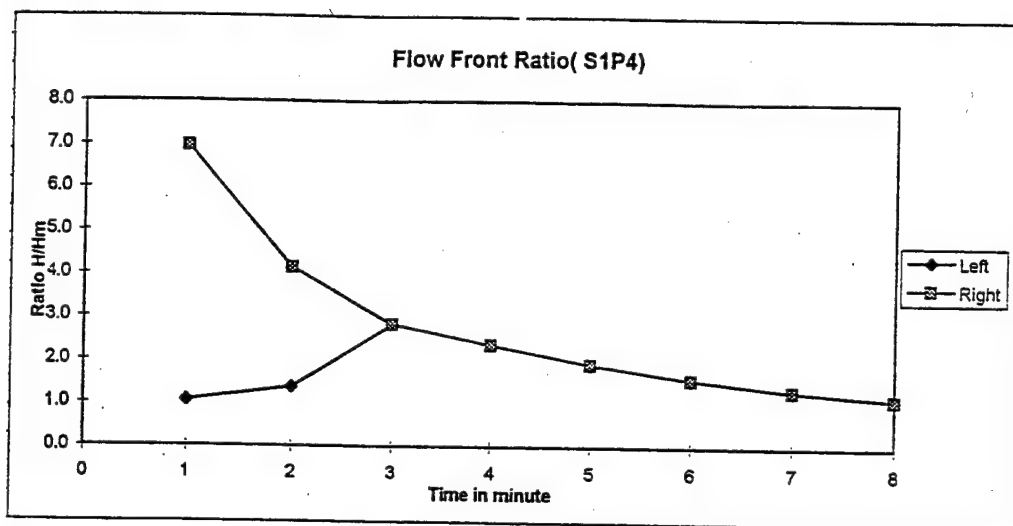


Figure 3-6 Plots of Flow Front Height Ratios - Sample 2

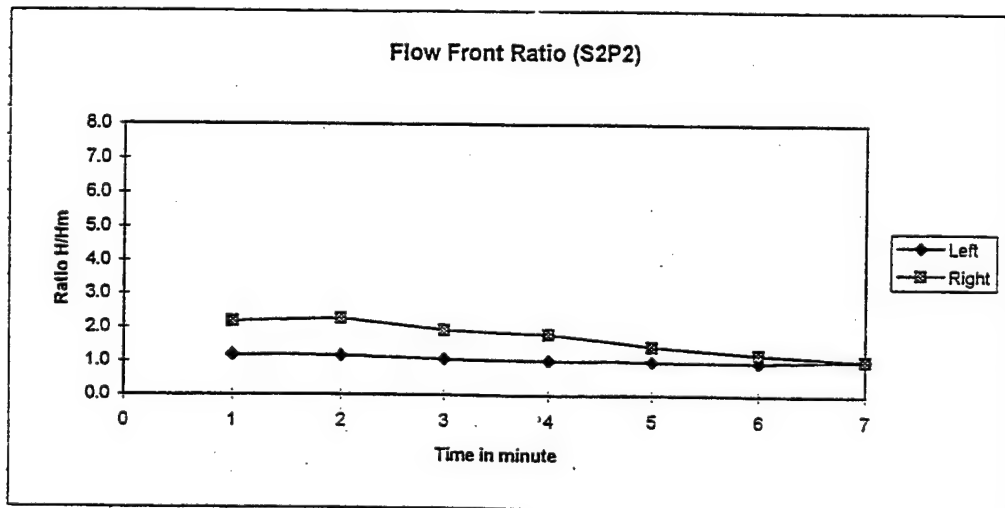


Figure 3-7 Plots of Flow Front Height Ratios - Sample 3

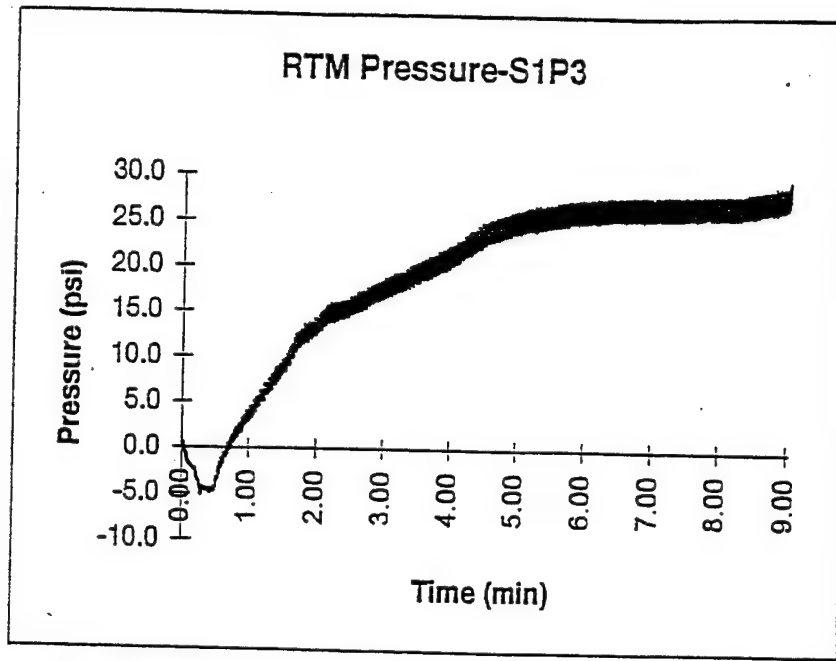


Figure 3-8 Plot of Inlet Pressure versus Time - Sample 1

### 3.2.2 Back Pressure

From the initial experiments, the rise in the resin back pressure was expected. The back pressure as recorded by the pressure transducer is sent to the data acquisition system and plotted. Typical plots are shown in Figures 3-8 to 3-10. The dynamic behavior of the system may be characterized through the analysis of the pressure data.

## 3.3 Material Properties

### 3.3.1 Compression Test

A typical example of data showing the Young's modulus, Poisson's ratio, and ultimate compressive strength are listed in Table 3-4. Six tests were performed for each panel. A sample was taken from each region of the panel as discussed in Section 2.11. Figure 3-11 shows a typical compressive stress-strain diagram. The maximum load prior to failure was used to calculate the ultimate compressive strength. The slope of the axial stress-strain curve was used to calculate the Young's Modulus and the ratio of the slopes of the transverse stress-strain curve and the axial stress-strain curve was used to determine the Poisson's ratio. The average Young's modulus, Poisson's ratio, and ultimate compressive strength for all ten panels are listed in Table 3-5.

$$F_{cu} = \frac{P_{\max}}{A}$$

$$E_a = \frac{\sigma_a}{\epsilon_a}$$

$$\nu_c = \frac{\Delta \epsilon_t}{\Delta \epsilon_a}$$



### RTM Pressure-S1P4

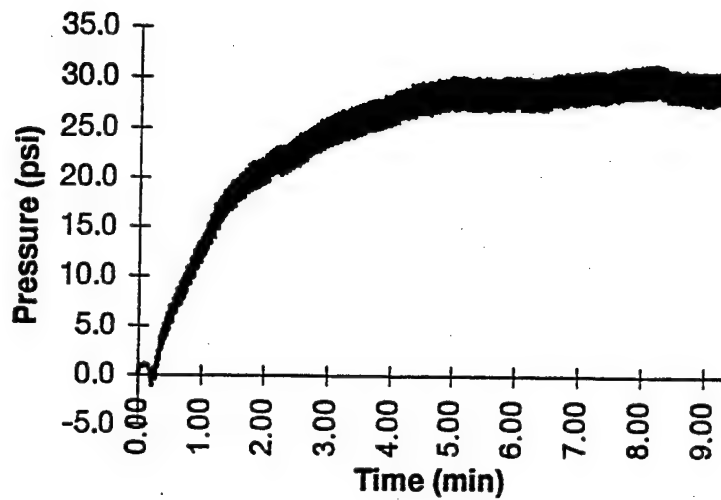


Figure 3-9 Plot of Inlet Pressure versus Time - Sample 2

### RTM Pressure-S2P2

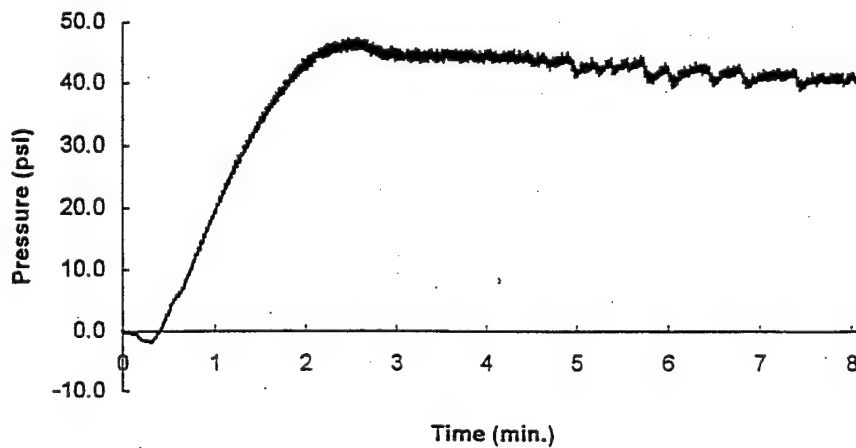


Figure 3-10 Plot of Inlet Pressure versus Time - Sample 3

Table 3-4: Compressive Strength – Sample Test Results (S2P1)

Specimen No.	Young's Modulus (Msi)	Poisson's Ratio	Ultimate Compressive Strength (ksi)
S2P1-C1	6.105	0.062	52.38
S2P1-C2	6.258	0.059	57.04
S2P1-C3	7.819	0.166	61.20
S2P1-C4	8.796	0.179	36.78
S2P1-C5	4.251	0.013	20.69
S2P1-C6	2.754	0.005	31.11
Average	5.997 ± 1.782	0.081 ± 0.060	43.20 ± 12.87

Table 3-5: Average Compressive Strengths of Panels

Panel No.	Young's Modulus (Msi)	Poisson's Ratio	Ultimate Compressive Strength (ksi)
S1P2	6.622	0.073	52.82
S1P3	5.580	0.039	51.29
S1P9	7.030	0.073	50.40
S1P10	6.420	0.057	49.83
S2P1	5.997	0.081	43.20
S2P9	5.227	0.161	38.39
S3P1	6.095	0.061	49.29
S3P2	4.256	0.068	35.93
S3P5	4.962	0.100	36.69
S3P6	6.129	0.063	46.45
Average	5.832 ± 0.516	0.077 ± 0.020	45.43 ± 3.97

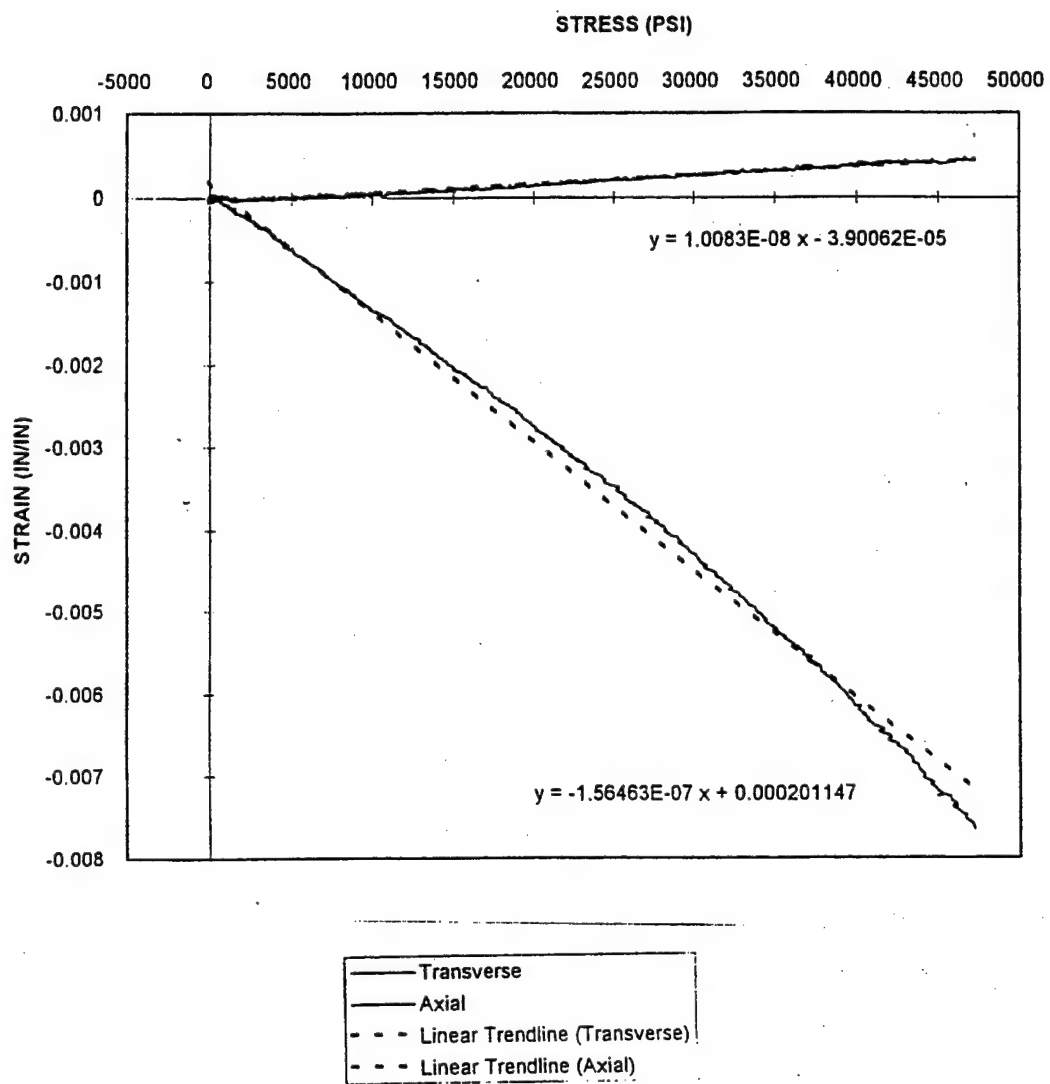


Figure 3-11 Typical Compressive Stress-Strain Diagram

Table 3-6: Shear Strength – Sample Test Results (S2P1)

Specimen No.	Thickness (in)	Width (in)	Breaking Load (lbf)	Shear Strength (ksi)
S2P1-S1	0.107	0.252	251.5	6.995
S2P1-S2	0.108	0.252	240.5	6.628
S2P1-S3	0.112	0.252	243.4	6.468
S2P1-S4	0.114	0.252	272.2	7.106
S2P1-S5	0.111	0.252	249.5	6.690
S2P1-S6	0.109	0.252	241.2	6.586
S2P1-S7	0.115	0.252	232.4	6.014
S2P1-S8	0.119	0.252	239.5	5.990
S2P1-S9	0.126	0.252	259.5	6.130
S2P1-S10	0.127	0.252	234.9	5.505
S2P1-S11	0.120	0.252	239.0	5.928
S2P1-S12	0.115	0.252	114.3	2.958
Average	0.115 ± 0.004	0.252 ± 0.000	234.8 ± 22.38	6.083 ± 0.617

### 3.3.2 Short-Beam Shear Test

The breaking load and shear strength of a typical specimen are listed in Table 3-6. Figure 3-12 shows a typical shear stress-strain diagram. The breaking load and cross-sectional area were used to calculate the shear strength. Shear strength varies between 3.679 ksi and 6.895 ksi. The average shear strength values for all 10 panels are listed in Table 3-7.

$$S_H = \frac{0.75 P_B}{A}$$

### 3.3.3 Specific Gravity, Fiber Volume Fraction and Void Content

A typical example of percent fiber weight and percent fiber volume is listed in Table 3-8. The weight of the fiber in the composite and the weight of the initial composite specimen were used to calculate the percent fiber weight. The fiber and composite densities were used to calculate the percent fiber volume. Percent fiber weight fraction varied between 44.47% and 57.80%. The average percent fiber weight and fiber volumes are listed in Table 3-9.

$$Fiber, wt\% = \left( \frac{W}{w} \right) \times 100$$

$$Fiber, vol\% = \left[ \left( \frac{W}{F} \right) / \left( \frac{w}{c} \right) \right] \times 100$$

S2P1-S4

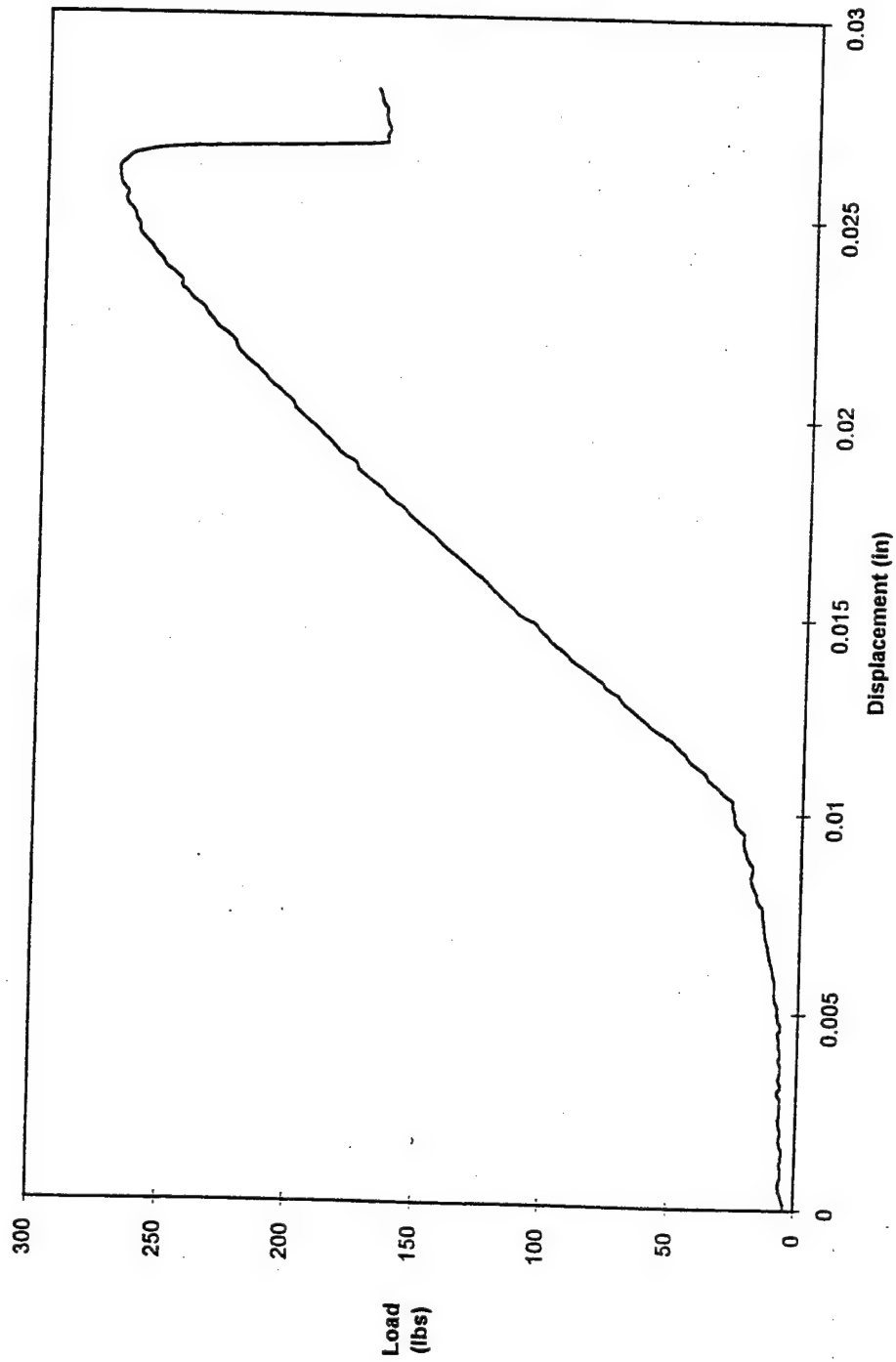


Figure 3-12 Typical Shear Stress-Strain Diagram

Table 3-7: Average Shear Strengths of Panels

Specimen No.	Thickness (in)	Width (in)	Breaking Load (lbf)	Shear Strength (ksi)
S1P2	0.106	0.252	233.9	6.289
S1P3	0.110	0.252	259.9	6.678
S1P9	0.114	0.252	268.4	6.551
S1P10	0.112	0.252	259.2	6.595
S2P1	0.115	0.252	217.4	5.302
S2P9	0.115	0.252	235.3	5.838
S3P1	0.143	0.249	345.4	6.895
S3P2	0.134	0.249	287.4	6.164
S3P5	0.131	0.250	172.0	3.679
S3P6	0.129	0.249	277.0	6.291
Average	0.121 ± 0.007	0.251 ± 0.001	255.6 ± 28.5	6.028 ± 0.584

The percent void content of S2P1 is listed in Table 3-10. The percent void content is obtained by subtracting the volume of the resin and fiber from the total volume of the composite. Values ranged from 0 % to 1.942 %. The average percent void content is listed in Table 3-11.

### 3.3.4 Ultrasonic Test Results

The C-Scan of each panel under consideration was obtained using the services of a third party. The amplitude of the signal was programmed to be color-coded and thus a 3-D color display system was plotted as the probe scans the surface of the panel. Figure 3-13 shows a typical example (S2P1) of the output of the system. These plots are obtained for each part before it was destructively tested to obtain the physical and the mechanical properties. The C-Scan results are provided in Appendix E. The colors are coded such that the darkest one represents 0% attenuation of the signal while the lightest one (white) represents 100% attenuation.

Table 3-8: Fiber Volume Fraction – Sample Test Results (S2P1)

Specimen. No	Crucible Weight (g)	Crucible & Fiber Weight (g)	Fiber Weight (g)	Composite Weight (g)	Composite Density (g/cm <sup>3</sup> )	Fiber Weight (%)	Fiber Volume (%)
S2P1-A1	35.80	37.11	1.311	2.411	1.435	54.38	43.61
S2P1-A2	35.57	36.88	1.307	2.598	1.402	50.31	39.40
S2P1-A3	35.80	37.08	1.285	2.433	1.426	52.82	42.09
S2P1-A4	35.69	37.15	1.456	2.377	1.478	61.24	50.58
S2P1-A5	35.80	37.34	1.543	2.509	1.483	61.50	50.95
S2P1-A6	35.70	37.06	1.367	2.418	1.452	56.56	45.87
Average	35.73 ± 0.07	37.10 ± 0.12	1.378 ± 0.082	2.457 ± 0.066	1.446 ± 0.025	56.14 ± 3.64	45.41 ± 3.72

Table 3-9: Average Fiber Volume Fraction of Panels

Panel No.	Crucible Weight (g)	Crucible & Fiber Weight (g)	Fiber Weight (g)	Composite Weight (g)	Composite Density (g/cm <sup>3</sup> )	Fiber Weight (%)	Fiber Volume (%)
S1P2	35.68	36.96	1.284	2.270	1.446	56.60	45.73
S1P3	35.59	36.94	1.347	2.335	1.440	57.80	46.51
S1P9	35.78	37.04	1.262	2.394	1.430	52.80	42.21
S1P10	35.78	37.07	1.296	2.353	1.435	55.13	44.21
S2P1	35.72	37.06	1.340	2.455	1.435	54.69	43.92
S2P9	35.69	37.02	1.329	2.434	1.425	54.63	43.55
S3P1	35.72	37.01	1.292	2.909	1.382	44.47	34.33
S3P2	35.69	37.02	1.329	2.434	1.425	54.63	43.55
S3P5	35.72	37.01	1.292	2.909	1.382	44.47	34.33
S3P6	35.68	37.08	1.403	2.746	1.408	51.02	40.19
Average	35.70 ± 0.033	37.02 ± 0.029	1.32 ± 0.025	2.52 ± 0.148	1.42 ± 0.014	52.62 ± 2.90	41.85 ± 2.68

Table 3.10: Percent Void Content – Sample Test Results (S2P1)

Specimen No.	Composite Wt. (gm)	Composite Density (g/cm <sup>3</sup> )	Composite Vol. (cm <sup>3</sup> )	Fiber Wt. (g)	Fiber Vol. (cm <sup>3</sup> )	Resin Wt. (g)	Resin Vol. (cm <sup>3</sup> )	Air Vol. (cm <sup>3</sup> )	Void Cont. (%)
S2P1-A1	2.411	1.435	1.679	1.311	0.732	1.100	0.941	0.006	0.346
S2P1-A2	2.598	1.402	1.853	1.307	0.730	1.291	1.105	0.018	0.977
S2P1-A3	2.433	1.426	1.706	1.285	0.718	1.148	0.982	0.006	0.326
S2P1-A4	2.377	1.478	1.608	1.456	0.813	0.921	0.788	0.006	0.385
S2P1-A5	2.509	1.483	1.692	1.543	0.862	0.966	0.827	0.003	0.192
S2P1-A6	2.418	1.452	1.665	1.367	0.764	1.050	0.899	0.003	0.158
Average	2.457	1.446	1.701	1.378	0.770	1.079	0.924	0.007	0.397
	± 0.066	± 0.025	± 0.066	± 0.082	± 0.046	± 0.106	± 0.091	± 0.005	± 0.238

Fiber Density 1.79 (g/cm<sup>3</sup>)Resin Density 1.1683 (g/cm<sup>3</sup>)

Table 3.11: Average Void Content of Panels

Specimen No.	Composite Wt. (g)	Composite Density (g/cm <sup>3</sup> )	Composite Vol. (cm <sup>3</sup> )	Fiber Wt. (g)	Fiber Vol. (cm <sup>3</sup> )	Resin Wt. (g)	Resin Vol. (cm <sup>3</sup> )	Air Vol. (cm <sup>3</sup> )	Void Cont. (%)
S1P2	2.291	1.444	1.587	1.287	0.719	1.004	0.859	0.009	0.570
S1P3	2.364	1.436	1.647	1.371	0.766	0.993	0.850	0.031	1.942
S1P9	2.430	1.426	1.705	1.254	0.701	1.176	1.007	0.000	0.000
S1P10	2.380	1.430	1.664	1.295	0.724	1.085	0.929	0.012	0.727
S2P1	2.480	1.421	1.746	1.301	0.727	1.179	1.010	0.010	0.550
S2P9	2.412	1.411	1.713	1.278	0.714	1.134	0.970	0.028	1.551
S3P1	2.943	1.379	2.134	1.294	0.723	1.649	1.411	0.000	0.000
S3P2	2.720	1.397	1.947	1.329	0.743	1.391	1.191	0.014	0.716
Average	2.503	1.418	1.768	1.301	0.727	1.201	1.028	0.013	0.757
	± 0.152	± 0.015	± 0.126	± 0.024	± 0.014	± 0.152	± 0.130	± 0.008	± 0.473

Fiber Density 1.79 (g/cm<sup>3</sup>)Resin Density 1.1683 (g/cm<sup>3</sup>)



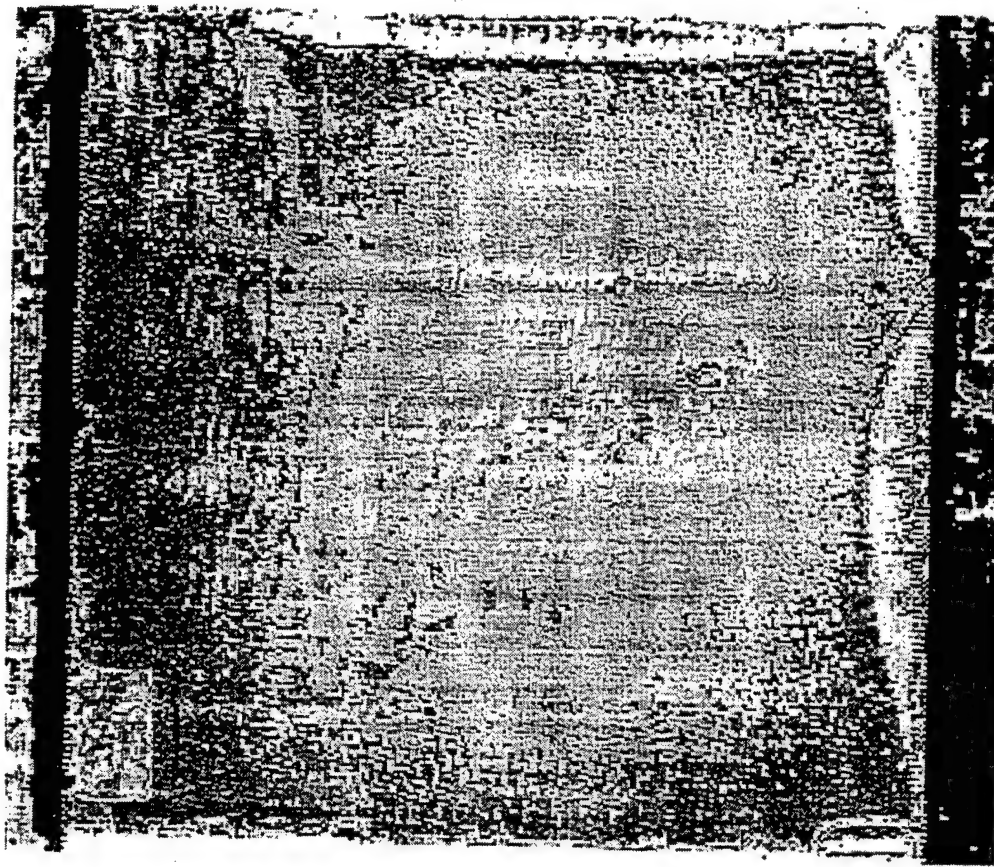
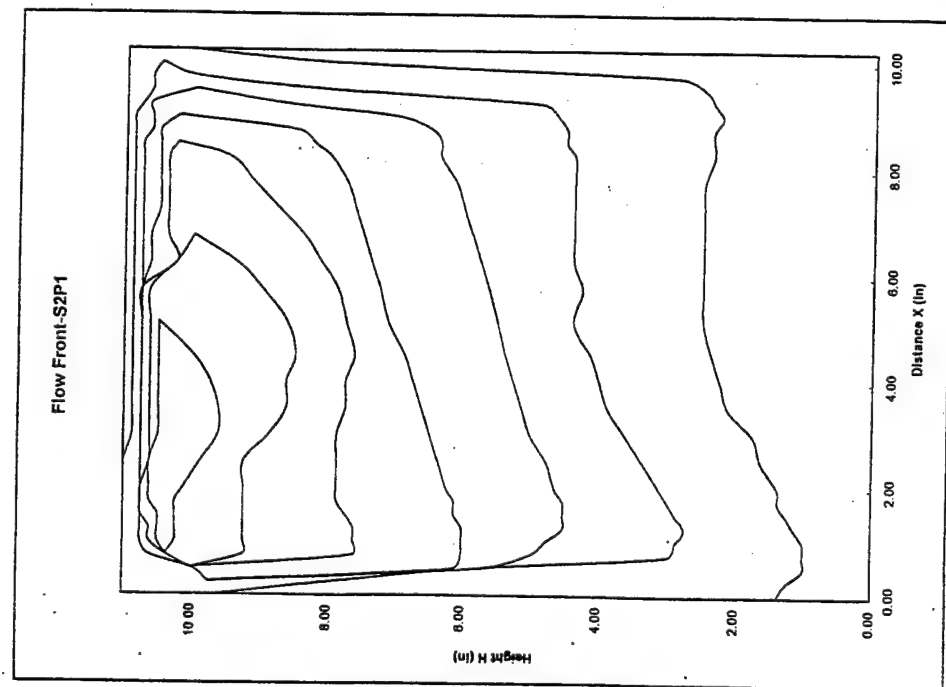


Figure 3-13 Typical Flow Front and Corresponding C-Scan Image (S2P1)

## CHAPTER 4

### ANALYSIS AND DISCUSSION OF RESULTS

The database assembled in Chapter 3 serves as the basis for the prediction of the nature of the flow front, race tracking, and the location of possible void or dry spot. The development of the technique is presented in this Chapter. Comparisons are frequently made between values developed to compare the left side with the right side of the mold. For reference, the left side is represented by the gas flows through ports (1, 2, and 5), whichever are open. Thus, with the all-ports-open configuration, the left side reflects flow through all the left ports (1, 2, and 5). With the top-ports-closed, the left side reflects flow through ports (1 and 2). With the lower-ports-closed, the value reflects that of ports (2 and 5). If the side ports are closed, the value reflects the flow through only port (5). Similarly, the right side is represented by the flows through ports (3, 4, and 7). Thus, with the all-ports-open configuration, the right side reflects flow through all the right ports. With the top ports closed, the right side reflects flow through ports (3 and 4). With the lower ports closed, the value reflects that of ports (3 and 7). If the side ports are closed, the value reflects the flow through port (7).

#### 4.1 Prediction of Skewness of Resin Flow Front

This method seeks to relate the behavior of nitrogen flow to the resin flow. Conceptually, the idea is to investigate the permeability of the ready-to-inject mold by probing the preform to determine the side with the lower resistance to the nitrogen flow and predict that the resin flow is likely to follow suit. The characteristics of the flow front are defined in terms of the skewness of the resin flow with respect to the central vertical axis of the mold. Now, the question becomes which ports should be used to represent the sides of the mold. By looking at the port orientation, ports (1, 2, and 5) are placed on the left side and ports (3, 4 and 7) are placed on the right side with port 6 being central. However, is it necessary to use the flow rates of all three ports from each side to make the decision or should we use combinations of the three ports for the decision making process? Various intuitive port combinations and gas flow quantities were tested to determine which ones would give the most consistent and accurate results.

##### 4.1.1 Prediction Based on Relative Percent Cumulative Flow

The raw nitrogen flow data were converted to percentages, which represent the right flow and left flow, respectively. As a first approximation, the no-port-closed configuration was utilized to check if the resin flow front could be predicted. Figures 4-1 to 4-5 show sample charts of the percentage flows for the no-ports-closed configuration and the corresponding digitized flow front. In these figures, comparisons of percent flows between the left and right ports are made. The percent flow under each experiment is used to predict the flow pattern of the resin. In Figure 4-1 there is a higher percentage of airflow through the right side and, thus, the resin flow is expected to follow suit. It can be seen that the corresponding flow front (S1P1) is skewed accordingly with more resin flow on the right side. The relative percentage gas flows of S1P2 (Figure 4-2) also predicts a flow pattern that favors the right side of the mold. The percentages of S1P3 (Figure 4-3)

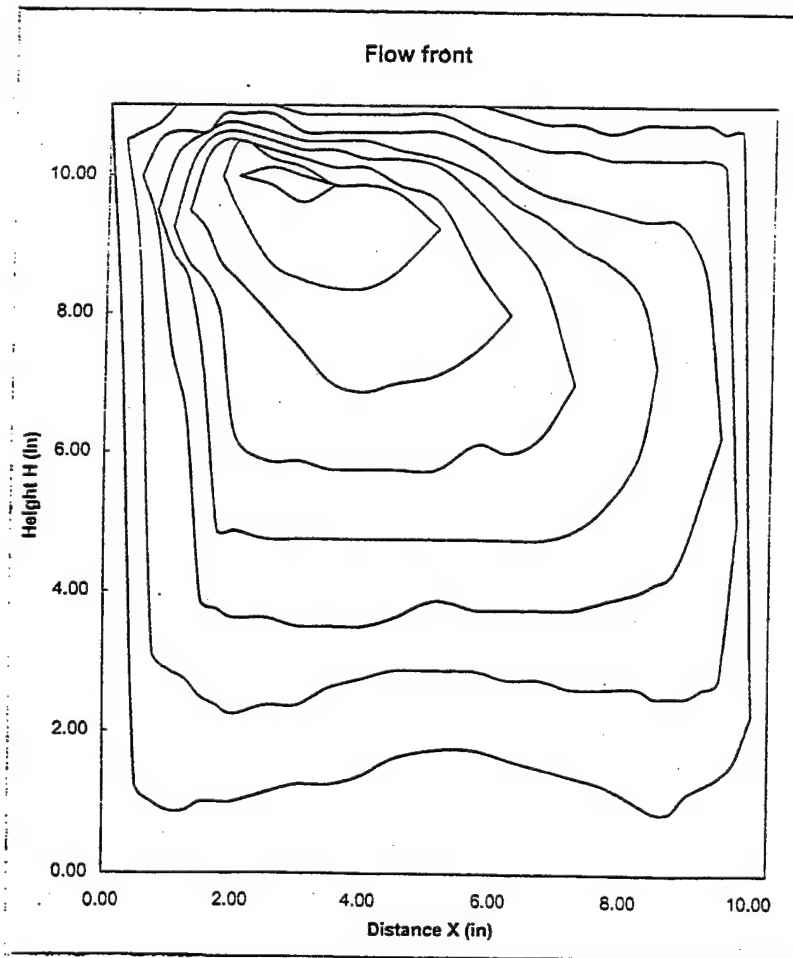
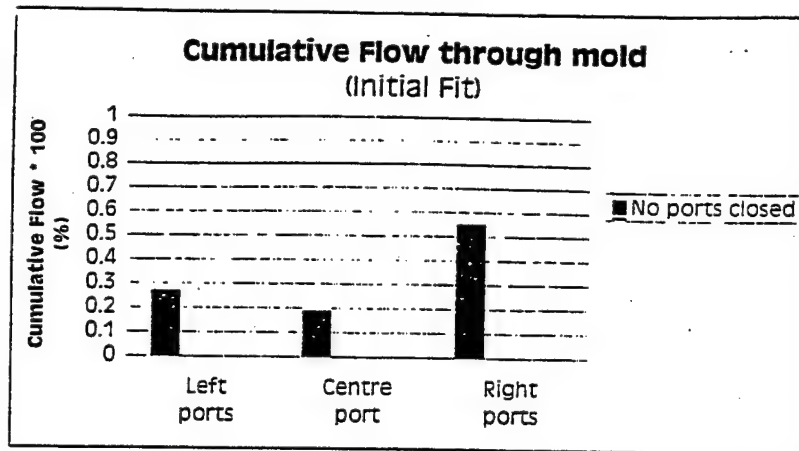


Figure 4-1      Airflow Data and Resin Flow Front for Panel S1P1

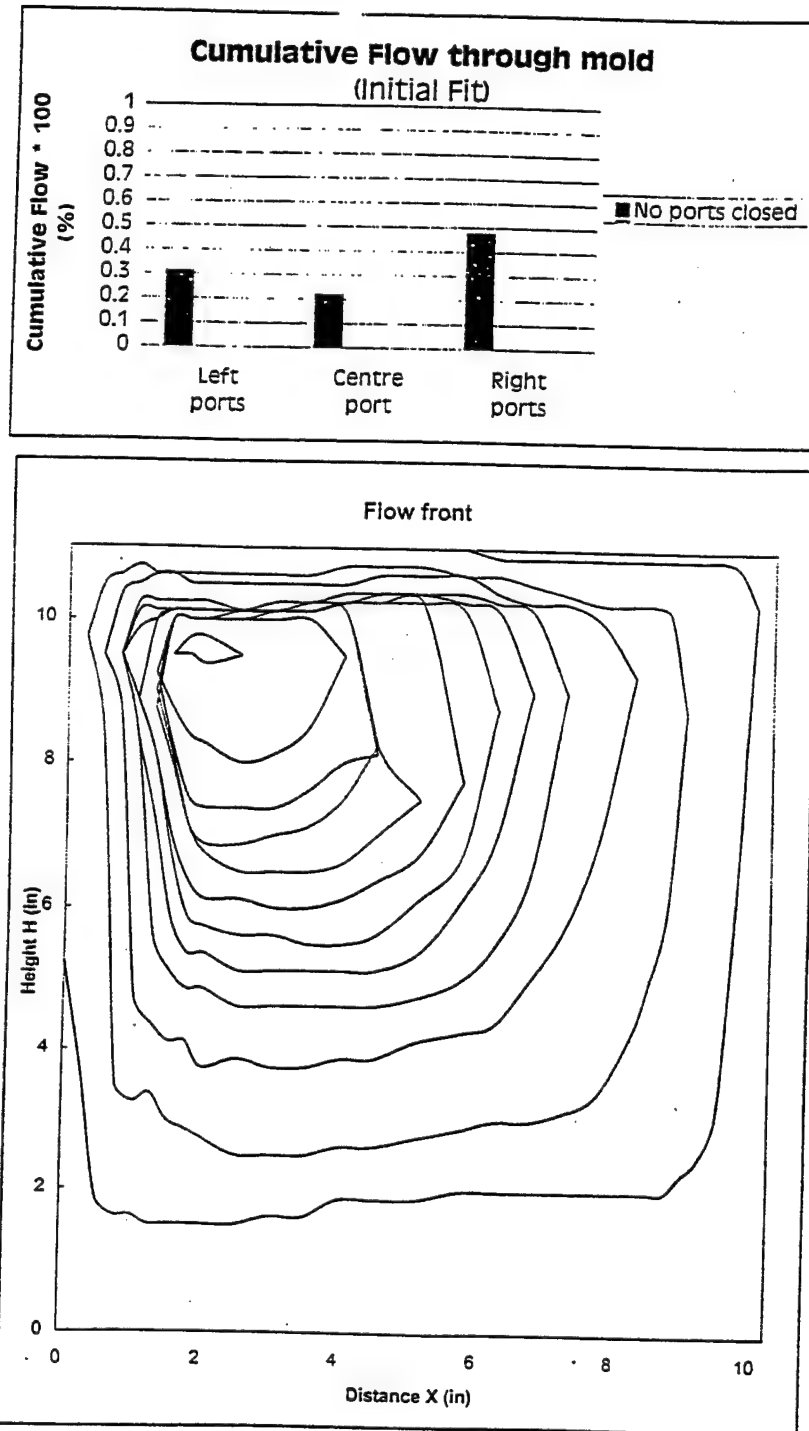


Figure 4-2      Airflow Data and Resin Flow Front for Panel S1P2

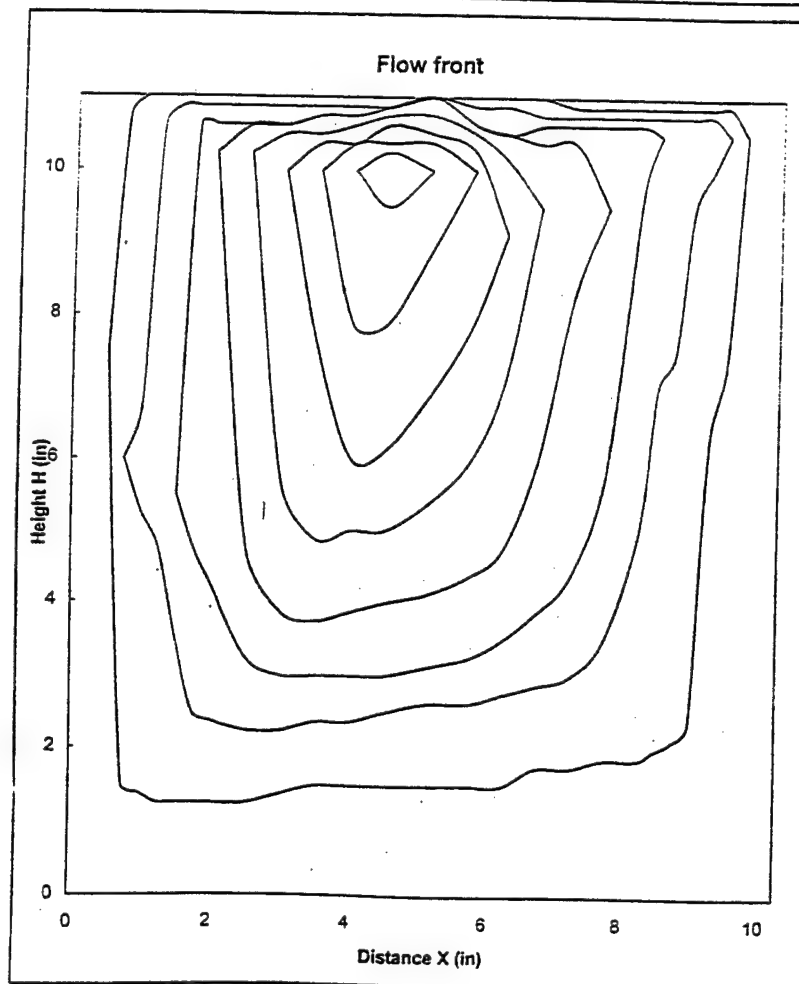
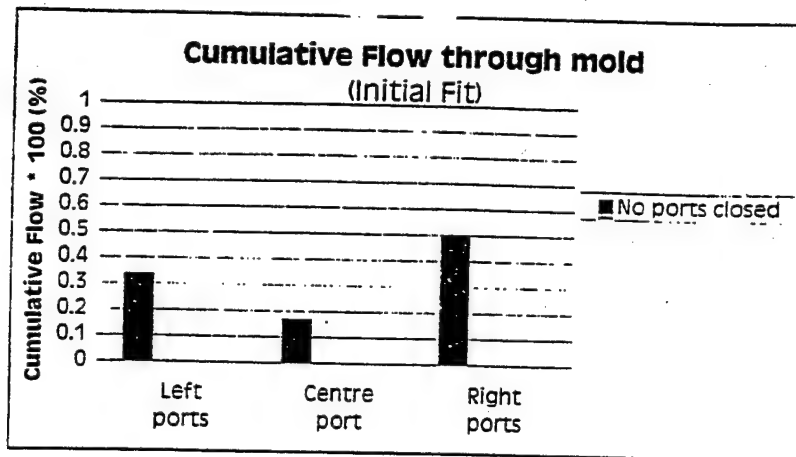


Figure 4-3      Airflow Data and Resin Flow Front for Panel S1P3

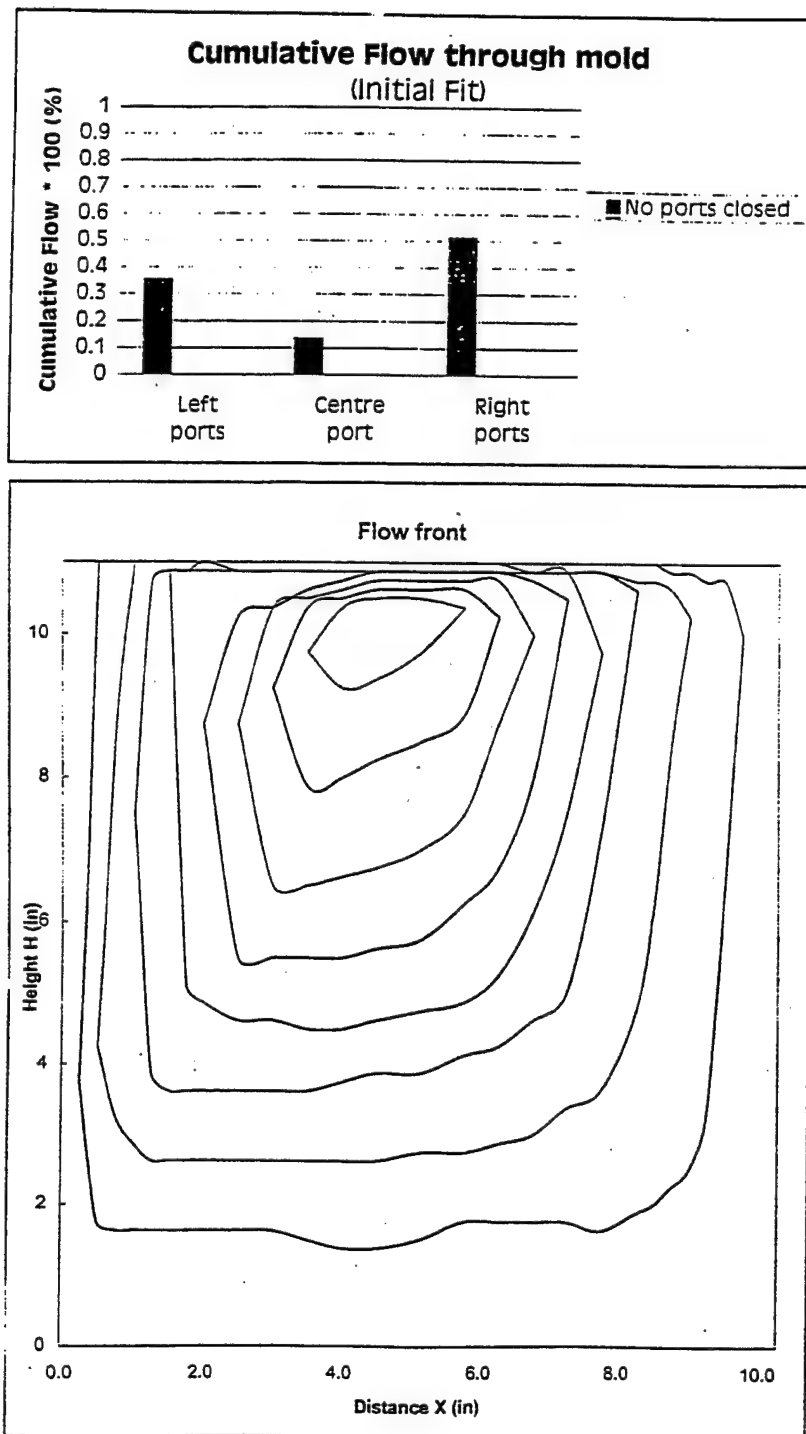


Figure 4-4      Airflow Data and Resin Flow Front for Panel S1P4

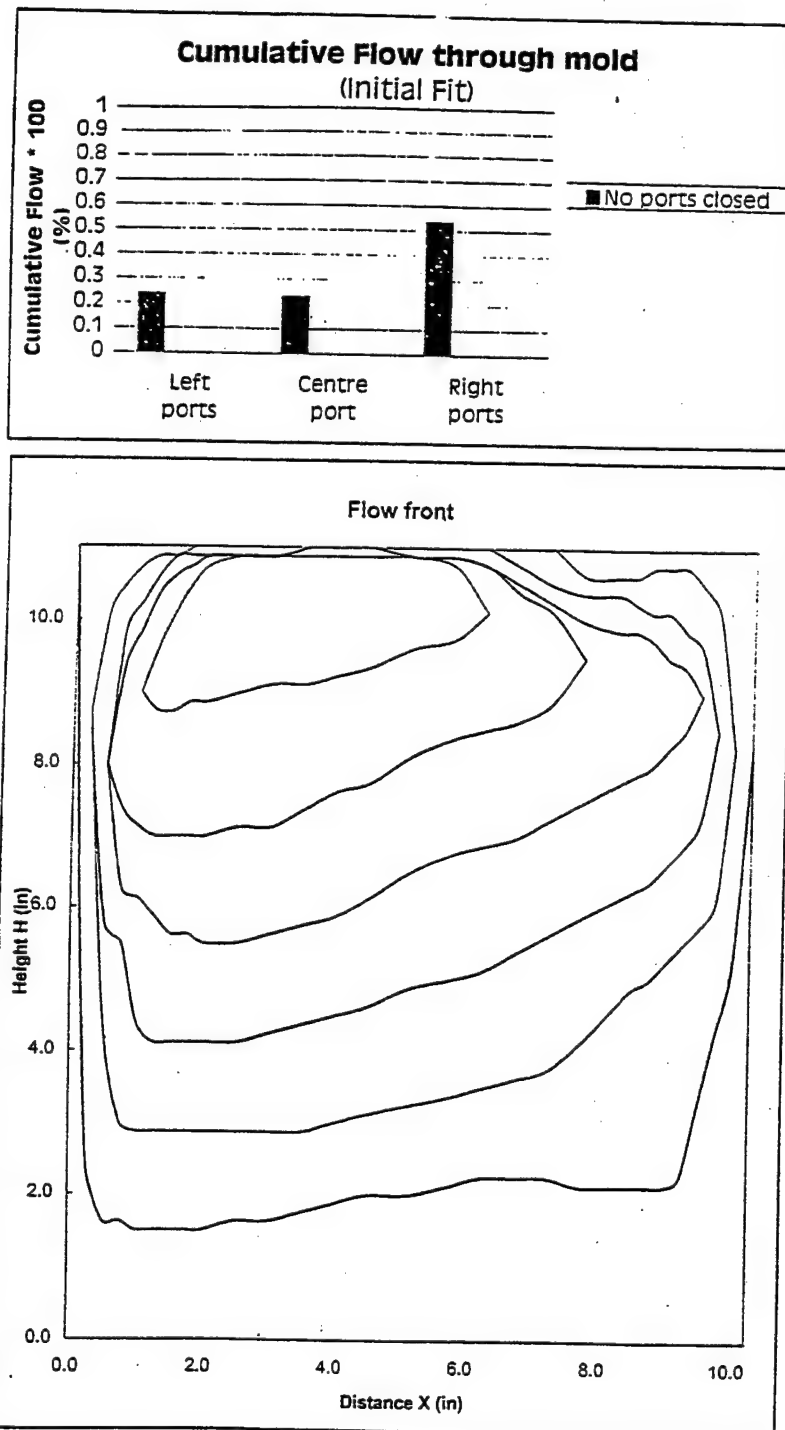


Figure 4-5      Airflow Data and Resin Flow Front for Panel S1P5

do not agree with the flow front. The resin flow is rather even on both sides of the mold. The flow front and the gas flow percentages also do not agree for experiment S1P4 (Figure 4-4) while there is an agreement for experiment S1P5 (Figure 4-5). Thus, when comparing the percentage flows through ports (1, 2 and 5) with ports (3, 4, and 7) and taking all ports into consideration, the prediction rate is 60% for the small sample size.

To determine how to improve the prediction rate, other combinations of flow were considered. In order to verify this prediction method, data for 14 more experiments were considered. The data representing the percentages of gas flow through the various port combinations is provided in Table 4-1.

A bar chart that represents these percentages, and the corresponding flow fronts, are provided in Appendix D. For each experiment, a prediction was made based on the relative percent gas flow through the appropriate left and right ports. The group of ports that possesses the higher flow percentage corresponds to more resin flow. Thus, in Table 4-1, the directional sub-categories under the columns *Skewness*, "E" represents even flow, "L" represents higher resin flow to the left side of the mold and "R" represents a higher resin flow to the right side. The location of the *Final Fill* represents the last spot to be impregnated. This location is predicted to be the side with the higher resistance to flow. If both sides have close to equal resistance to flow then the dry spot (last place to fill) is expected to be near the vertical axis of the mold and indicated as "Even" (E). Otherwise it is identified with respect to the vertical axis of the mold as being to the right (R) or left (L). This is the location in which the phenomena (*Skewness* or last place to fill) were actually observed and are also noted in the table. The number of correct predictions was obtained. The success rates are provided in Table 4-2.

Both Tables 4-1 and 4-2 show the comparison of ports (1, 2, and 5) and ports (3, 4, and 5) as already discussed. Percent gas flow through ports (2 and 5) is compared with that of ports (3 and 7) while the value through side ports (1 and 2) is compared with side ports (3 and 4). The relative percentages when comparing side ports (1 and 2) with side ports (3 and 4) yielded only 50% accuracy. However, when ports (2 and 5) are compared with ports (3 and 7), the results came closer to the experimental ones. This comparison suggests higher resin flows on the right side for experiments S1P1, S1P2, and S1P5. Also, since the percentages are closer (to within 5%) for S1P3 and S1P4, the data suggest a nearly even flow front which agrees with the actual flow front. Overall, comparing ports (2 and 5) with ports (3 and 7) yielded 75% prediction accuracy. Thus, it seems that the percent flow through ports (2 and 5) when compared with that through ports (3 and 7) could provide information regarding the general nature of the flow front, namely, skewness to the left, right or even.

#### 4.1.2 Predictions Based on Gas Flow Ratio

In an attempt to improve upon the prediction accuracy, a second method was developed based on the ratio of the normalized gas flow rates. Of the 20 panels fabricated, 14 panels were observed to have prominent race tracking on the right side of the mold during resin injection. Of the remaining six panels, three panels experienced race tracking on the left side and the remaining had even flows on both sides. A quick inspection of the ratios of the air flows provided a parameter,  $G_R$  the gas flow ratio where:



Table 4-1 Prediction Table Using Relative Percent Flow; All Ports Open

ID	Actual Flow	Predictions Based on Relative Cumulative Flows										Pred.	Ports (1,2)	Ports (3,4)	Pred.	Ports (1,2)	Ports (3,4)	Pred.
		port1	port2	port3	port4	port5	port6	port7	sum	Ports (1,2,5)	Ports (3,4,7)							
S1P1	R	2.101	1.028	3.925	3.745	2.795	3.5	2.681	19.775	29.96	52.34	R	19.33	33.41	R	15.82	38.79	R
S1P2	R	2.791	1	3.584	3.18	2.45	4.392	2.858	20.255	30.81	47.50	R	17.03	31.80	R	18.72	33.39	R
S1P3	E	1.377	2.52	1.77	3.961	1.587	2.734	2.432	16.381	33.48	49.83	R	25.07	25.65	E	23.79	34.99	R
S1P4	E	2.497	2.704	2.744	4.181	1.492	2.545	2.729	18.892	35.43	51.10	R	22.21	28.97	R	27.53	36.66	R
S1P5	R	1.061	1.383	1.408	2.625	1.104	3.428	3.947	14.956	23.72	53.36	R	16.63	35.81	R	16.34	26.97	R
S1P6	R	1.793	1.316	1.252	2.616	2.082	3.829	2.473	15.361	33.79	41.28	R	22.12	24.25	E	20.24	25.18	E
S1P7	E	1.418	0.898	0.592	1.903	2.313	1.133	2.464	10.721	43.18	46.26	E	29.95	28.50	E	21.60	23.27	E
S1P8	E	1.669	2.089	2.344	3.393	1.393	2.162	1.913	14.963	34.42	51.13	R	23.27	28.45	E	25.12	38.34	R
S1P9	L	1.202	0.813	1.129	1.103	4.294	1.389	3.098	13.028	48.43	40.91	L	39.20	32.45	L	15.47	17.13	E
S1P10	R	1.009	0.516	1.394	1.17	0.432	0.602	1.569	6.692	29.24	61.76	R	14.17	44.28	R	22.79	38.31	R
S2P1	R	0.737	0.726	1.122	2.526	1.537	1.507	1.076	9.231	32.50	51.18	R	24.52	23.81	E	15.85	39.52	R
S2P2	R	2.158	1.125	1.563	3.114	1.354	1.961	1.912	13.187	35.16	49.97	R	18.80	26.35	R	24.90	35.47	R
S2P3	E	3.476	0.71	0.638	1.607	1.632	1.938	1.166	11.167	52.10	30.55	L	20.97	16.15	E	37.49	20.10	L
S2P4	E	2.84	1.364	1.439	2.643	1.063	3.016	1.594	13.959	37.73	40.66	E	17.39	21.73	E	30.12	29.24	E
S2P5	E	3.294	2.284	1.644	2.058	0.85	2.227	1.388	13.745	46.77	37.03	L	22.80	22.06	E	40.58	26.93	L
S2P6	E	3.378	0.869	0.533	1.405	2.122	1.889	2.255	12.451	51.15	33.68	L	24.02	22.39	E	34.11	15.57	L
S2P7	R	3.622	1.336	0.734	1.719	0.939	2.536	1.489	12.375	47.65	31.85	L	18.38	17.96	E	40.06	19.82	L
S2P8	R	3.377	1.478	3.04	2.739	1.555	2.051	1.606	15.846	40.45	46.60	R	19.14	29.32	R	30.64	36.47	R
S2P9	E	1.732	1.231	0.988	2.375	1.24	1.859	1.091	10.516	39.97	42.35	E	23.50	19.77	E	28.18	31.98	E
S2P10	E	3.262	1.297	0.682	2.859	2.043	2.233	1.562	13.938	47.37	36.61	L	23.96	16.10	L	32.71	25.41	L

Table 4-2: Success Rate in Prediction using Relative Percent Gas Flow Rate; All Ports Open

Side Configuration	Skewness		Final Fill location	
	# tests	# correct      Accuracy (%)	# Correct      Accuracy (%)	
Ports (1,2,5) versus (3,4,7)	20	12              60.0	11              55.0	
Ports (2,5) versus (3,7)	20	15              75.0	11              55.0	
Ports (1,2) versus (3,4)	20	10              50.0	11              55.0	

$$G_R = \frac{\Sigma (\text{Normalized N}_2 \text{ gas flow of right sided ports})}{\Sigma (\text{Normalized N}_2 \text{ gas flow of left sided ports})}$$

Note that the sums of the normalized flows from the right side are always the dividend, and the sums of the normalized flows from the left, the divisor. In this way, values of  $G_R$  greater than 1.0 indicate resin flow to the right side of the mold whereas values below 1.0 indicate resin flow to the left side of the mold. By applying a standard error of  $\pm 0.1$  obtained from  $G_R$  data, we considered any ratio value  $G_R$  falling between 0.9 and 1.1 to be indicative of equal skewness on both sides.

Thus, from the analysis, if  $G_R > 1.1$ , it is predicted that the resin flow will be to the right side. If  $G_R < 0.9$ , the flow will be to the left. If  $0.9 < G_R < 1.1$ , then it is expected to be even. The complete data are provided in Appendix F, and Tables 4-3 to 4-7 provide summaries of the success rates. The results are inconclusive and, thus, another parameter is explored.

#### 4.1.3 Predictions Based on Gas Flow Parameter

The third prediction method used a statistical test of significance between the left and right flow parameters (paired comparison) and experimental error (Box, Hunter and Hunter, 1978) to determine whether the gas flow parameter is a good indicator of resin flow skewness to the left, right or both sides. Conceptually, if the value of  $P_R$  and  $P_L$ , from the right side ports and left side ports, respectively, are statistically equal, then the resin flow may be predicted to be even on both sides. If not, then the higher of the two would indicate the direction of skewness of resin flow.

During the experiments, it was discovered that for our mold configuration, race tracking is identified within the first 2 minutes of resin flow. Thus, using the position of the flow front at the 2-minute mark, the flow fronts were grouped into three categories, namely, left race tracking, right race tracking and even race tracking. For the right and left race tracking flow fronts, we expect real differences to exist between the gas flow parameters and no significant difference for the even race tracking. The statistical test is used to find out whether the differences are real or not.

The difference of the two gas flow parameters,  $P_R$  and  $P_L$ , for each experiment in each group was used as the random variable in a paired comparison test. The Student  $t$ -distribution test was applied to the gas flow parameters for the various port combinations. Prior to the  $t$ -test, the data were further segregated by mold configuration. During panel

Table 4-3: Success Rate in Prediction of Skewness using Gas Flow Ratio,  $G_R$ ; Ports (3 + 4 + 7) and (1 + 2 + 5)

Flow Configuration	Skewness			Final Fill location	
	# tests	# Correct	Accuracy (%)	# Correct	Accuracy (%)
No ports closed	20	12	60.0	11	55.0
Top ports closed	15	8	53.3	7	46.7
Lower ports closed	15	6	40.0	7	46.7
Side ports closed	15	9	60.0	8	53.3

Table 4-4: Success Rate in Prediction of Skewness using Gas Flow Ratio,  $G_R$ ; Ports (3 + 7) and (2 + 5)

Flow Configuration	Skewness			Final Fill location	
	# tests	# Correct	Accuracy (%)	# Correct	Accuracy (%)
No ports closed	20	11	55.0	8	40.0
Top ports closed	15	5	33.3	6	40.0
Lower ports closed	15	6	40.0	6	40.0
Side ports closed	15	9	60.0	7	46.7

Table 4-5: Success Rate in Prediction of Skewness using Gas Flow Ratio,  $G_R$ ; Ports (3) and (2)

Flow Configuration	Skewness			Final Fill location	
	# tests	# Correct	Accuracy (%)	# Correct	Accuracy (%)
No ports closed	20	9	45.0	8	40.0
Top ports closed	15	3	33.3	6	40.0
Lower ports closed	15	5	33.3	6	40.0
Side ports closed	--	--	--	--	--

Table 4-6: Success Rate in Prediction of Skewness using Gas Flow Ratio,  $G_R$ ; Ports (3+4) and (1+2)

Flow Configuration	Skewness			Final Fill location	
	# tests	# Correct	Accuracy (%)	# Correct	Accuracy (%)
No ports closed	20	10	50.0	10	50.0
Top ports closed	15	8	53.3	8	53.3
Lower ports closed	15	5	33.3	6	40.0
Side ports closed	--	--	--	--	--

Table 4-7: Success Rate in Prediction of Skewness using Gas Flow Ratio,  $G_R$ ; Ports (5) and (7)

Flow Configuration	Skewness			Final Fill location	
	# tests	# Correct	Accuracy (%)	# Correct	Accuracy (%)
No ports closed	20	10	50.0	8	40.0
Top ports closed	--	--	--	--	--
Lower ports closed	15	8	53.3	7	46.7
Side ports closed	15	8	53.3	7	46.7

fabrication, some panels experienced flow skewed to one side of the mold. The Student t-test is applied to those data to check if differences between  $P_R$  and  $P_L$  are significant.

The underlying assumption of the Student t-distribution test is that the means of  $P_R$  and  $P_L$  are equal (Null Hypothesis). Given a selected significance level, in this case 5 %, and the degrees of freedom of the data, any calculated t-value greater than value of the t-critical (from t-tables) is considered significant. Significance in this case means that the two variables,  $P_R$  and  $P_L$ , are statistically different at the 5 % significance.

Since  $P_R$  and  $P_L$  are paired values for each experiment, the paired comparison test method was employed. Tables 4-8 to 4-12 show the results of the test for the various port configurations. Consider Table 4-8 for example. Under no-ports-closed configuration,  $P_R$  has a value of 1.057 and  $P_L$  has a value of 0.875. Fourteen such experiments were observed; with resin flow skewed to the right. The calculated t-value based on the differences (paired) between  $P_R$  and  $P_L$  is 1.992. At the 5 % significance, t-critical is 1.771. Since t-stat is greater than t-critical, the difference between  $P_R$  and  $P_L$  is real and significant. Since the gas flow is significantly skewed, we expect the resin flow to follow suit. For all other configurations; top-ports-closed, lower-ports-closed, and side-ports-closed, the t-test results indicate that  $P_R$  and  $P_L$  are not significantly different, which is not the expected result. Similar explanations can be made for Tables 4-9 to 4-12.

Table 4-8: Significance Test for Difference of Gas Flow Parameters ( $P_L$ ,  $P_R$ ); ports (3+4+7) and (1+2+5)

	Avg. Ports (3+4+7)	Avg. Ports (1+2+5)	Observations	t-Statistical value	Critical t value
No ports closed	1.057	0.875	14	1.992	1.771
Top ports closed	1.171	1.163	10	0.055	1.833
Lower ports closed	0.905	0.796	10	1.019	1.833
Side ports closed	0.771	0.681	10	0.843	1.833

Table 4-9: Significance Test for Difference of Gas Flow Parameters ( $P_L$ ,  $P_R$ ); ports (3+7) and (2+5)

	Avg. Ports (3+7)	Avg. Ports (2+5)	Observations	t-Statistical value	Critical t value
No ports closed	0.914	0.714	14	2.293	1.771
Top ports closed	0.895	0.826	10	0.607	1.833
Lower ports closed	1.357	1.194	10	1.019	1.833
Side ports closed	1.157	1.021	10	0.843	1.833

Table 4-10: Significance Test for Difference of Gas Flow Parameters ( $P_L$ ,  $P_R$ ); ports (3+4) and (1+2)

	Avg. Ports (3+4)	Avg. Ports (1+2)	Observations	t-Statistical value	Critical t value
No ports closed	1.117	0.942	14	1.357	1.771
Top ports closed	1.756	1.744	10	0.055	1.833
Lower ports closed	0.615	0.556	10	0.647	1.833
Side ports closed	--	--	10	--	1.833

Table 4-11: Significance Test for Difference of Gas Flow Parameters ( $P_L$ ,  $P_R$ ); Ports (7) and (5)

	Avg. Port (7)	Avg. Port (5)	Observations	t-Statistical value	Critical t value
No ports closed	0.936	0.742	14	1.936	1.771
Top ports closed	--	--	10	--	1.833
Lower ports closed	1.484	1.275	10	1.005	1.833
Side ports closed	2.314	2.042	10	0.843	1.833

Table 4-12: Significance Test for Difference of Gas Flow Parameters ( $P_L$ ,  $P_R$ ); Ports (3) and (2)

	Avg. Port (3)	Avg. Port (2)	Observations	t-Statistical value	Critical t value
No ports closed	0.892	0.685	14	0.043	1.771
Top ports closed	1.651	1.790	10	0.228	1.833
Lower ports closed	1.113	1.230	10	0.262	1.833
Side ports closed	--	--	10	--	1.833

In Tables 4-8 - 4-12, the configurations and combinations of statistical significance are the pairings of ports (1+2+5) versus (3+4+7), ports (3+7) versus (2+5) and port (7) versus (5), with all having the mold configuration of *No-ports-closed*. The combination possessing the highest level of significance was ports (3+7) versus (2+5).

This result signifies that the use of the side ports (1,2) versus (3,4) would not provide accurate results since the gas flow parameters do not show any real differences even though the resin flow shows significant differences.

By means of the paired comparison technique, the experimental error was found to be 0.2 between the left flow and the right flow gas parameters,  $P_R$  and  $P_L$ , with no regard to the degree of race tracking. Thus,  $P_R$  and  $P_L$  are considered to be statistically equal if they are within 0.2 of each other. If they deviate by 0.2, then the resin flow direction is indicated by the higher of the two values. By using this method, predictions are made of the resin flow front. The prediction charts for the various port combinations are provided in Appendix F. Tables 4-13 to 4-17 show the summary of the results.

In the analysis of the prediction charts, the *No ports closed* configuration consistently yielded the highest number of correct predictions, regardless of the numerical combination.

Table 4-13: Success Rate in Prediction of Skewness using Gas Flow Parameters ( $P_L$ ,  $P_R$ ); Ports (3 + 4 + 7) and (1 + 2 + 5)

Flow Configuration	Skewness			Final Fill location	
	# tests	# Correct	Accuracy (%)	# Correct	Accuracy (%)
No ports closed	20	9	45.0	12	60.0
Top ports closed	15	5	33.3	9	60.0
Lower ports closed	15	7	46.0	6	40.0
Side ports closed	15	6	40.0	7	46.7

Table 4-14: Success Rate in Prediction of Skewness using Gas Flow Parameters ( $P_L$ ,  $P_R$ ); Ports (3 + 7) and (2 + 5)

Flow Configuration	Skewness			Final Fill location	
	# tests	# Correct	Accuracy (%)	# Correct	Accuracy (%)
No ports closed	20	14	70.0	10	50.0
Top ports closed	15	7	46.6	6	40.0
Lower ports closed	15	9	60.0	7	46.7
Side ports closed	15	7	46.7	6	40.0

Table 4-15: Success Rate in Prediction of Skewness using Gas Flow Parameters ( $P_L$ ,  $P_R$ ); Ports (3) and (2)

Flow Configuration	Skewness			Final Fill location	
	# tests	# Correct	Accuracy (%)	# Correct	Accuracy (%)
No ports closed	20	12	60.0	9	45.0
Top ports closed	15	3	20.0	6	40.0
Lower ports closed	15	5	33.3	5	33.3
Side ports closed	--	--	--	--	--

Table 4-16: Success Rate in Prediction of Skewness using Gas Flow Parameters ( $P_L$ ,  $P_R$ ); Ports (3 + 4) and (1 + 2)

Flow Configuration	Skewness			Final Fill location	
	# tests	# Correct	Accuracy (%)	# Correct	Accuracy (%)
No ports closed	20	10	50.0	10	50.0
Top ports closed	15	8	53.3	8	53.3
Lower ports closed	15	8	53.3	5	33.3
Side ports closed	15	--	--	--	--

Table 4-17: Success Rate in Prediction of Skewness using Gas Flow Parameters ( $P_L$ ,  $P_R$ ); Ports (5) and (7)

Flow Configuration	Skewness			Final Fill location	
	# tests	# Correct	Accuracy (%)	# Correct	Accuracy (%)
No ports closed	20	9	45.0	6	30.0
Top ports closed	15	--	--	--	--
Lower ports closed	15	7	46.6	6	40.0
Side ports closed	15	6	40.0	5	33.3

#### 4.1.4 Summary of Resin Flow Prediction Methods

Three distinct methods have been applied to investigate the port configurations (closed/open) for the nitrogen injection to determine which ports must be opened and which ones are to be closed during the nitrogen injection to predict the resin flow pattern.

The relative percentage flow method was done with all ports open. This method suggested that ports (3 and 7) when compared with ports (2 and 5) could provide information about the resin flow pattern. The gas flow ratio method was used for various port closing/openings and this method suggested that the all-ports-open method was quite appropriate. The gas flow parameter method validates the all-ports-open method for the gas data collection and three alternative ways to combine left and right ports for the analysis.

Analysis of the results from all three methods yields this conclusion: the most appropriate way to inject the gas is to have all the ports open; record the gas flow rate at all the ports; and use ports (3 and 7) to evaluate  $P_R$  and ports (2 and 5) to evaluate  $P_L$ . This technique is pursued for the rest of the work.

## 4.2 Prediction of Race Tracking

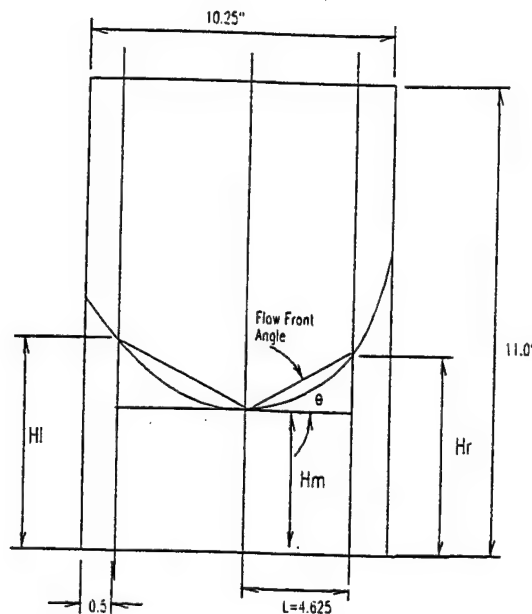
The next step is to determine the severity of the skewness of the resin flow front, which is an indication of race tracking. In order to do this, we need to develop a parameter that could be used to quantitatively describe the flow front and race tracking. This parameter may then be correlated with the gas flow parameters. This section describes two parameters which characterize the resin flow front, the correlation of the gas flow parameters and the resin flow front parameters and technique used to predict the severity of race tracking.

### 4.2.1 Characterization of Flow Front by Height Ratios

This was done by digitizing the flow front and obtaining the values of the height of the flow front from the base line with respect to time. Vertical reference lines were drawn at an approximate distance of 1/2 in. (12 mm) from the sidewalls to represent the flow at the edges. The location of the intersection of the flow front and these vertical lines and the flow front and the central vertical lines are monitored with respect to time. In Figure 4-6, the height from the base of the mold to the flow front is labeled as  $H_m$  at the vertical central axis,  $H_r$  to the right and  $H_L$  to the left.

Using these heights, the ratio  $R_r (= H_r / H_m)$  is defined as the right flow front ratio and ( $R_L = H_L / H_m$ ) is defined as the left flow front ratio. It is expected that these ratios will vary with time and, thus, may be used to characterize the flow front. Practically, these ratios should approach unity as the process progresses. For an even flow front, each of the two ratios should be near to unity from start to the end of the process since the central flow and the edge flow are essentially equal. For skewed resin flow fronts, the values must be large at the start of the process and approach unity at the end. Figures 4-7 and 4-8 show two flow fronts with their corresponding plots of the height ratios. Figure 4-7 (for S2P2), particularly, shows an acceptable flow front with no race tracking on the left side and a minimal race tracking on the right side of the mold. The plots of the ratios show that the values are apart along the entire filling time with the left ratio almost constant. The values of  $R_L$  being nearly equal to unity indicate that the left front and central front are nearly even for the entire process. The values of  $R_r$  converge to unity from the initial value, which indicates that the right flow front is ahead of the central flow for most of the process. Thus, the ratios may be used to describe how the flow front behaves on either side of the mold with respect to the central flow. Figure 4-8 shows a behavior in which both  $R_L$  and  $R_r$  exhibit identical patterns. Both ratios start from extremely high values and gradually approach unity. Such a pattern depicts that the side fronts run rapidly ahead of the central front, which is an indication of severe race tracking. For the good and the average fronts, the values of the ratios seem to be limited to approximately 2.0, while in the case of the poor fronts, the values seem to be unbounded at the start of the process and decrease as the process progresses.





### Flow Front Ratio

Left:  $R_L = H_L / H_m$

Right:  $R_R = H_R / H_m$

$$\Delta h = H - H_m$$

$$\tan \theta = \Delta h / L$$

### Flow Front Angle

$$\theta(t) = \tan^{-1} \Delta h(t) / L$$

Figure 4-6 Resin Flow Front Parameters

#### 4.2.2 Characterization of Flow Front by Flow Front Angle

Figure 4-6 also shows the definition of the flow front angle,  $\theta(t)$ . Since the skewness could be to either side of the mold, the flow front angle is calculated for both sides. Thus,  $\theta_L$  represents the left flow front angle and  $\theta_R$  represents the right.

It is expected that these angles vary with time and, thus, may also be used to characterize the resin flow front. Practically, these angles should approach zero at the end of the process. For an even flow front, each the two angles should be low (approximately zero) from the start to the end of the process since the central flow and the edge flows are essentially equal. For skewed resin flow fronts, the values must be large at the start of the process and approach zero at the end. In order to check the nature of variation of these angles with time, flow front angle plots were made for the flow fronts shown in Figures 4-7 and 4-8 for comparison. These are shown in Figures 4-9 and 4-10.

Figure 4-9 (for S2P2) particularly shows an acceptable flow front with no race tracking on the left side and a minimal race racking on the right side of the mold. The plots of the flow front angle show that the values are apart along the entire filling time with the flow front angle hovering around zero. The values of  $\theta_L$  being nearly zero indicate that the left front and central front are nearly even for the entire process. The values of  $\theta_R$  rise from an initial value and converge to zero, indicating that the right flow front is ahead of the central flow for the entire process. Thus, the flow front angle may also be used to describe how the flow front behaves on either side of the mold with respect to the central flow. Figure 4-10 (for S1P3) shows a behavior in which both



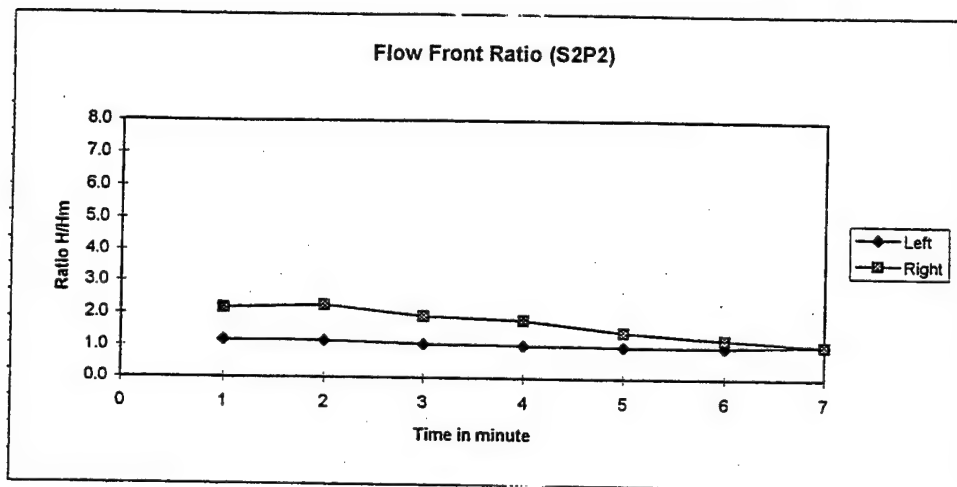


Figure 4-7 Height Ratio for a Good Flow Front (S2P2)

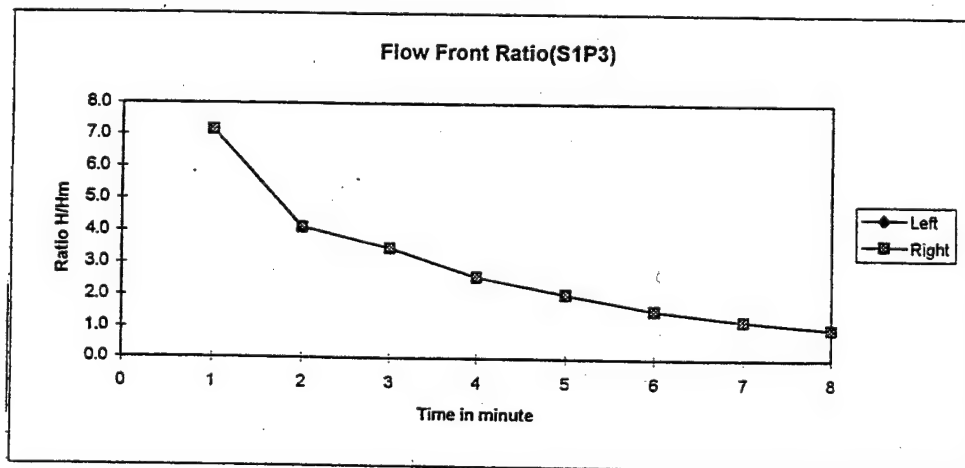


Figure 4-8 Height Ratio for a Poor Flow Front (S1P3)

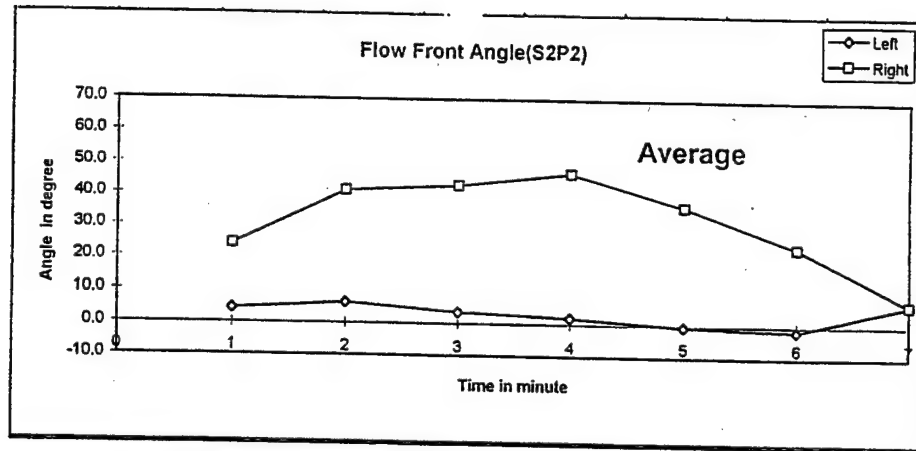


Figure 4-9 Flow Front Angle for a Good Flow Front (S2P2)

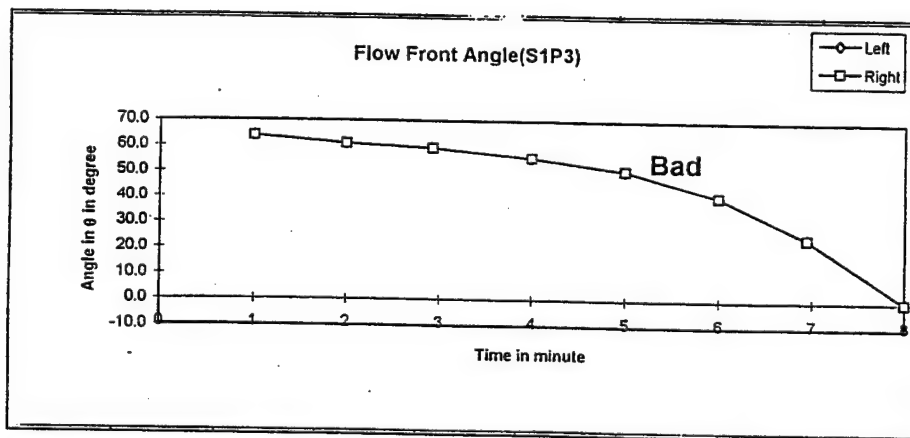


Figure 4-10 Flow Front Angle for a Poor Flow Front (S1P3)

$\theta_L$  and  $\theta_R$  exhibit identical patterns. Both angles start from extremely high values and gradually approach zero. Such a pattern depicts that the side fronts run rapidly ahead of the central front, which is an indication of severe race tracking. For the good flow fronts, the values of the angles seem to be limited to no more than  $45^\circ$  while in the case of the poor fronts the values seem to be higher. The plots of the flow front angles for the experiments are provided in Appendix G.

Unlike the height ratios, the flow front angle, even for the poor fronts have a limit which is dictated by the height of the mold and the length  $L$  from the central axis to the location of the reference lines at the sides of the mold. In our case, the mold height was 11 in. and the length  $L = 4.625$  in. As the resin reaches the top, the resin front height is kept at a constant value of 11 in. Thus, for the worst case scenario, the resin flow at the sides of the mold will race rapidly to the top of the mold before the central flow actually begins to rise. This gives an angle of  $67^\circ$ . If the height ratio is used to characterize the resin flow front for such a scenario, the value will be infinity, which is not appropriate for characterizing the resin flow. Thus, even though both the height ratios and the flow front angles are good measures for the characterization of the resin flow front, the flow front angle is pursued due to the fact it is a bounded parameter.

#### 4.2.3 Parameterization of Flow Front

Using the flow front angle, the next step is to develop a parameter that could be used to quantify the characteristics of the front. By inspecting the plot of the flow front angle, it can be seen that the area under the graph is obviously larger for the poor flow fronts than for the good ones. Thus, this area is explored as a parameter (index) to quantify the front. Figure 4-11 shows a general plot of the flow front angle with time. By dividing the area into simple trapezoids, the total area can be evaluated numerically.

Since the area must be evaluated for each side of the mold, the parameters  $A_L$  and  $A_R$  represent the weighted areas under  $\theta_L$  - time plot for the left side and the right side, respectively. Large values result from severe skewness (race tracking) and vice-versa. We need to determine whether there is any correlation between the results of the gas flow parameters and these area quantities.

#### 4.2.4 Correlation of Flow Front Parameter and Gas Flow Parameter

Figure 4-12 provides scatter plots of the resin flow front parameters ( $A_L$  and  $A_R$ ) versus the gas flow parameters ( $P_L$  and  $P_R$ ). These scatter plots suggest a linear correlation between  $A_L$  and  $P_L$  and also between  $A_R$  and  $P_R$ . In order to evaluate the statistical significance of the correlation, the flow on each side of the mold was classified as acceptable or non-acceptable based on the visual inspection of the severity of the race tracking. The flow front of each group was separately correlated with the corresponding gas flow data. Table 4-18 shows the summary of the results of the analysis. A statistically significant correlation was found to exist between the gas flow data ( $P_L$  and  $P_R$ ) and the corresponding flow front angle area ( $A_L$  and  $A_R$ ) at 5% significance. Thus, we could use the gas flow parameters to draw conclusions about the flow front area.

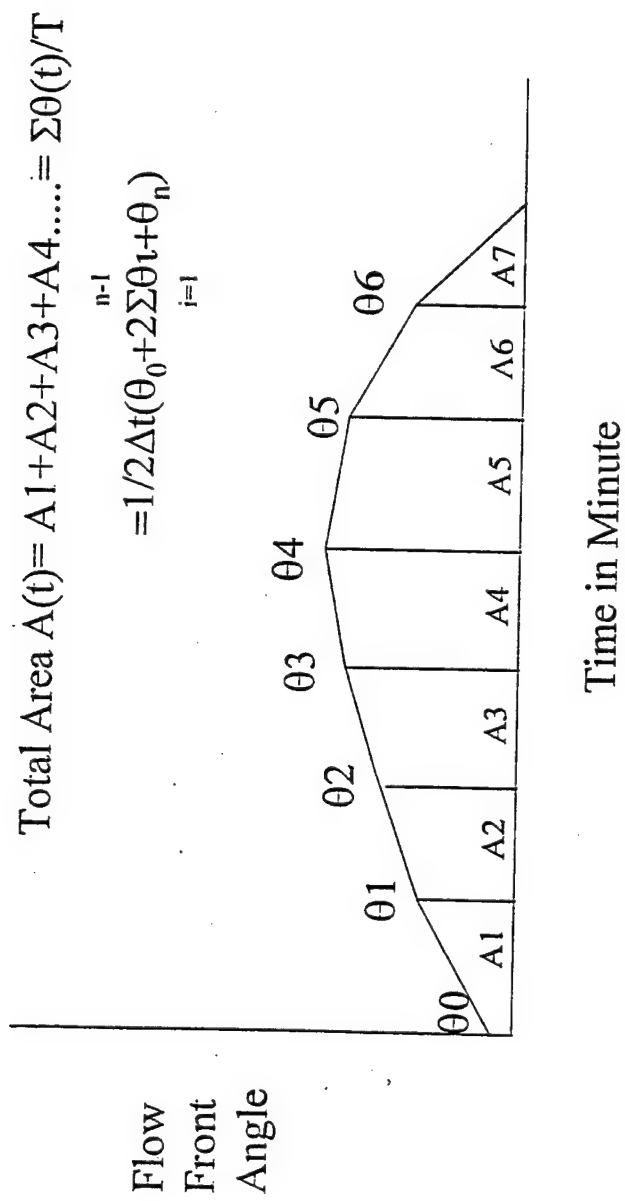


Figure 4-11 Definition of Flow Front Angle Area

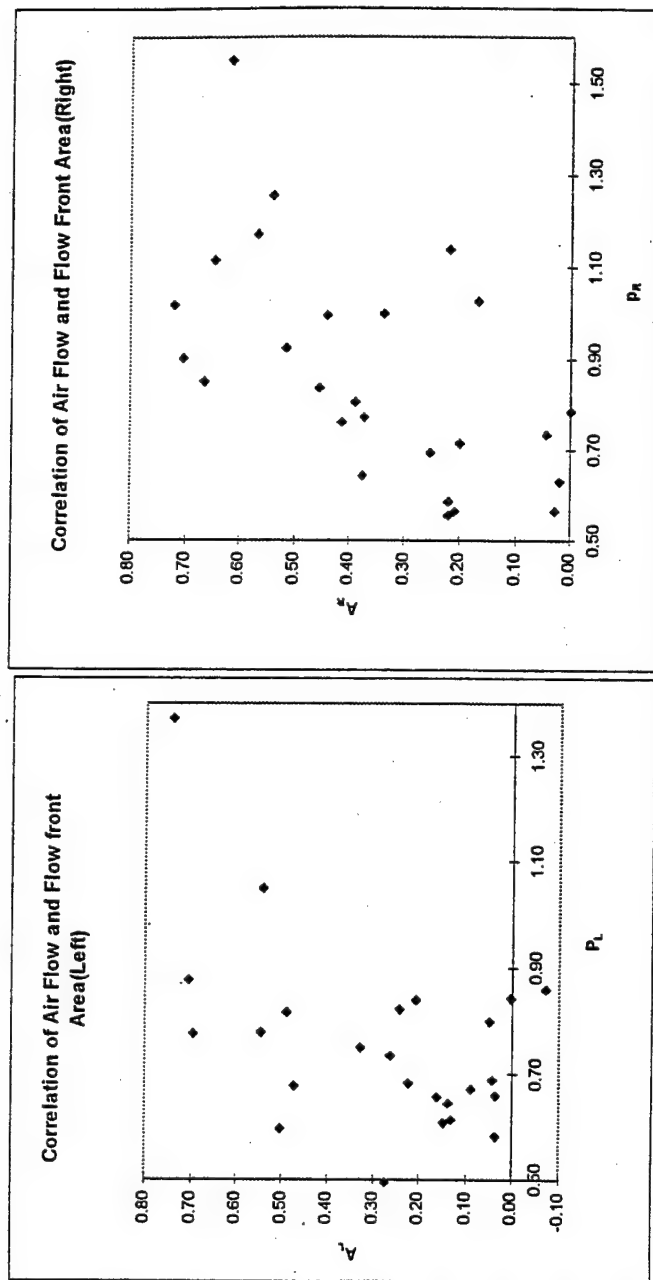


Figure 4-12 Scatter Plot of Gas Flow Parameters versus Flow Front Angle Area

Table 4-18 Correlation of Gas Flow Parameters versus Flow Front Angle Area

### SUMMARY OF CORRELATION-2

Air	Flow Area per min. (Radian)	Correlation Coefficient
Left		
$P_L = (P_2 + P_5)/2$	$A_L$	0.50
Right		
$P_R = (P_3 + P_7)/2$	$A_R$	0.59

Theoretical for 95% confidence level 0.381 for 25 degree of freedom

Observation

-Significant correlation between areas and air flows

-Air Flow can be used to predict degree of race tracking

Table 4-19: Limits of Gas Flow Parameter

Acceptable = Mean +/- Experimental Error

Upper limit =  $0.670 + 0.1 = 0.77$

Lower limit =  $0.670 - 0.1 = 0.57$

Unacceptable = Mean +/- Experimental Error

Upper limit =  $0.970 + 0.1 = 1.07$

Lower limit =  $0.970 - 0.1 = 0.87$

#### 4.2.5 Limits of Gas Flow Parameter

Since the flow front areas can be used to characterize race tracking, we could use the airflow data to characterize race tracking. Also since the correlation is positive, it implies that a higher value of the gas flow parameter would yield a higher value of the resin front parameter (severe race tracking). The cut-off point for an acceptable value of the gas flow parameters needs to be established. In order to do this; the flow fronts were grouped into acceptable and unacceptable fronts. It should be realized that one side of a particular resin flow might yield an acceptable flow while the other side may yield an unacceptable flow. Thus, each flow front was analyzed and each side of the front was characterized as acceptable or unacceptable. The statistics of the gas flow parameter for each group were obtained. Table 4-19 shows the summary of the results.

Assuming that the distribution is normal, we found that the mean of the gas flow parameter (P) was 0.670 with a standard deviation of 0.108 for the acceptable flow fronts while the mean for the unacceptable flow fronts was 0.972 with a standard deviation of 0.223. Based on the pooled standard deviation, the experimental error was determined to be  $\pm 0.1$  at the 95% confidence level. This provided the following air flow ranges:

Acceptable Flow Front:  $P_L$  or  $P_R = 0.670 \pm 0.1$  or (0.570, 0.770)

Unacceptable Flow Front:  $P_L$  or  $P_R = 0.872 \pm 0.1$  or (0.772, 0.972)

Figure 4-13 shows these two ranges on the normal distribution curves. The two ranges show no significant interference and, thus, could be concluded to come from two independent populations. Rounding off, we, thus, conclude that if the air flow parameter is 0.8 or less, we should expect an acceptable flow front and if higher, we should expect an unacceptable flow front with severe race tracking on that particular side of the front. Since the decisions are made independently for each side of the mold, we can predict separately for each side of the mold. It should be noticed that one side of the flow could be race tracking severely while the other side is not.

# ACCEPTANCE CHART

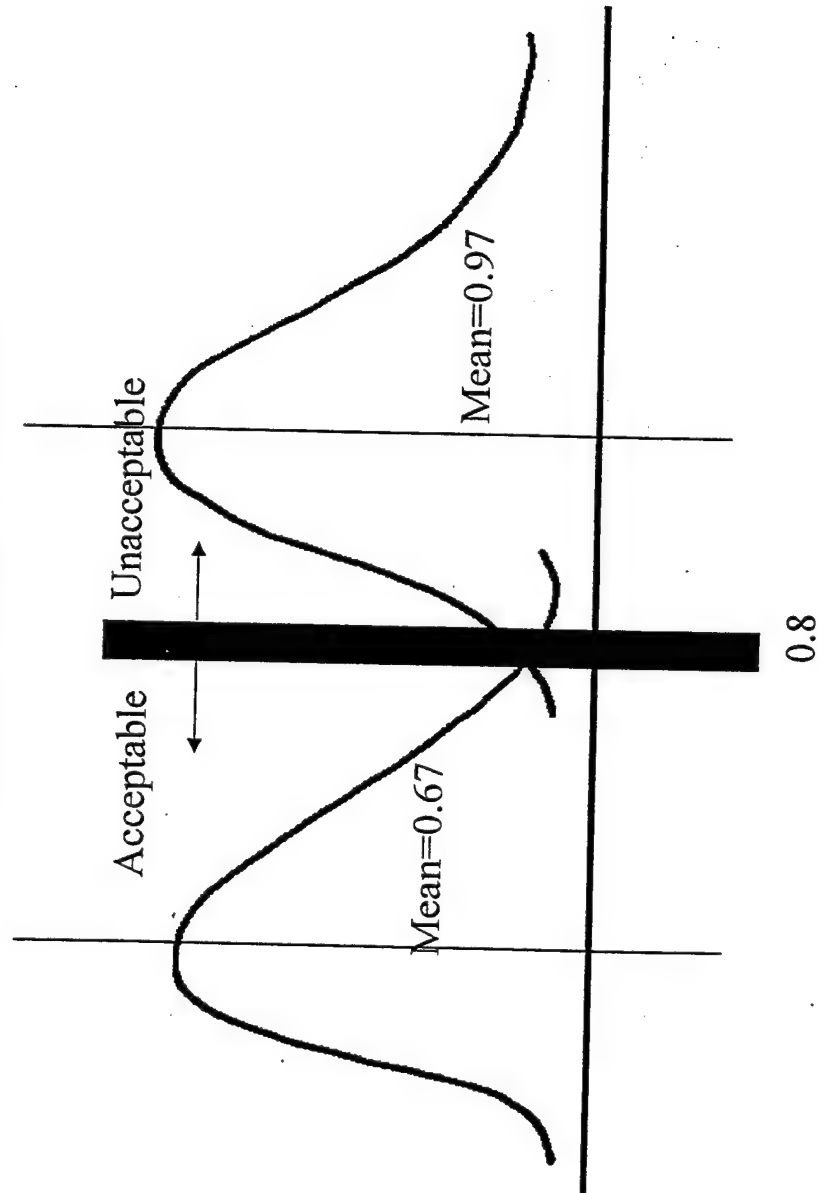


Figure 4-13 Normal Distribution Showing Limits of gas Flow Parameter



### 4.3 Verification of Method

Figure 4-14 illustrates the decision process model. The actual flow rate through each flow meter ( $q_i$ ) is recorded. The normalized flow rate for each port is calculated ( $Q_i = q_i/q_{avg}$ ). The left flow parameter [ $P_L = \text{Avg.}(Q_2, Q_5)$ ] and the right flow parameter [ $P_R = \text{Avg.}(Q_3, Q_7)$ ] are extracted. The skewness and the severity (race tracking) are then predicted using  $P_L$  and  $P_R$ .

**Skewness:** If the absolute difference between the two parameters  $P_L$  and  $P_R$  is greater than 0.2, then the flow will be skewed, otherwise it will be even. If the flow front is skewed and  $P_L > P_R$ , then the flow will favor the left side and the front will be skewed to the right side, otherwise it will be skewed to the left side.

**Race Tracking:** For an even flow, it is sufficient to check the severity on only one side. If  $P_R$  or  $P_L > (P_{lim} = 0.8)$ , then race tracking is severe on both sides. Otherwise, the race tracking is not severe, if it exists. For a left-skewed flow, if  $P_R > (P_{lim} = 0.8)$ , then race tracking is severe on the right side. Otherwise, right race tracking is not severe, if it exists. For a right-skewed flow, if  $P_L > (P_{lim} = 0.8)$ , then race tracking is severe on the left side. Otherwise, left race tracking is not severe, if it exists.

#### 4.3.1 Verification Using Flat Panels

A set of 6-ply flat panels was made to verify the methodology. All the ports were open during the air flow measurements. The experimental procedures used for the previous twenty panels were applied exactly. Before the resin injection, the LabView VI was used to predict the nature of the resin flow. Table 4-20 shows the values of the gas flow parameters.

Table 4-20: Normalized Data and Gas Flow Parameters ( $P_L, P_R$ ); 2-D Verification Part

Panel I.D. #	Port #1	Port #2	Port #3	Port #4	Port #5	Port #6	Port #7	Right Gas Index, $P_L$	Left Gas Index, $P_R$
S3P1	1.790	0.350	0.780	2.230	0.390	0.630	0.830	0.370	0.800
S3P2	2.170	0.620	0.630	1.730	0.480	0.680	0.690	0.554	0.656
S3P3	1.574	1.096	0.998	3.090	0.403	0.653	0.426	0.712	0.749
S3P4	1.293	0.474	0.464	1.456	0.753	0.742	0.707	0.585	0.614
S3P5	1.163	0.703	0.642	2.347	0.671	0.836	0.639	0.641	0.687
S3P6	1.856	0.751	0.985	1.831	0.610	0.483	0.482	0.733	0.681

Figures 4 -15 through 4 -20 show the resulting flow fronts. The difference between the gas flow parameters for S3P1 exceeds 0.2 and, thus, the flow is expected to be skewed with more resin flow to the right side of the mold. The last place to fill is, thus, expected to be at the left side of the vertical axis of the mold. The value of  $P_R$  (0.8) is right at the limit for severe race tracking on the right side while  $P_L$  (0.370) is considerably below the limit, corresponding to a nice even flow on the left side. The rest of the panels should experience even flows on both sides of the mold and none should possess severe race tracking. The flow fronts confirm these predictions. The outputs obtained from the LabView are presented in Appendix H. The LabView output shows following results:

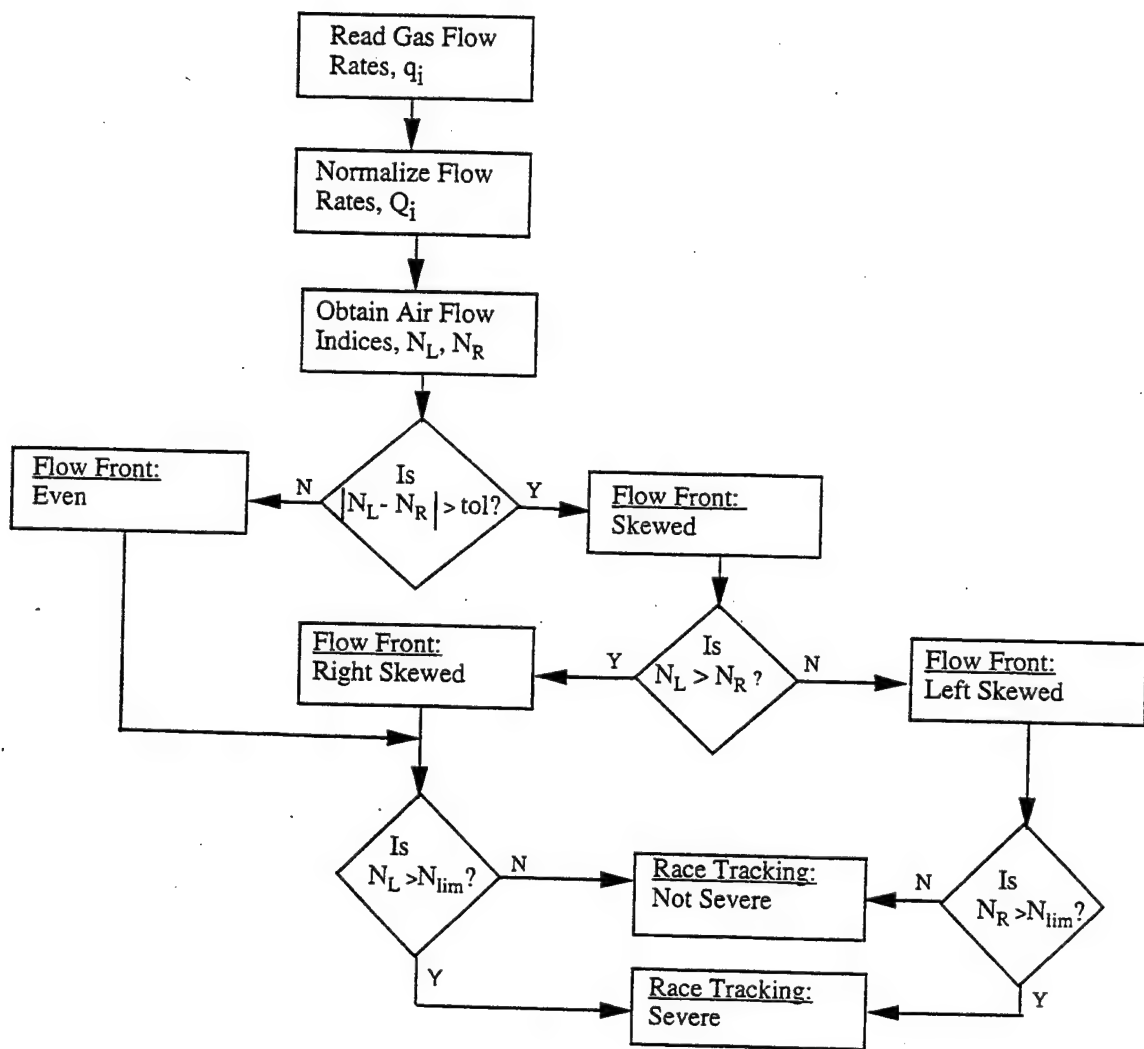


Figure 4-14 Flow Chart of Methodology for Prediction of Resin Flow

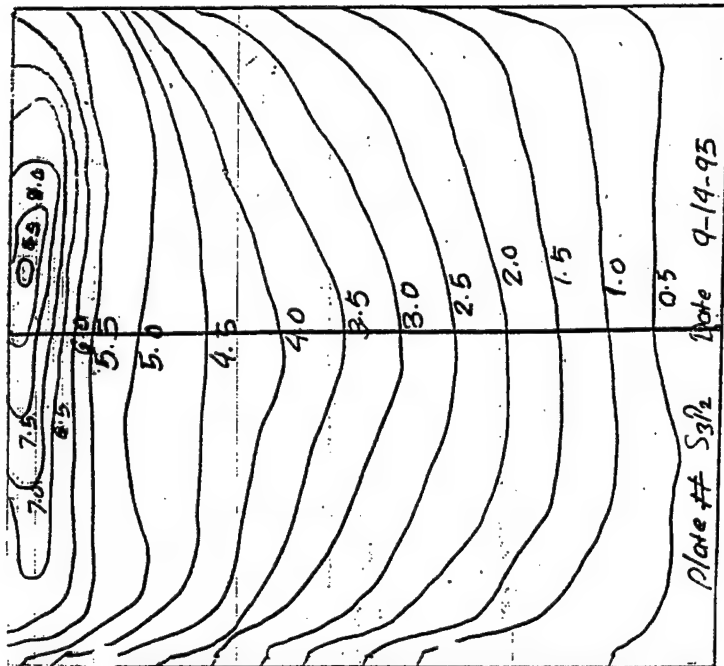


Figure 4-16 Flow Front for S3P2

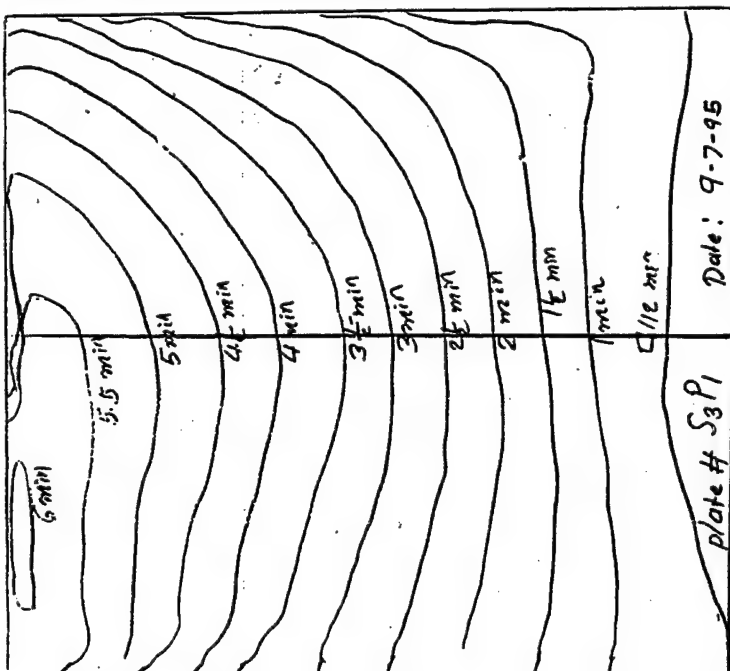


Figure 4-15 Flow Front for S3P1

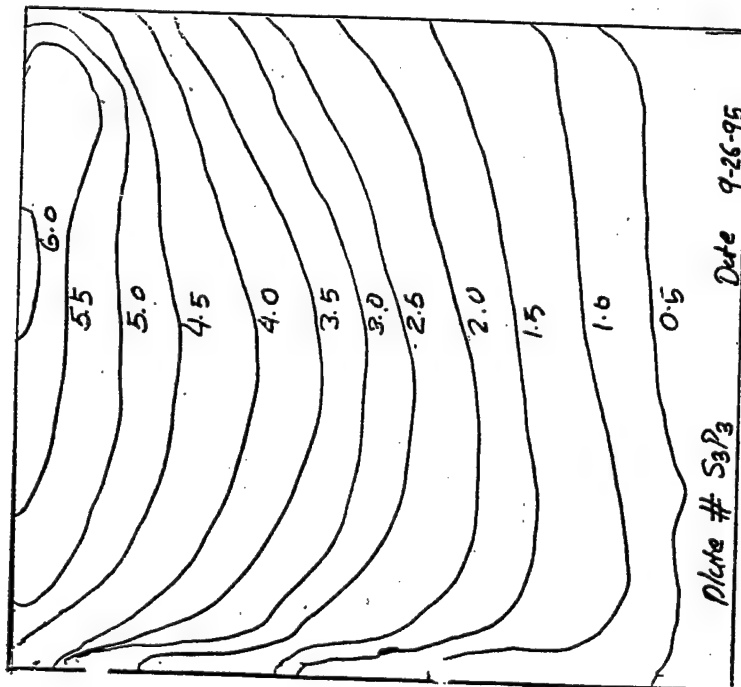


Figure 4-17 Flow Front for S3P3

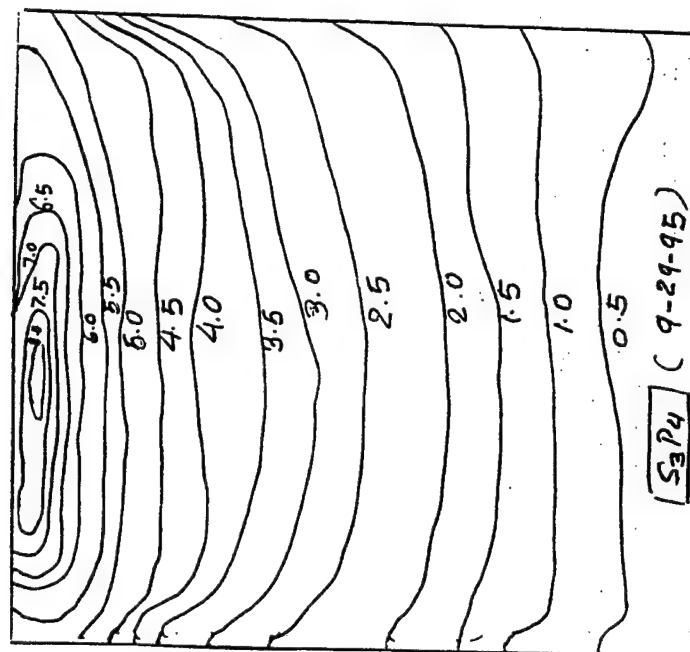


Figure 4-18 Flow Front for S3P4

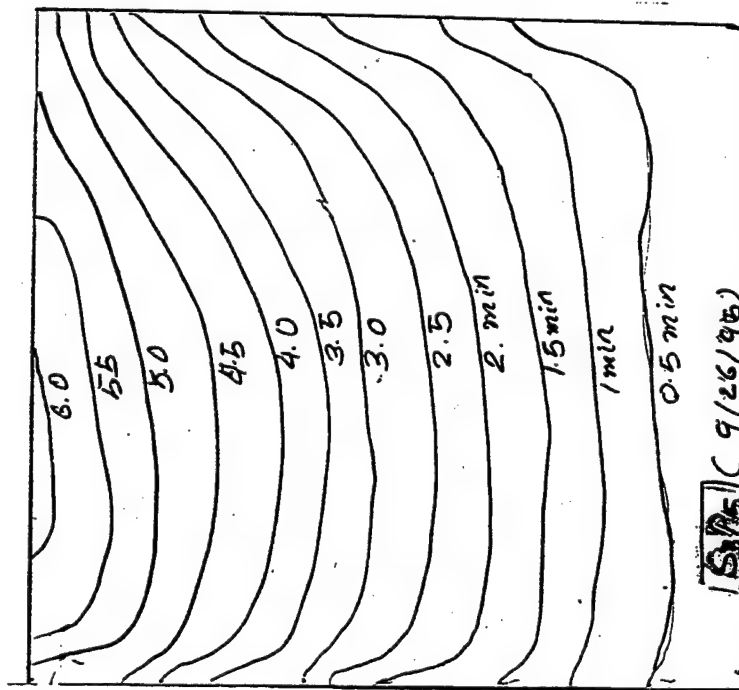


Figure 4-19 Flow Front for S3P5

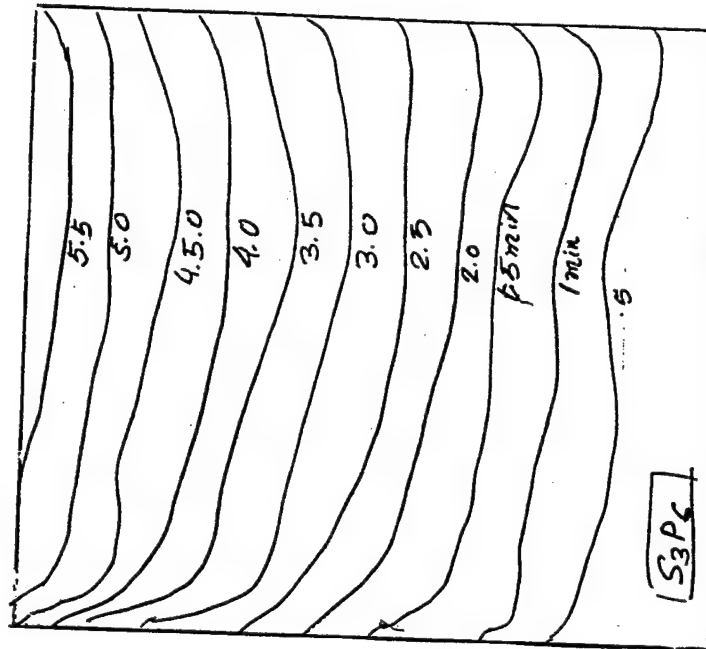


Figure 4-20 Flow Front for S3P6

1. raw air flow values for each port
2. bar chart representing these readings
3. normalized data
4. values of  $P_L$  and  $P_R$
5. skewness of the flow front
6. degree of race tracking

From the LabView predictions and flow fronts diagrams for all of the plates, the use of the developed methodology to predict the direction of the skewed resin flow is verified. The region of the mold with the higher gas flow parameter was expected to have the resin flow skewed to that region. In the instances in which the average flow values were within the experimental error range ( $\pm 0.2$ ), a prediction of equally skewed flow was given. For all the panels, this method proved successful in predicting the region of the skewed resin flow prior to resin injection. The degree of the severity of race tracking is also predicted and verified for the flat panels.

#### **4.3.2 Verification using 3-D Demonstration Part**

The methodology discussed above was developed using flat rectangular panels. In order to test its applicability to other geometries, the method was applied to a simple 3-D part. This section discusses the part geometry, the gas flow parameter and the results from the resin injection.

Figure 4-21 shows diagram of the demonstration part. This is essentially a 6-ply hat section of uniform cross section and width of 8 in. The special features include two sets of connecting corner radii and the direction of flow such that the resin flows over curved surfaces. The bottom of the part is in contact with the bottom half of the mold made of steel and the top is in contact with the acrylic top of the mold. Due to our experience with the flat panel, the mid section of the top acrylic mold is made heavier to prevent deflection due to the compressive stress applied to the graphite preform and warpage due to the thermal stresses during the curing operation.

The same process conditions were applied as before. The preform is made of graphite/epoxy, as is the flat panel. The set up and the data collection procedures are maintained as the same for the flat panel.

Table 4-21 shows the values of the gas flow parameters for the parts before the resin injection. Figures 4-22 to 4-26 show the resulting flow fronts.

The differences between the gas flow parameters do not exceed 0.2 (critical value), except for S4P1 which is right at the critical value and thus, the flows are expected to be even flow on both sides of each panel. The value of each gas flow parameter is much lower than the cut-off point of 0.8 required for severe race tracking and thus, these panels should experience even flows on both sides of the mold and none should possess severe race tracking. The flow fronts confirm these predictions.

#### **4.4 Material Properties**

The purpose of this section is to compare the properties of the panels produced with those achieved by other investigators to ensure that the conclusions drawn are valid.

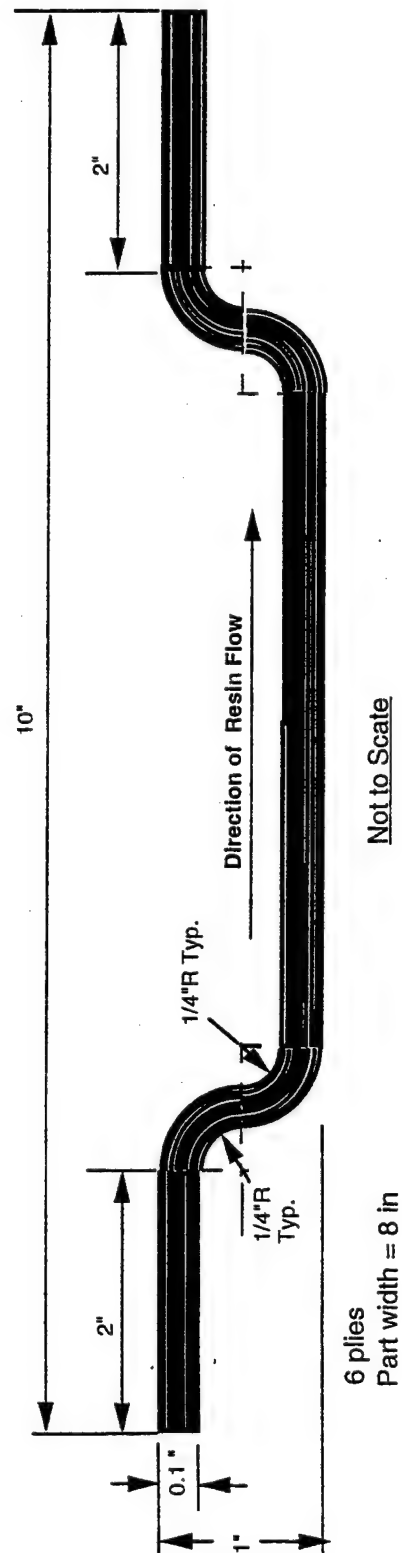


Figure 4-21 3-D Demonstration Part

Table 4-21: Normalized Data and Gas Flow Parameters ( $P_L$ ,  $P_R$ ); 3-D Demonstration Part

Panel I.D. #	Port #1	Port #2	Port #3	Port #4	Port #5	Port #6	Port #7	Right Gas Index, $P_L$	Left Gas Index, $P_R$
S4P1	4.917	0.010	0.007	1.923	0.080	0.243	0.536	0.045	0.272
S4P2	4.126	0.197	0.034	1.937	0.177	0.182	0.348	0.187	0.191
S4P3	4.509	0.088	0.158	1.712	0.170	0.188	0.174	0.129	0.166
S4P4	4.078	0.148	0.173	2.098	0.124	0.236	0.142	0.136	0.158
S4P5	3.670	0.223	0.305	2.285	0.130	0.218	0.170	0.177	0.238

#### 4.4.1 Physical Properties

Information regarding the mix ratios, viscosities, flow rates, and other related parameters were sought from on-going and past activities. Experiments have been performed by others (Senibi et al., 1993) to determine the number of plies to be used to attain at least 50 % fiber volume fraction. This was done by increasing the number of plies and measuring the specific gravity and the fiber content. Figures 4-27 and 4-28 show plots of the specific gravity and fiber volume fraction versus the number of plies, respectively. These experiments were performed using satin weave graphite fiber and Dow Chemical's Tactix 123 epoxy matrix. It was determined that for the given mold, a 54 % fiber volume is attainable with an 8-ply preform. The corresponding values for a 6-ply preform are approximately 1.42 specific gravity and 40% fiber volume. Our experiments yielded a specific gravity of  $1.418 \pm 0.015$  and fiber volume of  $41.85 \% \pm 2.68$  for the 6-ply panels. These values match the established ones and, thus, our experiments yielded accurate data for the analysis. The comparison with the graphite/epoxy system is of the most interest. The density is very close to the expected results. However, the fiber volume fraction is much lower than expected. This may be due to the fact that the fiber volume fraction is a function of the number of plies and we are using fewer plies than those reported.

Previous investigators have also studied the void content at various resin flow rates. Plots of the void content versus the flow rate for RRTM and VARTM are shown in Figure 4-29. It can be seen that the void content for the RRTM is always higher than that of the VARTM at all flow levels. Furthermore, at resin flow rates higher than 28 g/min., the void content of the regular RTM rises very sharply while that of the VARTM remains essentially constant. For our experiments using VARTM and 30 g/min. flow rate, we obtained an average void content of  $0.756 \% \pm 0.473$ , which compares quite well with previous results.

#### 4.4.2 Mechanical Properties

The two mechanical properties studied are the inter-laminar shear strength and the compressive strength and its associated Young's modulus. In the inter-laminar short beam shear test, the specimen could fail by rupture, micro-buckling or interlaminar cracking or a combination of modes depending on the loading conditions and the material geometry. The span length and overhang were varied and the part tested until shear failure was obtained. The importance of the interfacial bonding is evidenced by the well-



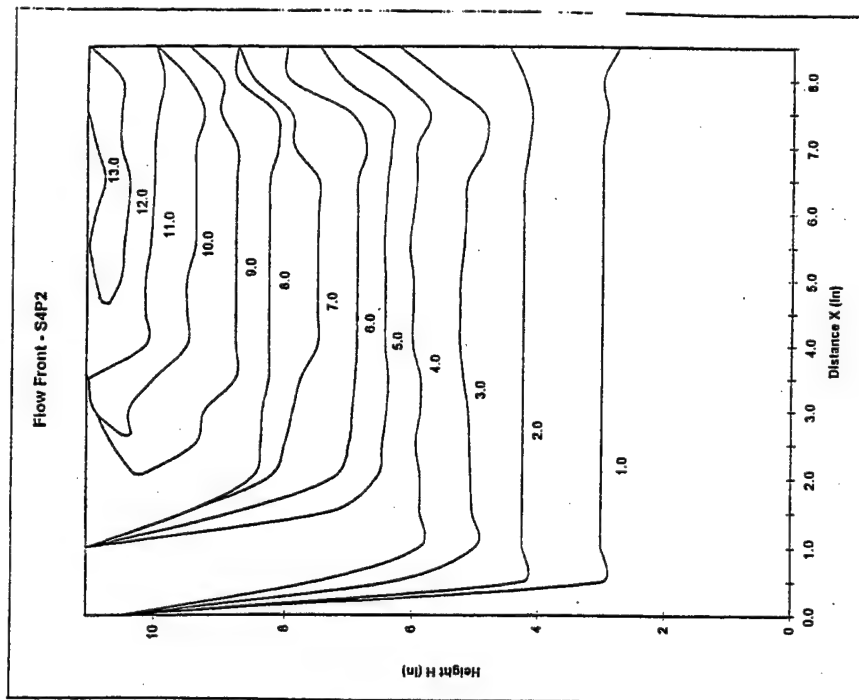


Figure 4-23 Flow Front for S4P2

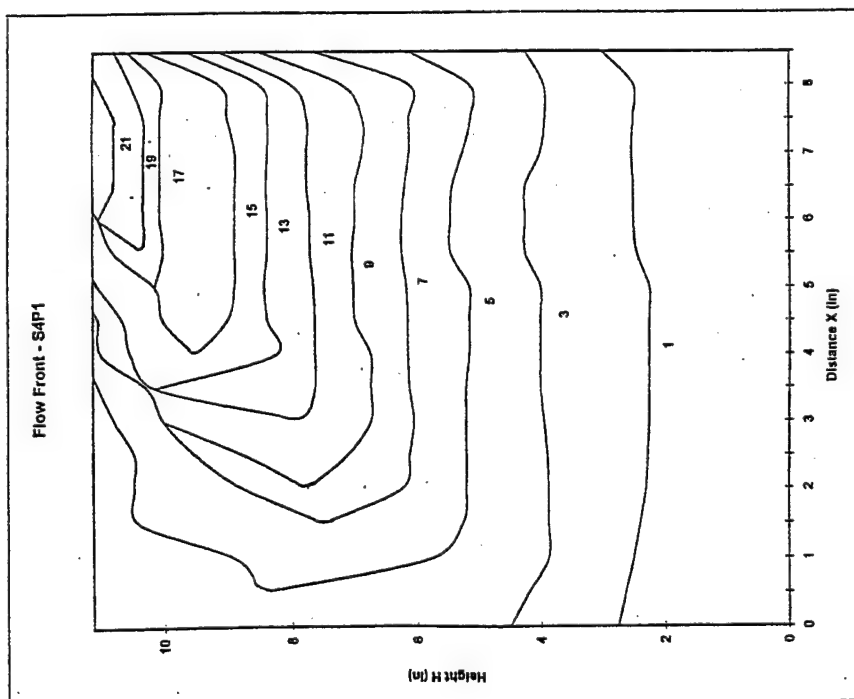


Figure 4-22 Flow Front for S4P1

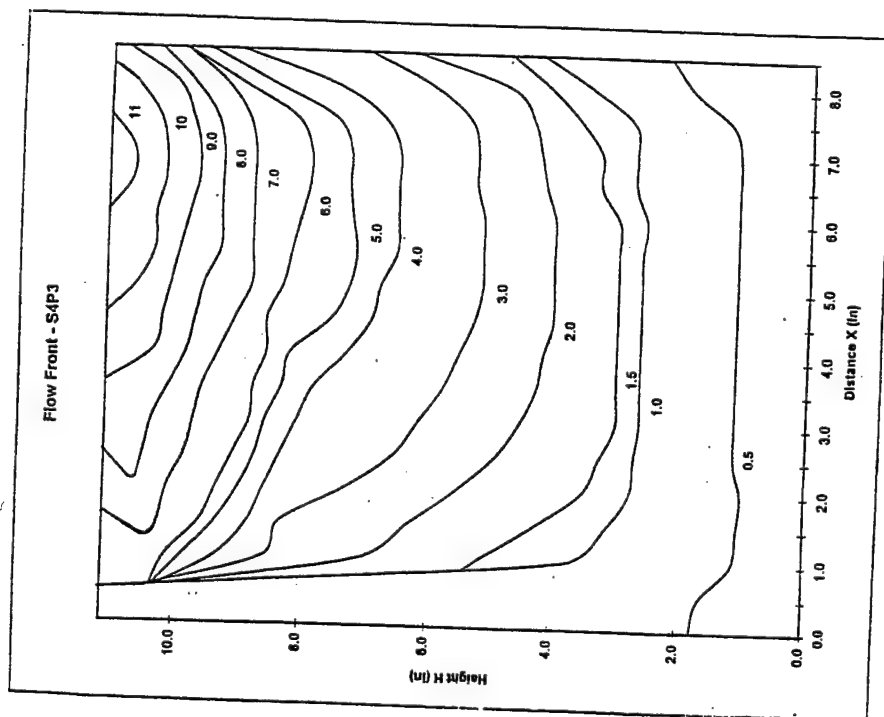


Figure 4-24 Flow Front for S4P3

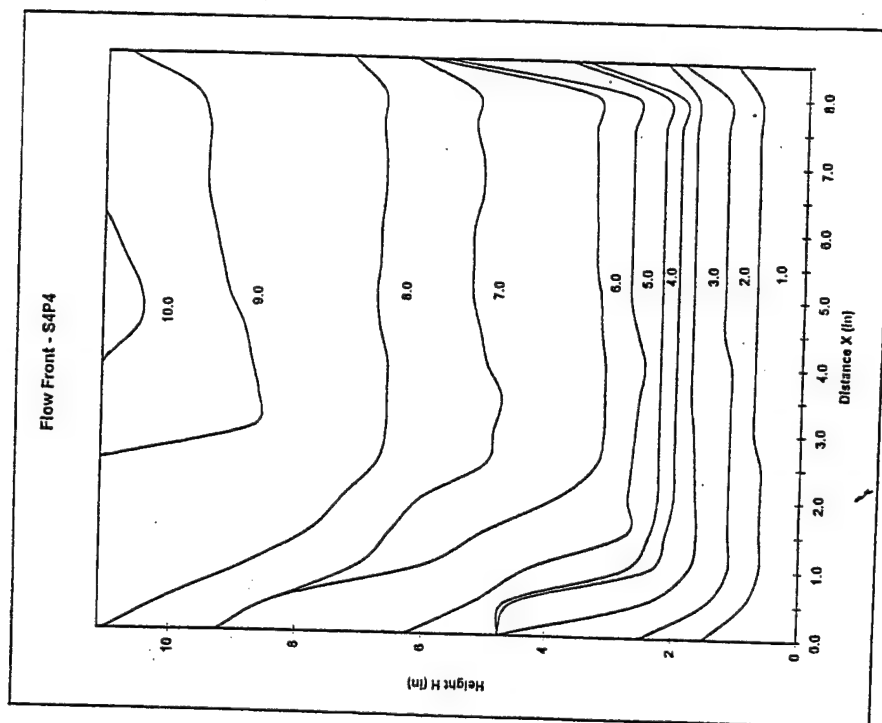


Figure 4-25 Flow Front for S4P4

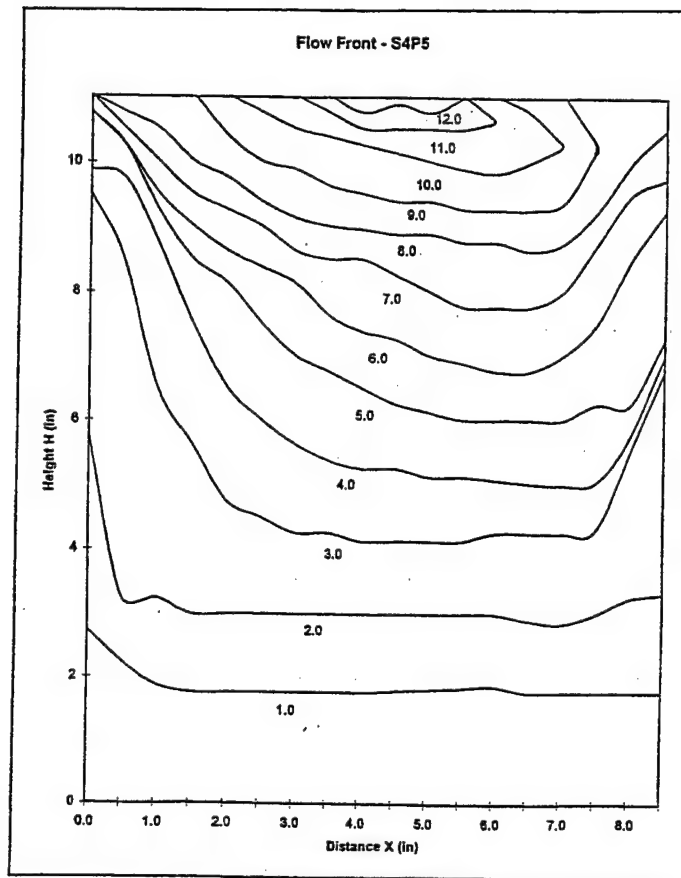


Figure 4-26 Flow Front for S4P5

known fact that glass-epoxy composites have higher inter-laminar shear strengths than those of vinyl ester and polyester composites. Our values average  $6.08 \pm 0.62$  ksi which is lower than those of typical graphite/epoxy systems due to the smaller number of plies used. Our values range from 2.96 to 7.1 ksi, so it seems that the failure mode was rather inconsistent and that could be the reason for the low shear strength values.

The panels from our experiments yielded  $45.4 \pm 0.97$  ksi for the compressive strengths. The longitudinal compressive strength of such  $0^\circ$  laminates depends on the fiber type, fiber volume fraction, matrix modulus, matrix yield strength, fiber straightness as well as the fiber-matrix bond strength. Thus, the effect of matrix-fiber interfacial bond is difficult to isolate. Even though the strength falls short of what is reported, the values are well within the acceptable range.

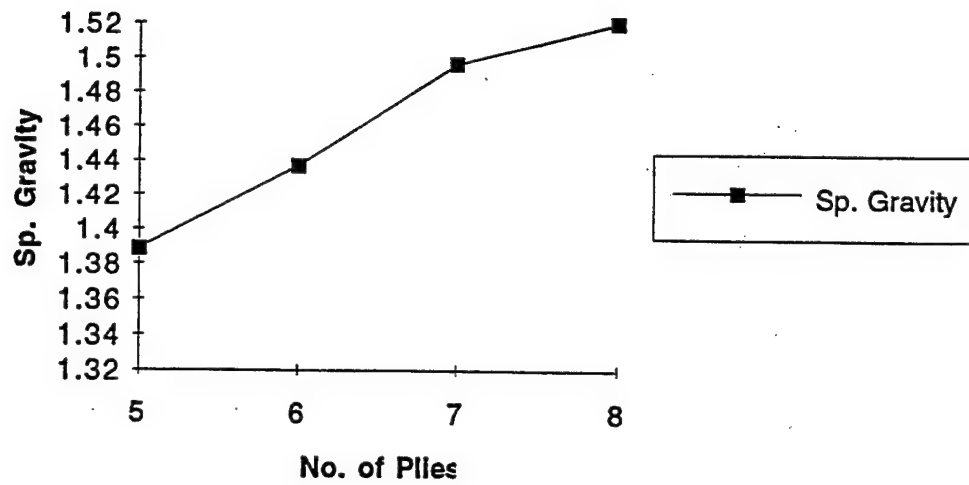


Figure 4-27 Specific Gravity versus Number of Plies

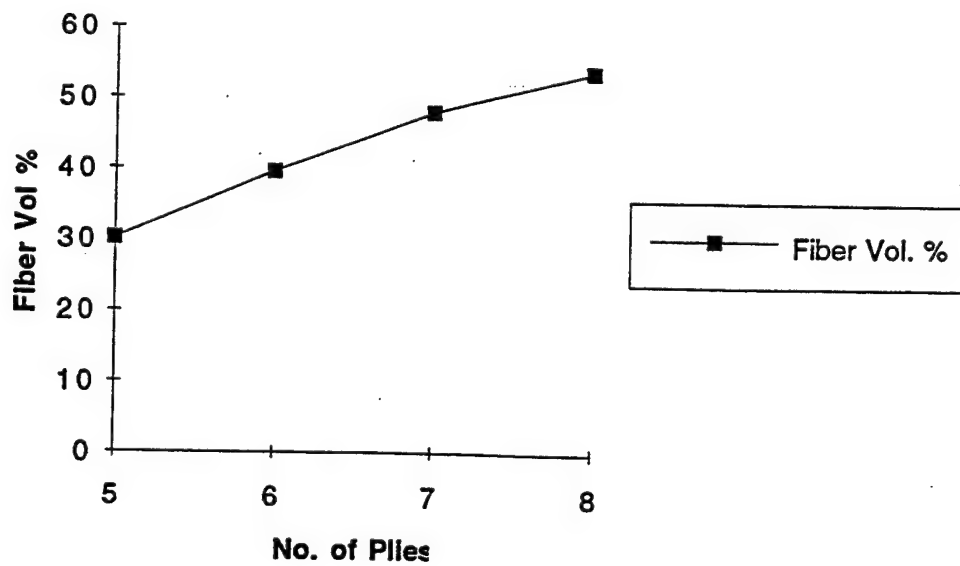


Figure 4-28 Fiber Volume versus Number of Plies

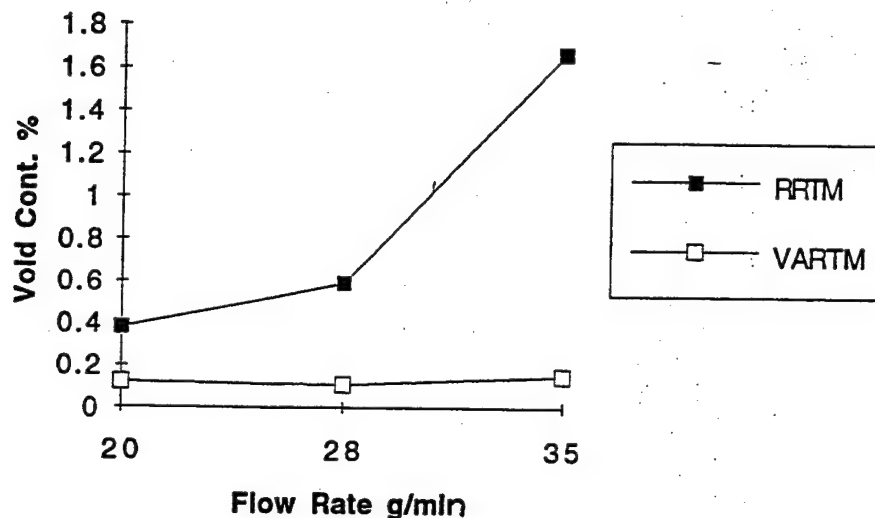


Figure 4-29 Void Content versus Resin Flow Rate

#### 4.4.3 Relationship among Material Properties

The physical and mechanical properties obtained in section 4.4.2 were analyzed to find the effects of the fill time and the race-tracking index. Ten panels were chosen as samples for this analysis. The specimens were taken from six regions of each panel, Lower Left, Lower Mid, Lower Right, Upper Left, Upper Mid, and Upper Right. Five were classified as severe race tracking, and five as acceptable race tracking. The idea was to investigate the correlation of the two sets of results. The results and analysis are discussed in this section.

The fill time (T) was the number of minutes it took for the resin to start rising from the intake manifold to the exit from the mold from all three top ports. The LabView data acquisition software automatically recorded the time. The race-tracking index ( $A_L$ ,  $A_R$ ) is essentially the rate at which the area of the panel fills per min. The index was split into right and left sides to determine the amount of race tracking that occurred on each side. Each of these two parameters was correlated with the Young's modulus, fiber volume, and the micro-void content. The complete results are provided in Appendix I. Tables 4-22 and 4-23 show the summary of the correlation coefficients. The fill time is analyzed against the properties resulting from the six regions of the panel while the race tracking index is analyzed against those obtained from either the left or the right edge since race-tracking does not relate to the central flow. Each correlation was performed at the 95% confidence level.

The Young's modulus was obtained from the results of IITRI compression test. There was no correlation found between the fill time and the Young's modulus. The Young's modulus in the first and fourth regions (left edge) was correlated against the left race-tracking index, and the Young's modulus in the third and sixth regions (right edge)

was correlated against the right race-tracking index. Again, there was no correlation found in each of these cases.

The interlaminar shear strength was obtained from the results of the transverse short-beam shear test. The shear strength was correlated against the results from the 10 panels from each region. There was no correlation between the fill time and the shear strength. There was no correlation between the shear strength and the race-tracking index.

The fiber volume fraction was obtained from the results of the acid digestion method. The fiber volume in each of the six regions was correlated against the fill time. There was a significant correlation between the fill time and the fiber volume of the lower section of the panel (regions 1, 2, and 3) while there was no correlation at the top section of the panel. The fiber volume percentage was also correlated against the race-tracking index and no significant correlation was detected.

The percent void content was also obtained from the results of the acid digestion method. The same specimens that were used for determining fiber volume were also used to determine the percent void content. The percentage void content was correlated against the fill time. There was no significant correlation between the two variables.

The percent void content was correlated with the race-tracking index. The averages of the first and fourth regions were correlated with the left side race-tracking index and the third and sixth regions were correlated with the right side race-tracking index. There was also no significant correlation between the race-tracking index and the percent void content.

Thus, the only case in which a correlation between the material properties of the panels and the process parameters of the VARTM process was the percent fiber volume versus fill time. Even though the results were not totally conclusive because there were only three cases from two regions of the panels which validated this analysis; it would seem that the fill time might have an influence on the fiber volume.

Table 4-22 Correlation Coefficients between Material Properties and Fill Time

Properties	Region					
	Lower Region			Upper Region		
	1. Left	2. Middle	3. Right	4. Left	5. Middle	6. Right
Physical						
Fiber Volume % vs Fill time	0.898	0.745	0.628	0.483	-0.127	0.342
Void Content % vs Fill time	0.699	0.578	-0.09	0.023	-0.246	-0.151
Mechanical						
Young's Modulus vs Fill time	-0.28	-0.095	-0.45	0.197	0.517	0.058
Shear Strength vs Fill time	0.232	0.130	0.200	0.214	0.306	0.356

Table 4-23: Correlation Coefficients between Material Properties and Race-Tracking Index

Properties	Race-tracking Index	
Physical	Left Side	Right Side
Fiber Volume % vs Race-tracking Index	0.497	0.347
Fiber Content % vs Race-tracking Index	0.350	0.064
Mechanical		
Young's Modulus vs Race-tracking Index	0.107	0.154
Shear Strength vs Race-tracking Index	0.413	0.109



## CHAPTER 5

### CONCLUSIONS AND RECOMMENDATIONS

The primary goal of this work was to develop a technique for predicting the characteristics of the resin flow in RTM prior to resin impregnation and to develop an intelligent advisory system to assist the user. The secondary goals include the determination of the severity of race tracking, the determination of the relationship between the process response and the material properties.

The technique developed involved the probing of the ready-to-inject mold/preform assembly with nitrogen. The nitrogen is injected through the resin injection port and allowed to exit through ports located along the periphery of the mold. Seven ports are used in this project with two at each vertical side of the mold and three at the top of the mold. The air flow rates are monitored by electronic mass flow meters and interfaced with a data acquisition system which is programmed to evaluate the mold-preform fit.

The first challenge was to determine the manner in which the ports must be opened or closed to provide a nitrogen flow pattern that may match the resin flow pattern. Thus, experiments were run with (1) no-ports-closed, (2) side-ports closed, (3) lower-ports-closed and (4) top-ports-closed to vary the flow pattern of the gas. The relative percent of the gas flow through the remaining ports was compared with the skewness of the resin flow and it was concluded that the no-ports-closed configuration provided the best scheme for the prediction of the resin flow pattern.

Various port combinations were observed, alongside the various ways to represent the flow pattern of the resin. It was determined that the gas flow parameter, obtained by normalizing the airflow through each port by the average flow rate, is appropriate to evaluate the flow through each port. The normalized flow through the corner exit ports (ports (2 and 5) and ports (3 and 7) in this case); when used to evaluate the gas flow parameter, provides the best parameter to estimate the resin flow pattern under the *No-ports-closed* configuration of the mold. The skewness is predicted as either right, left or even depending on the relative values of the left and right gas flow parameters ( $P_L$  and  $P_R$ ). In our experiments, the skewness is considered to be significant if the values of  $P_L$  and  $P_R$  deviate by 20% (0.2). These parameters provide a guideline for indicating the probability of skewed resin flow and race tracking in a particular region of the mold. Thus, it may be concluded that the permeability along the periphery of the ready-to-inject mold can be determined by probing the system with a low pressure inert-gas, such as nitrogen, and by monitoring the flow rates of the gas along pre-determined exit ports. The mold used is an upright mold and the flow through the exit ports near the two top corners of the mold provided the basis for the prediction of the behavior of the flow front.

A flow front-angle parameter ( $\theta_L$  and  $\theta_R$ ) has been determined to represent the dynamic behavior of the flow front. The magnitude of the area under the  $\theta$  - time plot ( $A_L$  and  $A_R$ ) has been determined to correlate with the normalized nitrogen flow rate parameters ( $P_L$  and  $P_R$ ). In our experiments, the typical flow fronts along the edges of the mold were ahead of those near middle section of the mold. Thus, race tracking may be considered to be an unavoidable phenomenon associated with resin transfer molding. Its

severity could be predicted by the level of the gas flow parameters ( $P_L$  and  $P_R$ ). Higher values indicate more severe race tracking. In our experiments, it was concluded that values greater than 0.8 would lead to severe race-tracking. The value of  $N_{lim}$  should be established for that particular setup.

The specific gravity, percent fiber volume, and the percent micro-void content are used to characterize the physical properties of the material. The inter-laminar shear strength, the ultimate compressive strength and the Young's modulus were used as the mechanical properties of the material. The fill time and the flow front parameter are used to represent the process response. Tests were performed to evaluate these material properties in order to ensure that the results agreed with the literature and to validate the experiments. The comparisons show that for the 6-ply panels the results are acceptable and, thus, the data is trustworthy. The process response and the materials properties are correlated with inconclusive results. The only probable correlation is with the fill time versus the fiber volume and the fill time versus the micro-void content. Both seem to indicate that as the fill time increases the fiber volume and the micro-void content increase at the lower region of the mold. More tests must be run to verify these results.

Non-destructive ultrasonic tests were used in an attempt to indirectly evaluate the material properties. It was discovered that a number of factors, such as the transducer material, signal frequency, type of couplant, orientation of the probe with respect to the defect, distance from the surface, type of display and many others influence the results of the ultrasound technique. It was, therefore, concluded that a separate extensive investigation must be done to interpret the C-Scan data and that the state-of-the-art is not yet at that level.

### Recommendations

1. The resin flow rate was selected to enable us to run the experiments at a rate fast enough to prevent gelation of the resin and slow enough to enable the peristaltic pump to handle the back pressure. It must be determined how the characteristics of the resin flow fronts as indicated by  $\theta_L$  and  $\theta_R$  will change with changes in the resin flow rates. The accuracy of the prediction method developed depends on the characteristics of the flow front. It is worth investigating the robustness of the method for a range of flow rates.
2. Both the test panels and the demonstration panels are thin sheets (6-ply) of about 0.1 inch thick. Investigations are needed to determine how the flow front and the prediction scheme is affected by the thickness of the panel (No. of plies).
3. The re-work used during the project involved opening the mold, shifting the panel based on the prediction of the flow and closing the mold again. Even by just opening and closing the mold without shifting the preform provides a new gas flow pattern. Appendix D shows bar charts for the gas flow rates for the second fit as well as the first fit for some of the panels. This indicates that the airflow pattern may be varied this way. This method can be used to change the permeability. However, it could be very tedious and, thus, a monitoring and control scheme needs to be developed based on the predictions.

4. Back pressure can be used to monitor and control the dynamics of the flow front. The pump can be controlled from the computer, and the settings changed while it is running. Advantage can be taken of this feature. It may be possible to extract the dynamics of race tracking by monitoring the back pressure. The pump speed may then be controlled on-line to respond to the behavior of the resin flow, especially to race tracking.
5. C-Scan image interpretation can be improved. Tests performed are inconclusive as to what changes in material properties are reflected in the color codes. Further research should be conducted to correlate the flow patterns, the relative velocities and measurable quantities of the material and mechanical properties to the C-Scan results.

In essence, the flow rate of the resin during injection should be monitored. From this, further conclusions may be made about the effects of race tracking upon the overall flow patterns of the resin. Once a database has been assembled which quantifies the flow rates and dynamics internal to the mold, this information may be used to evaluate the various aspects of the RTM process, including the injection rate, the mold dimensions, exit port locations and eventual automation of the entire process. Ultimately, a comprehensive profile of the RTM process may be developed, one that encompasses the improvement of all pertinent factors of resin transfer molding. This profile would then supply the foundation upon which to fabricate composite panels with reduced defects and acceptable material and mechanical properties.

## CHAPTER 6

### REFERENCES

- Addison, R.C., Jr., A.D.W. McKie, T.L.T. Liao, H.S. Ryang. "In Situ Process Monitoring Using Laser-Based Ultrasound." 1992 Ultrasonics Symposium: 783-786.
- Brosius, D., M. Wadsworth. "RTM of a Complex Composite Aircraft Structure." In *Composites In Manufacturing: Case Studies*, edited by A. Brent Strong, Society of Manufacturing Engineers, 1991: 111-120, 127.
- Chao, L. P., M.V. Gandhi, B.S. Thompson. "A Design-for-Manufacture Methodology for Incorporating Manufacturing Uncertainties in the Robust Design of Fibrous Laminated Composite Structures." *Journal of Composite Materials* 27, no. 2, (1993): 175-194.
- Fong, L., L.J. Lee. "Preforming Analysis of Thermoformable Fiber mats-Preforming Effects on Mold Filling." *Journal of Reinforced Plastics and Composites* 13 (July 1994): 637-662.
- Gong, H. "Pressure Distribution in Resin Transfer Molding with a Non-Rigid Fiber Preform." *Journal of Materials Processing Technology* 37 (1993): 363-371.
- Han, K., Cheng-Hsien Wu, L.J. Lee. "Characterization and Simulation of Resin Transfer Molding-Race Tracking and Dry Spot Formation." Conference Proceedings-Advanced Composite Technologies, Dearborn, MI, (Nov. 8 - 11, 1993): 19-36.
- Hayward, J.S., B. Harris. "Effect of Process Variables on the Quality of RTM Mouldings." *SAMPE Journal* 26, (May/June 1990): 39-46.
- Jones, R. M. *Mechanics of Composite Materials*. Scripta Book Co. Washington D.C., 1975, 5, 11, 13 - 17.
- Kikuchi, A., E. Higuerey, J. Coulter. "An Experimental Investigation of Resin Flow Sensing During Molding Processes." *Journal of Engineering Materials and Technology* 117 (January 1995): 83-86.
- Mallick, P.K. *Fiber Reinforced Composites*. Marcel-Dekker, Inc. New York, NY 1988, 2.
- Matthews, F.D., R.D. Rawlings. *Composite Materials: Engineering and Sciences*. Chapman and Hall, New York, NY. 1994, 179, 182 - 200.
- Patel, N., V. Rohatgi, L. J. Lee. "Micro Scale Flow Behavior and Void Formation Mechanism During Impregnation Through a Unidirectional Stitched Fiberglass Mat." *Polymer Engineering and Science* 35, no. 10 (May 1995): 837-851.

- Pitchumani, R., S. Yao. "Non-Dimensional Analysis of an Idealized Thermoset Composites Manufacture." *Journal of Composite Materials* 27, no. 6 (1993): 613-636.
- Senebi. S., E.C. Clang, R.L. Sadler, V.S. Avva. "Resin Transfer Molding Experiments with Vacuum Assisted Methods": 529-536.
- Shah, D. "On-Line Monitoring of the Vacuum-Assisted Resin Transfer Molding Process." M.S.M.E. thesis, North Carolina A&T State University, 1995.
- Stabler. W.S., "Void Minimization in RTM of Graphite/Epoxy Resin." M.S.M.E. thesis, North Carolina A&T State University, 1991.
- Wang. Y., J. Li. "Properties of Composites Reinforced with E-Glass Nonwoven Fabrics." *Journal of Advanced Materials*. (April 1995): 28-34.
- Young, Wen-Bin, Chaw-Wu Tseng. "Study on the Pre-Heated Temperatures and Injection Pressures of the RTM Process." *Journal of Reinforced Plastics and Composites* 13, (May 1994): 467-482.
- Zhu, Y.T., G. Zong "On the Application of the Statistical Strength Model of Fiber-Reinforced Composites." *Journal of Composite Materials* 27, no. 9 (1993): 944-959.
- "ASTM D2393 - Standard Test Method for Viscosity of Epoxy Resins and Related Components." *Annual Book of ASTM Standards*. American Society for Testing and Materials, 1993: 1-3.
- "Omega Mass Flowmeters Operator's Manual." Omega Engineering, Inc. 1993: 22-23.
- "LabView for Macintosh Demonstration Guide." National Instruments Corp., November 1992: 1.1-1.10.

**APPENDIX A**  
**NITROGEN FLOW RATE DATA**

**Table A.1** N<sub>2</sub> Flow rates through Ports 1 - 7 (standard liters per minute)

<b>Plate ID: SIP1</b>	<i>Port #1</i>	<i>Port #2</i>	<i>Port #3</i>	<i>Port #4</i>	<i>Port #5</i>	<i>Port #6</i>	<i>Port #7</i>	<i>Pressure (psig)</i>
No ports closed	2.101	1.028	3.925	3.745	2.795	3.500	2.681	4.620
<b>Plate ID: SIP2</b>	<i>Port #1</i>	<i>Port #2</i>	<i>Port #3</i>	<i>Port #4</i>	<i>Port #5</i>	<i>Port #6</i>	<i>Port #7</i>	<i>Pressure (psig)</i>
No ports closed	2.791	1.000	3.584	3.180	2.450	4.392	2.858	2.940
<b>Plate ID: SIP3</b>	<i>Port #1</i>	<i>Port #2</i>	<i>Port #3</i>	<i>Port #4</i>	<i>Port #5</i>	<i>Port #6</i>	<i>Port #7</i>	<i>Pressure (psig)</i>
No ports closed	1.377	2.520	1.770	3.961	1.587	2.734	2.432	2.300
<b>Plate ID: SIP4</b>	<i>Port #1</i>	<i>Port #2</i>	<i>Port #3</i>	<i>Port #4</i>	<i>Port #5</i>	<i>Port #6</i>	<i>Port #7</i>	<i>Pressure (psig)</i>
No ports closed	2.497	2.704	2.744	4.181	1.492	2.545	2.729	2.710
<b>Plate ID: SIP5</b>	<i>Port #1</i>	<i>Port #2</i>	<i>Port #3</i>	<i>Port #4</i>	<i>Port #5</i>	<i>Port #6</i>	<i>Port #7</i>	<i>Pressure (psig)</i>
No ports closed	1.061	1.383	1.408	2.625	1.104	3.428	3.947	3.610
<b>Plate ID: SIP6</b>	<i>Port #1</i>	<i>Port #2</i>	<i>Port #3</i>	<i>Port #4</i>	<i>Port #5</i>	<i>Port #6</i>	<i>Port #7</i>	<i>Pressure (psig)</i>
No ports closed	1.793	1.316	1.252	2.616	2.082	3.829	2.473	2.710
Top ports closed	1.985	1.978	2.503	2.729	0.000	0.000	0.000	2.640
Lower ports closed	0.000	1.280	1.379	0.000	1.968	4.076	2.800	2.620
Side ports closed	0.000	0.000	0.000	0.000	2.565	5.215	3.689	2.710
<b>Plate ID: SIP7</b>	<i>Port #1</i>	<i>Port #2</i>	<i>Port #3</i>	<i>Port #4</i>	<i>Port #5</i>	<i>Port #6</i>	<i>Port #7</i>	<i>Pressure (psig)</i>
No ports closed	1.418	0.898	0.592	1.903	2.313	1.133	2.464	2.160
Top ports closed	2.463	2.639	1.928	2.953	0.000	0.000	0.000	2.460
Lower ports closed	0.000	1.503	1.024	0.000	3.257	1.767	3.373	2.440
Side ports closed	0.000	0.000	0.000	0.000	4.317	2.351	4.250	2.560
<b>Plate ID: SIP8</b>	<i>Port #1</i>	<i>Port #2</i>	<i>Port #3</i>	<i>Port #4</i>	<i>Port #5</i>	<i>Port #6</i>	<i>Port #7</i>	<i>Pressure (psig)</i>
No ports closed	1.669	2.089	2.344	3.393	1.393	2.162	1.913	2.300
Top ports closed	2.761	3.599	4.432	4.617	0.000	0.000	0.000	2.520
Lower ports closed	0.000	3.076	3.642	0.000	2.055	3.147	2.905	2.520
Side ports closed	0.000	0.000	0.000	0.000	3.061	4.774	4.792	2.720
<b>Plate ID: SIP9</b>	<i>Port #1</i>	<i>Port #2</i>	<i>Port #3</i>	<i>Port #4</i>	<i>Port #5</i>	<i>Port #6</i>	<i>Port #7</i>	<i>Pressure (psig)</i>
No ports closed	1.202	0.813	1.129	1.103	4.294	1.389	3.098	1.870
Top ports closed	1.980	2.191	3.275	1.759	0.000	0.000	0.000	1.940
Lower ports closed	0.000	0.999	1.331	0.000	4.230	1.395	3.156	1.850
Side ports closed	0.000	0.000	0.000	0.000	5.382	1.919	4.494	1.980

<b>Plate ID: S1P10</b>	<i>Port #1</i>	<i>Port #2</i>	<i>Port #3</i>	<i>Port #4</i>	<i>Port #5</i>	<i>Port #6</i>	<i>Port #7</i>	<i>Pressure (psig)</i>
No ports closed	1.009	0.516	1.394	1.170	0.432	0.602	1.569	1.770
Top ports closed	1.398	1.014	2.750	1.771	0.000	0.000	0.000	1.880
Lower ports closed	0.000	0.859	2.073	0.000	0.745	0.999	2.329	1.900
Side ports closed	0.000	0.000	0.000	0.000	1.331	1.700	3.988	2.020
<b>Plate ID: S2P1</b>	<i>Port #1</i>	<i>Port #2</i>	<i>Port #3</i>	<i>Port #4</i>	<i>Port #5</i>	<i>Port #6</i>	<i>Port #7</i>	<i>Pressure (psig)</i>
No ports closed	0.737	0.726	1.122	2.526	1.537	1.507	1.076	1.860
Top ports closed	1.339	2.608	2.688	3.597	0.000	0.000	0.000	2.040
Lower ports closed	0.000	1.207	1.689	0.000	3.364	2.513	2.198	2.050
Side ports closed	0.000	0.000	0.000	0.000	4.518	2.742	2.937	2.130
<b>Plate ID: S2P2</b>	<i>Port #1</i>	<i>Port #2</i>	<i>Port #3</i>	<i>Port #4</i>	<i>Port #5</i>	<i>Port #6</i>	<i>Port #7</i>	<i>Pressure (psig)</i>
No ports closed	2.158	1.125	1.563	3.114	1.354	1.961	1.912	3.590
Top ports closed	2.143	2.411	2.756	2.963	0.000	0.000	0.000	3.390
Lower ports closed	0.000	1.720	2.062	0.000	2.114	2.934	2.716	3.920
Side ports closed	0.000	0.000	0.000	0.000	3.362	3.779	3.889	4.060
<b>Plate ID: S2P3</b>	<i>Port #1</i>	<i>Port #2</i>	<i>Port #3</i>	<i>Port #4</i>	<i>Port #5</i>	<i>Port #6</i>	<i>Port #7</i>	<i>Pressure (psig)</i>
No ports closed	3.476	0.710	0.638	1.607	1.632	1.938	1.166	3.210
Top ports closed	4.362	2.086	1.649	2.027	0.000	0.000	0.000	3.350
Lower ports closed	0.000	1.166	0.967	0.000	2.542	2.845	1.719	3.410
Side ports closed	0.000	0.000	0.000	0.000	3.378	3.366	2.250	3.470
<b>Plate ID: S2P4</b>	<i>Port #1</i>	<i>Port #2</i>	<i>Port #3</i>	<i>Port #4</i>	<i>Port #5</i>	<i>Port #6</i>	<i>Port #7</i>	<i>Pressure (psig)</i>
No ports closed	2.840	1.364	1.439	2.643	1.063	3.016	1.594	2.970
Top ports closed	3.568	3.146	3.011	3.113	0.000	0.000	0.000	3.180
Lower ports closed	0.000	1.920	1.918	0.000	1.633	4.124	2.292	3.230
Side ports closed	0.000	0.000	0.000	0.000	2.582	5.472	3.390	3.380
<b>Plate ID: S2P5</b>	<i>Port #1</i>	<i>Port #2</i>	<i>Port #3</i>	<i>Port #4</i>	<i>Port #5</i>	<i>Port #6</i>	<i>Port #7</i>	<i>Pressure (psig)</i>
No ports closed	3.294	2.284	1.644	2.058	0.850	2.227	1.388	2.990
Top ports closed	3.926	4.258	2.973	2.381	0.000	0.000	0.000	3.100
Lower ports closed	0.000	3.300	2.306	0.000	1.402	3.346	2.100	3.230
Side ports closed	0.000	0.000	0.000	0.000	2.875	4.800	3.589	3.390
<b>Plate ID: S2P6</b>	<i>Port #1</i>	<i>Port #2</i>	<i>Port #3</i>	<i>Port #4</i>	<i>Port #5</i>	<i>Port #6</i>	<i>Port #7</i>	<i>Pressure (psig)</i>
No ports closed	3.378	0.869	0.533	1.405	2.122	1.889	2.255	2.960
Top ports closed	4.374	2.802	1.802	1.865	0.000	0.000	0.000	3.160
Lower ports closed	0.000	1.342	0.825	0.000	3.027	2.694	3.084	3.170
Side ports closed	0.000	0.000	0.000	0.000	4.058	3.145	3.889	3.270



<b>Plate ID: S2P7</b>	<i>Port #1</i>	<i>Port #2</i>	<i>Port #3</i>	<i>Port #4</i>	<i>Port #5</i>	<i>Port #6</i>	<i>Port #7</i>	<i>Pressure (psig)</i>
No ports closed	3.622	1.336	0.734	1.719	0.939	2.536	1.489	2.660
Top ports closed	4.525	3.184	2.161	2.159	0.000	0.000	0.000	2.840
Lower ports closed	0.000	2.121	1.234	0.000	1.651	3.766	2.277	2.930
Side ports closed	0.000	0.000	0.000	0.000	2.789	5.013	3.170	3.030

<b>Plate ID: S2P8</b>	<i>Port #1</i>	<i>Port #2</i>	<i>Port #3</i>	<i>Port #4</i>	<i>Port #5</i>	<i>Port #6</i>	<i>Port #7</i>	<i>Pressure (psig)</i>
No ports closed	3.377	1.478	3.040	2.739	1.555	2.051	1.606	2.470
Top ports closed	4.082	3.287	5.135	3.198	0.000	0.000	0.000	2.620
Lower ports closed	0.000	2.288	4.096	0.000	2.489	3.027	2.433	2.700
Side ports closed	0.000	0.000	0.000	0.000	4.605	4.606	4.219	2.970

<b>Plate ID: S2P9</b>	<i>Port #1</i>	<i>Port #2</i>	<i>Port #3</i>	<i>Port #4</i>	<i>Port #5</i>	<i>Port #6</i>	<i>Port #7</i>	<i>Pressure (psig)</i>
No ports closed	1.732	1.231	0.988	2.375	1.240	1.859	1.091	2.410
Top ports closed	2.386	2.767	2.415	2.747	0.000	0.000	0.000	2.530
Lower ports closed	0.000	1.803	1.481	0.000	1.866	2.710	1.708	2.600
Side ports closed	0.000	0.000	0.000	0.000	2.900	3.735	2.940	2.690

<b>Plate ID: S2P10</b>	<i>Port #1</i>	<i>Port #2</i>	<i>Port #3</i>	<i>Port #4</i>	<i>Port #5</i>	<i>Port #6</i>	<i>Port #7</i>	<i>Pressure (psig)</i>
No ports closed	3.262	1.297	0.682	2.859	2.043	2.233	1.562	2.230
Top ports closed	4.430	3.481	1.955	3.493	0.000	0.000	0.000	2.430
Lower ports closed	0.000	2.158	1.184	0.000	3.448	2.790	2.721	2.490
Side ports closed	0.000	0.000	0.000	0.000	4.868	3.612	3.774	2.600

**APPENDIX B**  
**NORMALIZED GAS FLOW DATA**

Normalized N<sub>2</sub> Flow rates through ports 1 - 7

<i>Plate ID: SIP1</i>	<i>Avg. flow</i>	<i>Port #1</i>	<i>Port #2</i>	<i>Port #3</i>	<i>Port #4</i>	<i>Port #5</i>	<i>Port #6</i>	<i>Port #7</i>
No ports closed	2.825	0.744	0.364	1.389	1.326	0.989	1.239	0.949

<i>Plate ID: SIP2</i>	<i>Avg. flow</i>	<i>Port #1</i>	<i>Port #2</i>	<i>Port #3</i>	<i>Port #4</i>	<i>Port #5</i>	<i>Port #6</i>	<i>Port #7</i>
No ports closed	2.894	0.964	0.346	1.238	1.099	0.847	1.518	0.988

<i>Plate ID: SIP3</i>	<i>Avg. flow</i>	<i>Port #1</i>	<i>Port #2</i>	<i>Port #3</i>	<i>Port #4</i>	<i>Port #5</i>	<i>Port #6</i>	<i>Port #7</i>
No ports closed	2.340	0.588	1.077	0.756	1.693	0.678	1.168	1.039

<i>Plate ID: SIP4</i>	<i>Avg. flow</i>	<i>Port #1</i>	<i>Port #2</i>	<i>Port #3</i>	<i>Port #4</i>	<i>Port #5</i>	<i>Port #6</i>	<i>Port #7</i>
No ports closed	2.699	0.925	1.002	1.017	1.549	0.553	0.943	1.011

<i>Plate ID: SIP5</i>	<i>Avg. flow</i>	<i>Port #1</i>	<i>Port #2</i>	<i>Port #3</i>	<i>Port #4</i>	<i>Port #5</i>	<i>Port #6</i>	<i>Port #7</i>
No ports closed	2.137	0.497	0.647	0.659	1.229	0.517	1.604	1.848

<i>Plate ID: SIP6</i>	<i>Avg. flow</i>	<i>Port #1</i>	<i>Port #2</i>	<i>Port #3</i>	<i>Port #4</i>	<i>Port #5</i>	<i>Port #6</i>	<i>Port #7</i>
No ports closed	2.195	0.817	0.600	0.571	1.192	0.949	1.745	1.127
Top ports closed	1.314	1.511	1.506	1.905	2.077	0.000	0.000	0.000
Lower ports closed	1.643	0.000	0.779	0.839	0.000	1.198	2.480	1.704
Side ports closed	1.639	0.000	0.000	0.000	0.000	1.566	3.183	2.252

<i>Plate ID: SIP7</i>	<i>Avg. flow</i>	<i>Port #1</i>	<i>Port #2</i>	<i>Port #3</i>	<i>Port #4</i>	<i>Port #5</i>	<i>Port #6</i>	<i>Port #7</i>
No ports closed	1.532	0.926	0.586	0.387	1.242	1.510	0.740	1.608
Top ports closed	1.426	1.727	1.850	1.352	2.071	0.000	0.000	0.000
Lower ports closed	1.561	0.000	0.963	0.656	0.000	2.087	1.132	2.162
Side ports closed	1.560	0.000	0.000	0.000	0.000	2.768	1.507	2.725

<i>Plate ID: SIP8</i>	<i>Avg. flow</i>	<i>Port #1</i>	<i>Port #2</i>	<i>Port #3</i>	<i>Port #4</i>	<i>Port #5</i>	<i>Port #6</i>	<i>Port #7</i>
No ports closed	2.138	0.781	0.977	1.097	1.587	0.652	1.011	0.895
Top ports closed	2.201	1.254	1.635	2.013	2.097	0.000	0.000	0.000
Lower ports closed	2.118	0.000	1.453	1.720	0.000	0.970	1.486	1.372
Side ports closed	1.804	0.000	0.000	0.000	0.000	1.697	2.647	2.656

<i>Plate ID: SIP9</i>	<i>Avg. flow</i>	<i>Port #1</i>	<i>Port #2</i>	<i>Port #3</i>	<i>Port #4</i>	<i>Port #5</i>	<i>Port #6</i>	<i>Port #7</i>
No ports closed	1.861	0.646	0.437	0.607	0.593	2.307	0.746	1.665
Top ports closed	1.315	1.506	1.666	2.491	1.338	0.000	0.000	0.000
Lower ports closed	1.587	0.000	0.629	0.839	0.000	2.665	0.879	1.988
Side ports closed	1.685	0.000	0.000	0.000	0.000	3.194	1.139	2.667

<i>Plate ID: S1P10</i>	<i>Avg. flow</i>	<i>Port #1</i>	<i>Port #2</i>	<i>Port #3</i>	<i>Port #4</i>	<i>Port #5</i>	<i>Port #6</i>	<i>Port #7</i>
No ports closed	0.956	1.056	0.540	1.459	1.224	0.452	0.630	1.641
Top ports closed	0.990	1.411	1.024	2.777	1.778	0.000	0.000	0.000
Lower ports closed	1.001	0.000	0.858	2.071	0.000	0.745	0.999	2.328
Side ports closed	1.003	0.000	0.000	0.000	0.000	1.327	1.695	3.978

<i>Plate ID: S2P1</i>	<i>Avg. flow</i>	<i>Port #1</i>	<i>Port #2</i>	<i>Port #3</i>	<i>Port #4</i>	<i>Port #5</i>	<i>Port #6</i>	<i>Port #7</i>
No ports closed	1.319	0.559	0.551	0.851	1.916	1.165	1.143	0.816
Top ports closed	1.462	0.916	1.784	1.839	2.461	0.000	0.000	0.000
Lower ports closed	1.516	0.000	0.796	1.114	0.000	2.219	1.420	1.450
Side ports closed	1.457	0.000	0.000	0.000	0.000	3.101	1.883	2.016

<i>Plate ID: S2P2</i>	<i>Avg. flow</i>	<i>Port #1</i>	<i>Port #2</i>	<i>Port #3</i>	<i>Port #4</i>	<i>Port #5</i>	<i>Port #6</i>	<i>Port #7</i>
No ports closed	1.884	1.146	0.597	0.829	1.653	0.719	1.041	1.015
Top ports closed	1.468	1.460	1.643	1.878	2.019	0.000	0.000	0.000
Lower ports closed	1.650	0.000	1.043	1.250	0.000	1.282	1.779	1.647
Side ports closed	1.576	0.000	0.000	0.000	0.000	2.134	2.398	2.468

<i>Plate ID: S2P3</i>	<i>Avg. flow</i>	<i>Port #1</i>	<i>Port #2</i>	<i>Port #3</i>	<i>Port #4</i>	<i>Port #5</i>	<i>Port #6</i>	<i>Port #7</i>
No ports closed	1.595	2.179	0.445	0.400	1.007	1.023	1.215	0.731
Top ports closed	1.446	3.016	1.442	1.140	1.402	0.000	0.000	0.000
Lower ports closed	1.320	0.000	0.884	0.733	0.000	1.926	2.155	1.302
Side ports closed	1.285	0.000	0.000	0.000	0.000	2.629	2.620	1.751

<i>Plate ID: S2P4</i>	<i>Avg. flow</i>	<i>Port #1</i>	<i>Port #2</i>	<i>Port #3</i>	<i>Port #4</i>	<i>Port #5</i>	<i>Port #6</i>	<i>Port #7</i>
No ports closed	1.994	1.424	0.684	0.772	1.326	0.533	1.512	0.799
Top ports closed	1.834	1.946	1.716	1.642	1.697	0.000	0.000	0.000
Lower ports closed	1.698	0.000	1.131	1.130	0.000	0.961	2.428	1.350
Side ports closed	1.635	0.000	0.000	0.000	0.000	1.579	3.347	2.074

<i>Plate ID: S2P5</i>	<i>Avg. flow</i>	<i>Port #1</i>	<i>Port #2</i>	<i>Port #3</i>	<i>Port #4</i>	<i>Port #5</i>	<i>Port #6</i>	<i>Port #7</i>
No ports closed	1.963	1.678	1.163	0.837	1.048	0.433	1.134	0.707
Top ports closed	1.934	2.030	2.202	1.537	1.231	0.000	0.000	0.000
Lower ports closed	1.779	0.000	1.855	1.296	0.000	0.788	1.881	1.180
Side ports closed	1.609	0.000	0.000	0.000	0.000	1.786	2.983	2.230

<i>Plate ID: S2P6</i>	<i>Avg. flow</i>	<i>Port #1</i>	<i>Port #2</i>	<i>Port #3</i>	<i>Port #4</i>	<i>Port #5</i>	<i>Port #6</i>	<i>Port #7</i>
No ports closed	1.779	1.899	0.489	0.300	0.790	1.193	1.062	1.268
Top ports closed	1.549	2.824	1.809	1.163	1.204	0.000	0.000	0.000
Lower ports closed	1.567	0.000	0.856	0.526	0.000	1.931	1.718	1.968
Side ports closed	1.586	0.000	0.000	0.000	0.000	2.558	1.983	2.458

<i>Plate ID: S2P7</i>	<i>Avg. flow</i>	<i>Port #1</i>	<i>Port #2</i>	<i>Port #3</i>	<i>Port #4</i>	<i>Port #5</i>	<i>Port #6</i>	<i>Port #7</i>
No ports closed	1.768	2.049	0.756	0.415	0.972	0.531	1.434	0.842
Top ports closed	1.719	2.633	1.853	1.258	1.256	0.000	0.000	0.000
Lower ports closed	1.578	0.000	1.344	0.782	0.000	1.046	2.386	1.442
Side ports closed	1.567	0.000	0.000	0.000	0.000	1.779	3.198	2.022

<i>Plate ID: S2P8</i>	<i>Avg. flow</i>	<i>Port #1</i>	<i>Port #2</i>	<i>Port #3</i>	<i>Port #4</i>	<i>Port #5</i>	<i>Port #6</i>	<i>Port #7</i>
No ports closed	2.264	1.492	0.653	1.343	1.210	0.687	0.906	0.709
Top ports closed	2.243	1.820	1.465	2.289	1.426	0.000	0.000	0.000
Lower ports closed	2.048	0.000	1.117	2.000	0.000	1.216	1.478	1.188
Side ports closed	1.919	0.000	0.000	0.000	0.000	2.400	2.401	2.199

<i>Plate ID: S2P9</i>	<i>Avg. flow</i>	<i>Port #1</i>	<i>Port #2</i>	<i>Port #3</i>	<i>Port #4</i>	<i>Port #5</i>	<i>Port #6</i>	<i>Port #7</i>
No ports closed	1.502	1.153	0.819	0.658	1.581	0.826	1.237	0.726
Top ports closed	1.473	1.619	1.878	1.639	1.864	0.000	0.000	0.000
Lower ports closed	1.367	0.000	1.319	1.084	0.000	1.365	1.983	1.250
Side ports closed	1.368	0.000	0.000	0.000	0.000	2.120	2.731	2.149

<i>Plate ID: S2P10</i>	<i>Avg. flow</i>	<i>Port #1</i>	<i>Port #2</i>	<i>Port #3</i>	<i>Port #4</i>	<i>Port #5</i>	<i>Port #6</i>	<i>Port #7</i>
No ports closed	1.991	1.638	0.651	0.343	1.436	1.026	1.121	0.785
Top ports closed	1.908	2.321	1.824	1.025	1.830	0.000	0.000	0.000
Lower ports closed	1.757	0.000	1.228	0.674	0.000	1.962	1.587	1.548
Side ports closed	1.751	0.000	0.000	0.000	0.000	2.781	2.063	2.156

**APPENDIX C**  
**GAS FLOW PARAMETERS**

Table 4.3: Combinations of Normalized N<sub>2</sub> Flow Data

<b>Plate ID: SIP1</b>	<i>Ports</i> 1+2+5	<i>Ports</i> 3+4+7	<i>Ports</i> 2+5	<i>Ports</i> 3+7	<i>Ports</i> 1+2	<i>Ports</i> 3+4	<i>Port</i> #6
No ports closed	0.699	1.221	0.677	1.169	0.554	1.358	1.239
<b>Plate ID: SIP2</b>	<i>Ports</i> 1+2+5	<i>Ports</i> 3+4+7	<i>Ports</i> 2+5	<i>Ports</i> 3+7	<i>Ports</i> 1+2	<i>Ports</i> 3+4	<i>Port</i> #6
No ports closed	0.719	1.108	0.596	1.113	0.655	1.169	1.518
<b>Plate ID: SIP3</b>	<i>Ports</i> 1+2+5	<i>Ports</i> 3+4+7	<i>Ports</i> 2+5	<i>Ports</i> 3+7	<i>Ports</i> 1+2	<i>Ports</i> 3+4	<i>Port</i> #6
No ports closed	0.781	1.163	0.877	0.898	0.833	1.224	1.168
<b>Plate ID: SIP4</b>	<i>Ports</i> 1+2+5	<i>Ports</i> 3+4+7	<i>Ports</i> 2+5	<i>Ports</i> 3+7	<i>Ports</i> 1+2	<i>Ports</i> 3+4	<i>Port</i> #6
No ports closed	0.827	1.192	0.777	1.014	0.964	1.283	0.943
<b>Plate ID: SIP5</b>	<i>Ports</i> 1+2+5	<i>Ports</i> 3+4+7	<i>Ports</i> 2+5	<i>Ports</i> 3+7	<i>Ports</i> 1+2	<i>Ports</i> 3+4	<i>Port</i> #6
No ports closed	0.553	1.245	0.582	1.253	0.572	0.944	1.604
<b>Plate ID: SIP6</b>	<i>Ports</i> 1+2+5	<i>Ports</i> 3+4+7	<i>Ports</i> 2+5	<i>Ports</i> 3+7	<i>Ports</i> 1+2	<i>Ports</i> 3+4	<i>Port</i> #6
No ports closed	0.789	0.963	0.774	0.849	0.708	0.881	1.745
Top ports closed	1.006	1.328	0.753	0.953	1.509	1.991	0.000
Lower ports closed	0.659	0.848	0.988	1.272	0.389	0.420	2.480
Side ports closed	0.522	0.751	0.783	1.126	0.000	0.000	3.183
<b>Plate ID: SIP7</b>	<i>Ports</i> 1+2+5	<i>Ports</i> 3+4+7	<i>Ports</i> 2+5	<i>Ports</i> 3+7	<i>Ports</i> 1+2	<i>Ports</i> 3+4	<i>Port</i> #6
No ports closed	1.007	1.079	1.048	0.998	0.756	0.815	0.740
Top ports closed	1.192	1.141	0.925	0.676	1.789	1.711	0.000
Lower ports closed	1.017	0.939	1.525	1.409	0.482	0.328	1.132
Side ports closed	0.923	0.908	1.384	1.362	0.000	0.000	1.507
<b>Plate ID: SIP8</b>	<i>Ports</i> 1+2+5	<i>Ports</i> 3+4+7	<i>Ports</i> 2+5	<i>Ports</i> 3+7	<i>Ports</i> 1+2	<i>Ports</i> 3+4	<i>Port</i> #6
No ports closed	0.803	1.193	0.815	0.996	0.879	1.342	1.011
Top ports closed	0.963	1.370	0.818	1.007	1.445	2.055	0.000
Lower ports closed	0.808	1.030	1.211	1.546	0.726	0.860	1.486
Side ports closed	0.566	0.885	0.848	1.328	0.000	0.000	2.647
<b>Plate ID: SIP9</b>	<i>Ports</i> 1+2+5	<i>Ports</i> 3+4+7	<i>Ports</i> 2+5	<i>Ports</i> 3+7	<i>Ports</i> 1+2	<i>Ports</i> 3+4	<i>Port</i> #6
No ports closed	1.130	0.955	1.372	1.136	0.541	0.600	0.746
Top ports closed	1.057	1.276	0.833	1.245	1.586	1.914	0.000
Lower ports closed	1.098	0.942	1.647	1.413	0.315	0.419	0.879
Side ports closed	1.065	0.889	1.597	1.333	0.000	0.000	1.139

<b>Plate ID: S1P10</b>	<i>Ports</i> <i>1+2+5</i>	<i>Ports</i> <i>3+4+7</i>	<i>Ports</i> <i>2+5</i>	<i>Ports</i> <i>3+7</i>	<i>Ports</i> <i>1+2</i>	<i>Ports</i> <i>3+4</i>	<i>Port #6</i>
No ports closed	0.682	1.441	0.496	1.550	0.798	1.341	0.630
Top ports closed	0.812	1.521	0.512	1.388	1.218	2.282	0.000
Lower ports closed	0.534	1.466	0.801	2.199	0.429	1.036	2.328
Side ports closed	0.442	1.326	0.664	1.989	0.000	0.000	3.978

<b>Plate ID: S2P1</b>	<i>Ports</i> <i>1+2+5</i>	<i>Ports</i> <i>3+4+7</i>	<i>Ports</i> <i>2+5</i>	<i>Ports</i> <i>3+7</i>	<i>Ports</i> <i>1+2</i>	<i>Ports</i> <i>3+4</i>	<i>Port #6</i>
No ports closed	0.758	1.194	0.858	0.833	0.555	1.383	1.143
Top ports closed	0.900	1.433	0.892	0.919	1.350	2.150	0.000
Lower ports closed	1.005	0.855	1.508	1.282	0.398	0.557	1.420
Side ports closed	1.034	0.672	1.551	1.008	0.000	0.000	1.883

<b>Plate ID: S2P2</b>	<i>Ports</i> <i>1+2+5</i>	<i>Ports</i> <i>3+4+7</i>	<i>Ports</i> <i>2+5</i>	<i>Ports</i> <i>3+7</i>	<i>Ports</i> <i>1+2</i>	<i>Ports</i> <i>3+4</i>	<i>Port #6</i>
No ports closed	0.820	1.116	0.658	0.922	0.871	1.241	1.041
Top ports closed	1.034	1.299	0.821	0.939	1.552	1.948	0.000
Lower ports closed	0.775	0.996	1.162	1.448	0.521	0.625	1.779
Side ports closed	0.711	0.823	1.067	1.234	0.000	0.000	2.398

<b>Plate ID: S2P3</b>	<i>Ports</i> <i>1+2+5</i>	<i>Ports</i> <i>3+4+7</i>	<i>Ports</i> <i>2+5</i>	<i>Ports</i> <i>3+7</i>	<i>Ports</i> <i>1+2</i>	<i>Ports</i> <i>3+4</i>	<i>Port #6</i>
No ports closed	1.216	0.713	0.734	0.566	1.312	0.704	1.215
Top ports closed	1.486	0.847	0.721	0.570	2.229	1.271	0.000
Lower ports closed	0.937	0.678	1.405	1.017	0.442	0.366	2.155
Side ports closed	0.876	0.584	1.315	0.876	0.000	0.000	2.260

<b>Plate ID: S2P4</b>	<i>Ports</i> <i>1+2+5</i>	<i>Ports</i> <i>3+4+7</i>	<i>Ports</i> <i>2+5</i>	<i>Ports</i> <i>3+7</i>	<i>Ports</i> <i>1+2</i>	<i>Ports</i> <i>3+4</i>	<i>Port #6</i>
No ports closed	0.880	0.949	0.608	0.761	1.054	1.024	1.512
Top ports closed	1.220	1.113	0.858	0.821	1.831	1.669	0.000
Lower ports closed	0.697	0.826	1.046	1.240	0.565	0.565	2.428
Side ports closed	0.526	0.691	0.790	1.037	0.000	0.000	3.347

<b>Plate ID: S2P5</b>	<i>Ports</i> <i>1+2+5</i>	<i>Ports</i> <i>3+4+7</i>	<i>Ports</i> <i>2+5</i>	<i>Ports</i> <i>3+7</i>	<i>Ports</i> <i>1+2</i>	<i>Ports</i> <i>3+4</i>	<i>Port #6</i>
No ports closed	1.091	0.864	0.798	0.772	1.421	0.943	1.134
Top ports closed	1.411	0.923	1.101	0.769	2.116	1.384	0.000
Lower ports closed	0.881	0.825	1.321	1.238	0.927	0.648	1.881
Side ports closed	0.595	0.743	0.893	1.115	0.000	0.000	2.983

<b>Plate ID: S2P6</b>	<i>Ports</i> <i>1+2+5</i>	<i>Ports</i> <i>3+4+7</i>	<i>Ports</i> <i>2+5</i>	<i>Ports</i> <i>3+7</i>	<i>Ports</i> <i>1+2</i>	<i>Ports</i> <i>3+4</i>	<i>Port #6</i>
No ports closed	1.194	0.786	0.841	0.784	1.194	0.545	1.062
Top ports closed	1.544	0.789	0.905	0.582	2.316	1.184	0.000
Lower ports closed	0.929	0.831	1.394	1.247	0.428	0.263	1.718
Side ports closed	0.853	0.819	1.279	1.229	0.000	0.000	1.983



<b>Plate ID: S2P7</b>	<i>Ports</i> 1+2+5	<i>Ports</i> 3+4+7	<i>Ports</i> 2+5	<i>Ports</i> 3+7	<i>Ports</i> 1+2	<i>Ports</i> 3+4	<i>Port #6</i>
No ports closed	1.112	0.743	0.643	0.629	1.402	0.694	1.434
Top ports closed	1.495	0.838	0.927	0.629	2.243	1.257	0.000
Lower ports closed	0.796	0.742	1.195	1.112	0.672	0.391	2.386
Side ports closed	0.593	0.674	0.890	1.011	0.000	0.000	3.198

<b>Plate ID: S2P8</b>	<i>Ports</i> 1+2+5	<i>Ports</i> 3+4+7	<i>Ports</i> 2+5	<i>Ports</i> 3+7	<i>Ports</i> 1+2	<i>Ports</i> 3+4	<i>Port #6</i>
No ports closed	0.944	1.087	0.670	1.026	1.072	1.277	0.906
Top ports closed	1.095	1.238	0.733	1.145	1.643	1.857	0.000
Lower ports closed	0.778	1.063	1.166	1.594	0.559	1.000	1.478
Side ports closed	0.800	0.733	1.200	1.100	0.000	0.000	2.401

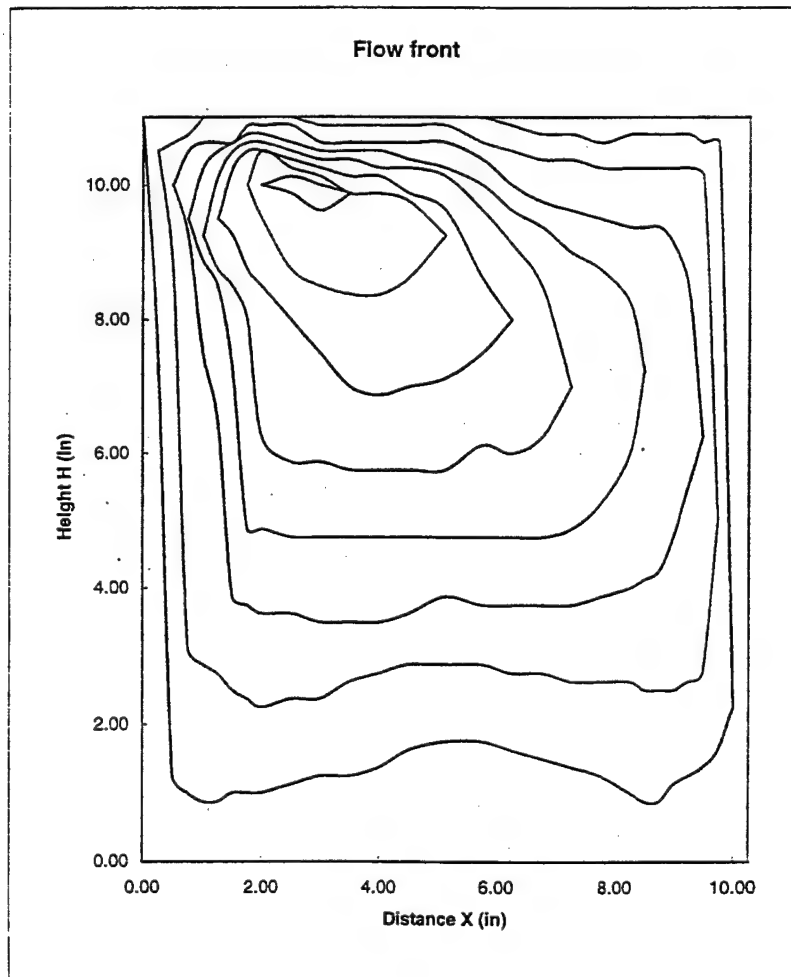
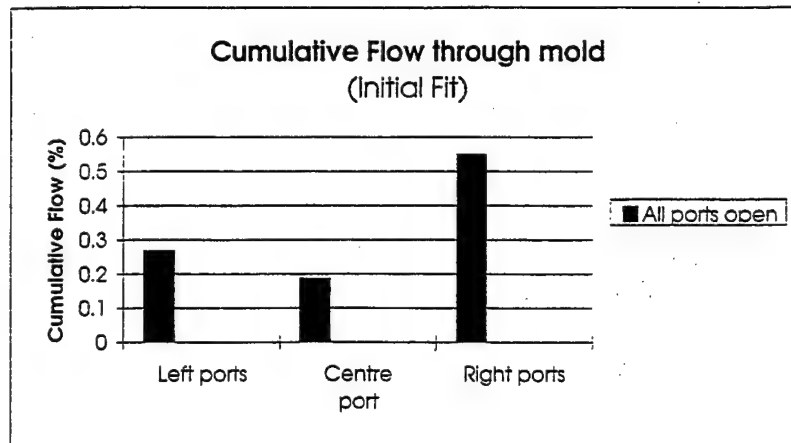
  

<b>Plate ID: S2P9</b>	<i>Ports</i> 1+2+5	<i>Ports</i> 3+4+7	<i>Ports</i> 2+5	<i>Ports</i> 3+7	<i>Ports</i> 1+2	<i>Ports</i> 3+4	<i>Port #6</i>
No ports closed	0.933	0.988	0.823	0.692	0.986	1.119	1.237
Top ports closed	1.166	1.168	0.939	0.820	1.748	1.752	0.000
Lower ports closed	0.895	0.778	1.342	1.167	0.660	0.542	1.983
Side ports closed	0.707	0.716	1.060	1.075	0.000	0.000	2.731

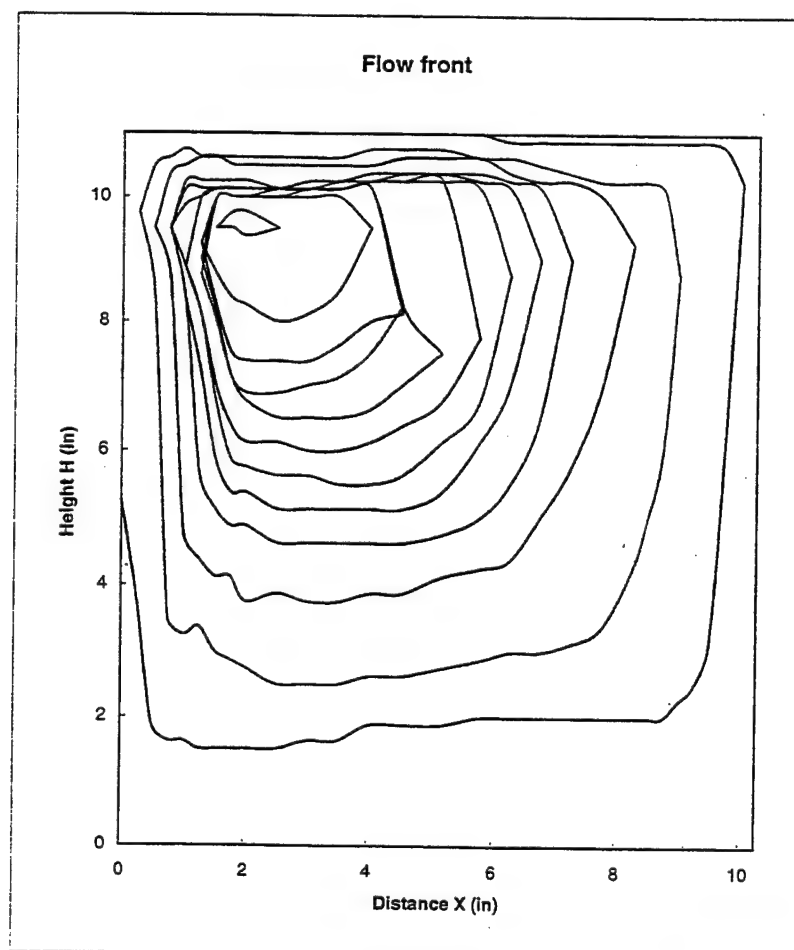
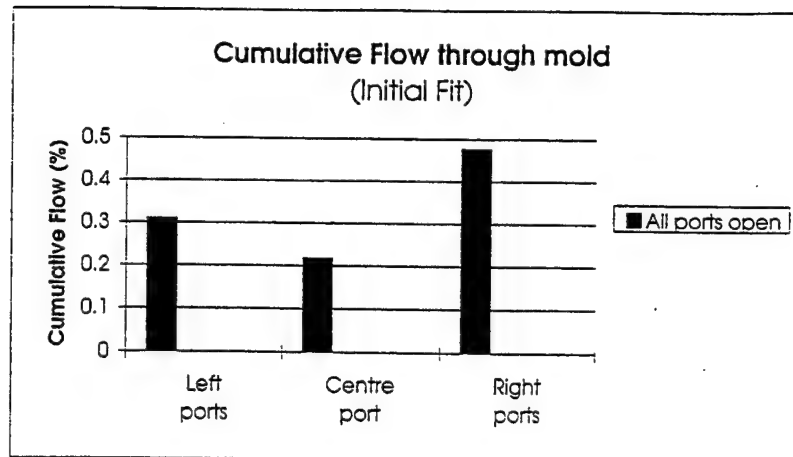
  

<b>Plate ID: S2P10</b>	<i>Ports</i> 1+2+5	<i>Ports</i> 3+4+7	<i>Ports</i> 2+5	<i>Ports</i> 3+7	<i>Ports</i> 1+2	<i>Ports</i> 3+4	<i>Port #6</i>
No ports closed	1.105	0.854	0.839	0.564	1.145	0.889	1.121
Top ports closed	1.382	0.952	0.912	0.512	2.073	1.427	0.000
Lower ports closed	1.063	0.741	1.595	1.111	0.614	0.337	1.587
Side ports closed	0.927	0.719	1.390	1.078	0.000	0.000	2.063

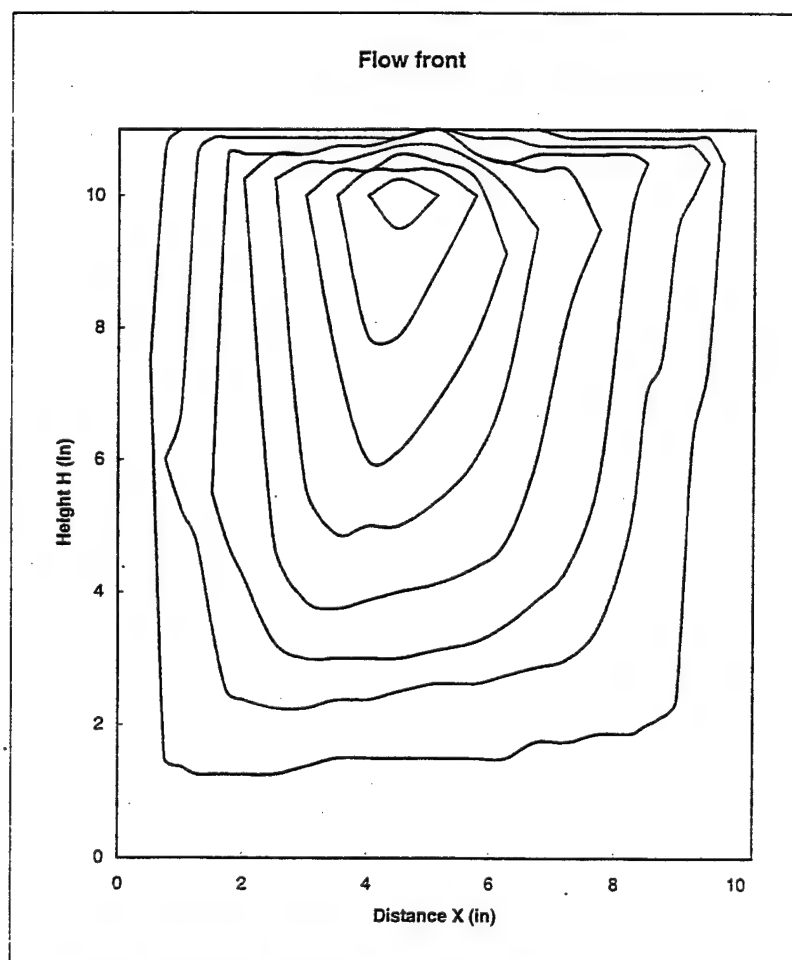
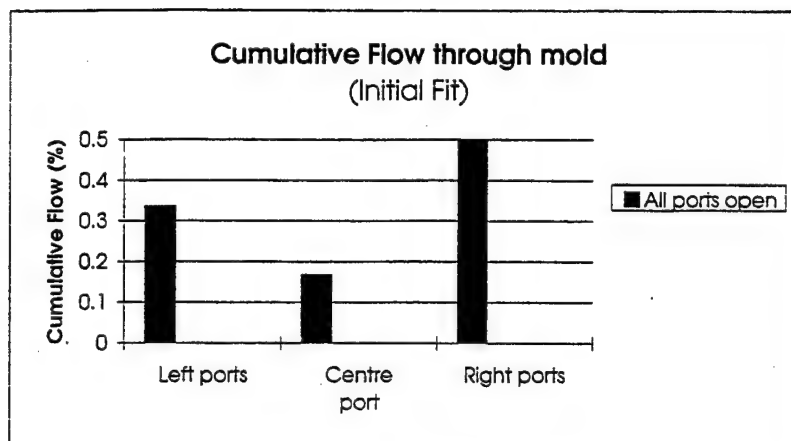
**APPENDIX D**  
**GAS FLOW DATA WITH DIGITIZED FLOW FRONTS**



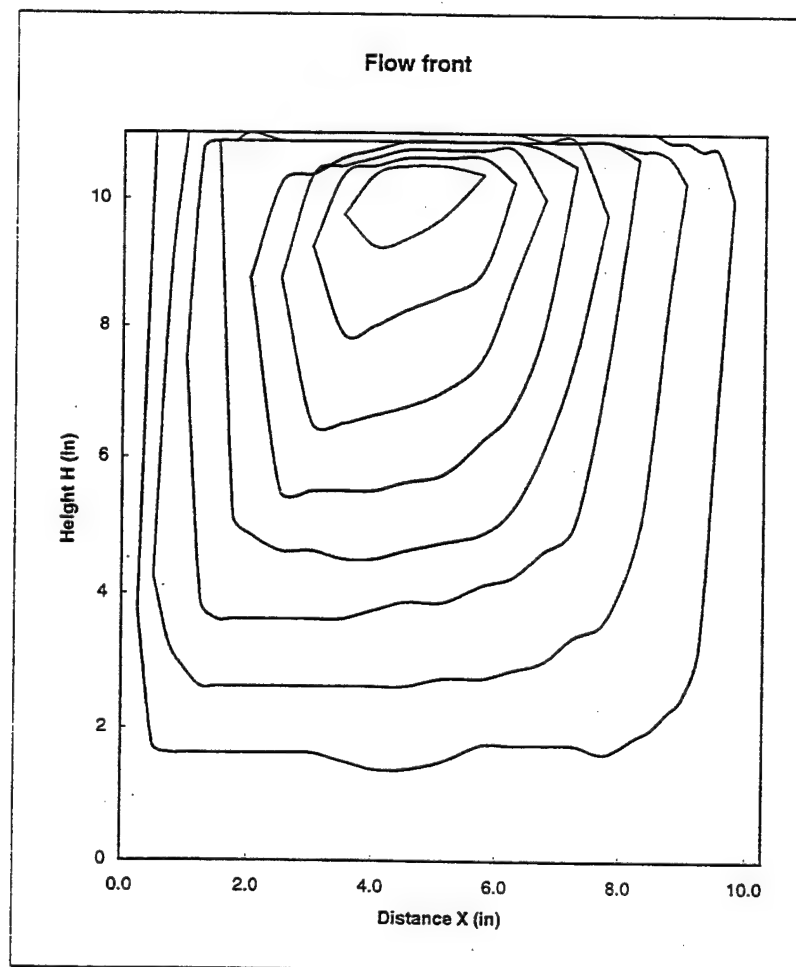
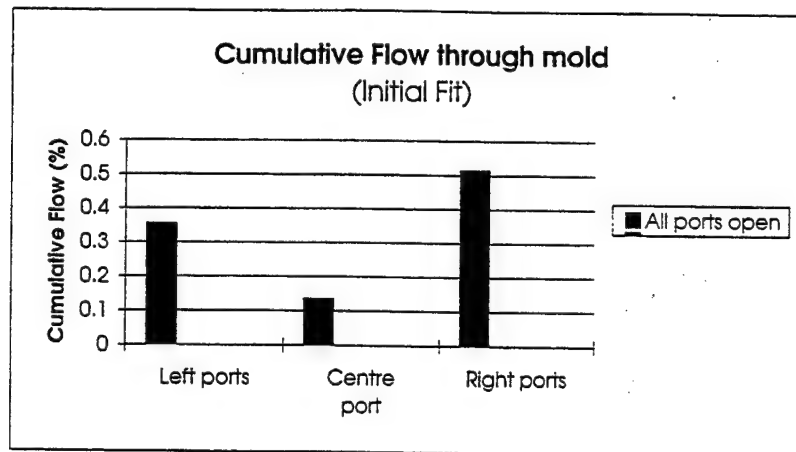
Flow data for Plate S1P1



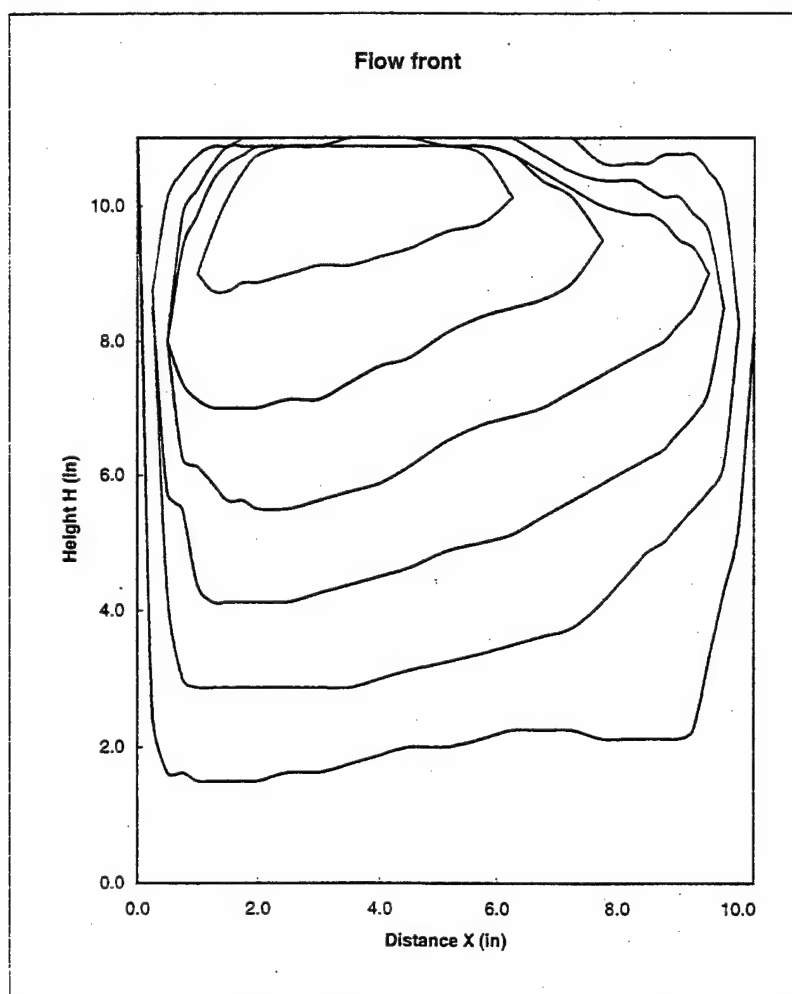
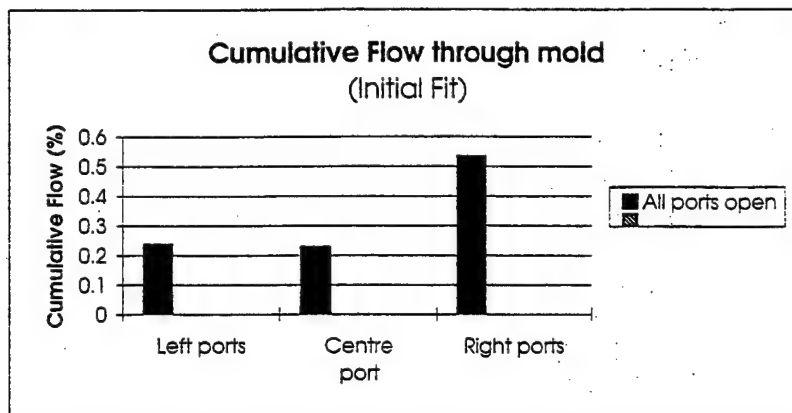
Flow data for Plate S1P2



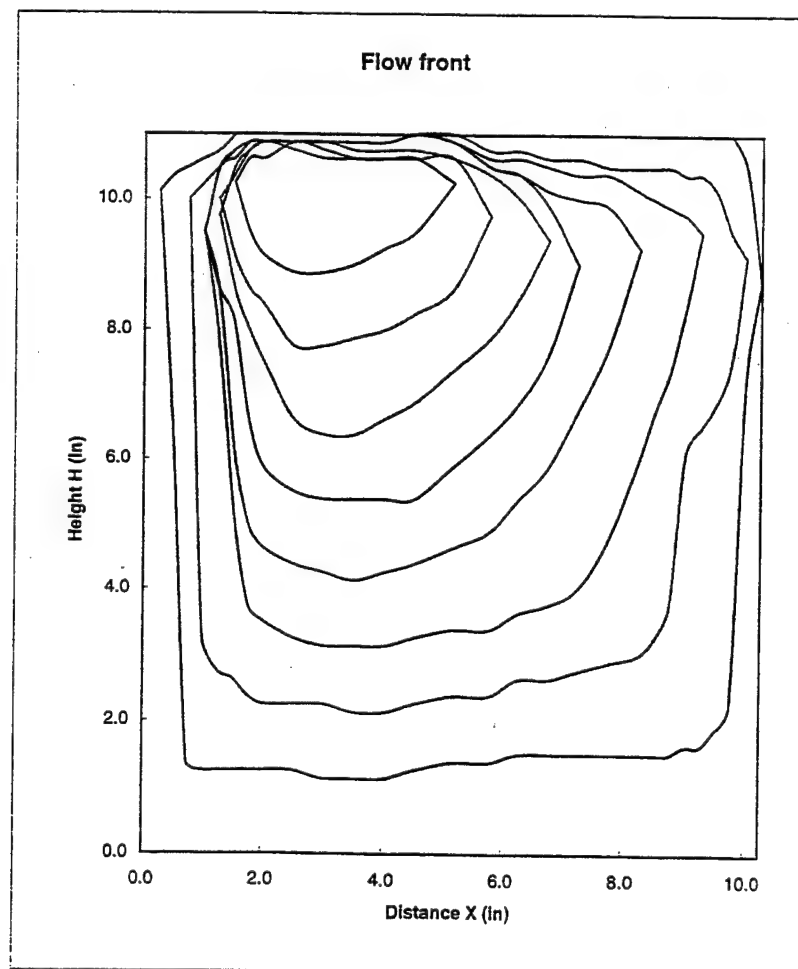
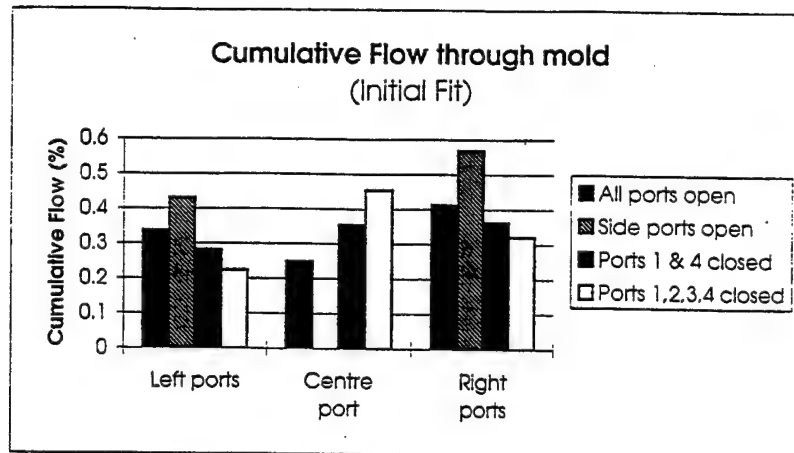
Flow data for Plate S1P3



Flow data for Plate S1P4

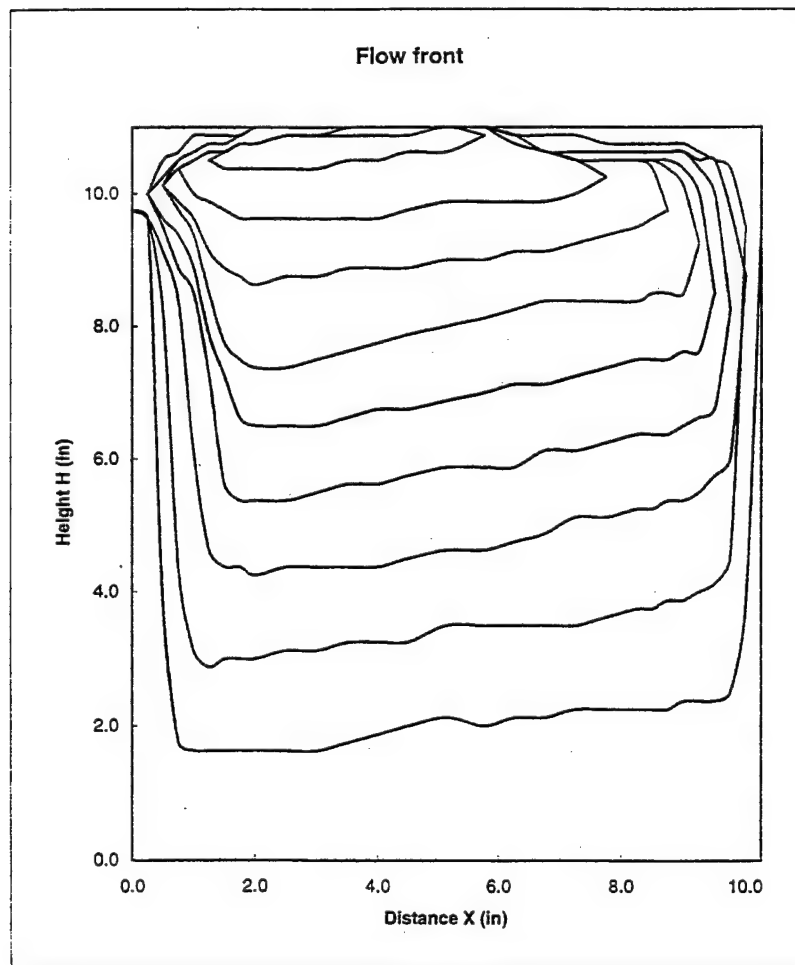
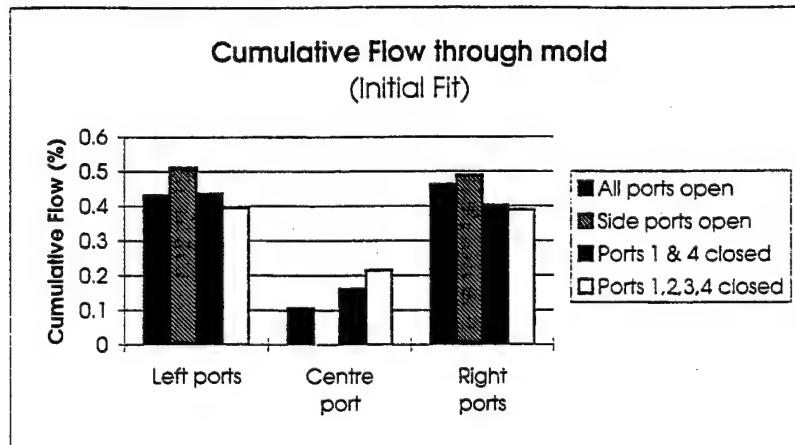


Flow data for Plate S1P5

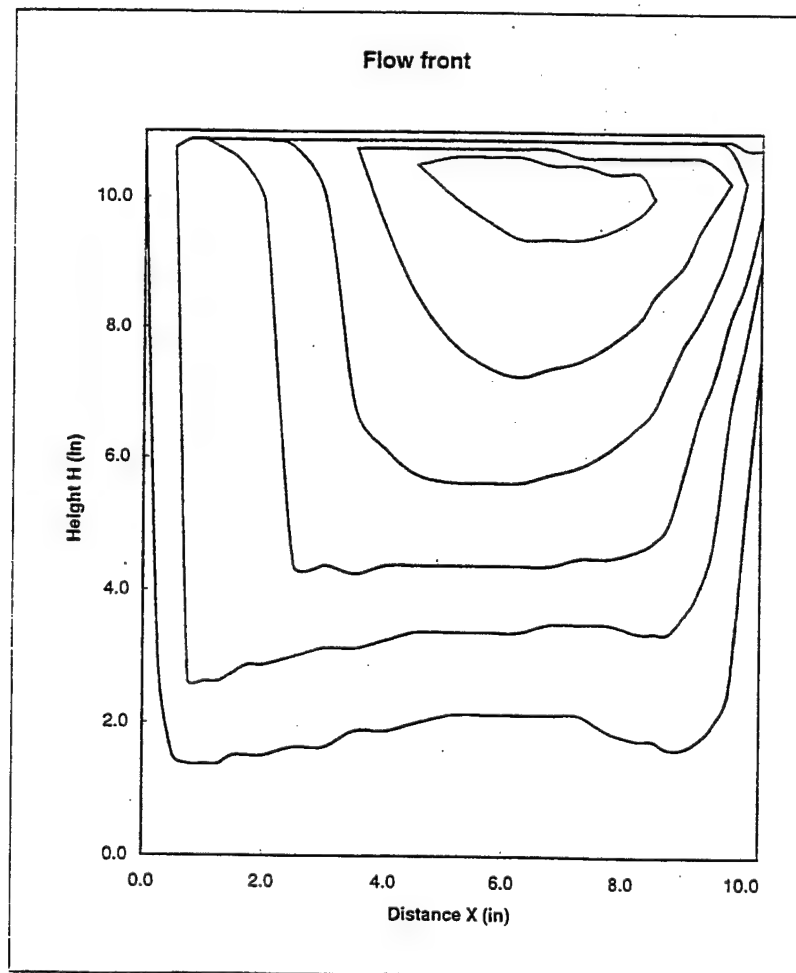
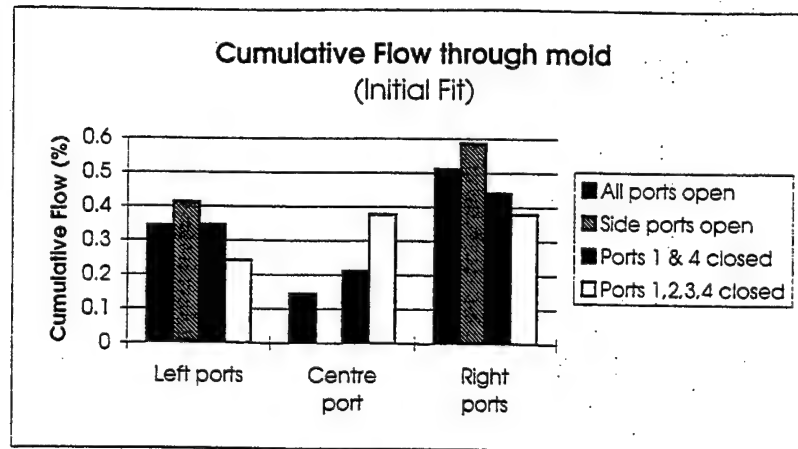


Flow data for Plate S1P6

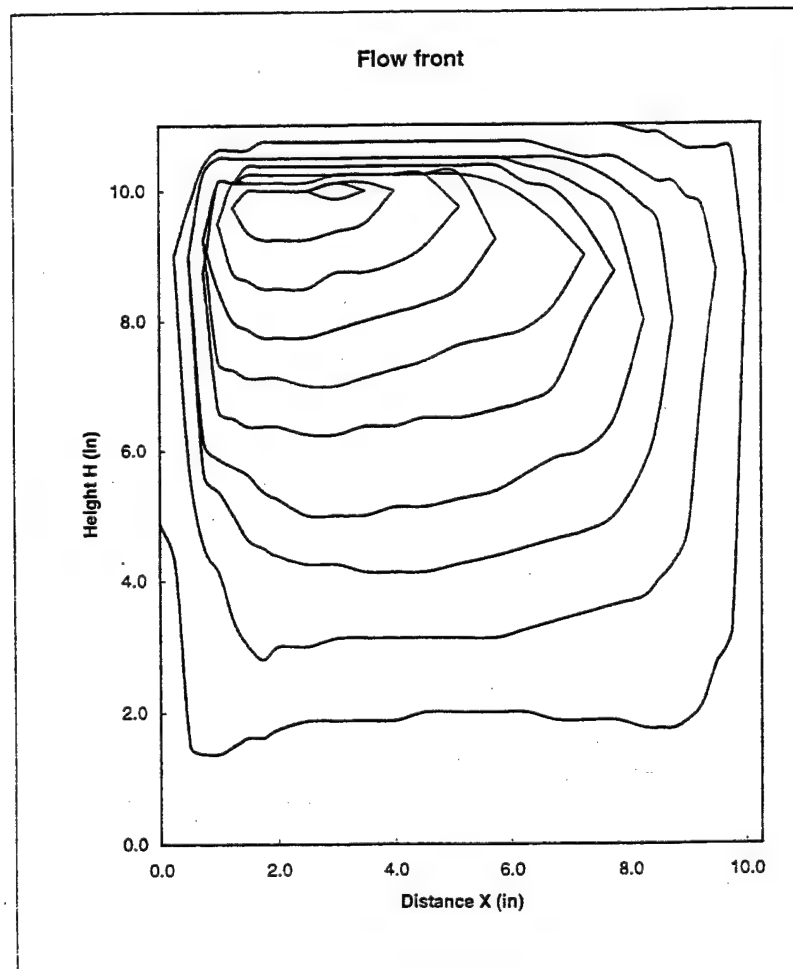
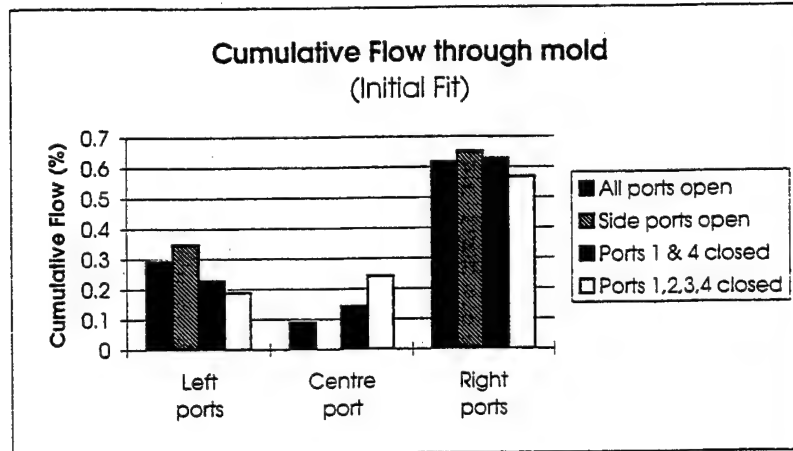




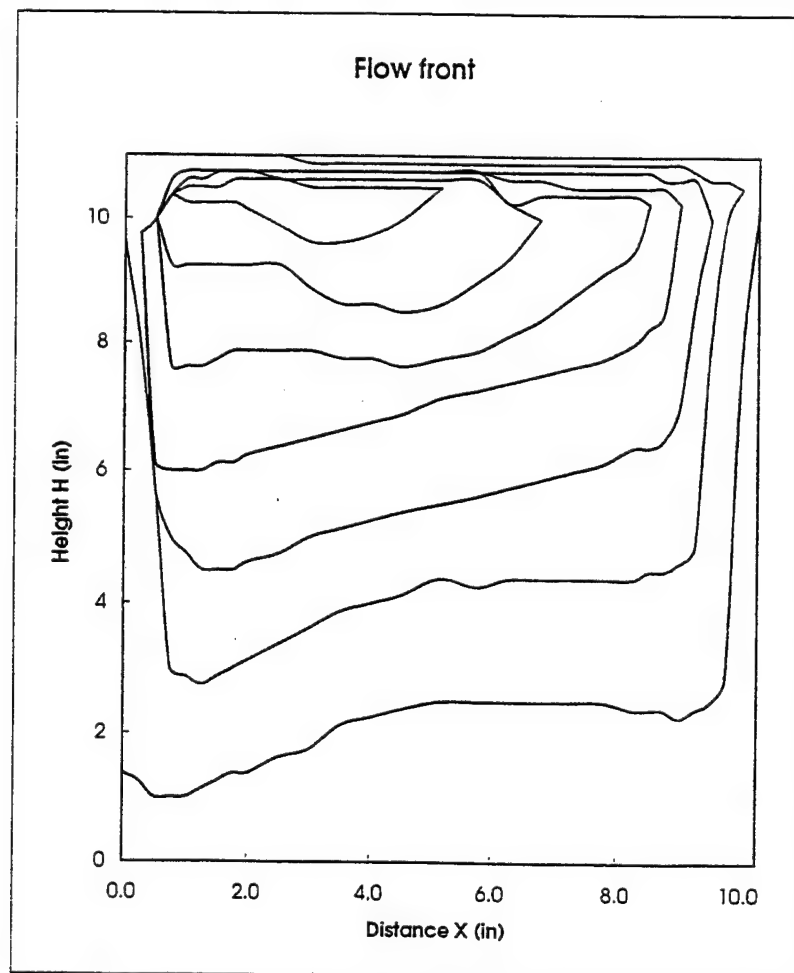
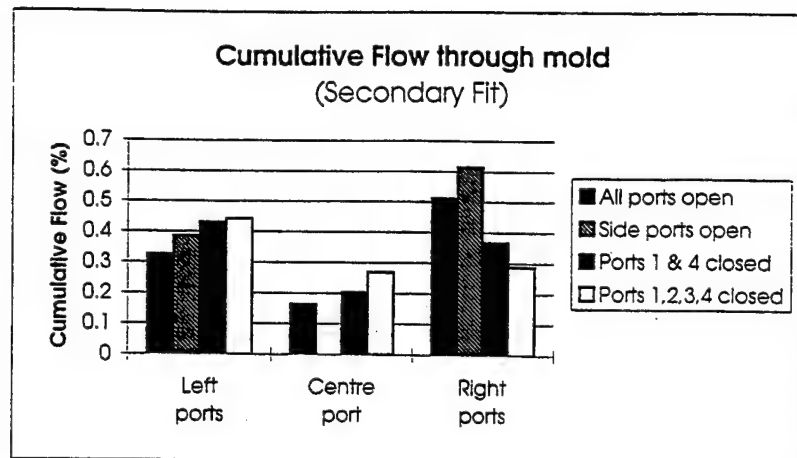
Flow data for Plate S1P7



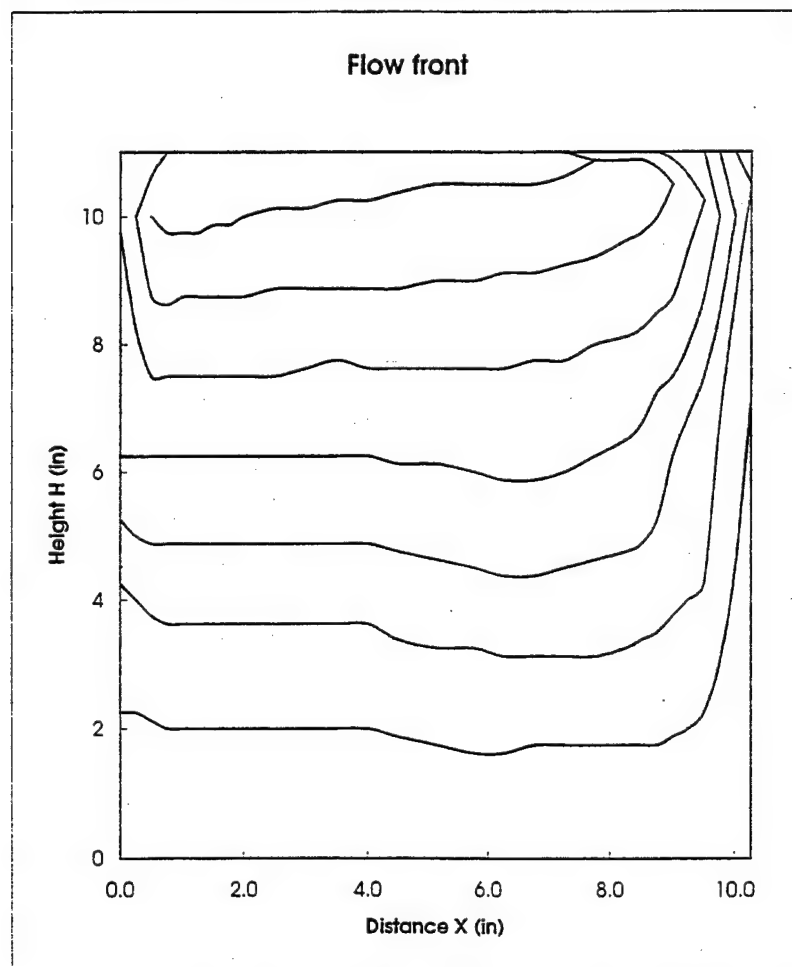
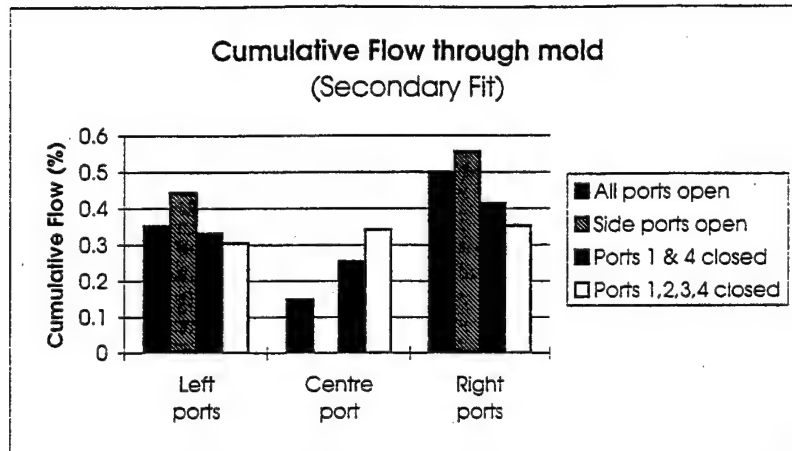
Flow data for Plate S1P8



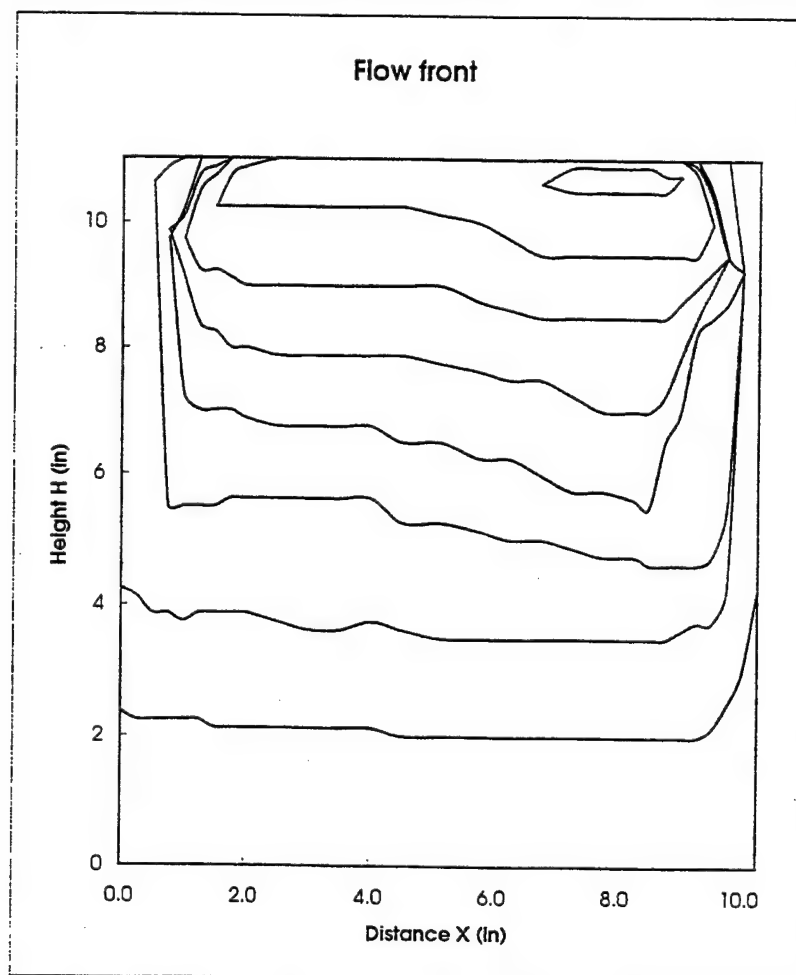
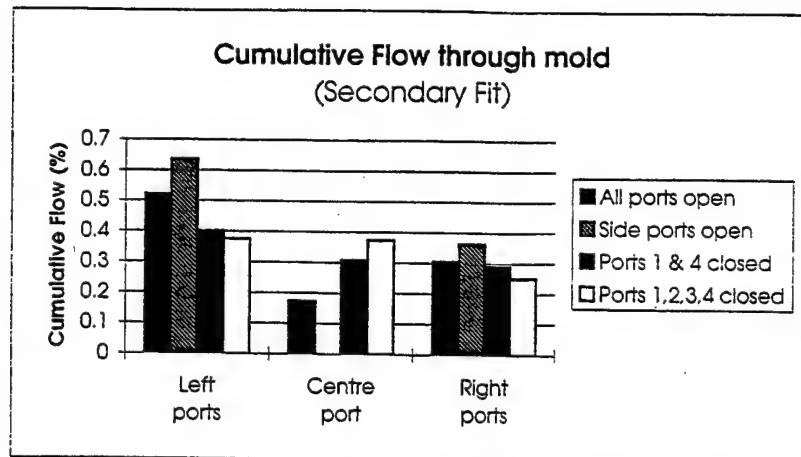
Flow data for Plate S1P10



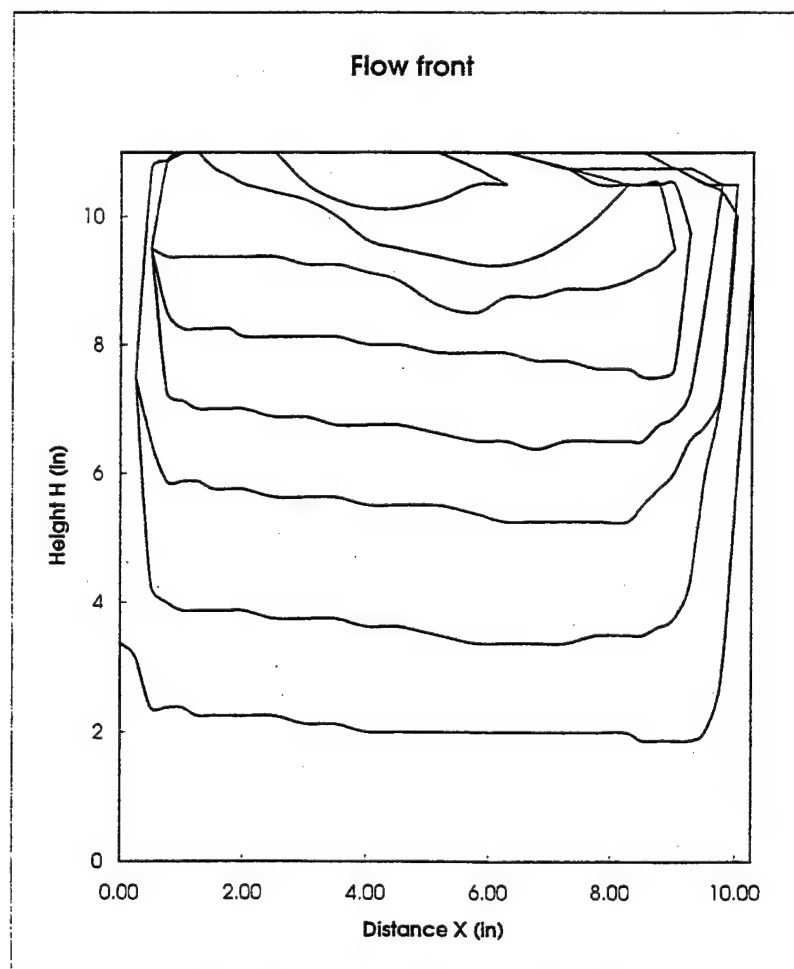
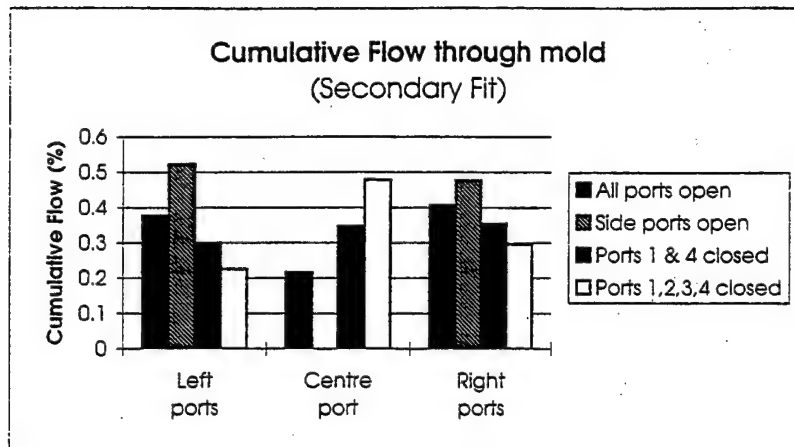
Flow data for Plate S2P1



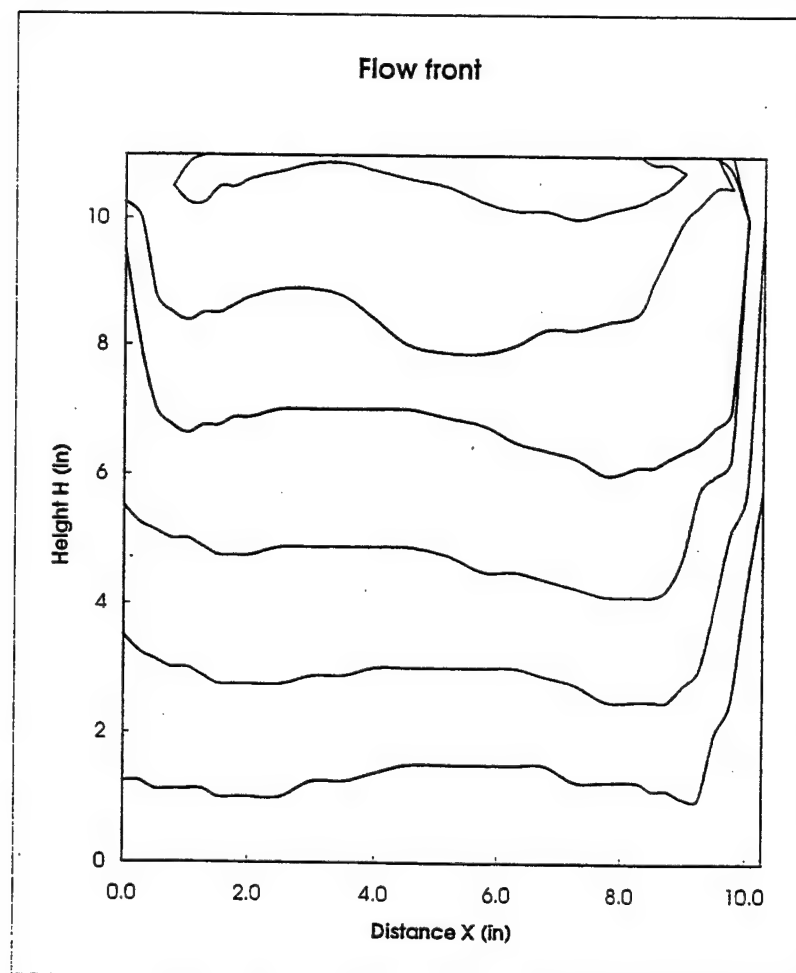
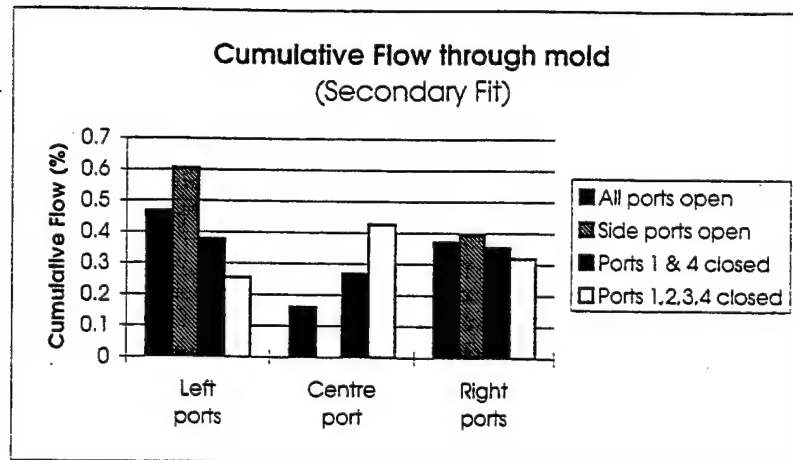
Flow data for Plate S2P2



Flow data for Plate S2P3

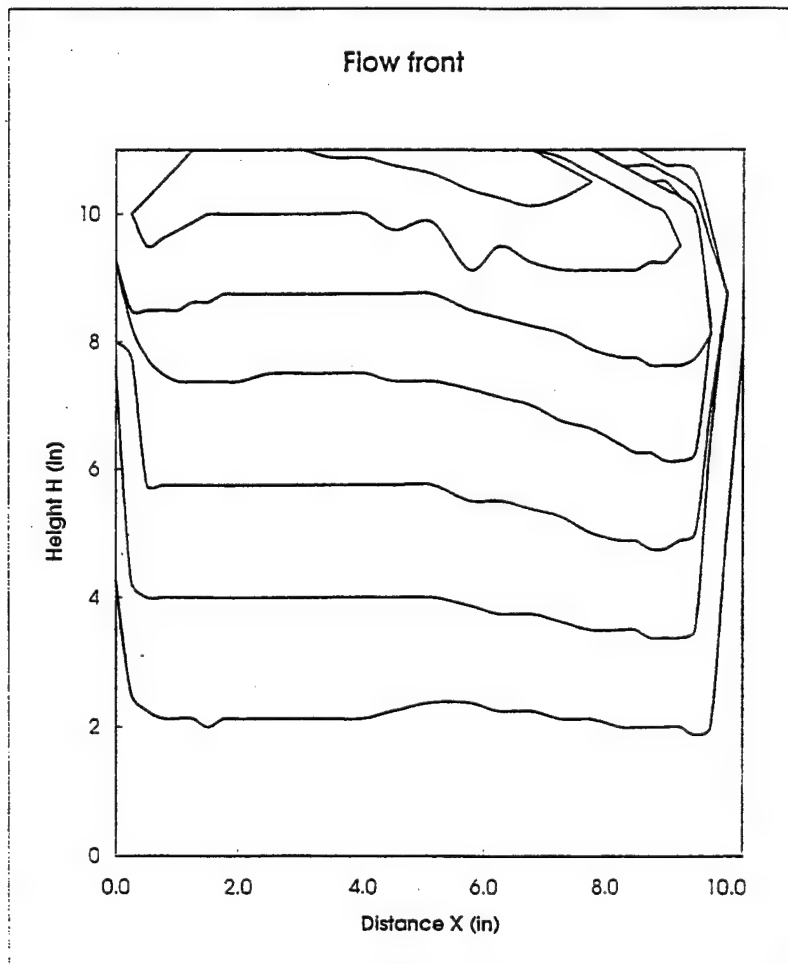
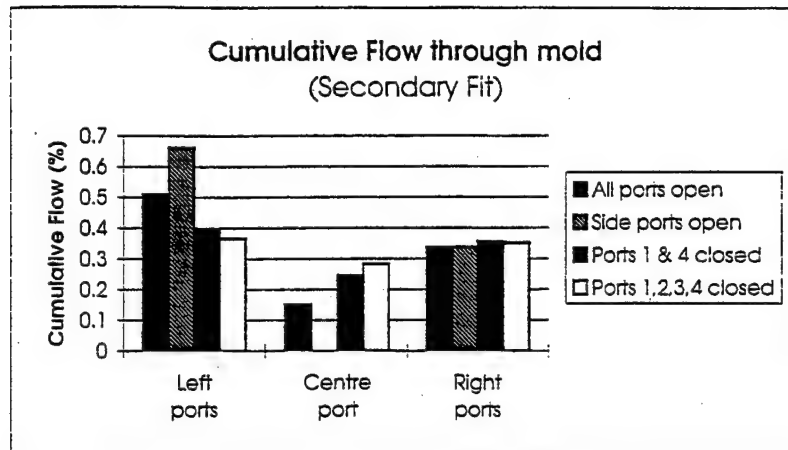


Flow data for Plate S2P4

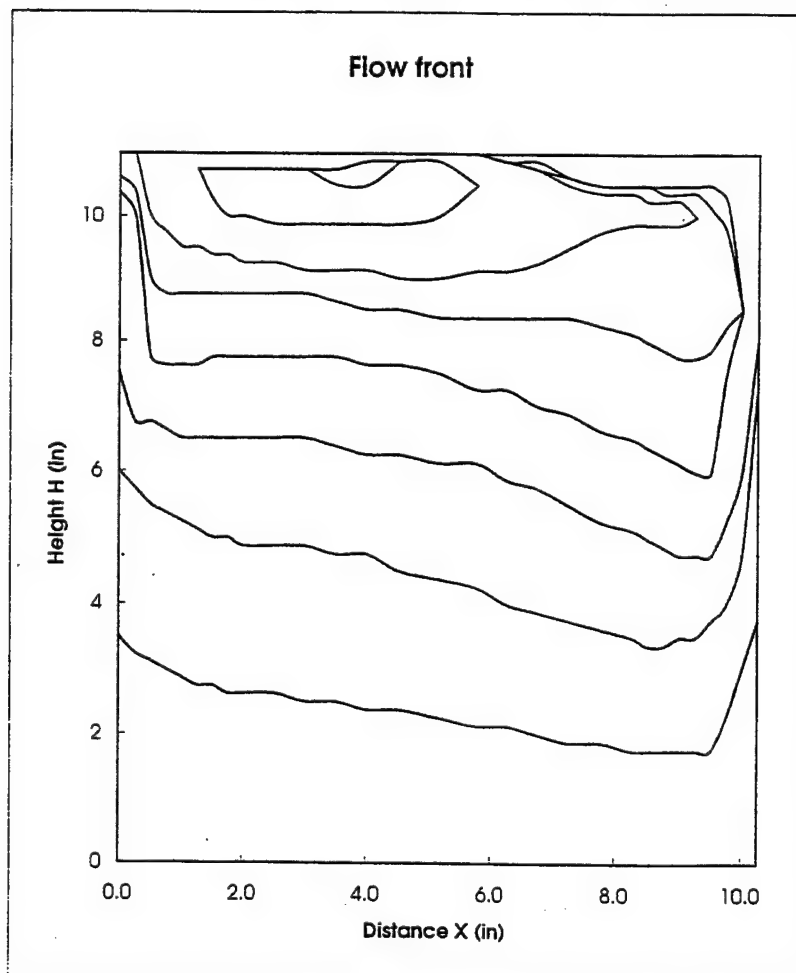
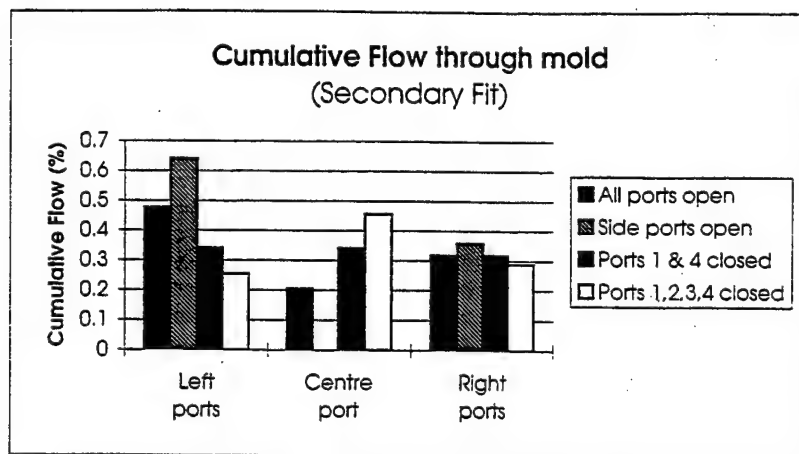


Flow data for Plate S2P5

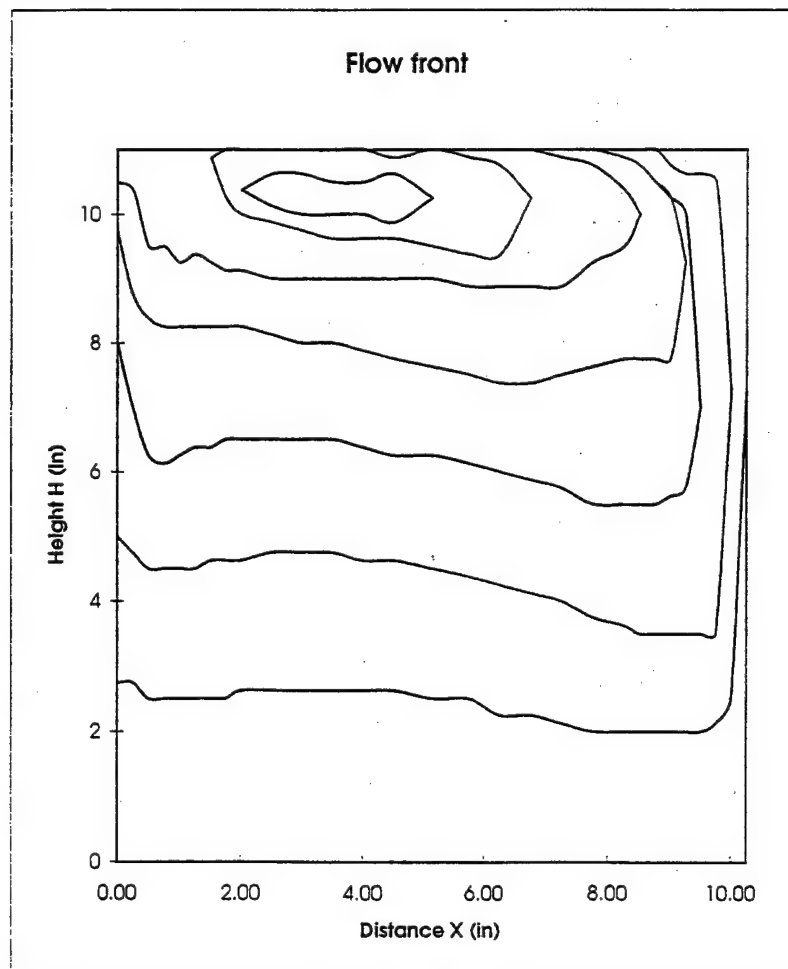
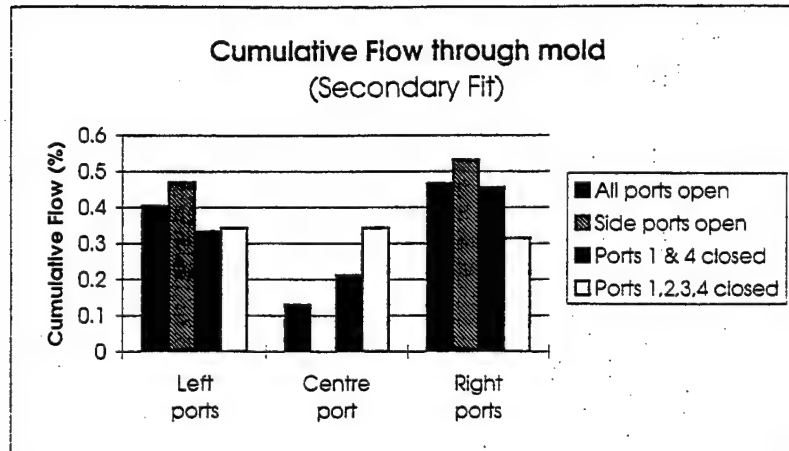




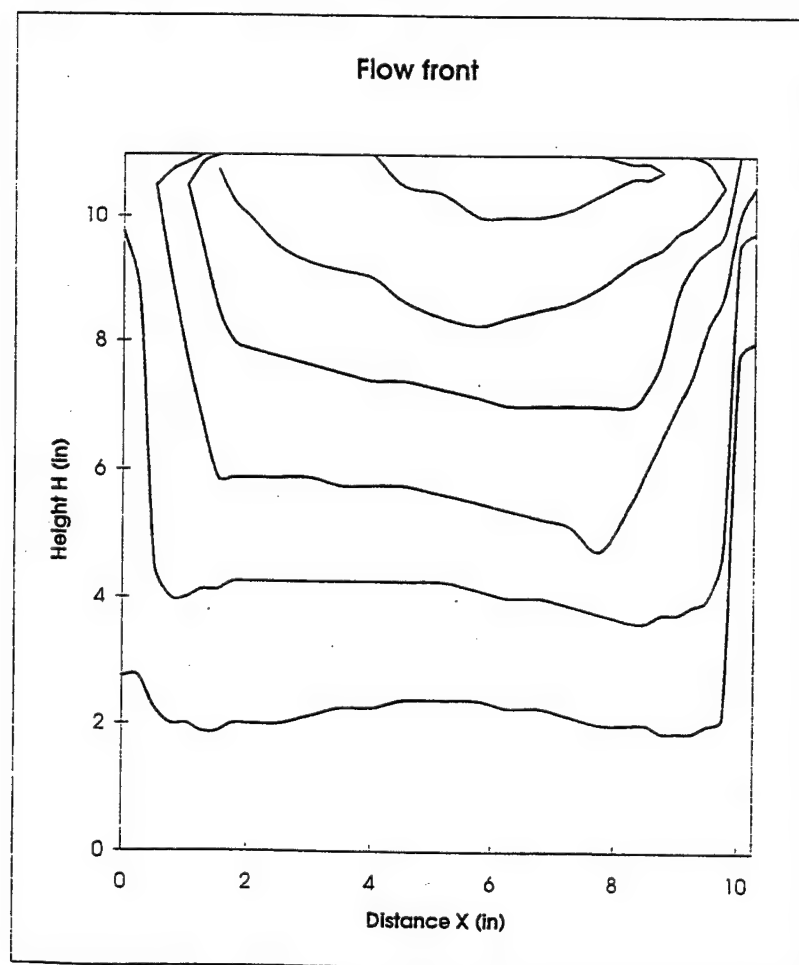
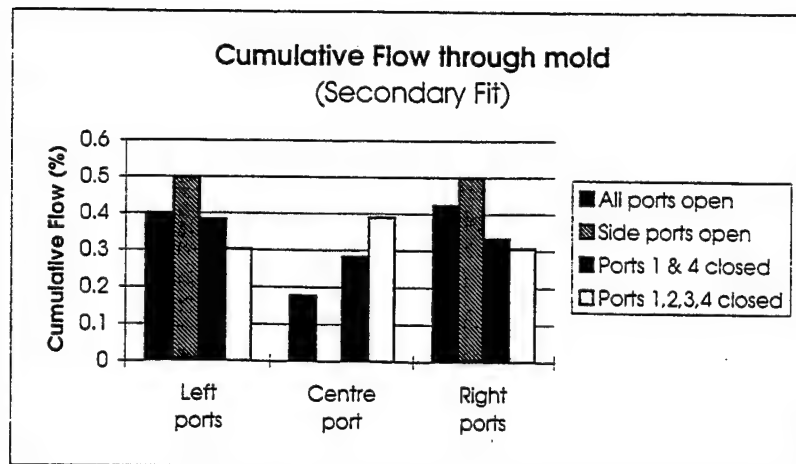
Flow data for Plate S2P6



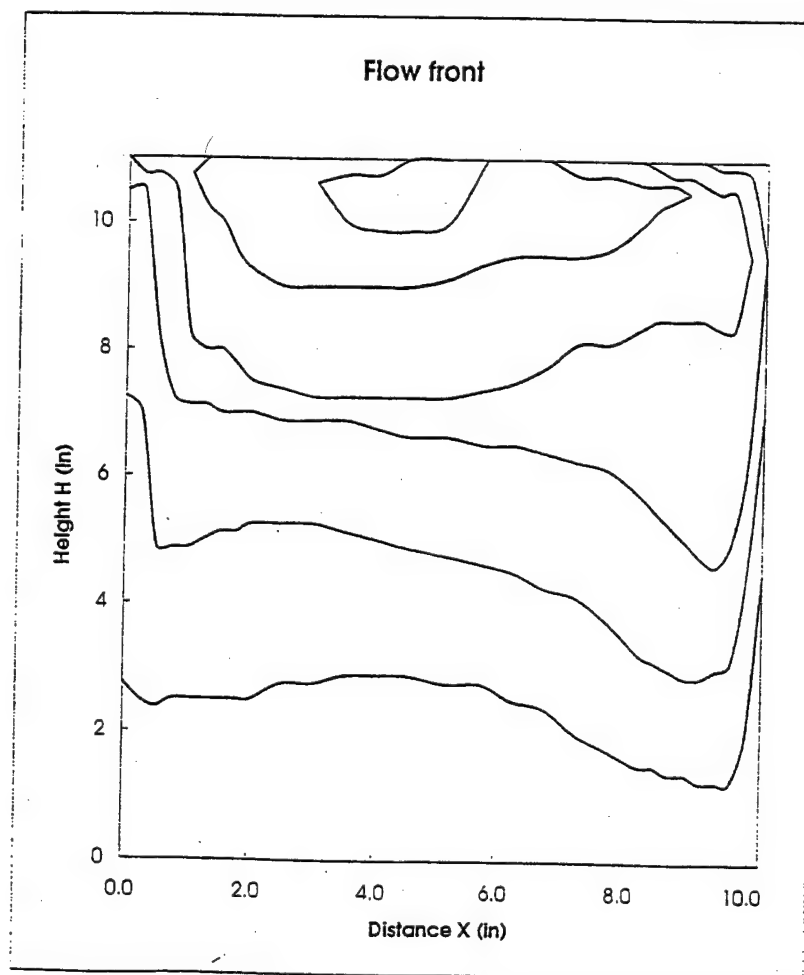
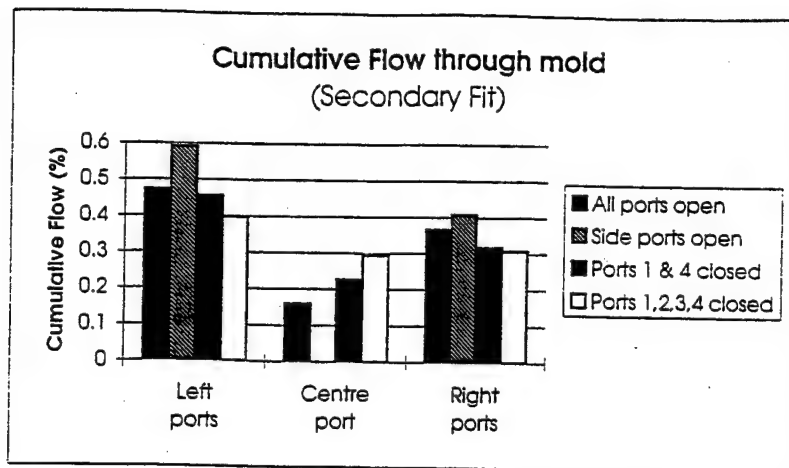
Flow data for Plate S2P7



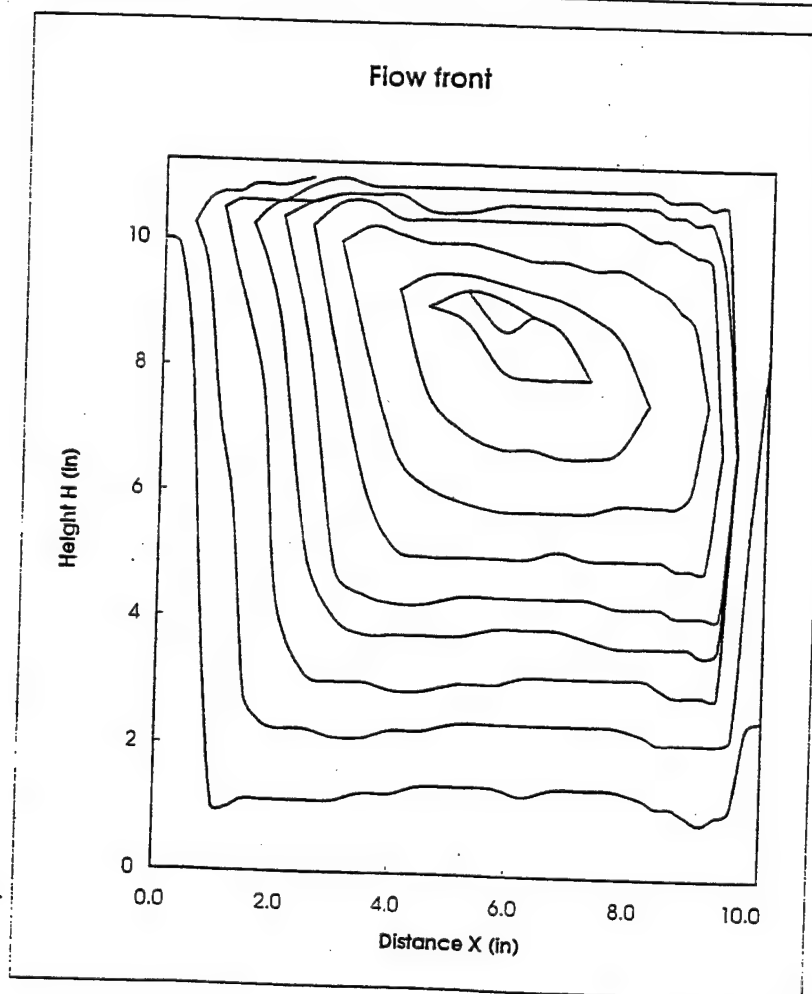
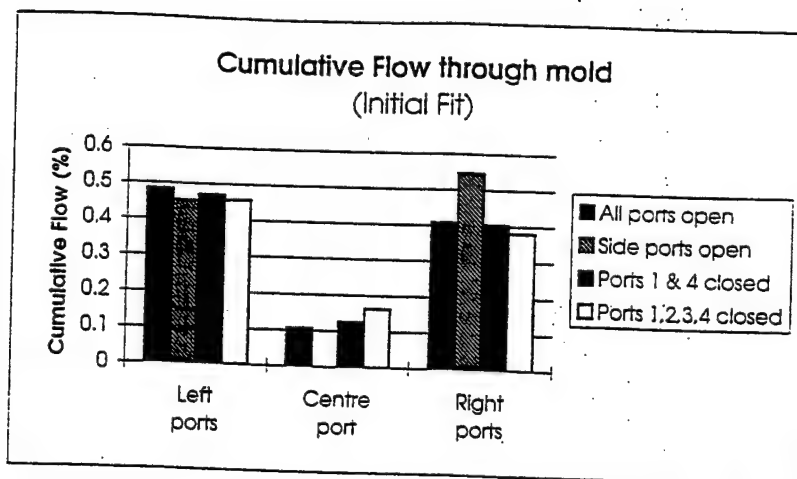
Flow data for Plate S2P8



Flow data for Plate S2P9



Flow data for Plate S2P10



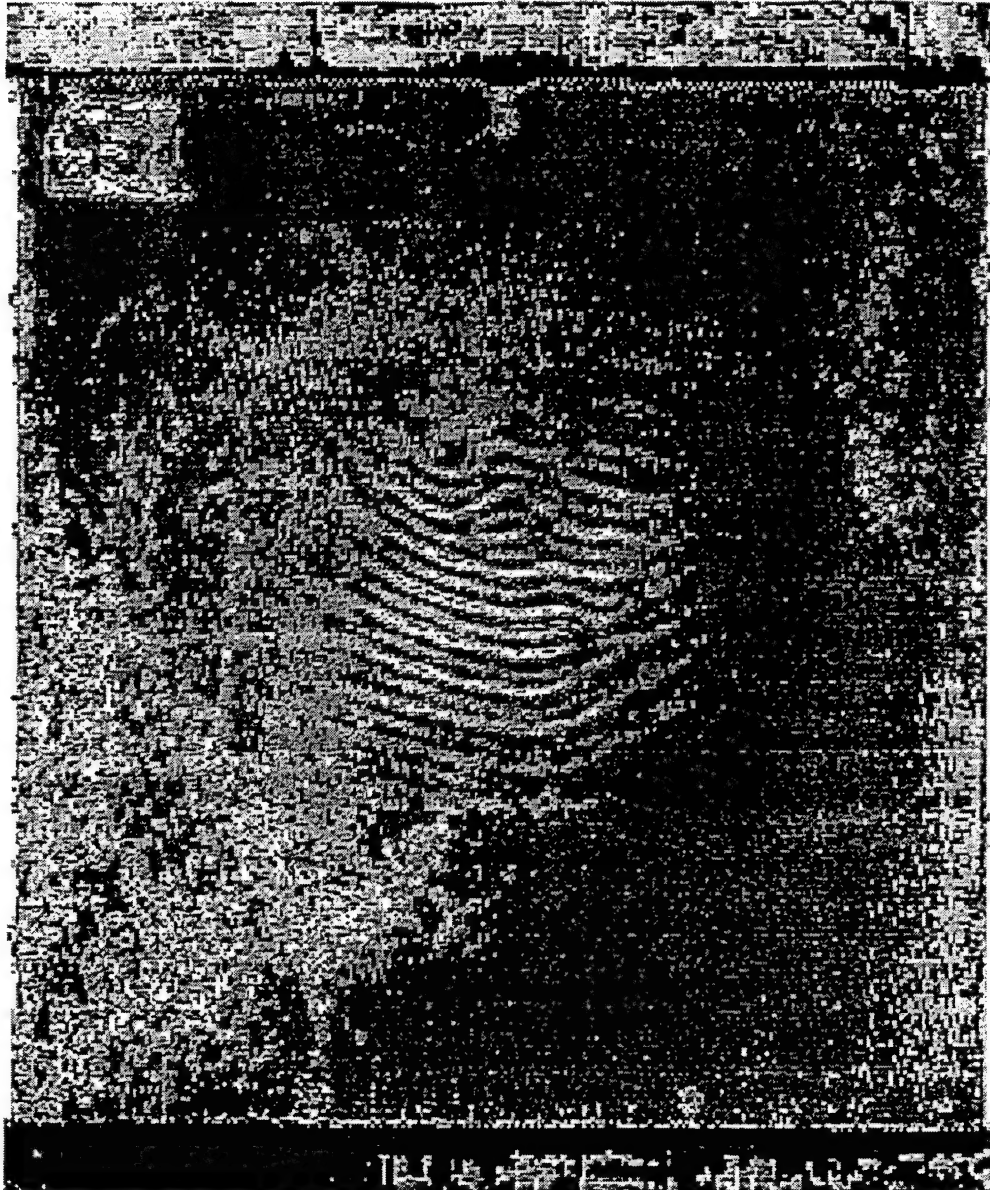
Flow data for Plate S1P9

**APPENDIX E**  
**C-SCAN IMAGES FOR PANELS S2P1 – S2P10**





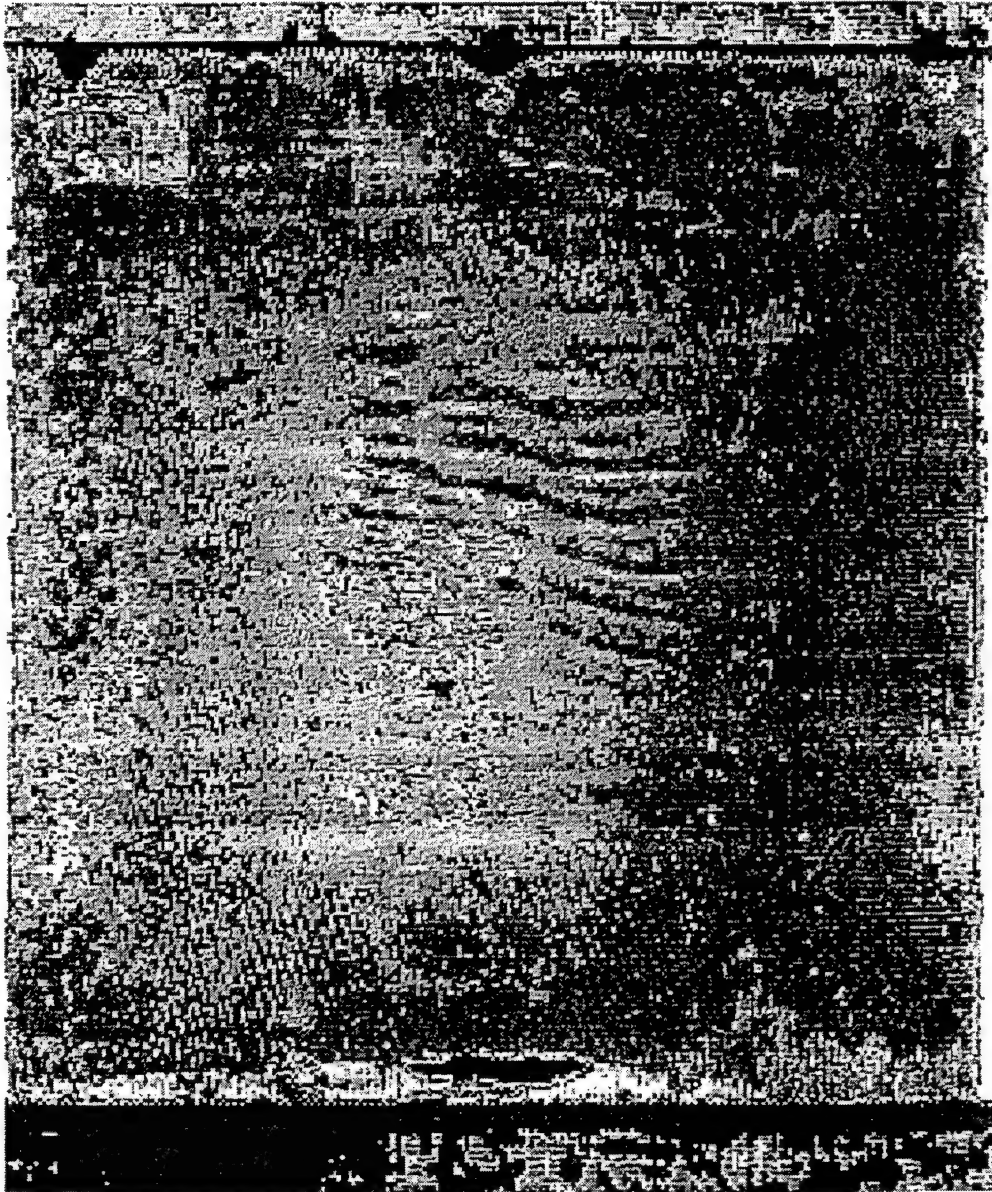
S2P2-0M1



S2P2.CM



5274.001



S2P5.DM1





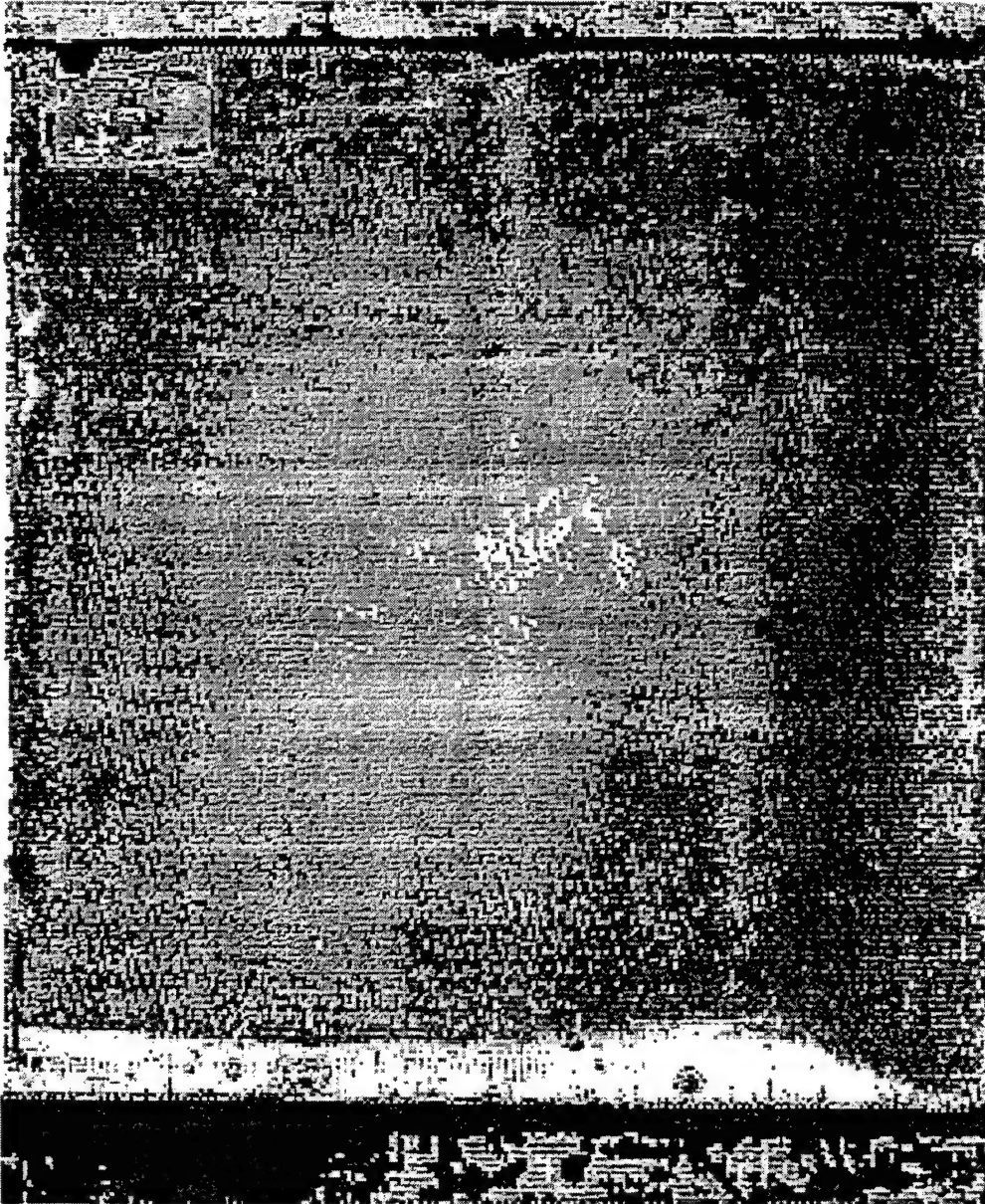
SZP6.CHI



5297.CHI



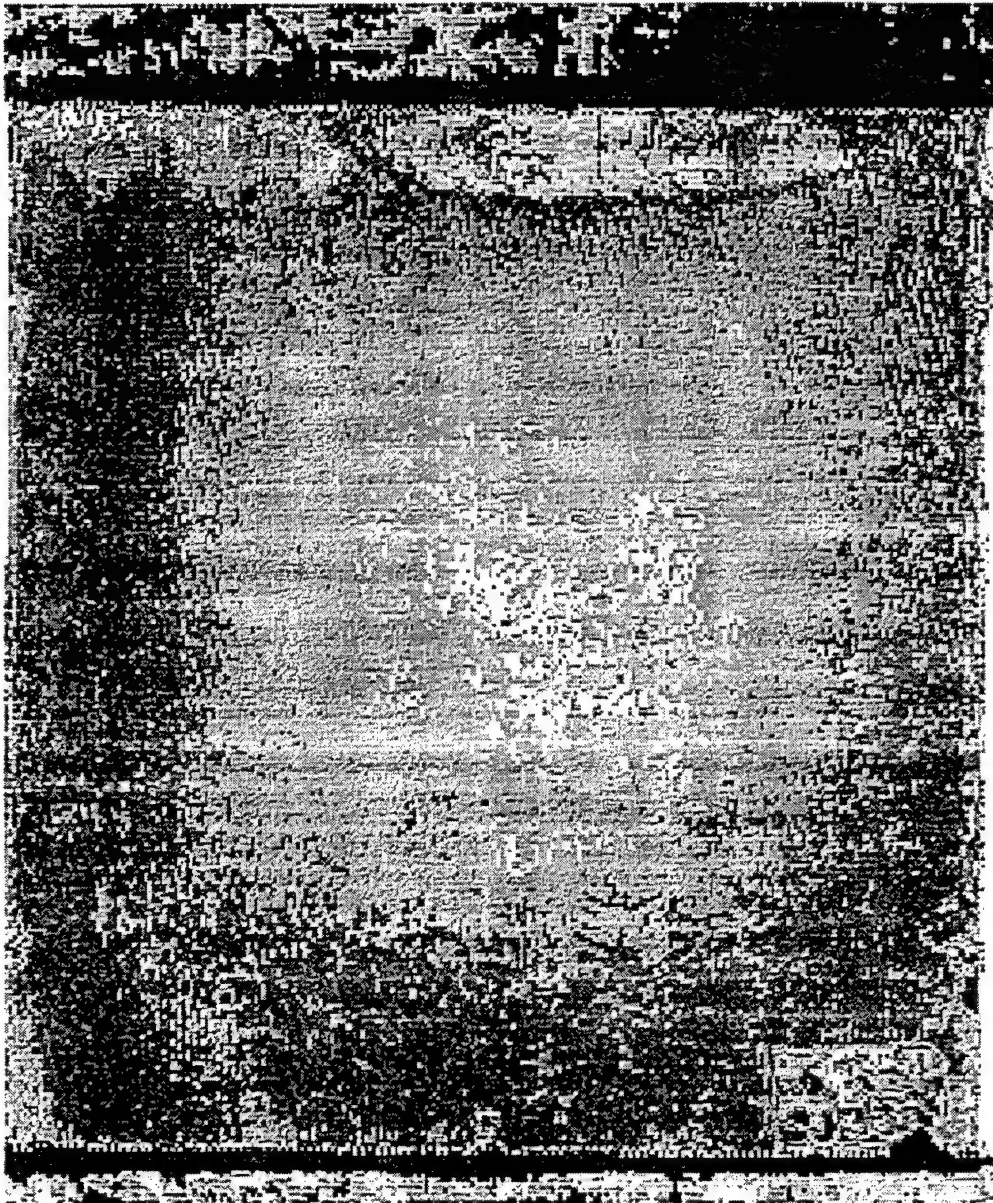
5296.DMS



0299.002







20070225

**APPENDIX F**  
**RACE TRACKING/FINAL FILL PREDICTION CHARTS**  
**A. Predictions Based on Relative Percent Flow**  
**B. Predictions Based on Gas Ratio**  
**C. Predictions Based on Gas Flow Parameter**

ID	Actual Flow	Predictions Based on Relative Percent Flows										Pred.	Ports (1,2)	Ports (3,4)	Pred.	Ports (3,7)	Ports (2,5)	Pred.	Ports (3,4,7)	Ports (1,2,5)	sum	port7	port6	port5	port4	port3	port2	port1
		port1	port2	port3	port4	port5	port6	port7	sum	Ports (1,2,5)	Ports (3,4,7)																	
S1P1	R	2.101	1.028	3.925	3.745	2.795	3.5	2.681	19.775	29.96	52.34	R	15.82	38.79	R	19.33	33.41	R	52.34	29.96								
S1P2	R	2.791	1	3.584	3.18	2.45	4.392	2.858	20.255	30.81	47.50	R	18.72	33.39	R	17.03	31.80	R	47.50	30.81								
S1P3	E	1.377	2.52	1.77	3.961	1.587	2.734	2.432	16.381	33.48	49.83	R	23.79	34.99	R	25.07	25.65	E	49.83	33.48								
S1P4	E	2.497	2.704	2.744	4.181	1.492	2.545	2.729	18.892	35.43	51.10	R	27.53	36.66	R	22.21	28.97	R	51.10	35.43								
S1P5	R	1.061	1.383	1.408	2.625	1.104	3.428	3.947	14.956	23.72	53.36	R	16.34	26.97	R	16.63	35.81	R	53.36	23.72								
S1P6	R	1.793	1.316	1.252	2.616	2.082	3.829	2.473	15.361	33.79	41.28	R	20.24	25.18	E	22.12	24.25	E	41.28	33.79								
S1P7	E	1.418	0.898	0.592	1.903	2.313	1.133	2.464	10.721	43.18	46.26	E	21.60	23.27	E	29.95	28.50	E	46.26	43.18								
S1P8	E	1.669	2.089	2.344	3.393	1.393	2.162	1.913	14.963	34.42	51.13	R	25.12	38.34	R	23.27	28.45	E	51.13	34.42								
S1P9	L	1.202	0.813	1.129	1.103	4.294	1.389	3.098	13.028	48.43	40.91	L	15.47	17.13	E	39.20	32.45	L	40.91	48.43								
S1P10	R	1.009	0.516	1.394	1.17	0.432	0.602	1.569	6.692	29.24	61.76	R	22.79	38.31	R	14.17	44.28	R	61.76	29.24								
S2P1	R	0.737	0.726	1.122	2.526	1.537	1.507	1.076	9.231	32.50	51.18	R	15.85	39.52	R	24.52	23.81	E	51.18	32.50								
S2P2	R	2.158	1.125	1.563	3.114	1.354	1.961	1.912	13.187	35.16	49.97	R	24.90	35.47	R	18.80	26.35	R	49.97	35.16								
S2P3	E	3.476	0.71	0.638	1.607	1.632	1.938	1.166	11.167	52.10	30.55	L	37.49	20.10	L	20.97	16.15	E	30.55	52.10								
S2P4	E	2.84	1.364	1.439	2.643	1.063	3.016	1.594	13.959	37.73	40.66	E	30.12	29.24	E	17.39	21.73	E	40.66	37.73								
S2P5	R	3.294	2.284	1.644	2.058	0.85	2.227	1.388	13.745	46.77	37.03	L	40.58	26.93	L	22.80	22.06	E	37.03	46.77								
S2P6	E	3.378	0.869	0.533	1.405	2.122	1.889	2.255	12.451	51.15	33.68	L	34.11	15.57	L	24.02	22.39	E	33.68	51.15								
S2P7	R	3.622	1.336	0.734	1.719	0.939	2.536	1.489	12.375	47.65	31.85	L	40.06	19.82	L	18.38	17.96	E	31.85	47.65								
S2P8	R	3.377	1.478	3.04	2.739	1.555	2.051	1.606	15.846	40.45	46.60	R	30.64	36.47	R	19.14	29.32	R	46.60	40.45								
S2P9	E	1.732	1.231	0.988	2.375	1.24	1.859	1.091	10.516	39.97	42.35	E	28.18	31.98	E	23.50	19.77	E	42.35	39.97								
S2P10	E	3.262	1.297	0.682	2.859	2.043	2.233	1.562	13.938	47.37	36.61	L	32.71	25.41	L	23.96	16.10	L	36.61	47.37								

Gas Ratio

	PREDICTIONS	BASED ON	GAS	RATIO			
EXPT. ID	Actual Flow Char.	G <sub>R</sub> (1,2,5) vs (3,4,7)	Predictions	G <sub>R</sub> (2,5) vs (3,7)	Prediction	G <sub>R</sub> (1,2) vs (3,4)	Predictions
SIP1	R						
No Ports Closed		1.75	R	1.73	R	2.45	R
SIP2	R						
No Ports Closed		1.54	R	1.87	R	1.78	R
SIP3	E						
No Ports Closed		1.49	R	1.02	E	1.47	R
SIP4	E						
No Ports Closed		1.44	R	1.42	R	1.33	R
SIP5	R						
No Ports Closed		2.25	R	2.15	R	1.65	R
SIP6	R						
No Ports Closed		1.22	R	1.12	R	1.24	R
Top Ports Closed		1.32	R	1.27	R	1.32	R
Lower Ports Closed		1.29	R	1.29	R	1.08	E
Side Ports Closed		1.44	R	1.44	R	-	
SIP7	E						
No Ports Closed		1.07	E	0.95	E	1.08	E
Top Ports Closed		0.96	E	0.73	L	0.96	E
Lower Ports Closed		0.92	E	0.92	E	0.68	L
Side Ports Closed		0.98	E	0.98	E	-	
SIP8	E						
No Ports Closed		1.49	R	1.22	R	1.53	R
Top Ports Closed		1.42	R	1.23	R	1.42	R
Lower Ports Closed		1.27	R	1.28	R	1.18	R
Side Ports Closed		1.56	R	1.57	R	-	

<b>S1P9</b>	<b>L</b>	0.85	L	0.83	L	1.11	R
No Ports Closed		1.21	R	1.49	R	1.21	R
Top Ports Closed		0.86	L	0.86	L	1.33	R
Lower Ports Closed		0.83	L	0.83	L	-	
Side Ports Closed							
<b>S1P10</b>	<b>R</b>	2.11	R	3.13	R	1.68	R
No Ports Closed		1.87	R	2.71	R	1.87	R
Top Ports Closed		2.75	R	2.75	R	2.41	R
Lower Ports Closed		3.00	R	3.00	R	-	
Side Ports Closed							
<b>S2P1</b>	<b>R</b>	1.58	R	0.97	E	2.49	R
No Ports Closed		1.59	R	1.03	E	1.59	R
Top Ports Closed		0.85	L	0.85	L	1.40	R
Lower Ports Closed		0.65	L	0.65	L	-	
Side Ports Closed							
<b>S2P2</b>	<b>R</b>	1.36	R	1.40	R	1.42	R
No Ports Closed		1.26	R	1.14	R	1.26	R
Top Ports Closed		1.29	R	1.25	R	1.20	R
Lower Ports Closed		1.16	R	1.16	R	-	
Side Ports Closed							
<b>S2P3</b>	<b>E</b>	0.59	L	0.77	L	0.54	L
No Ports Closed		0.57	L	0.79	L	0.57	L
Top Ports Closed		0.72	L	0.72	L	0.83	L
Lower Ports Closed		0.67	L	0.67	L	-	
Side Ports Closed							
<b>S2P4</b>	<b>E</b>	1.08	E	1.25	R	0.97	E
No Ports Closed		0.91	E	0.96	E	0.91	E
Top Ports Closed		1.19	R	1.19	R	1.00	E
Lower Ports Closed		1.31	R	1.31	R	-	
Side Ports Closed							

<b>S2P5</b>	R	0.79 0.65 0.94 1.25	L L E R	0.97 0.70 0.94 1.25	E L E R	0.66 0.65 0.70 -	L L L
<b>S2P6</b>	E	0.66 0.51 0.89 0.96	L L L E	0.93 0.64 0.89 0.96	E L L E	0.46 0.51 0.61 -	L L L
<b>S2P7</b>	R	0.66 0.56 0.93 1.14	L L E R	0.98 0.68 0.93 1.14	E L E R	0.50 0.56 0.58 -	L L L
<b>S2P8</b>	R	1.15 1.13 1.37 0.92	R R R E	1.53 1.56 1.37 0.92	R R R E	1.19 1.13 1.79 -	R R R
<b>S2P9</b>	E	1.06 1.00 0.87 1.01	E E L E	0.84 0.87 0.87 1.01	L L L E	1.13 1.00 0.82 -	R E L
<b>S2P10</b>	E	0.77 0.69 0.70 0.78	L L L L	0.67 0.56 0.70 0.78	L L L L	0.78 0.69 0.55	L L L
<b>Legend:</b> E = Even Flow R = Right Flow L = Left Flow							

GAS Flow Parameter

		Predictions Based on Gas Flow Parameter							
EXPT. ID	Actual Flow Char.	$\Delta P = P_R - P_L$ (1,2,5) vs (3,4,7)	Predictions	$\Delta P = P_R - P_L$ (2,5) vs (3,7)	Prediction	$\Delta P = P_R - P_L$ (1,2) vs (3,4)	Predictions		
S1P1	R								
No Ports Closed		0.52	R	0.49	R	0.80	R		
S1P2	R								
No Ports Closed		0.39	R	0.52	R	0.51	R		
S1P3	E								
No Ports Closed		0.38	R	0.02	E	0.39	R		
S1P4	E								
No Ports Closed		0.37	R	0.33	R	0.32	R		
S1P5	R								
No Ports Closed		0.69	R	0.67	R	0.37	R		
S1P6	R								
No Ports Closed		0.17	E	0.10	E	0.17	E		
Top Ports Closed		0.32	R	0.20	R	0.48	R		
Lower Ports Closed		0.19	E	0.28	R	0.03	E		
Side Ports Closed		0.23	R	0.34	R	-	-		
S1P7	E								
No Ports Closed		0.07	E	-0.05	E	0.06	E		
Top Ports Closed		-0.05	E	-0.25	L	-0.08	E		
Lower Ports Closed		-0.08	E	-0.12	E	-0.15	E		
Side Ports Closed		-0.02	E	-0.02	E	-	-		
S1P8	E								
No Ports Closed		0.39	R	0.18	E	0.46	R		
Top Ports Closed		0.41	R	0.19	E	0.61	R		
Lower Ports Closed		0.22	R	0.34	R	0.13	E		
Side Ports Closed		0.32	R	0.48	R	-	-		

## GAS Flow Parameter

[illegible]

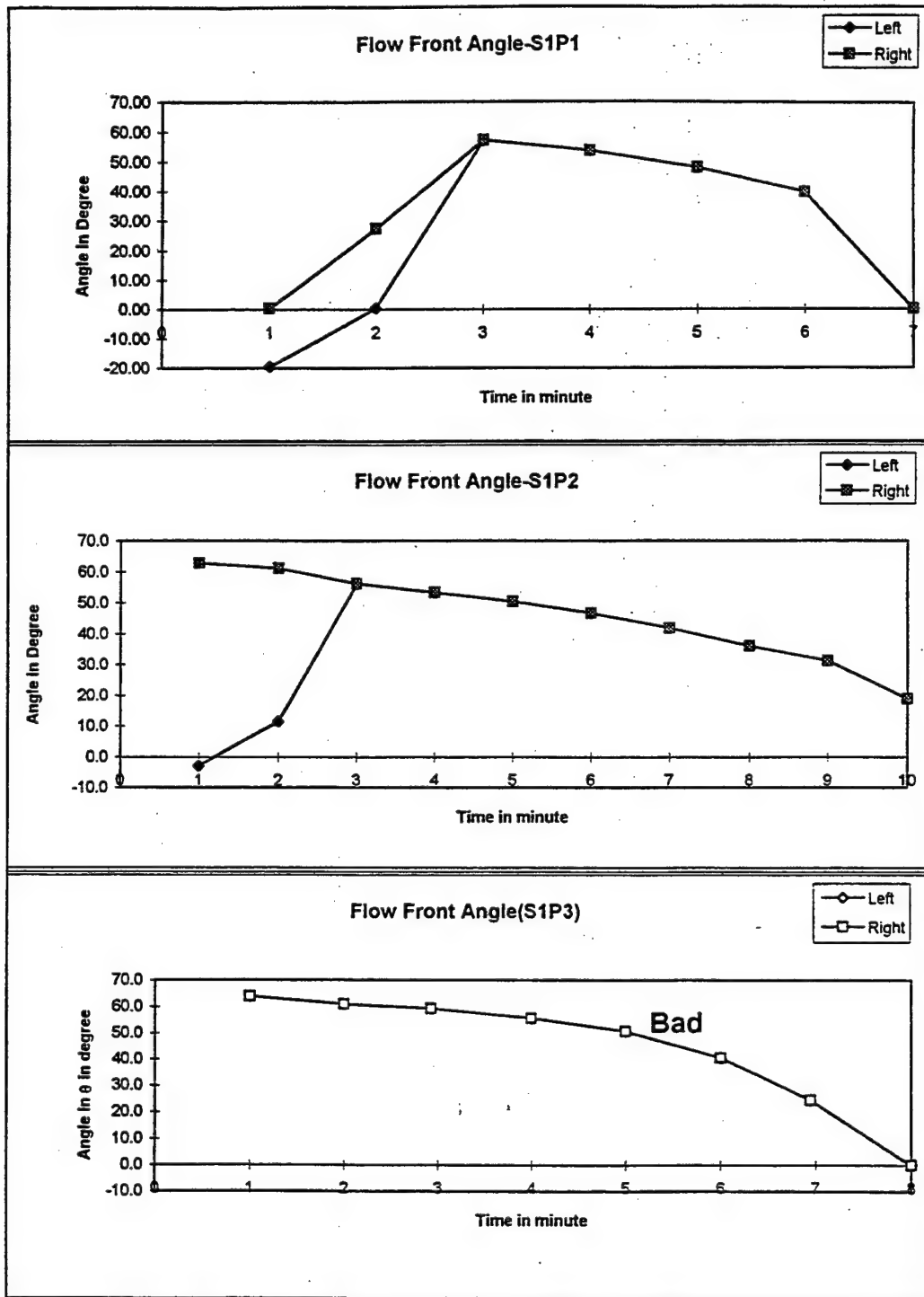


# GAS Flow Parameter

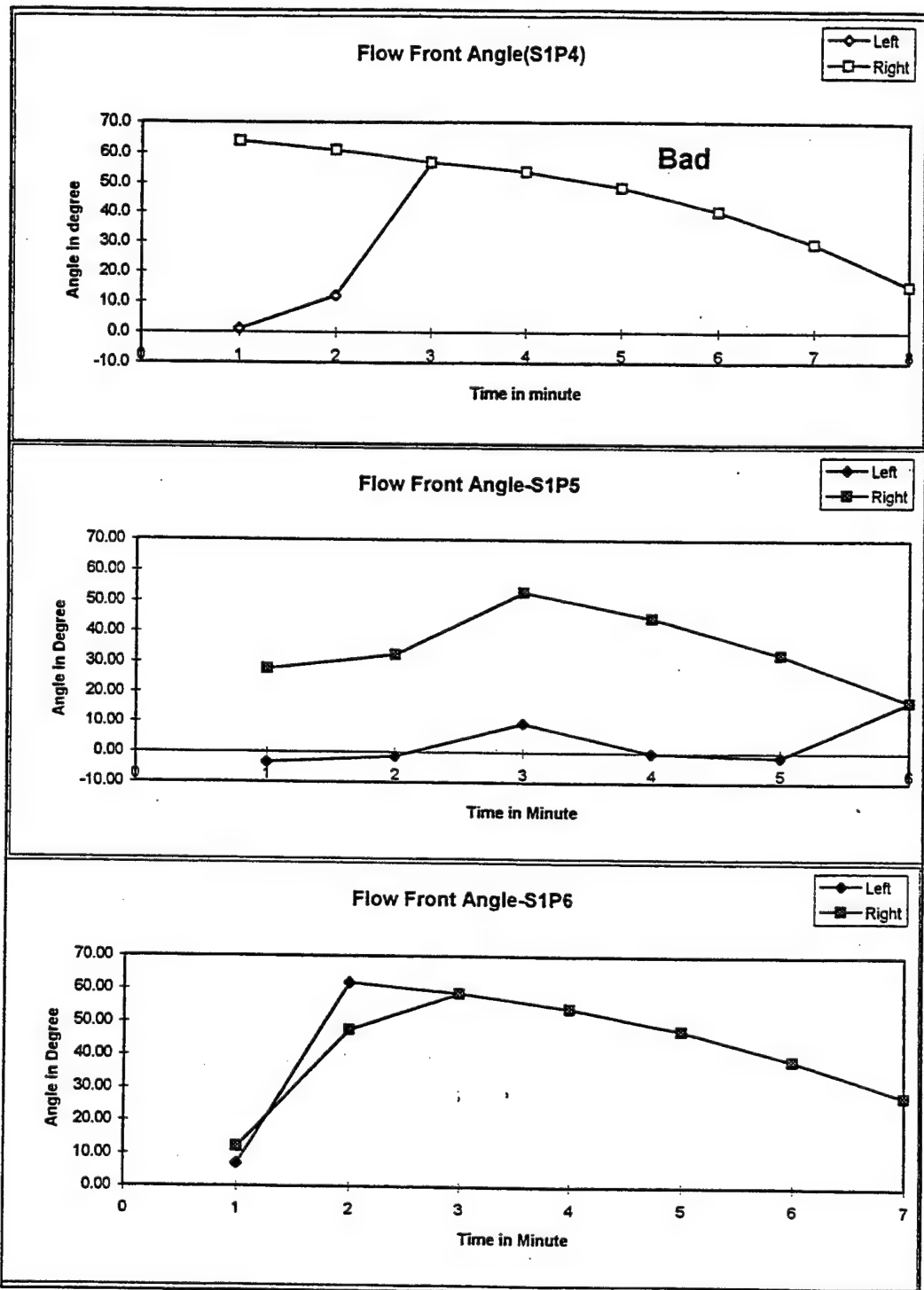
<b>S2P5</b>	R								
No Ports Closed		-0.23	L	-0.03	E	-0.48	L		
Top Ports Closed		-0.49	L	-0.33	L	-0.73	L		
Lower Ports Closed		-0.06	E	-0.08	E	-0.28	L		
Side Ports Closed		0.15	E	0.22	R	-			
<b>S2P6</b>	E								
No Ports Closed		-0.41	L	-0.06	E	-0.65	L		
Top Ports Closed		-0.76	L	-0.32	L	-1.13	L		
Lower Ports Closed		-0.10	E	-0.15	E	-0.17	E		
Side Ports Closed		-0.03	E	-0.05	E	-			
<b>S2P7</b>	R								
No Ports Closed		-0.38	L	-0.01	E	-0.71	L		
Top Ports Closed		-0.66	L	-0.30	L	-0.99	L		
Lower Ports Closed		-0.05	E	-0.08	E	-0.28	L		
Side Ports Closed		0.08	E	0.12	E	-			
<b>S2P8</b>	R								
No Ports Closed		0.14	E	0.36	R	0.21	R		
Top Ports Closed		0.14	E	0.41	R	0.21	R		
Lower Ports Closed		0.29	R	0.43	R	0.44	R		
Side Ports Closed		-0.07	E	-0.10	E	-			
<b>S2P9</b>	E								
No Ports Closed		0.05	E	-0.13	E	0.13	E		
Top Ports Closed		0.00	E	-0.12	E	0.00	E		
Lower Ports Closed		-0.12	E	-0.18	E	-0.12	E		
Side Ports Closed		0.01	E	0.01	E	-			
<b>S2P10</b>	E								
No Ports Closed		-0.25	L	-0.28	L	-0.26	L		
Top Ports Closed		-0.43	L	-0.40	L	-0.65	L		
Lower Ports Closed		-0.32	L	-0.48	L	-0.28	L		
Side Ports Closed		-0.21	L	-0.31	L	-			
<b>Legend:</b>	E = Even Flow	R = Right Flow	L = Left Flow						

**APPENDIX G**  
**FLOW FRONT ANGLES**

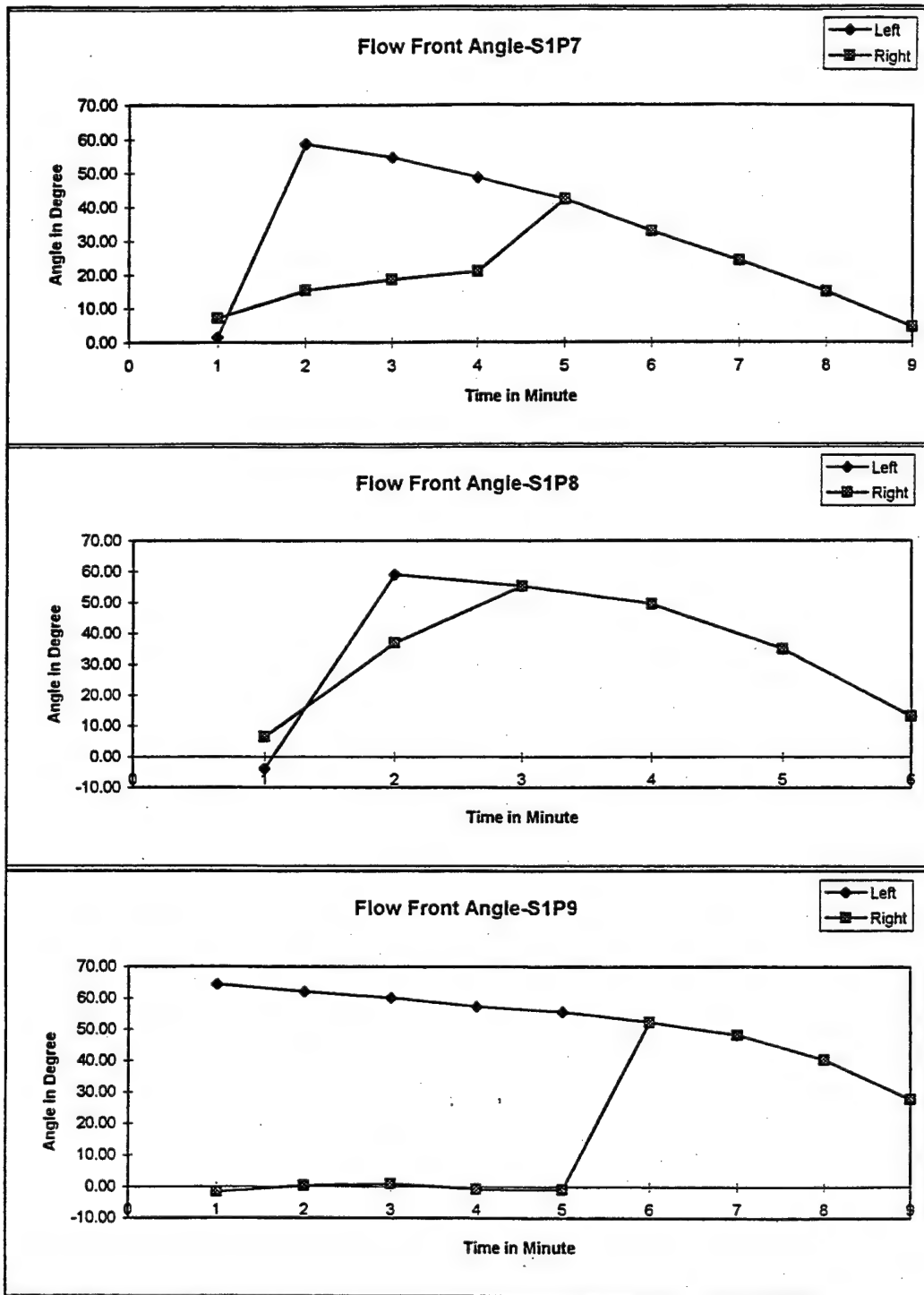
# Flow Front Angle Chart



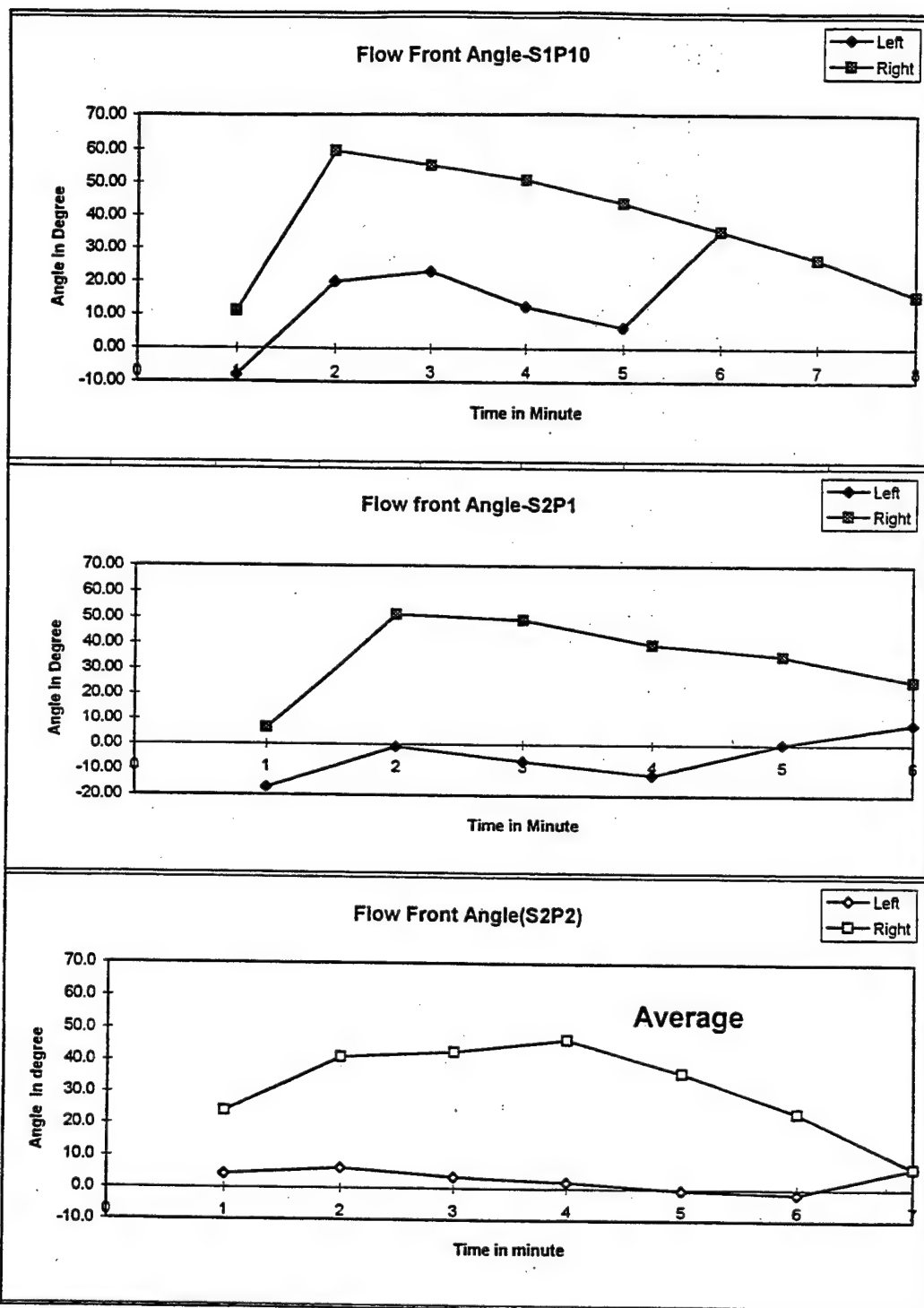
Flow Front Angle Chart



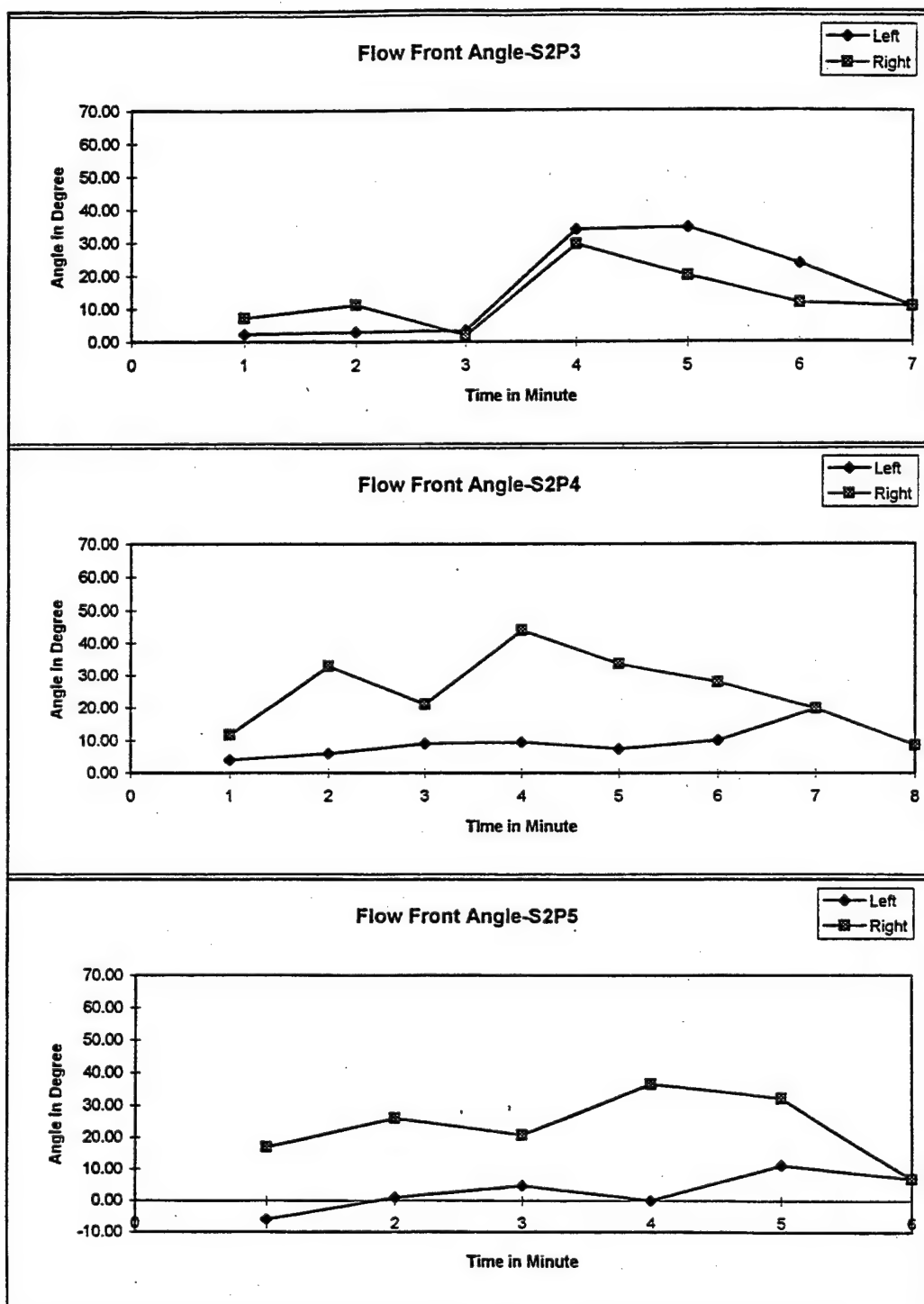
# Flow Front Angle Chart



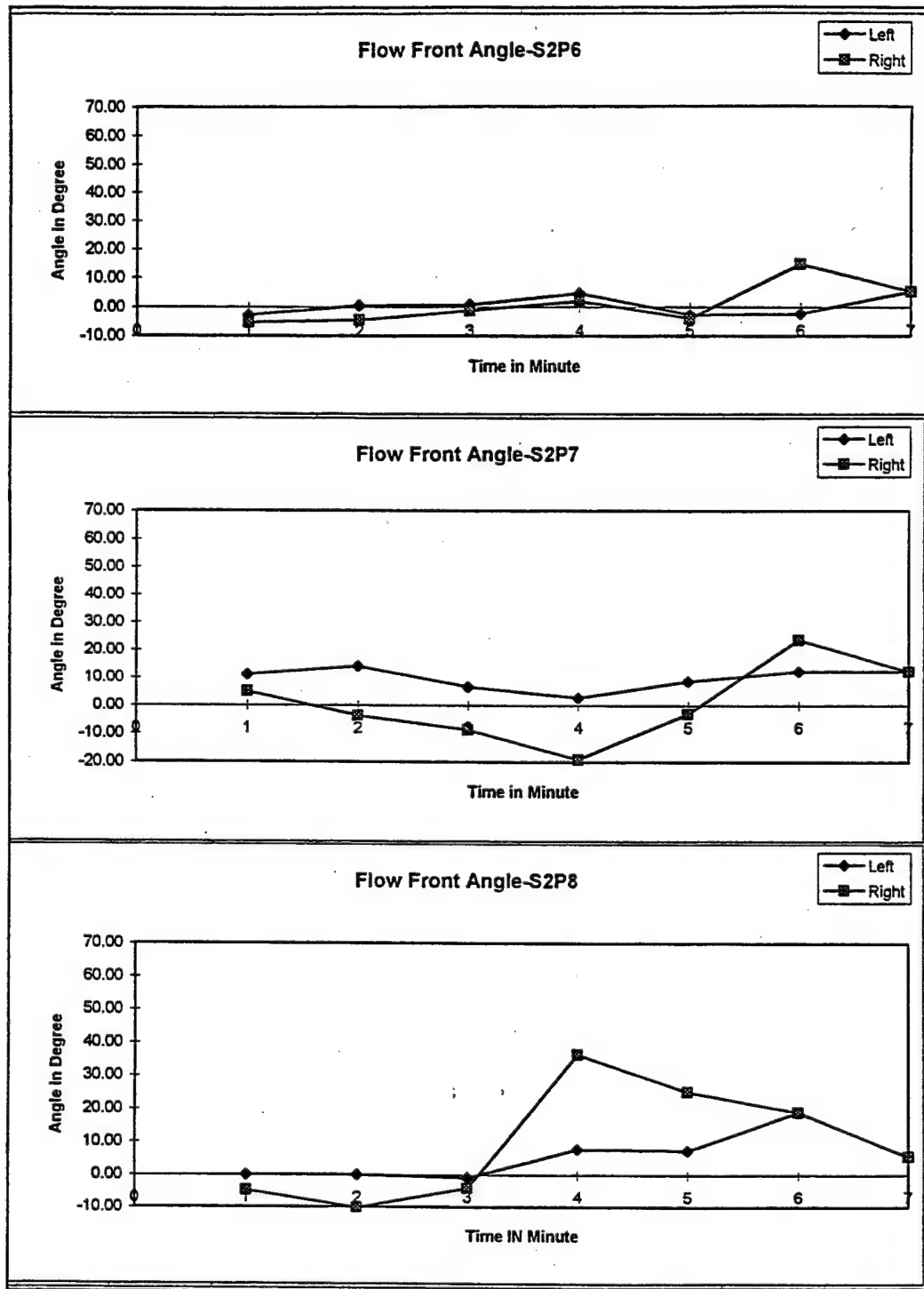
# Flow Front Angle Chart



# Flow Front Angle Chart

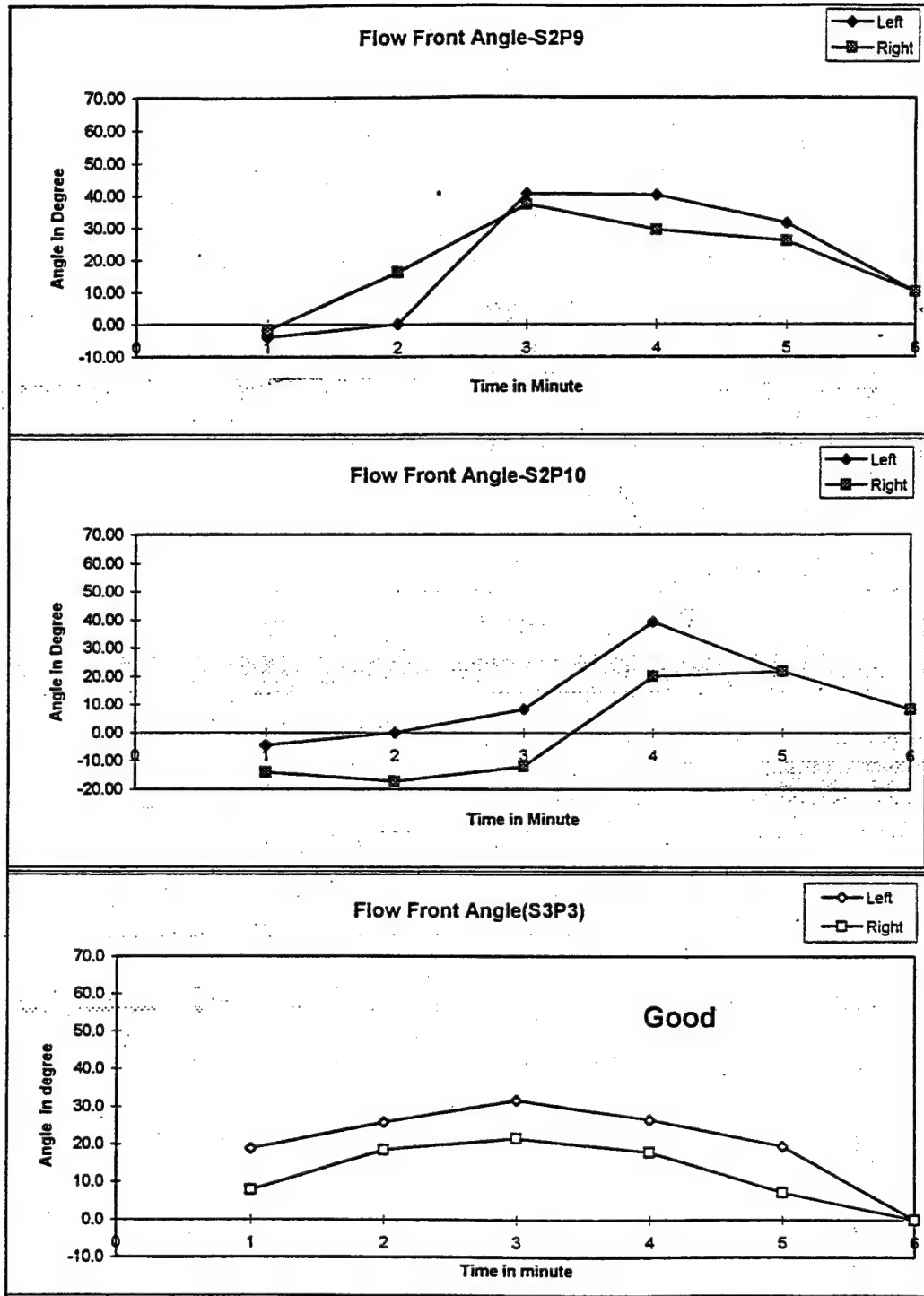


# Flow Front Angle Chart

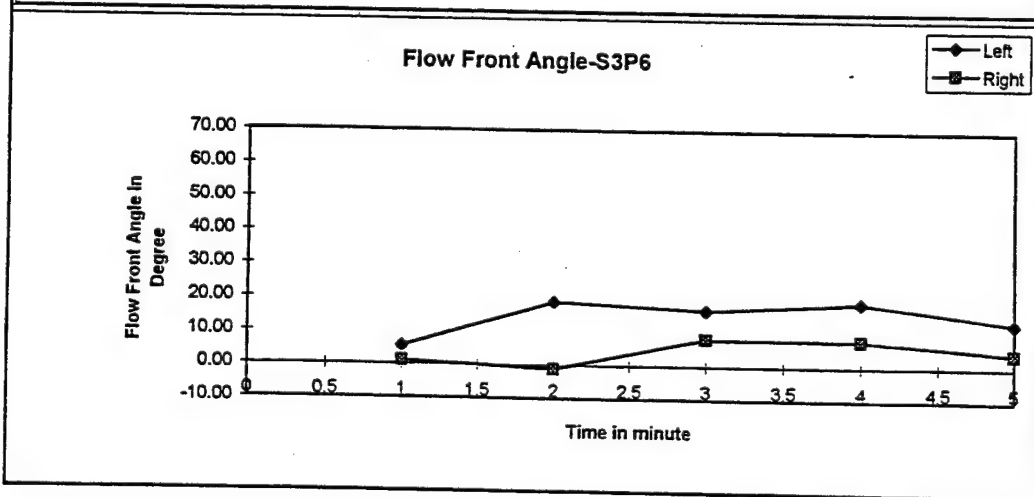
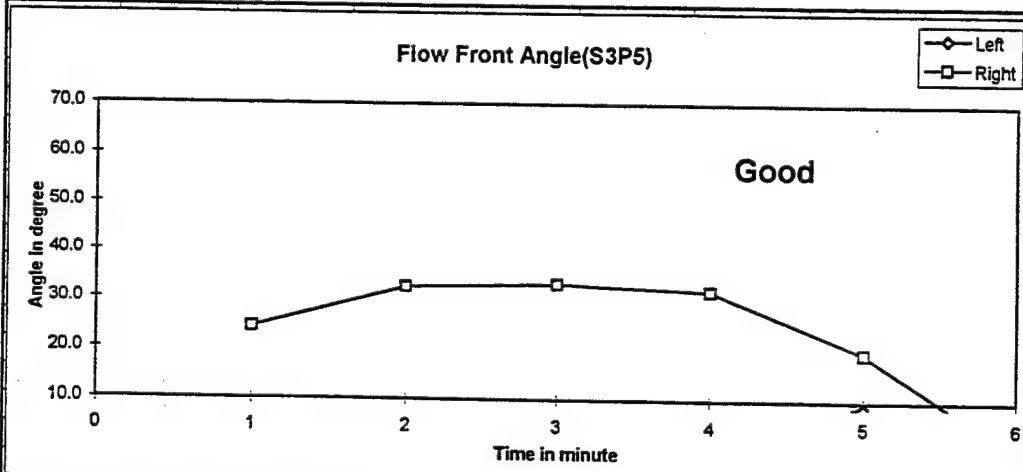
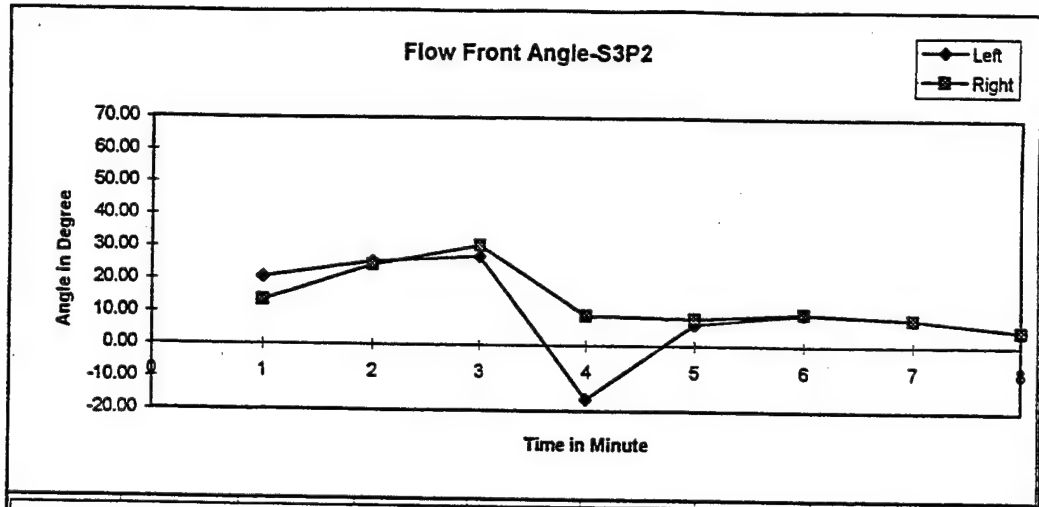




# Flow Front Angle Chart

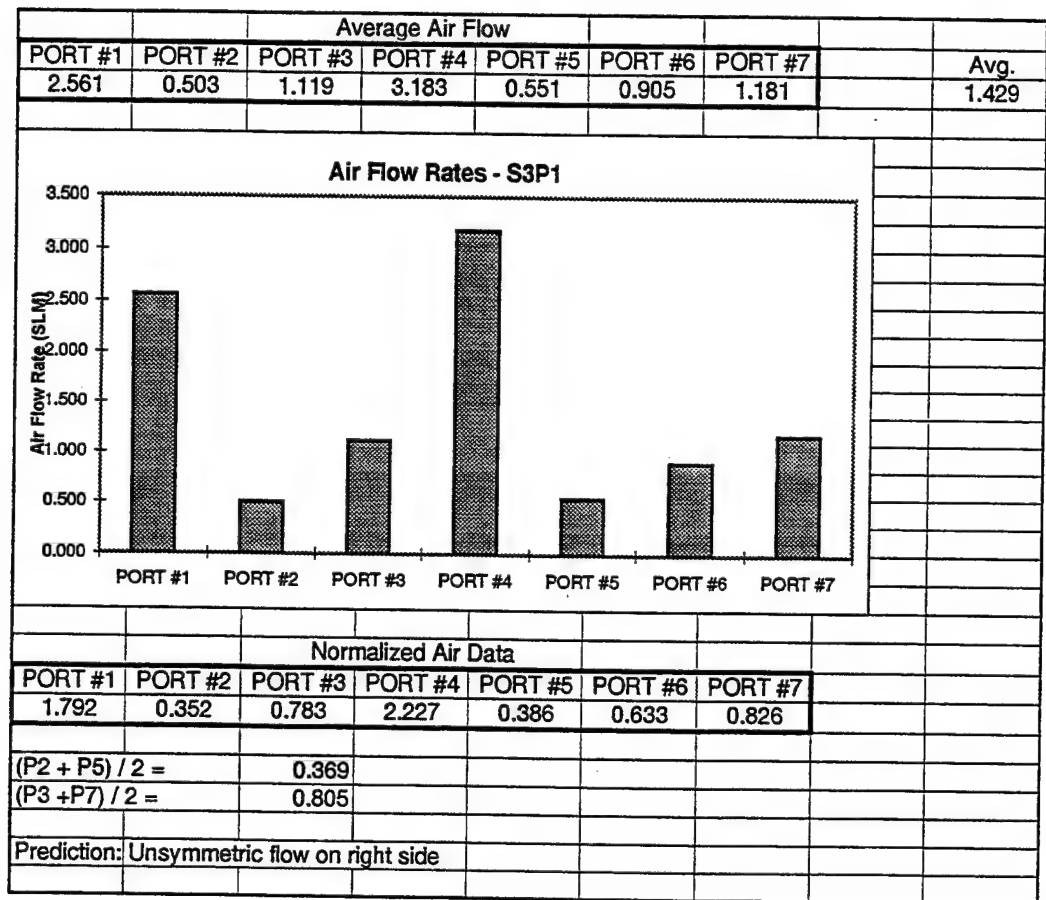


# Flow Front Angle Chart

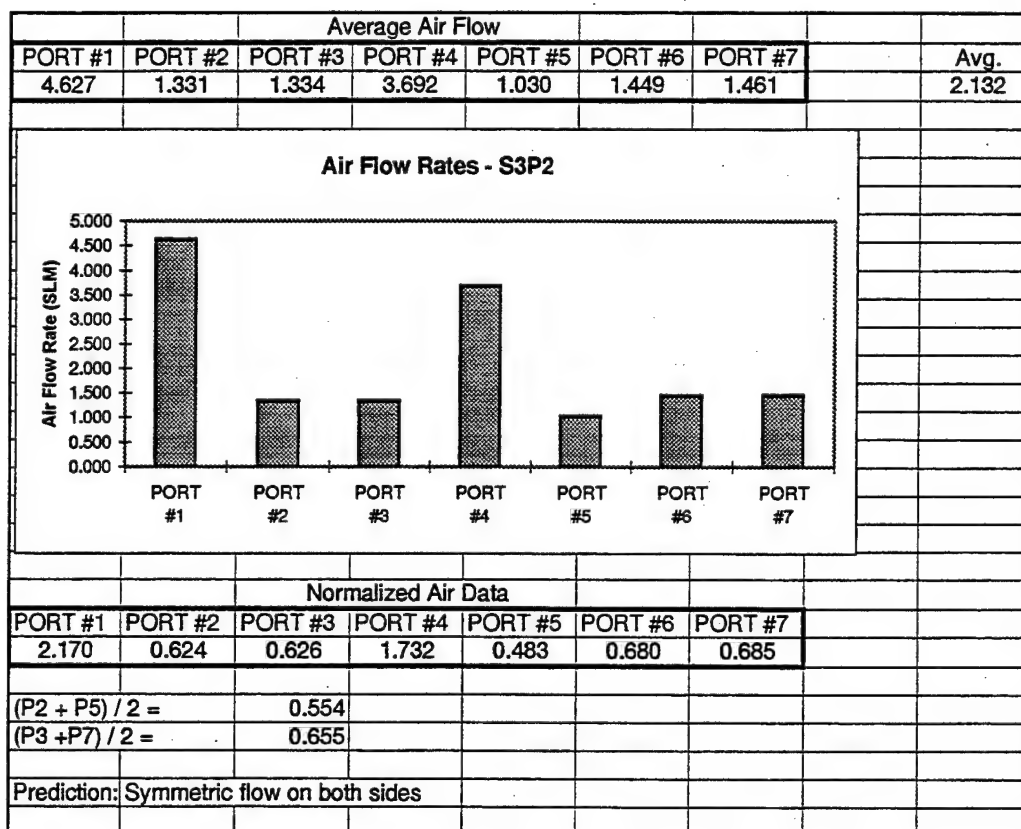


**APPENDIX H**  
**LABVIEW OUTPUT - VERIFICATION TESTS**  
**A. Flat Panels**  
**B. 3-D Demonstration Part**

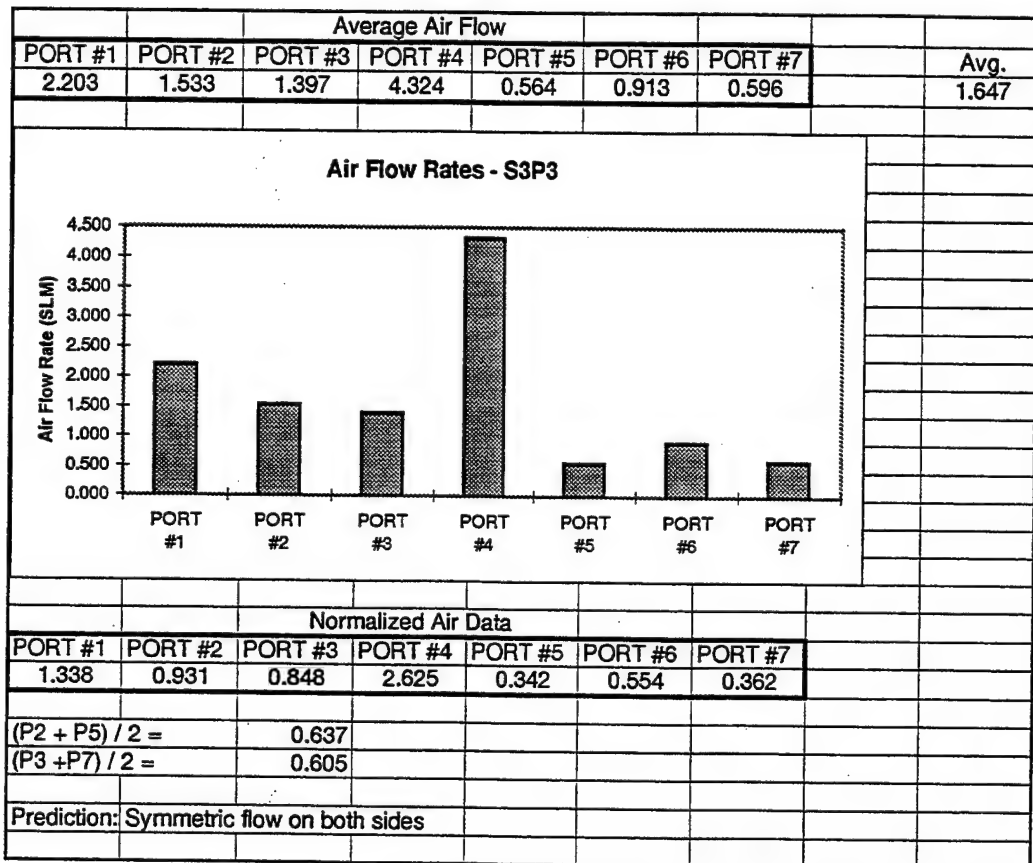
# Air Flow Data



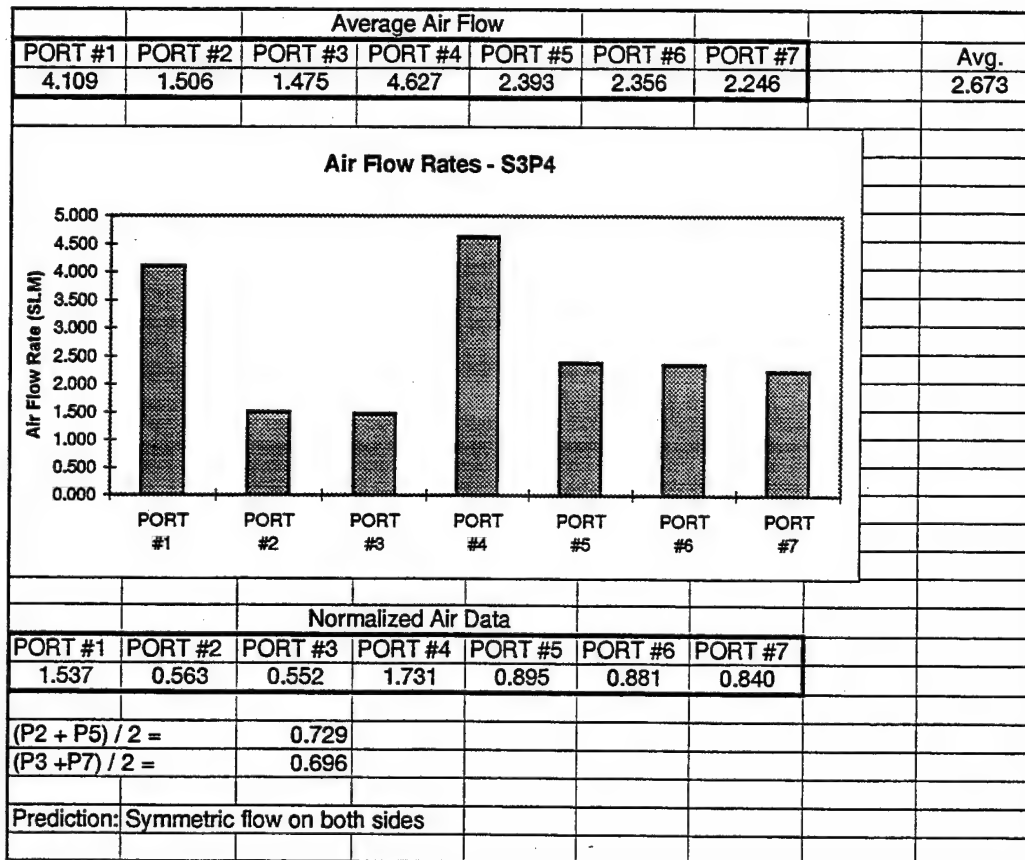
# Air Flow Data



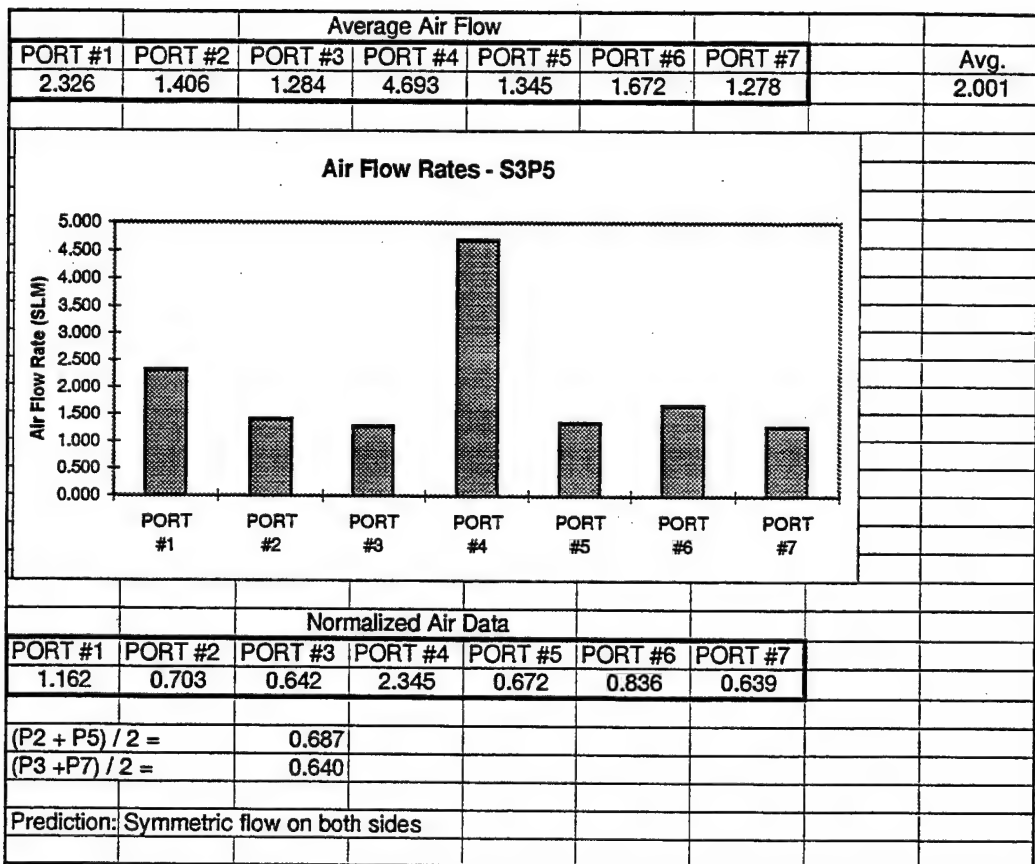
# Air Flow Data



# Air Flow Data

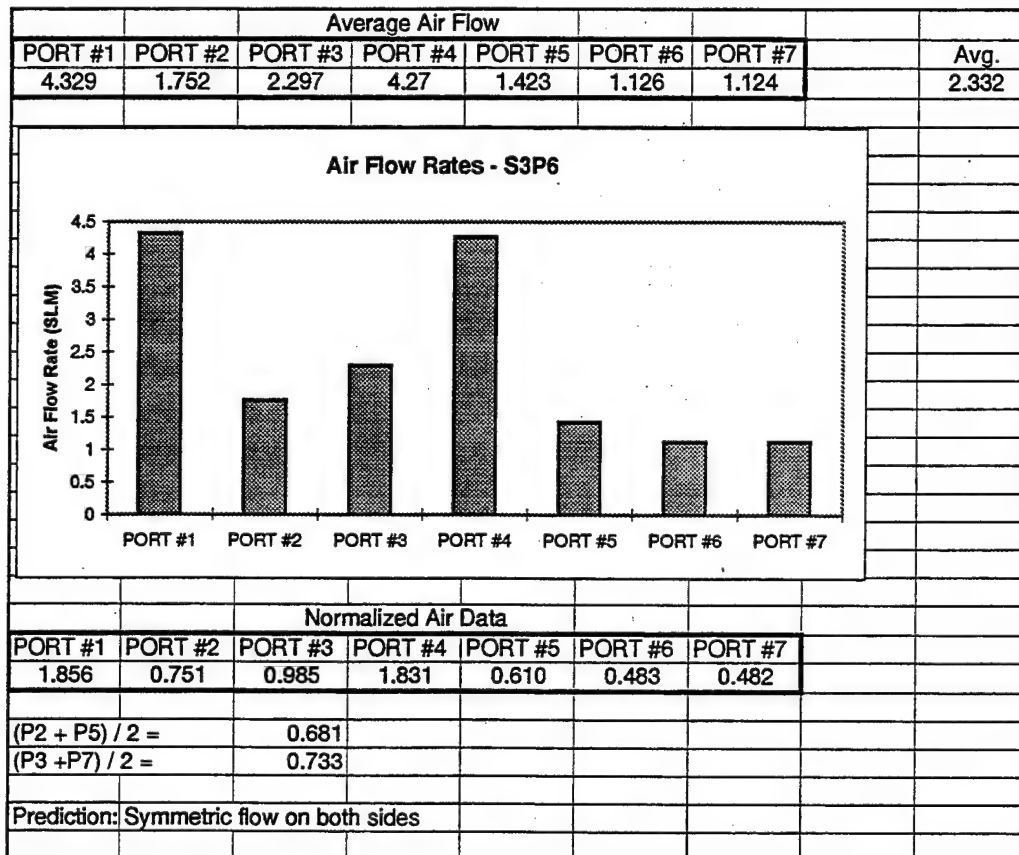


# Air Flow Data

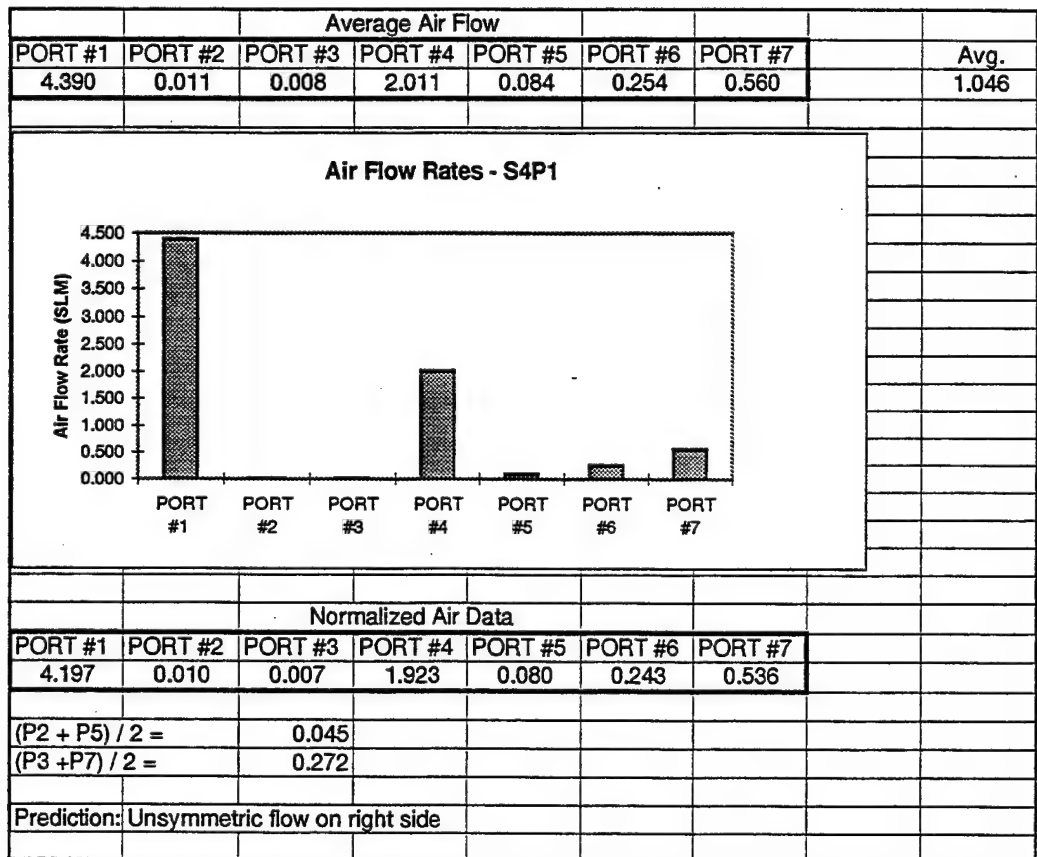




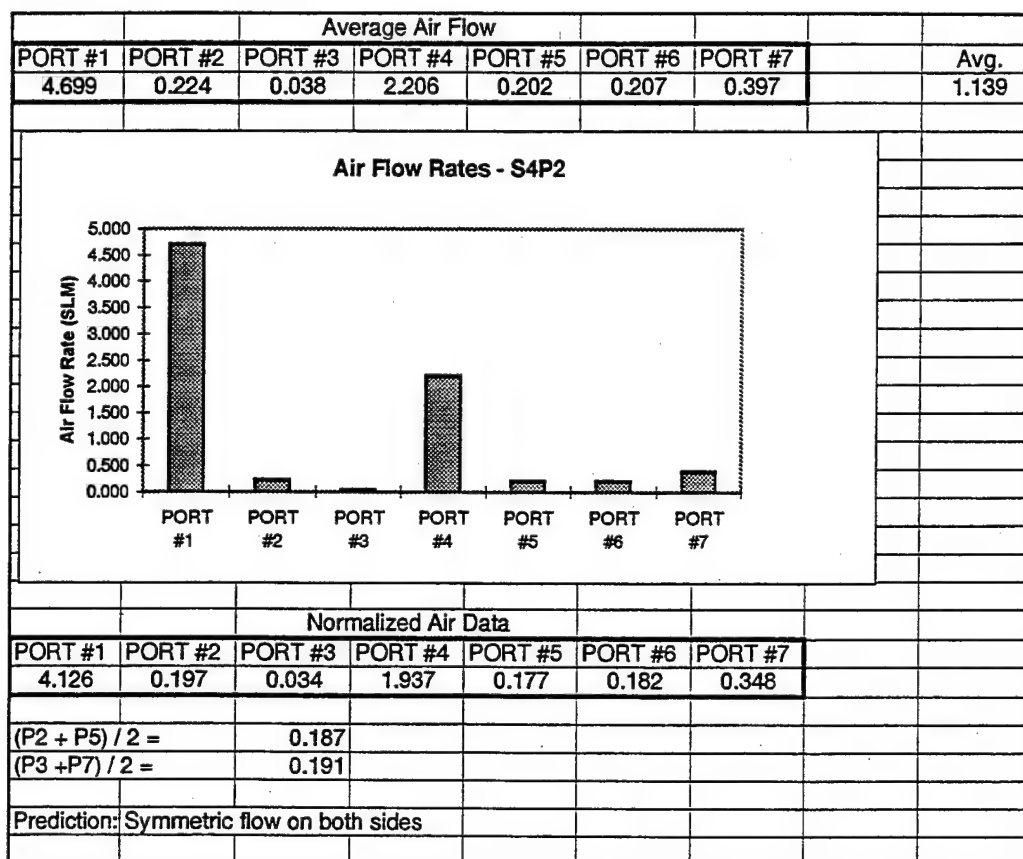
# Air Flow Data



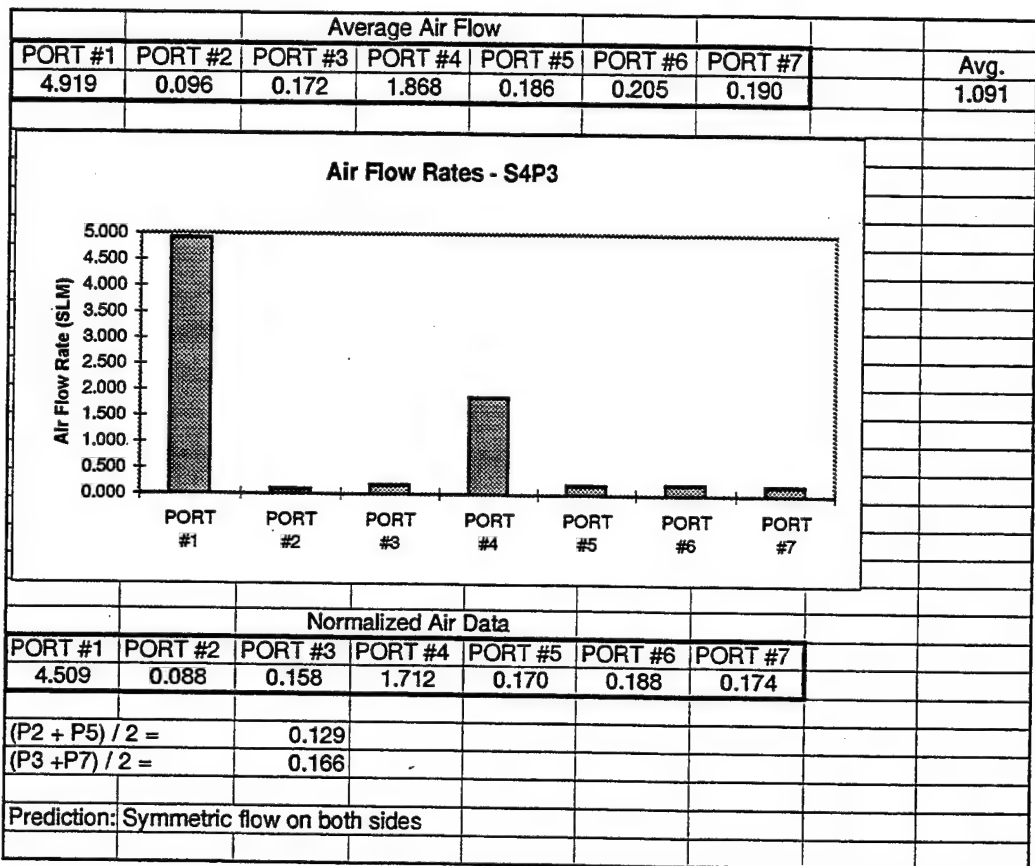
# Air Flow Data



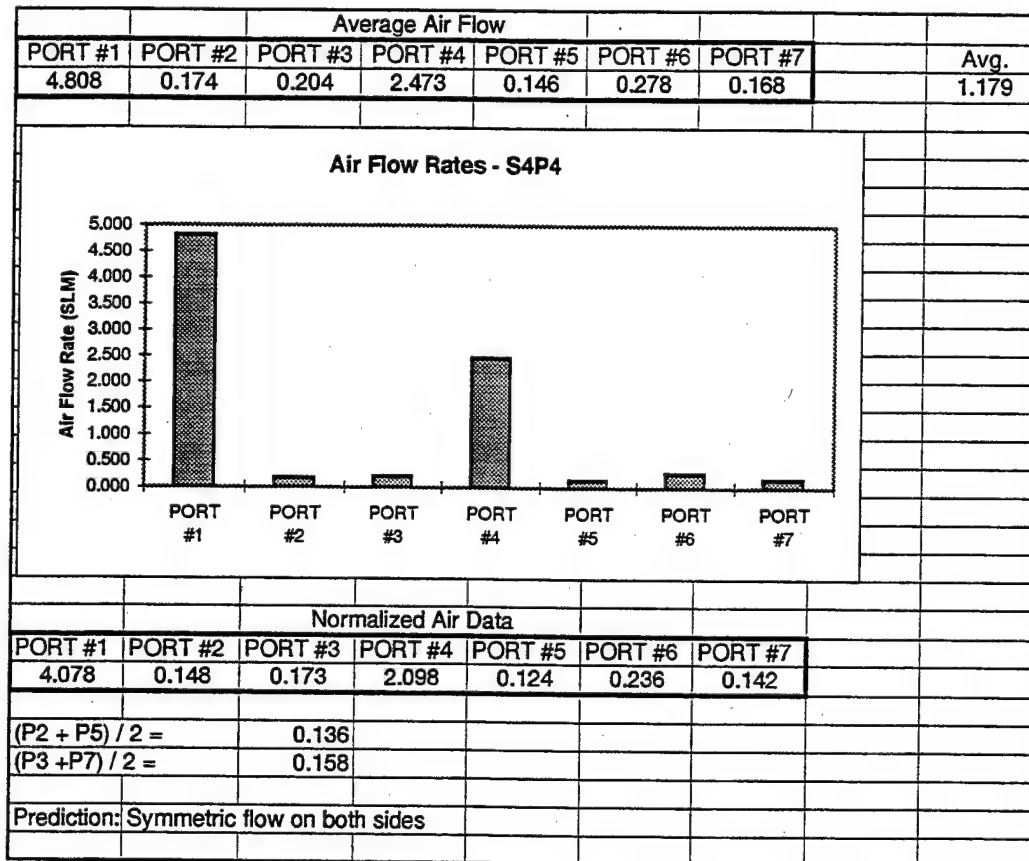
# Air Flow Data



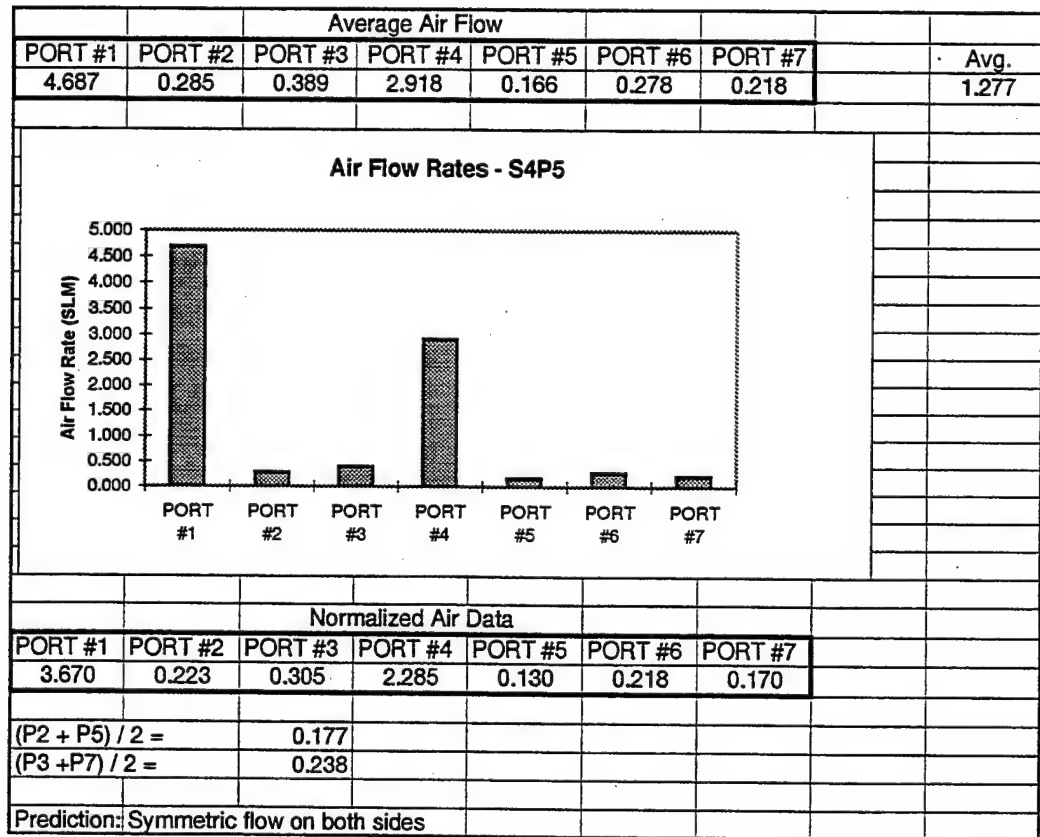
# Air Flow Data



# Air Flow Data



# Air Flow Data



**APPENDIX I**  
**RESULTS - MATERIAL PROPERTIES**

Table I-1: Correlation between Filltime and Young's Modulus for Regions 1 - 3.

Region 1			Region 2			Region 3		
Panel No.	Filltime (min)	Youngs Modulus (Msi)	Panel No.	Filltime (min)	Youngs Modulus (Msi)	Panel No.	Filltime (min)	Youngs Modulus (Msi)
S3P6	5	7.520	S3P6	5	5.750	S3P6	5	12.80
S3P5	6	5.520	S3P5	6	6.060	S3P5	6	6.620
S3P2	6	5.430	S3P2	6	5.620	S3P2	6	5.560
S3P1	6	6.330	S3P1	6	5.290	S3P1	6	7.870
S1P9	6	6.930	S1P9	6	7.370	S1P9	6	7.100
S2P9	7	6.430	S2P9	7	6.950	S2P9	7	7.270
S2P1	8	6.110	S2P1	8	6.260	S2P1	8	7.820
S1P2	10	6.050	S1P2	10	7.130	S1P2	10	6.290
S1P10	10	6.720	S1P10	10	6.170	S1P10	10	5.710
S1P3	12	5.750	S1P3	12	5.020	S1P3	12	6.740
Corr.		-0.275	Corr.		-0.095	Corr.		-0.454

Table I-2: Correlation between Filltime and Young's Modulus for Regions 4 - 6.

Region 4			Region 5			Region 6		
Panel No.	Filltime (min)	Youngs Modulus (Msi)	Panel No.	Filltime (min)	Youngs Modulus (Msi)	Panel No.	Filltime (min)	Youngs Modulus (Msi)
S3P6	5	5.650	S3P6	5	5.320	S3P6	5	6.410
S3P5	6	3.280	S3P5	6	3.310	S3P5	6	4.980
S3P2	6	2.180	S3P2	6	3.380	S3P2	6	3.370
S3P1	6	7.040	S3P1	6	4.630	S3P1	6	5.410
S1P9	6	6.910	S1P9	6	6.690	S1P9	6	7.190
S2P9	7	3.750	S2P9	7	3.300	S2P9	7	3.660
S2P1	8	8.800	S2P1	8	4.250	S2P1	8	2.750
S1P2	10	7.560	S1P2	10	7.440	S1P2	10	5.260
S1P1	10	5.610	S1P10	10	7.410	S1P10	10	6.890
S1P3	12	4.870	S1P3	12	5.660	S1P3	12	5.440
Corr.		0.197	Corr.		0.517	Corr.		0.058



Table I-3: Correlation between Race-Tracking Index and Average Young's Modulus for Regions 1, 4 and 3, 6.

Filltime (min)	Panel No.	Left RT-Index	Avg. Youngs Modulus (Msi)	Region 1	Region 4
8	S2P1	-0.07	7.455	6.110	8.800
6	S3P5	0.04	4.400	5.520	3.280
6	S3P1	0.09	6.685	6.330	7.040
6	S3P2	0.16	3.805	5.430	2.180
5	S3P6	0.22	6.585	7.520	5.650
7	S2P9	0.24	5.090	6.430	3.750
10	S1P10	0.27	6.165	6.720	5.610
10	S1P2	0.50	6.805	6.050	7.560
12	S1P3	0.71	5.310	5.750	4.870
6	S1P9	0.74	6.920	6.930	6.910
Correlation		0.107			

Filltime (min)	Panel No.	Right RT-Index	Avg. Youngs Modulus (Msi)	Region 3	Region 6
6	S3P2	0.22	9.605	5.560	3.370
6	S1P9	0.22	4.465	7.100	7.190
6	S2P9	0.25	7.145	7.270	3.660
6	S3P5	0.37	5.465	6.620	4.980
7	S3P1	0.39	5.800	7.870	5.410
8	S2P1	0.45	6.640	7.820	2.750
10	S1P10	0.62	5.285	5.710	6.890
10	S1P2	0.65	6.300	6.290	5.260
12	S1P3	0.71	5.775	6.740	5.440
Correlation		0.154			

Table I-4: Correlation between Filltime and Shear Strength for Regions 1 - 3.

Region 1				Region 2				Region 3			
Panel No.	Filltime (min)	Shear 1	Shear 2	Panel No.	Filltime (min)	Shear 3	Shear 4	Panel No.	Filltime (min)	Shear 5	Shear 6
S3P6	5	6.688	6.351	S3P6	5	6.382		S3P6	5	6.591	6.494
S3P5	6	6.633	6.629	S3P5	6	6.390	6.305	S3P5	6	6.766	6.817
S3P2	6	4.858	4.595	S3P2	6	6.068	5.737	S3P2	6	2.947	5.544
S3P1	6	6.548	6.896	S3P1	6	6.858	6.446	S3P1	6	6.741	6.832
S1P9	6	6.771	6.430	S1P9	6	6.419	6.614	S1P9	6	6.950	6.667
S2P9	7	6.185	6.190	S2P9	7	4.622	6.963	S2P9	7	6.357	5.724
S2P1	8	6.995	6.628	S2P1	8	6.468	7.106	S2P1	8	6.690	6.586
S1P2	10	6.394	6.265	S1P2	10	6.466	6.470	S1P2	10	6.657	6.236
S1P1	10	6.678	6.628	S1P1	10	6.328	6.028	S1P1	10	6.600	5.812
S1P3	12	6.711	6.322	S1P3	12	6.567	6.458	S1P3	12	6.553	6.457
Corr.		0.232	0.144	Corr.		0.130	0.016	Corr.		0.200	-

Table I-5: Correlation between Filltime and Shear Strength for Regions 4 - 6

Region 4				Region 5				Region 6			
Panel No.	Filltime (min)	Shear 7	Shear 8	Panel No.	Filltime (min)	Shear 9	Shear 10	Panel No.	Filltime (min)	Shear 11	Shear 12
S3P6	5	6.241	6.309	S3P6	5	6.157	6.140	S3P6	5	6.090	6.760
S3P5	6	3.591	3.147	S3P5	6	3.176	4.204	S3P5	6	3.718	4.151
S3P2	6	6.313	6.286	S3P2	6	6.233	5.586	S3P2	6	6.133	6.580
S3P1	6	7.384	6.933	S3P1	6	7.088	7.315	S3P1	6	6.424	6.714
S1P9	6	6.667	6.631	S1P9	6	6.413	6.810	S1P9	6	6.271	6.628
S2P9	7	6.389	6.376	S2P9	7	4.741	4.783	S2P9	7	6.819	6.472
S2P1	8	6.014	5.990	S2P1	8	6.130	5.505	S2P1	8	5.928	2.958
S1P2	10	6.573	6.452	S1P2	10	6.370	6.207	S1P2	10	6.199	6.217
S1P1	10	6.802	6.576	S1P1	10	6.294	6.703	S1P10	10	6.861	6.540
S1P3	12	6.447	6.501	S1P3	12	6.705	6.873	S1P3	12	6.571	6.739
Corr.		0.214	0.234	Corr.		0.288	0.306	Corr.		0.356	0.054

Table I-6: Correlation between left race-tracking index and average shear strength for regions 1, 4.

Filltime (min)	Panel No.	Left RT-Index	Avg. Shear Strength (ksi)	Region 1		Region 4	
8	S2P1	-0.07	6493	6995	6628	6014	5990
6	S3P5	0.04	4890	6633	6629	3591	3147
6	S3P1	0.09	6741	6548	6896	7384	6933
6	S3P2	0.16	5572	4858	4596	6313	6286
5	S3P6	0.22	6499	6688	6351	6241	6309
7	S2P9	0.24	6281	6185	6190	6389	6376
10	S1P10	0.27	6627	6678	6628	6802	6576
10	S1P2	0.50	6423	6394	6265	6573	6452
12	S1P3	0.71	6606	6711	6322	6447	6501
6	S1P9	0.74	6701	6771	6430	6667	6631
Correlation 0.413							

Table I-7: Correlation between Right Race-Tracking Index and Average Shear Strength for Regions 3, 6

Filltime (min)	Panel No.	Right RT-Index	Avg. Shear Strength (ksi)	Region 3		Region 6	
5	S3P6	0.04	6676	6591	6494	6090	6760
6	S3P2	0.22	4764	2947	5544	6133	6580
6	S1P9	0.22	6789	6950	6667	6271	6628
7	S2P9	0.25	6415	6357	5724	6819	6472
6	S3P5	0.37	5459	6766	6817	3718	4151
6	S3P1	0.39	6728	6741	6832	6424	6714
8	S2P1	0.45	4824	6690	6586	5928	2958
10	S1P10	0.62	6570	6600	5812	6861	6540
10	S1P2	0.65	6437	6657	6236	6199	6217
12	S1P3	0.71	6646	6553	6457	6571	6739
Correlation 0.109							

Table I-8: Correlation between Filltime and Fiber Volume Percentage for Regions 1 - 3.

Region 1			Region 2			Region 3		
Panel No.	Filltime (min)	Fiber Vol. %	Panel No.	Filltime (min)	Fiber Vol. %	Panel No.	Filltime (min)	Fiber Vol. %
S3P6	5	38.14	S3P6	5	38.98	S3P6	5	37.54
S3P5	6	37.59	S3P5	6	37.86	S3P5	6	37.36
S3P2	6	38.16	S3P2	6	37.23	S3P2	6	39.02
S3P1	6	34.09	S3P1	6	32.39	S3P1	6	35.27
S1P9	6	42.67	S1P9	6	38.18	S1P9	6	42.63
S2P9	7	40.35	S2P9	7	38.35	S2P9	7	46.41
S2P1	8	43.61	S2P1	8	39.40	S2P1	8	42.09
S1P2	10	46.79	S1P2	10	43.95	S1P2	10	45.27
S1P1	10	44.36	S1P1	10	41.26	S1P10	10	44.99
S1P3	12	54.63	S1P3	12	42.37	S1P3	12	42.95
Correlation 0.898			Correlation 0.745			Correlation 0.628		

Table I-9: Correlation between Filltime and Fiber Volume Percentage for Regions 4 - 6.

Region 4			Region 5			Region 6		
Panel No.	Filltime (min)	Fiber Vol. %	Panel No.	Filltime (min)	Fiber Vol. %	Panel No.	Filltime (min)	Fiber Vol. %
S3P6	5	39.09	S3P6	5	38.72	S3P6	5	36.89
S3P5	6	41.59	S3P5	6	42.47	S3P5	6	41.51
S3P2	6	46.33	S3P2	6	44.24	S3P2	6	46.12
S3P1	6	35.59	S3P1	6	36.31	S3P1	6	36.30
S1P9	6	45.35	S1P9	6	42.99	S1P9	6	43.30
S2P9	7	48.44	S2P9	7	48.59	S2P9	7	48.60
S2P1	8	50.58	S2P1	8	50.95	S2P1	8	45.87
S1P2	10	46.92	S1P2	10	31.47	S1P2	10	45.18
S1P10	10	46.22	S1P10	10	43.48	S1P10	10	42.76
S1P3	12	46.10	S1P3	12	40.96	S1P3	12	43.47
Correlation 0.483			Correlation -0.127			Correlation 0.342		

Table I-10: Correlation between Left Race-Tracking Index and Average Fiber Volume Percentage for Regions 1, 4.

Filltime (min)	Panel No.	Left RT-Index	Fiber Vol. %	Region 1	Region 4
8	S2P1	-0.07	47.09	43.61	50.58
6	S3P5	0.04	39.59	37.59	41.59
6	S3P1	0.09	34.84	34.09	35.59
6	S3P2	0.16	42.25	38.16	46.33
5	S3P6	0.22	38.61	38.14	39.09
7	S2P9	0.24	44.4	40.35	48.44
10	S1P10	0.27	45.29	44.36	46.22
10	S1P2	0.5	46.85	46.79	46.92
12	S1P3	0.71	50.36	54.63	46.1
6	S1P9	0.74	44.01	42.67	45.35
Correlation		0.497			

Table I-11: Correlation between Right Race-Tracking Index and Average Fiber Volume Percentage for Regions 3, 6.

Filltime (min)	Panel No.	Right RT-Index	Fiber Vol. %	Region 3	Region 6
5	S3P6	0.04	37.21	37.54	36.89
6	S3P2	0.22	42.57	39.02	46.12
6	S1P9	0.22	42.96	42.63	43.3
7	S2P9	0.25	47.5	46.41	48.6
6	S3P5	0.37	39.44	37.36	41.51
6	S3P1	0.39	35.78	35.27	36.3
8	S2P1	0.45	43.98	42.09	45.87
10	S1P10	0.62	43.87	44.99	42.76
10	S1P2	0.65	45.23	45.27	45.18
12	S1P3	0.71	43.21	42.95	43.47
Correlation		0.347			

Table I-12: Correlation between Filltime and Void Content Percentage for Regions 1 - 3.

Panel No.	Region 1 Filltime (min)	Void Content %	Panel No.	Region 2 Filltime (min)	Void Content %	Panel No.	Region 3 Filltime (min)	Void Content %
S3P6	5	0.000	S3P6	5	0.029	S3P6	5	0.200
S3P5	6	0.000	S3P5	6	0.412	S3P5	6	1.142
S3P2	6	0.841	S3P2	6	0.373	S3P2	6	0.933
S3P1	6	0.068	S3P1	6	0.019	S3P1	6	0.000
S1P9	6	0.000	S1P9	6	0.000	S1P9	6	0.303
S2P9	7	0.294	S2P9	7	4.234	S2P9	7	0.124
S2P1	8	0.346	S2P1	8	0.977	S2P1	8	0.326
S1P2	10	0.496	S1P2	10	0.474	S1P2	10	0.741
S1P10	10	0.743	S1P10	10	0.702	S1P10	10	0.735
S1P3	12	5.326	S1P3	12	0.625	S1P3	12	0.000
Corr.		0.739	Corr.		0.079	Corr.		-0.086

Table I-13: Correlation between Filltime and Void Content Percentage for Regions 4 - 6.

Panel No.	Region 4 Filltime (min)	Void Content %	Panel No.	Region 5 Filltime (min)	Void Content %	Panel No.	Region 6 Filltime (min)	Void Content %
S3P6	5	0.264	S3P6	5	0.300	S3P6	5	0.000
S3P5	6	0.000	S3P5	6	0.256	S3P5	6	2.525
S3P2	6	1.201	S3P2	6	1.468	S3P2	6	1.439
S3P1	6	0.000	S3P1	6	1.121	S3P1	6	0.223
S1P9	6	0.474	S1P9	6	0.509	S1P9	6	0.286
S2P9	7	0.309	S2P9	7	5.669	S2P9	7	0.478
S2P1	8	0.385	S2P1	8	0.192	S2P1	8	0.158
S1P2	10	0.547	S1P2	10	0.000	S1P2	10	0.444
S1P10	10	0.610	S1P10	10	0.272	S1P10	10	0.000
S1P3	12	0.180	S1P3	12	0.000	S1P3	12	0.000
Corr.		0.023	Corr.		-0.246	Corr.		-0.151

Table I-14: Correlation between Race-Tracking Index and Void Content Percentage for Regions 1, 4 and 3, 6.

Filltime (min)	Panel No.	Left RT-Index	Avg. Void Content %	Region 1	Region 4
5	S3P6	0.22	0.104	-0.055	0.264
6	S3P5	0.04	0.000	0.000	0.000
6	S3P2	0.16	1.021	0.841	1.201
6	S3P1	0.09	0.034	0.068	0.000
6	S1P9	0.74	0.237	0.000	0.474
7	S2P9	0.24	0.302	0.294	0.309
8	S2P1	-0.07	0.365	0.346	0.385
10	S1P2	0.50	0.521	0.496	0.547
10	S1P10	0.27	0.677	0.743	0.610
12	S1P3	0.71	2.753	5.326	0.180
Corr.	0.526				

Filltime (min)	Panel No.	Right RT-Index	Avg. Void Content %	Region 3	Region 6
5	S3P6	0.04	0.100	0.200	0.000
6	S3P5	0.37	1.834	1.142	2.525
6	S3P2	0.22	1.186	0.933	1.439
6	S3P1	0.39	0.111	0.000	0.223
6	S1P9	0.22	0.295	0.303	0.286
7	S2P9	0.25	0.301	0.124	0.478
8	S2P1	0.45	0.242	0.326	0.158
10	S1P2	0.65	0.592	0.741	0.444
10	S1P10	0.62	0.368	0.735	0.000
12	S1P3	0.71	0.000	0.000	0.000
Corr.	-0.109				